UNIVERSITÀ DEGLI STUDI DI PAVIA
DOTTORATO DI RICERCA IN FISICA – XXX CICLO

Applications of Light-Front Quantization in QED and QCD

Luca Mantovani

2017

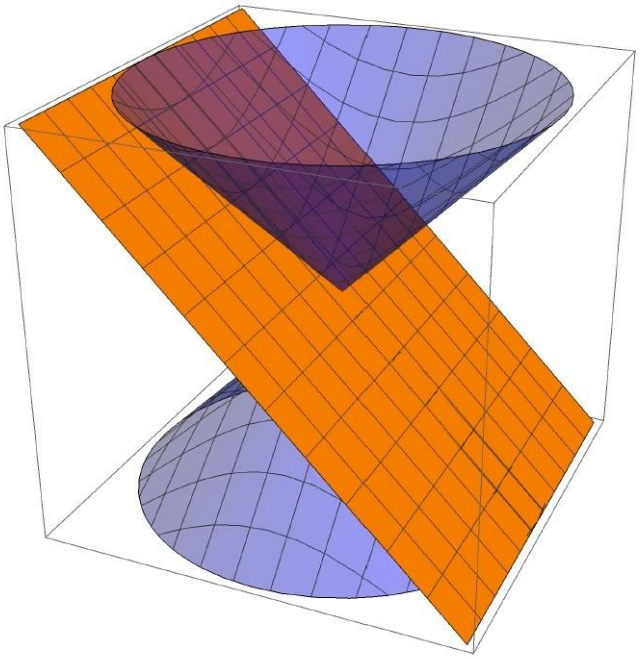

This thesis is partly based on the following publications:

1. A. Bacchetta, L. Mantovani, and B. Pasquini. Electron in three-dimensional momentum space. *Phys. Rev.*, D93(1):013005, 2016.

2. L. Mantovani, A. Bacchetta, and B. Pasquini. The Electron in Three-Dimensional Momentum Space. *Few Body Syst.*, 57(7):515, 2016.

3. L. Mantovani, B. Pasquini, X. Xiong, and A. Bacchetta. Revisiting the equivalence of light-front and covariant QED in the light-cone gauge. *Phys. Rev.*, D94(11):116005, 2016.

4. L. Mantovani, A. Bacchetta, B. Pasquini, and X. Xiong. The Gauge-Field Propagator in Light-Cone Gauge: Which is the Correct One? *Few Body Syst.*, 58(2):84, 2017.

5. C. Lorcé, L. Mantovani, and B. Pasquini. Spatial distribution of angular momentum inside the nucleon. arXiv:1704.08557 [hep-ph]. Submitted to *Phys. Lett.,* B, 2017.

Contents

Notations and conventions

Throughout this thesis, we will use natural units $\hbar = c = 1$. Light italic roman type will be used for four-vectors, while boldface italic will be used for three-vectors and two-vectors. The latter will be also indicated with the "$\perp$" suffix. Greek indices range from 0 to 3 and refer to Lorentz components; Latin indices range from 1 to 3 and refer to spatial components, namely $(a^1, a^2, a^3) = (a_x, a_y, a_z)$. Einstein's convention for summation of repeated Latin indices will always be assumed, whereas repeated Lorentz indices are meant to be contracted with the metric tensor: $a^\mu b_\mu = a^\mu g_{\mu\nu} b^\nu$.
We will consider the Levi-Civita totally-antisymmetric tensor in four dimensions with the convention $\varepsilon_{0123} = 1$; accordingly, in three dimensions we will take $\varepsilon^{ijk} = \varepsilon_{0ijk}$, while in two dimensions ε^{ij} is defined through $\varepsilon^{12} = -\varepsilon^{21} = 1$, $\varepsilon^{11} = \varepsilon^{22} = 0$
We will use the Standard representation for Dirac matrices:

$$\gamma^0 = \begin{pmatrix} \mathbb{1} & 0 \\ 0 & -\mathbb{1} \end{pmatrix}, \quad \gamma^i = \begin{pmatrix} 0 & \sigma^i \\ -\sigma^i & 0 \end{pmatrix}, \quad \gamma^5 = \begin{pmatrix} 0 & \mathbb{1} \\ \mathbb{1} & 0 \end{pmatrix},$$

where σ^i are the 2×2 Pauli's matrices

$$\sigma^1 = \begin{pmatrix} 0 & 1 \\ 1 & 0 \end{pmatrix}, \quad \sigma^2 = \begin{pmatrix} 0 & -i \\ i & 0 \end{pmatrix}, \quad \sigma^3 = \begin{pmatrix} 1 & 0 \\ 0 & -1 \end{pmatrix}.$$

The commutator of Dirac matrices is $\sigma^{\mu\nu} = \frac{i}{2}[\gamma^\mu, \gamma^\nu]$. We will also adopt Feynman's slash notation $\not{p} = \gamma^\mu p_\mu$.

Chapter 1

Introduction

In this thesis we will discuss examples of applications of the light-front quantization formalism in Quantum Field Theories. The purpose of this Introduction is to describe the background of our studies and to provide the motivations that inspired this research.

1.1 Quantum Field Theory

In the mid 1920s, when Quantum Mechanics was emerging as the formalism that describes Physics at the subatomic scale, the theory of Special Relativity was already well-established. A lot of effort was therefore immediately devoted to reconcile the two theories in a unified framework. It soon became clear that the approach offered by Quantum Field Theory (QFT), as presented in the pioneering works by Born, Jordan, Heisenberg and Dirac [1, 2], was the most suitable to attack the problem. Quantum Electrodynamics (QED), in particular, proved to be extremely successful in the description of the interactions between radiation and matter.
Thanks to the subsequent introduction of renormalization techniques, which made it possible to obtain an incredibly precise predictive power, QED has become over the years the best-tested and one of the most consolidated theories in all of Physics [3]. Quantum Field Theory is nowadays the underlying framework of the Standard Model (SM), that describes elementary particles and the fundamental forces ruling their interactions.

In the canonical QFT formulation, given some boundary condition on a three-dimensional hypersurface at fixed time $t = 0$, the state associated to a given system is evolved in the time direction according to the Schrödinger equation. As noticed already by Dirac in 1949 [4], however, the choice of a preferred direction for the evolution of the system is somewhat arbitrary: there are (infinitely many, in principle) equivalent possibilities, or *forms* of relativistic dynamics, as Dirac called them. The canonical one is referred to as the

instant form. The *light-front form*, instead, mixes the direction of time and of the z coordinate, thus rotating the $t = 0$ hypersurface to make it tangent to the light cone centered at the origin. The formulation of QFT in the light-front form is named *light-front quantization*.

As we will extensively discuss throughout this thesis, the different forms of dynamics eventually provide perfectly equivalent results. Nevertheless, they turn out to be more or less suitable for the analysis of a given problem. In the framework of Particle Physics, light-front quantization proves to be an elegant language for the description of a composite particle in terms of its elementary constituents. For this reason, this formalism is effectively employed in the context of Hadron Physics and Quantum Chromodynamics (QCD), although it can be in principle applied to any QFT.

1.2 Hadronic Physics and QCD

The main goal of Hadronic Physics is to describe the global properties of nucleons (namely, protons and neutrons) in terms of the underlying properties of their constituents (namely, quarks and gluons) and of the interactions among them. The latter are ruled by QCD, which is the Standard-Model theory of strong interactions. Its non-Abelian nature makes it far different from the electroweak sector of the SM, introducing in particular the phenomena of asymptotic freedom and confinement. These aspects complicate the treatment of QCD both from the theoretical and the experimental side, making the final goal extremely challenging to achieve.
Besides lacking a complete mathematical formulation, QCD misses to explain the nature of fundamental physical quantities related to protons and neutrons. Over the last few years, tremendous progresses have been made in matching the QCD theoretical predictions of nucleons' fundamental physical quantities, mainly through the lattice-QCD approach. Nevertheless, QCD still lacks a complete mathematical formulation; it cannot therefore, at present, provide a method for the analytical derivation of such quantities, and eventually explain of their generation mechanisms. Typical examples in this regard are given by the origin of the nucleons' mass (which amounts to about 99% of the mass of the visible universe) as due to the gluon dynamics [5,6], and the decomposition of the nucleons' spin in terms of contributions from spin and orbital angular momentum of the constituents [7].
The fundamental primary tools for the inspection of the internal structure of nucleons are the partonic distribution functions, which provide us with multi-dimensional maps of the inside of nucleons both in momentum and position space. A proper determination of these functions, both from the theoretical and the experimental point of view, would hence be key to shed light on the above-mentioned open problems. For this reason, over the last few decades the worldwide Hadronic Physics community has spent a major effort in their

investigation.
The light-front quantization formalism is a precious theoretical instrument for the study of partonic distributions since, other than simplifying practical calculations, it allows one to have an intuitive physical interpretation of their content [8]. Furthermore, the possibility to apply it to a generic Quantum Field Theory makes it a suitable common ground for the comparison of theories with different properties, such as QED and QCD, thus highlighting their similarities and differences.

1.3 Outline of the thesis

The goal of this thesis is to present some novel applications of the light-front quantization formalism to the fields of QED and QCD.
In Chapter 2 we will review the basic concepts that form the foundations of light-front quantization. We will adopt a historical perspective, stressing at the same time the advantages of this formalism with respect to the usual instant-form quantization.
In Chapter 3 we will prove that light-front Time-Ordered Perturbation Theory and the covariant Feynman-diagram approach in light-front coordinates and in light-cone gauge are equivalent at one-loop level in QED. As we work in a gauge theory, the presence of instantaneously-propagating photons makes the problem non-trivial. Our proof clarifies which form should be used for the gauge-field propagator in light-cone gauge.
In Chapter 4 we will give a brief overview of the available distribution functions in Hadronic Physics. These instruments allow one to investigate the internal structure of composite particles in terms of their constituents. Examples of their application both in the field of QED and in that of QCD will be showed in Chapters 5 and 6.
In Chapter 5 we will study the α-order structure of the dressed electron, considering it as composed of a bare electron and a virtual photon[1]. To this aim, we will consider the Generalized Transverse-Momentum Dependent and the Transverse-Momentum Dependent distribution functions in QED. We will provide their analytical calculation and discuss their gauge-invariance, with particular focus on the role of the transverse gauge link. Besides the academic interest in viewing the point-like electron in a new perspective as a composite system, the purpose of working in the QED framework is to gain a deeper knowledge of light-front quantization methods by enlightening their general features.
In Chapter 6 we will turn our attention to Hadronic Physics and describe angular-momentum distributions of quarks in position space inside the nu-

[1] In the field-theoretical picture, the electron cloud contains (in principle) an infinite number of virtual photons and electron-positron pairs, consistently with the quantum numbers of the physical electron. Here we will restrict ourselves to the dominant electron-photon component.

cleon. At the level of densities, the interpretation of contributions from orbital angular momentum and spin of the constituents to the total spin of the nucleon is not straightforward, due to divergence terms that vanish upon integration. A correct assessment of these quantities is nonetheless crucial if we want to understand how the nucleon's spin originates from the properties of the partons. We will illustrate our findings in the scalar-diquark model of the nucleon, in terms of Generalized Parton Distribution functions in the impact-parameter space.
We will finally summarize our results and offer some outlooks for future perspective of this work in Chapter 7.

Chapter 2

Light-front quantization

All throughout the present work, we will adopt the formalism of light-front quantization, discussing some of its applications in the contexts of Quantum ElectroDynamics (QED) and Quantum ChromoDynamics (QCD). Over the last few decades, light-front quantization has become a well-established language for the investigation of composite systems in Quantum Field Theory, providing a clear intuition of the physical picture under analysis and relevant simplifications of the practical calculations. In this Chapter we recall the basic ideas behind this approach and show some of the advantages that it offers, mainly following the discussion in Ref. [9].

2.1 Foundations

Quantum Field Theories provide a quantum-mechanical description of a physical system in the arena of a flat, four-dimensional Minkowski spacetime $(\mathcal{M}, g)$, endowed with the metric

$$g_{\mu\nu} = \begin{pmatrix} 1 & 0 & 0 & 0 \\ 0 & -1 & 0 & 0 \\ 0 & 0 & -1 & 0 \\ 0 & 0 & 0 & -1 \end{pmatrix} \tag{2.1}$$

and with coordinates written canonically as $x^\mu = (x^0, x^1, x^2, x^3) = (t, \mathbf{x})$. Let $\psi(t, \mathbf{x})$ be the state that describes the system at a certain point in spacetime. As we deal with the dynamics of the system, the "time" coordinate t plays a special role, since $\psi(t, \mathbf{x})$ evolves along the time-like direction through the Schrödinger equation

$$i\frac{\partial}{\partial t}\psi(t, \mathbf{x}) = P_0\psi(t, \mathbf{x}) \, . \tag{2.2}$$

Eq. (2.2) is uniquely solved once we have fixed some boundary conditions $\psi(t_0, \mathbf{x}_0)$ on a *space-like* hypersurface at fixed time $t = 0$, and yields an operational definition for the Hamiltonian P_0 as a displacement operator with

respect to time t.
It is easy to realize that the concepts of "time" and "space" are to some extent arbitrary in the context of a covariant theory: one can obtain a new parametrization of spacetime by taking some generalized coordinates $\tilde{x}^\mu(x^\mu) = (\tilde{x}^0, \tilde{\mathbf{x}})(x^\mu)$ and considering initial conditions $\psi(\tilde{x}^0_0, \tilde{\mathbf{x}}_0)$ on the *null-time* hypersurface $\tilde{x}^0 = 0$. The system would then evolve in the direction of the new "time" $\tilde{x}^0$, orthogonal to the null-time hypersurface, still according to the Schrödinger equation:

$$i\frac{\partial}{\partial\tilde{x}^0}\psi(\tilde{x}^0, \tilde{\mathbf{x}}) = \tilde{P}_0\psi(\tilde{x}^0, \tilde{\mathbf{x}}) \,, \tag{2.3}$$

which we can interpret as the definition of the Hamiltonian operator $\tilde{P}_0$ in the new coordinates.

The minimal constraint to be required for the transformation $\tilde{x}^\mu$ is that it should be an invertible function of the canonical coordinates. The metric tensor in turn changes according to

$$\tilde{g}_{\mu\nu} = \left(\frac{\partial x^\rho}{\partial\tilde{x}^\mu}\right) g_{\rho\lambda} \left(\frac{\partial x^\lambda}{\partial\tilde{x}^\nu}\right) \equiv C^\rho_\mu \, g_{\rho\lambda} \, C^\lambda_\nu \,, \tag{2.4}$$

thus conserving the volume element $ds^2 = g_{\mu\nu}dx^\mu dx^\nu = \tilde{g}_{\mu\nu}d\tilde{x}^\mu d\tilde{x}^\nu$. Such a transformation would of course leave the physics of the system unaffected. There are, in principle, infinite possibilities for the choice of the parametrization. One must exclude, however, all those which are connected to each other through a Lorentz transformation, since they are already included in a covariant formalism. In fact, it turns out that only five independent parameterizations [10] survive; each of them can be characterized, in general, by the respective null-time hypersurface (see also Fig. 2.1). In 1949, Dirac [4] identified three of them, which he referred to as *forms of relativistic dynamics*:

- The *instant form*, which refers to the canonical coordinates $x^\mu = (x, t)$ and to the metric tensor (2.1). The null-time hypersurface is given by the condition $t = 0$.

- The *front form*, which is associated to the transformation $\tilde{x}^\mu(x^\mu) = (\tilde{x}^0, \tilde{x}^3, \tilde{x}^1, \tilde{x}^2) = (x^+, x^-, \boldsymbol{x}_\perp)$, where:

  $$x^+ = \frac{1}{\sqrt{2}}(x^0 + x^3) \,, \quad x^- = \frac{1}{\sqrt{2}}(x^0 - x^3) \,, \quad \boldsymbol{x}_\perp = (x^1, x^2) \,. \tag{2.5}$$

  In this case, the null-time hypersurface $x^+ = 0$ is obtained via rotation of the hyperplane $t = 0$ by an angle of $\pi/4$, making it tangent to the light-cone centered at the origin. For this reason, the coordinates in Eq. (2.5) are called *light-front coordinates* and the front-form dynamics is referred to also as *light-front quantization*. The new metric reads

  $$\tilde{g}_{\mu\nu} = \begin{pmatrix} 0 & 1 & 0 & 0 \\ 1 & 0 & 0 & 0 \\ 0 & 0 & -1 & 0 \\ 0 & 0 & 0 & -1 \end{pmatrix} . \tag{2.6}$$

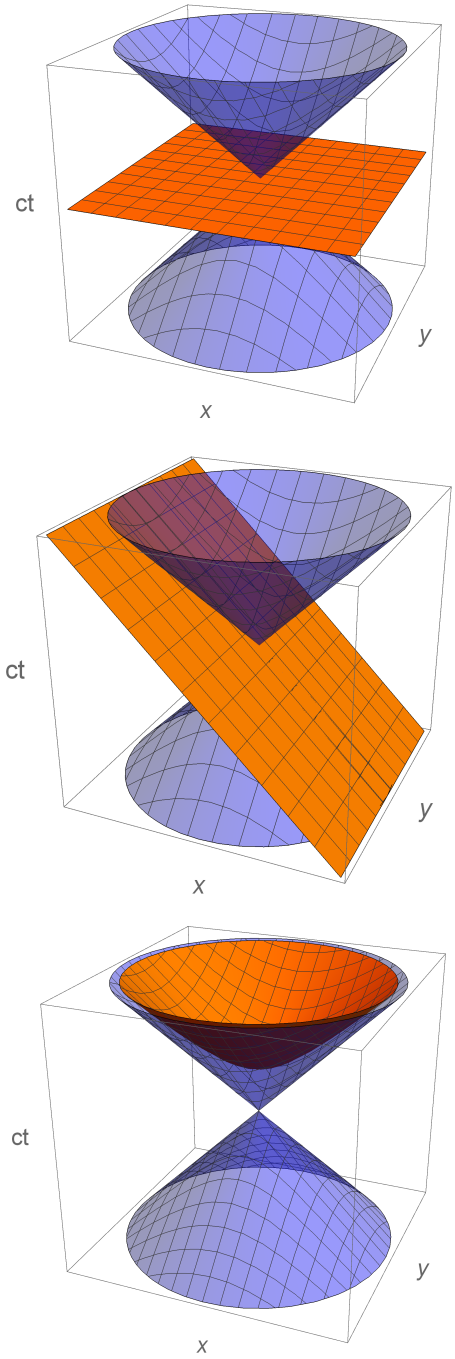

Figure 2.1: Null-time hyperplanes in Dirac's forms of relativistic dynamics. From top to bottom: hyperplane $t = 0$ (instant form), hypersurface $x^+ = 0$ tangent to the light-cone (front form), hypersurface $x^2 = 1$ (point form).

- The *point form*, which is associated to the transformation that takes $x^\mu = (\tau\cosh\omega, \tau\sinh\omega\sin\theta\cos\phi, \tau\sinh\omega\sin\theta\sin\phi, \tau\sinh\omega\cos\theta)$ into $\tilde{x}^\mu(x^\mu) = (\tau, \omega, \theta, \phi)$, with the new metric given by

$$\tilde{g}_{\mu\nu} = \begin{pmatrix} 1 & 0 & 0 & 0 \\ 0 & -\tau^2 & 0 & 0 \\ 0 & 0 & -\tau^2\sinh^2\omega & 0 \\ 0 & 0 & 0 & -\tau^2\sinh^2\omega\sinh^2\theta \end{pmatrix} .$$

  The corresponding null-time hypersurface is identified by the condition $x^2 - a^2 = 0$, with $x^0 > 0$.

The two remaining parameterizations are characterized by the following null-time hypersurfaces:

- $(x^0)^2 - (x^1)^2 - (x^3)^2 - a^2 = 0$, with $x^0 > 0$.
- $(x^0)^2 - (x^3)^2 - a^2 = 0$, with $x^0 > 0$.

Although the five forms eventually produce the same physical results, they may be more or less suitable for attacking different problems. For the purposes of this work, we will focus on the front form, which turns out to offer a particularly intuitive framework when dealing with many-body systems. We will enlighten some of the motivations supporting this choice in the next Sections.

2.2 Relation with the infinite-momentum frame

After Dirac's work in 1949, the alternative forms of dynamics were not further investigated until the late 60's and early 70's, when considerable interest grew around the possibility of studying current algebras and scattering processes in a reference frame moving with velocity close the speed of light [11–20]. It was later recognized that this approach (which offers significant simplifications, as we will briefly illustrate) is completely equivalent to that of light-front quantization.

Let us consider a reference frame moving along the z direction with velocity $-v$ ($v > 0$) with respect to a given "ordinary" reference frame. If a particle travels with four-momentum $p = (E, p_x, p_y, p_z)$ as observed in the ordinary frame, Lorentz transformations provide us with the components of the corresponding four-momentum p' in the moving frame:

$$E' = \frac{1}{\sqrt{1-v^2}}\left(E + vp_z\right) , \tag{2.7}$$

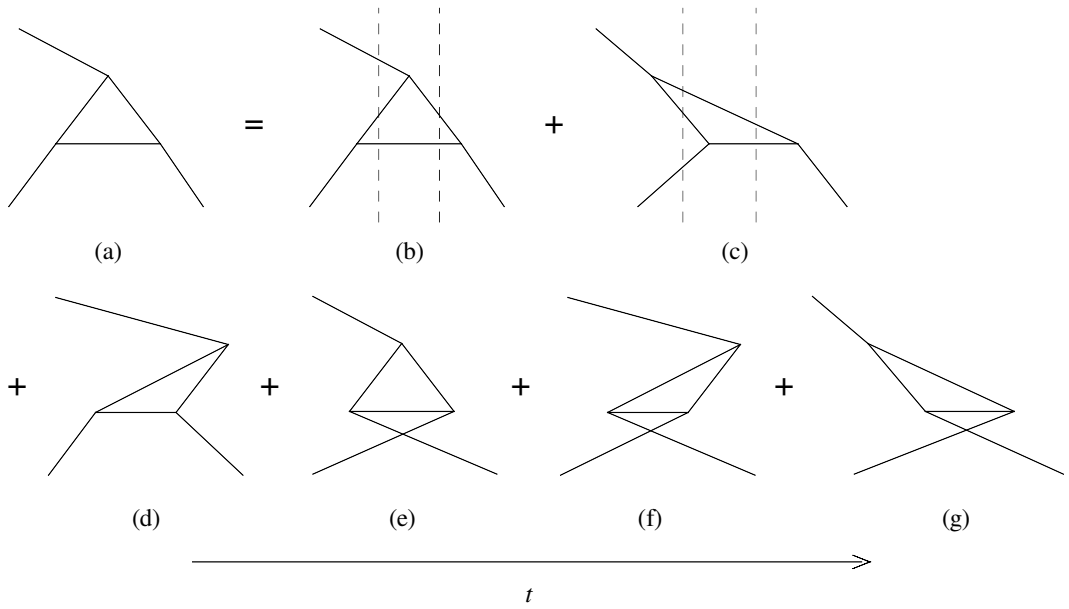

Figure 2.2: Triangle diagram for the scalar ϕ^3 theory (a), as a sum of the corresponding time-ordered diagrams (b)-(g). Time t flows from left to right and dashed lines indicate intermediate states at a fixed value of time.

$$p'_x = p_x \ , \tag{2.8}$$

$$p'_y = p_y \ , \tag{2.9}$$

$$p'_z = \frac{1}{\sqrt{1-v^2}} \left(p_z + vE\right) . \tag{2.10}$$

By taking the limit $v \to c = 1$ of a frame moving with velocity close to the speed of light, the momentum along the z direction becomes infinite; it is thus justified to refer to such a frame as *Infinite-Momentum Frame* (IMF).
Weinberg [12] was the first to examine the consequences of working in the IMF by discussing the rules of old-fashioned Time-Ordered Perturbation Theory (TOPT) in the infinite-momentum limit, for a scalar ϕ^n theory. We briefly recall that in order to calculate a scattering amplitude $\mathcal{M}_{\alpha\beta}$ for a given process with initial and final states $|\alpha\rangle$ and $|\beta\rangle$, respectively, the TOPT rules prescribe that one should:

- Sum the contributions from all possible diagrams for the process $\alpha \to \beta$, drawn by assigning to each interaction vertex a time index $i = 1, \dots n$ and by considering as distinct the $n!$ diagrams which have a different ordering of the vertices. We show in Fig. 2.2 an example for the case of the triangle diagram in the scalar ϕ^3 theory.

- Require conservation of three-momentum (and not of energy) at each vertex, considering each intermediate state on the mass-shell.

Notice that the last requirement marks a difference with respect to the Feynman diagram approach, where four-momentum is conserved at each ver-

tex, but particles in the intermediate states are virtual. Moreover, in TOPT manifest covariance is lost, since a single diagram is not Lorentz-invariant (while their sum of course is); on the other hand, unitarity is explicit, since all particles propagate forward in time.
Weinberg showed that, by taking the limit of the total incident momentum $P = |\mathbf{P}|$ to infinity, all time-ordered diagrams containing vacuum fluctuations (i.e. creation from / annihilation into vacuum of two or more particles) vanish, since they are power-suppressed as P^{-2} [1]. This means that in the case of the triangle diagram shown in Fig. 2.2, out of the six possible time-ordered diagrams, only two [namely (b) and (c)] survive in the infinite-momentum frame. It was later suggested that the infinite-momentum-frame results could be achieved through a simple change of variables, without needing to take explicitly the limit of infinite momenta [13, 14]. Chang and Ma [15], in particular, proved that it is possible to reproduce the rules of TOPT for the scalar ϕ^3 theory in the infinite-momentum frame by introducing new variables $\eta = t + z$ and $s = t - z$. More recently, Sawicki [22] considered again the triangle diagram in the same model to prove that the TOPT formalism in light-front coordinates exactly reproduces the covariant result in the Feynman approach. We will come back to this argument in Chapter 3 in the framework of QED.
A rigorous extension of the IMF formalism to the case of QED was obtained by Bjorken, Kogut and Soper [17,23], using the light-front coordinates (2.5). They also derived the rules for the fermion and photon propagators from the expansion of the Scattering matrix S. We finally mention that the first application to the quark parton model of QCD is due to Drell, Levy and Yan [18–20].

2.3 Poincaré group on the light-front

In general, a field theory is described by a Lagrangian density

$$\mathscr{L} = \mathscr{L}(\varphi_r(x), \partial_\mu \varphi_r(x), x) \tag{2.11}$$

depending on the fields $\varphi_r(x)$ along with their derivatives. Invariance of the theory under translations results, via Noether's theorem, into conservation of the energy-momentum tensor

$$T^{\mu\nu}(x) = \pi_r^\mu \partial^\nu \varphi_r(x) \,, \qquad \partial_\mu T^{\mu\nu} = 0 \,, \tag{2.12}$$

where

$$\pi_r^\mu = \frac{\partial \mathscr{L}}{\partial \left(\partial_\mu \varphi_r(x)\right)}$$

is the momentum conjugate to the field $\phi_r(x)$. Lorentz invariance leads instead to the conservation of the so-called generalized angular momentum density

$$J^{\mu\nu\rho}(x) = L^{\mu\nu\rho}(x) + S^{\mu\nu\rho}(x) \,, \qquad \partial_\mu J^{\mu\nu\rho} = 0 \,. \tag{2.13}$$

[1] The same argument is also reviewed in [21].

Here

$$L^{\mu\nu\rho}(x) = x^\nu T^{\mu\rho}(x) - x^\rho T^{\mu\nu}(x) \tag{2.14}$$

is a Orbital Angular Momentum (OAM) contribution, while

$$S^{\mu\nu\rho}(x) = -i\pi_r^\mu \left(\Sigma^{\nu\rho}\right)_s^r \varphi_s(x) \tag{2.15}$$

is interpreted as the intrinsic spin contribution to the total angular momentum density. The spin operator is [7]:

$$\left(\Sigma^{\mu\nu}\right)_s^r = 0 \,, \qquad \text{spin-0 particle } \phi_r(x) \,, \tag{2.16}$$

$$\left(\Sigma^{\mu\nu}\right)_s^r = \frac{i}{2}\left(\left[\gamma^\mu, \gamma^\nu\right]\right)_s^r \,, \qquad \text{spin-1/2 Dirac particle } \psi_r(x) \,, \tag{2.17}$$

$$\left(\Sigma^{\mu\nu}\right)_\alpha^\beta = i\left(\delta_\alpha^\mu g^{\nu\beta} - \delta_\alpha^\nu g^{\mu\beta}\right) \,, \qquad \text{spin-1 particle } A_\alpha(x) \,. \tag{2.18}$$

The conserved charges associated with the quantities in Eqs. (2.12) and (2.13) are, respectively, the four-momentum vector

$$P^\nu = \int \mathrm{d}^4x\, T^{0\nu}(x) \tag{2.19}$$

and the angular momentum tensor

$$M^{\mu\nu} = \int \mathrm{d}^4x \left[x^\mu T^{0\nu}(x) - x^\nu T^{0\mu}(x) + S^{0\mu\nu}(x)\right] . \tag{2.20}$$

Let us now consider these objects as operators at the level of algebraic quantum-mechanics. The algebra of operators is generated by x^μ, p^μ and the identity $\mathbb{1}$ with the canonical commutation relation

$$\left[x^\mu, p^\nu\right] = -i\mathbb{1} \,. \tag{2.21}$$

If we write $P^\mu = p^\mu$, $M^{\mu\nu} = x^\mu p^\nu - x^\nu p^\mu$, we find

$$\left[P^\mu, P^\nu\right] = 0 \,, \tag{2.22}$$

$$\left[M^{\mu\nu}, P^\rho\right] = -i\left(g^{\mu\rho}P^\nu - g^{\nu\rho}P^\mu\right) \,, \tag{2.23}$$

$$\left[M^{\mu\nu}, M^{\rho\sigma}\right] = -i\left(g^{\mu\rho}M^{\nu\sigma} - g^{\mu\sigma}M^{\nu\rho} - g^{\nu\rho}M^{\mu\sigma} + g^{\nu\sigma}M^{\mu\rho}\right) \,. \tag{2.24}$$

These coincide with the commutation relations of the Lie algebra that generates the Poincaré group, where P^μ are the translations and $M^{\mu\nu}$ the Lorentz transformations. In the instant form, rewriting the Lorentz group generators in terms of rotations $J^i = \varepsilon^{ijk}M^{jk}$ and boosts $K^i = M^{0i}$, we can equivalently express the relations (2.23)-(2.24) as

$$\left[J^i, P^l\right] = i\varepsilon^{ilm}P^m \,, \tag{2.25}$$

$$\left[J^i, P^0\right] = 0 \,, \tag{2.26}$$

$$\left[K^i, P^l\right] = -i\delta^{il}P^0 \,, \tag{2.27}$$

$$\left[K^i, P^0\right] = -iP^i \,, \tag{2.28}$$

$$\left[J^i, J^l\right] = i\varepsilon^{ilm} J^m \,, \tag{2.29}$$

$$\left[J^i, K^l\right] = i\varepsilon^{ilm} K^m \,, \tag{2.30}$$

$$\left[K^i, K^l\right] = -i\varepsilon^{ilm} J^m \,. \tag{2.31}$$

We distinguish two types of operators, calling *kinematic operators* those which leave the hypersurface $t = 0$ invariant; the remaining ones, which evolve equal-time hypersurfaces along the direction of time, are referred to as *dynamical operators* or *Hamiltonians*, in the spirit of Eq. (2.2) [4]. Kinematic operators do not depend on the interaction, whereas dynamical operators do. In instant form, the three rotations J^i and the three space-translations P^i are kinematic, while time translation P^0 and the three boosts K^i are dynamical.

The interpretation of the algebra of Poincaré generators in light-front quantization is one of the crucial features of the formalism. In order to obtain the commutation relations corresponding to Eqs. (2.22) and (2.25) to (2.31) in light-front coordinates, we apply the transformation $M^{\mu\nu} \to \tilde{M}^{\mu\nu} = C^\mu_\rho M^{\rho\sigma} C^\nu_\sigma$, with C^μ_ν defined in Eq. (2.4). One finds [17]:

$$\tilde{M}^{\mu\nu} = \begin{pmatrix} 0 & -K^3 & B^1 & B^2 \\ K^3 & 0 & S^1 & S^2 \\ -B^1 & -S^1 & 0 & J^3 \\ -B^2 & -S^2 & -J^3 & 0 \end{pmatrix} , \tag{2.32}$$

where

$$B^1 = \frac{1}{\sqrt{2}}\left(K^1 + J^2\right) \,, \qquad B^2 = \frac{1}{\sqrt{2}}\left(K^2 - J^1\right) \,, \tag{2.33}$$

$$S^1 = \frac{1}{\sqrt{2}}\left(K^1 - J^2\right) \,, \qquad S^2 = \frac{1}{\sqrt{2}}\left(K^2 + J^1\right) \,. \tag{2.34}$$

The ten generators of the Poincaré group in light-front coordinates are then $P^\mu = (P^+, P^-, \boldsymbol{P}_\perp)$, $\boldsymbol{B}_\perp = (B^1, B^2)$, $J_z = J^3$, $\boldsymbol{S}_\perp = (S^1, S^2)$, $K_z = K^3$. Note that, in terms of the angular momentum tensor in light-front coordinates, we can write[2] $B^i_\perp = M^{+i}$, $S^i_\perp = M^{-i}$, $K_z = M^{-+}$ and $J_z = M^{12}$. Furthermore, in terms of the energy-momentum tensor, from Eqs. (2.19) and (2.20) we have

$$P^\nu = \int \mathrm{d}^4x\, T^{+\nu}(x) \,, \tag{2.35}$$

$$M^{\mu\nu} = \int \mathrm{d}^4x\, \left[x^\mu T^{+\nu}(x) - x^\nu T^{+\mu}(x) + S^{+\mu\nu}(x)\right] \,. \tag{2.36}$$

The generators satisfy the following commutation relations:

$$\left[P^\mu, P^\nu\right] = \left[J_z, P^+\right] = \left[J_z, P^-\right] = \left[B^i_\perp, P^+\right] = 0 \,, \tag{2.37}$$

[2] We omit the tilde for light-front operators, from now on.

$$\left[P^-, B^i_\perp\right] = iP^i_\perp \,, \tag{2.38}$$
$$\left[J_z, P^i_\perp\right] = i\varepsilon^{il}P^l_\perp \,, \tag{2.39}$$
$$\left[J_z, B^i_\perp\right] = i\varepsilon^{il}B^l_\perp \,, \tag{2.40}$$
$$\left[P^i_\perp, B^l_\perp\right] = i\delta^{il}P^+ \,, \tag{2.41}$$
$$\left[B^i_\perp, B^l_\perp\right] = \left[S^i_\perp, P^-\right] = \left[S^i_\perp, S^l_\perp\right] = \left[J_z, K_z\right] = \left[P^i_\perp, K_z\right] = 0 \,, \tag{2.42}$$
$$\left[B^i_\perp, K_z\right] = iB^i_\perp \,, \tag{2.43}$$
$$\left[P^\pm, K_z\right] = \pm iP^\pm \,, \tag{2.44}$$
$$\left[S^i, K_z\right] = -iS^i_\perp \,, \tag{2.45}$$
$$\left[J_z, S^i_\perp\right] = i\varepsilon^{il}S^l_\perp \,, \tag{2.46}$$
$$\left[S^i_\perp, B^l_\perp\right] = i\left(\delta^{il}K_z + \varepsilon^{il}J_z\right) \,, \tag{2.47}$$
$$\left[P^+, S^i_\perp\right] = iP^i_\perp \,, \tag{2.48}$$
$$\left[P^i_\perp, S^l_\perp\right] = i\delta^{il}P^+ \,, \tag{2.49}$$

as can be readily checked from Eqs. (2.25) to (2.31).
The relations (2.37) to (2.41) are particularly interesting since they allow us to single out a subgroup of the Poincaré group spanned by P^μ, $\boldsymbol{B}_\perp$ and J_z and isomorphic to the two-dimensional subgroup of non-relativistic Galilean transformations. To this extent, we can identify P^- with the Hamiltonian, P^+ with the mass and $\boldsymbol{P}_\perp$, $\boldsymbol{B}_\perp$ and J_z respectively with translations, Galilean boosts and rotations in the *transverse* plane of coordinates x, y [13,17]. Notice also from Eqs. (2.42) to (2.45) that the boost operator along the z direction K_z simply acts as a rescaling of the other generators, as can be explicitly seen by exponentiating: we have, for instance,

$$e^{i\omega K_z}P^\pm e^{-i\omega K_z} = e^{\pm\omega}P^\pm$$

and similarly for the other generators.
We will now naturally transpose the nomenclature adopted for the instant form to the light-front scenario and call kinematic the operators that leave invariant the hypersurfaces at instant-form time $\tau = 0$. It is easy to check that this is the case for the generators P^+, $\boldsymbol{P}_\perp$, $\boldsymbol{B}_\perp$ and J^3 belonging to the Galilean subgroup. This entails, in particular, that boosts in the transverse plane are independent of the interaction; that is a crucial difference compared to the instant-form case, whose consequences will be pointed out later in more detail.
A final remark concerns the interpretation of the P^- generator as the Hamiltonian of the system. If we compute the on-shell relation $M^2 = P^\mu P_\mu = 2P^+P^- - \boldsymbol{P}^2_\perp$ in light-front coordinates, we can rewrite

$$P^- \equiv H = \frac{\boldsymbol{P}^2_\perp}{2P^+} + \frac{M^2}{2P^+} \,, \tag{2.50}$$

which has a manifestly non-relativistic form. Furthermore, the operator P^- acts as a translation with respect to the light-front time τ, accordingly with

Eq. (2.3). We also notice that Eq. (2.50) helps to support the interpretation of P^+ as a mass parameter, which is in fact justified by the fact that P^+ is a positive semi-definite operator.

2.3.1 The Impact-Parameter space

The isomorphism between generators of the Poincaré group on the light front and generators of the two-dimensional Galilean subgroup of Lorentz transformation helps us to interpret the structure of composite systems in the transverse plane, as we will be better illustrate in Section 4.4.1. Here we introduce some key concepts to this extent.

In non-relativistic quantum mechanics, when dealing with a composite system, if the Hamiltonian is invariant under translations it is possible to separate the dynamics of the center of mass

$$\boldsymbol{R} = \sum_{i=1} x_i \boldsymbol{r}_i \tag{2.51}$$

from that of the constituents and work in the center-of-mass frame. In Eq. (2.51) each constituent contributes with a fraction $x_i = m_i/M$ to the total mass M of the system and has coordinates $\boldsymbol{r}_i$ in position space. It should be emphasized here that the center of mass also corresponds the generator $\boldsymbol{B}$ of (three-dimensional) Galilean boosts up to a factor of M [24]:

$$\boldsymbol{B} = -M\boldsymbol{R}\,. \tag{2.52}$$

Let us now restrict to the description in the transverse plane. Recall that the isomorphism described in Section 2.3 associates the mass M with the translation operator along the longitudinal direction P^+ and the transverse boosts $\boldsymbol{B}_\perp$ with the operators B_i introduced in Eq. (2.33), suggesting us to define the *center of transverse momentum*

$$\boldsymbol{R}_\perp = \sum_{i=1} \frac{k_i^+}{P^+} \boldsymbol{r}_{i,\perp} = \sum_{i=1} x_i \boldsymbol{r}_{i,\perp}\,, \tag{2.53}$$

where now

$$x_i = k_i^+/P^+ \tag{2.54}$$

is the boost-invariant longitudinal momentum fraction carried by the i-th parton. This means that Eq. (2.52), in two dimensions, will correspond to

$$\boldsymbol{R}_\perp = -\frac{1}{P^+}\boldsymbol{B}_\perp\,. \tag{2.55}$$

Another way to justify the relation (2.55) is to consider the field-theoretical definition of center of transverse momentum [25]

$$\boldsymbol{R}_\perp = \int \mathrm{d}x^- \mathrm{d}^2\boldsymbol{x}_\perp\, \boldsymbol{x}_\perp\, T^{++}(x) = -\frac{1}{P^+}\boldsymbol{B}_\perp\,, \tag{2.56}$$

where $T^{\mu\nu}$ is the energy momentum tensor and hence $T^{++}(x)$ represents the light-front momentum density. In order to recover the right-hand side of Eq. (2.56), we write $B^i = M^{+i}$ and use Eq. (2.36) in the limit[3] $x^+ = 0$.
We define the coordinates of the i-th parton in the transverse plane relative to the center of transverse momentum as the *impact parameter*

$$\boldsymbol{b}_{i,\perp} = \boldsymbol{r}_{i,\perp} - \boldsymbol{R}_\perp \ . \tag{2.57}$$

In particular, we call *impact-parameter space* the coordinate system $\boldsymbol{b}_\perp = (b_x, b_y)$ in the transverse plane whose origin coincides with the center of transverse momentum, namely $\boldsymbol{R}_\perp = \boldsymbol{0}_\perp$.

2.4 Light-Front Wave Functions

We now address explicitly the problem of describing the state of a composite particle in terms of its elementary constituents. Light-front quantization provides an elegant language for this purpose, in terms of the so-called Light-Front Wave Function representation [26].

2.4.1 Light-front helicity states

In the following, we will focus on composite particles endowed with a spin degree of freedom. To this end, in the context of light-front quantization, it is useful to introduce the concept of light-front helicity [24].
Consider the operator

$$j_z = J_z - \boldsymbol{R}_\perp \times \boldsymbol{P}_\perp \ ,$$

where $\boldsymbol{R}_\perp$ is given by Eq. (2.55). It is defined as the difference between the longitudinal component J_z of the total angular momentum operator and the orbital angular momentum operator along the z direction $\boldsymbol{R}_\perp \times \boldsymbol{P}_\perp$, thus deserving the interpretation as an "intrinsic" angular momentum operator. It can be proved [17, 24] that j_z coincides with the ordinary helicity operator $\boldsymbol{p}\cdot\boldsymbol{S}/p$ in the infinite-momentum-frame limit. We label with $|p,\Lambda\rangle \equiv |p^+, \boldsymbol{p}_\perp, \Lambda\rangle$ an eigenstate of j_z which is, at the same time, an eigenstate of the momentum operators P^+ and $\boldsymbol{P}_\perp$ with eigenvalues p^+ and $\boldsymbol{p}_\perp$, respectively. The eigenvalue Λ satisfying

$$j_z|p,\Lambda\rangle = \Lambda|p,\Lambda\rangle \tag{2.58}$$

is the *light-front helicity* of the particle. Strictly speaking, we can consider ordinary and light-front helicities to be equivalent in the infinite-momentum limit up to effects of order M/p^+.

[3] We will discuss in Chapter 6 how to deal with time dependence of angular-momentum densities.

2.4.2 Fock-state decomposition

Let $|\Psi\rangle$ be the state that describes a composite, or parent, particle of mass M and light-front helicity Λ, satisfying the eigenvalue equation for the Hamiltonian H

$$H|\Psi\rangle = \frac{M^2 + \boldsymbol{P}_\perp^2}{2P^+}|\Psi\rangle \ . \tag{2.59}$$

The state $|\Psi\rangle$ will be in general dependent on M, P^+, $\boldsymbol{P}_\perp$ and Λ. It can be conveniently decomposed in terms of Fock states $\{|\mu_n(\omega_n)\rangle\}_{n\in\mathbb{N}}$, where $|\mu_n(\omega_n)\rangle$ is a state of n free quanta depending on the collective index $\omega_n = \{k_i^+, \mathbf{k}_{i,\perp}, \lambda_i\}_{i=1\dots n}$. Here k_i^+, $\mathbf{k}_{i,\perp}$ and λ_i are respectively the longitudinal momentum, the transverse momentum and the light-front helicity of the i-th parton.
Fock states are constructed in a very simple way by acting with creation operators on the vacuum, which has a trivial structure in light-front quantization. One can indeed postulate the vacuum $|0\rangle$ to be the lowest-energy state (assuming the vacuum's energy to be zero) and to be invariant under Lorentz transformations [27]. This means in particular that the vacuum must be an eigenstate of the generators of space translations, namely

$$P^+|0\rangle = 0 \ , \tag{2.60}$$

$$\boldsymbol{P}_\perp|0\rangle = \mathbf{0}_\perp \ . \tag{2.61}$$

Recalling that P^+ is a positive semi-definite operator, Eq. (2.60) implies that the vacuum coincides with the zero-particle Fock state[4]: it is not possible to make the total momentum along the longitudinal direction vanish by summing only positive contributions. This is the reason why diagrams with vacuum fluctuations are null on the light-front, consistently with the description in the Infinite-Momentum Frame (see Section 2.2).
We consequently construct the Fock states as:

$$|\mu_n(\omega_n)\rangle = \prod_{i=1}^{n} a_i^\dagger(k_i^+, \mathbf{k}_{i,\perp}, \lambda_i)|0\rangle \ , \tag{2.62}$$

with proper ladder operators $a_i^\dagger$ that can be related to scalar particles, fermions or gauge bosons. Fock states form a basis of the Hilbert space of $|\Psi\rangle$:

$$\sum_n \not\int \mathrm{d}\omega \, |\mu_n(\omega_n)\rangle\langle\mu_n(\omega_n)| = \mathbb{1} \ , \tag{2.63}$$

where the $\not\int$ symbol means that we integrate over the continuous variables, such as momenta, and sum over the discrete variables, namely parton helicities. We

[4] Actually this is true, strictly speaking, only up to corrections proportional to $\delta(P^+)$. Some issues arise concerning the limit $P^+ \to 0$ of particles in the ground state with vanishingly small longitudinal momentum; they become relevant especially in the QCD case (see Ref. [9, 15]). We do not discuss this problem in the present work. This issue is beyond the scope of this thesis.

can therefore rewrite

$$|\Psi\rangle = \sum_n \not\int \mathrm{d}\omega\, \Psi_n(\omega_n)|\mu_n(\omega_n)\rangle \,. \tag{2.64}$$

The coefficients of the combination (2.64) are the Light-Front Wave Functions (LFWFs)

$$\Psi_n(\omega_n) \equiv \Psi^{\Lambda}_{n,\lambda_i}(x_i, \mathbf{k}_{i,\perp}) = \langle \Psi|\mu_n(\omega_n)\rangle \,. \tag{2.65}$$

In the notation used in Eq. (2.65), Λ indicates the light-front helicity of the parent particle, while $x^i = k^i/P^+$ is the longitudinal momentum fraction in Eq. (2.54). By construction, LFWFs are eigenstates of the longitudinal component J^z of the total angular momentum operator, with eigenvalue Λ, and of the momentum operators P^+ and $\boldsymbol{P}_\perp$, with eigenvalues

$$\boldsymbol{P}_\perp = \sum_{i=1}^{n} k_{i,\perp} \,, \qquad P^+ = \sum_{i=1}^{n} k_i^+ \,. \tag{2.66}$$

The longitudinal momentum fractions are therefore normalized as

$$\sum_{i=1}^{n} x_i = 1 \,. \tag{2.67}$$

Notice that LFWFs do not actually depend on the transverse momentum $\boldsymbol{P}_\perp$ of the composite particle, due to the fact that transverse boosts are kinematic. Therefore it is convenient to set $\boldsymbol{P}_\perp = 0$ in practical calculations: from Eq. (2.66), this results into the condition

$$\sum_{i=1}^{n} k_{i,\perp} = \mathbf{0}_\perp \,. \tag{2.68}$$

The frame of reference where the state has zero transverse momentum is also called *hadron frame*. It is possible to connect the coordinates of a given four-vector v in a generic frame to those in the hadron frame via the light-front boost:

$$(v^+, v^-, \boldsymbol{v}_\perp) \longrightarrow \left(v^+, v^- - \frac{\boldsymbol{v}_\perp \cdot \boldsymbol{a}_\perp}{a^+} + \frac{v^+ \boldsymbol{a}_\perp^2}{2(a^+)^2}, \boldsymbol{v}_\perp - \frac{v^+}{a^+}\boldsymbol{a}_\perp \right) \,, \tag{2.69}$$

where the boost parameters must be chosen as $a^+ = v^+$, $\boldsymbol{a}_\perp = \boldsymbol{v}_\perp$ so as to obtain zero for the transverse component in the new frame.
The square modulus $|\Psi^{\Lambda}_n(\omega_n)|^2$ also enjoys the interpretation of probability density in three-momentum space of finding n partons, in the states specified by the collective index ω_n, inside a parent particle with light-front helicity Λ.

2.4.3 Light-cone gauge

When we consider a gauge theory, such as QED or QCD, it is convenient to fix a certain gauge to work with. Since light-front quantization selects a preferred

direction along the light cone, the most natural choice in this case is the axial gauge

$$n_\mu A^\mu = 0 \,, \qquad n^\mu = (0, 1, \mathbf{0}_\perp) \,, \tag{2.70}$$

where A^μ indicates the gauge-boson field. The gauge condition (2.70), often written simply as $A^+ = 0$, is referred to as *light-cone gauge*.
We will discuss extensively the consequences of working in this gauge rather than in the covariant Feynman gauge, usually adopted in instant-form quantization. What we would like to enlighten here is that LFWFs do depend on the gauge choice; hereafter it will always be assumed that they are evaluated in the light-cone gauge. In this case it can be shown [26, 28] that for a longitudinally polarized particle, the LFWFs are also eigenstates of the longitudinal component L_z of the OAM operator L (see Eq. (2.14)), with eigenvalue

$$l_z = \Lambda - \sum_i \lambda_i \,. \tag{2.71}$$

In view of the afore-mentioned properties of the LFWFs, it is justified to assert that they encode all the information about the internal structure of composite system as described in terms of their components.

Chapter 3

Gauge-field propagator in light-cone gauge

The explicit proof of the equivalence between the instant-form and the light-front form of dynamics has been the subject of several works [12, 15, 17, 21, 22, 29–36] with applications over a wide range of field theories: some examples include scalar ϕ^3 theory [22], Yukawa interaction [32, 33], scalar QED [34] and standard QED [35, 36]. In this Chapter we are going to prove the equivalence at one-loop level in QED by using the same argument proposed by Sawicki in Ref. [22] in the context of a ϕ^3 model (see also Section 2.2): we compare old-fashioned time-ordered perturbation theory with the covariant approach of Feynman diagrams in the light-front quantization framework, i.e. in light-cone gauge $n_\mu A^\mu = 0$ [with $n^\mu = (0, 1, \mathbf{0}_\perp)$] *and* using light-front coordinates. We mainly follow the discussion in Refs. [37, 38].
When dealing with a gauge theory, one is confronted with the problem of matching the presence of particles that propagate instantaneously; furthermore, the use of a non-covariant gauge makes it non-trivial to determine which of the gauge boson's degrees of freedom have to be taken into account. As we will motivate in the following, these difficulties are ultimately related to the correct assessment of which form should be used for the gauge-field propagator in the covariant formulation, when working in the light-cone gauge. Our derivation allows one to eventually provide an answer to this question.

3.1 Overview of the problem

As mentioned in Chapter 2, Feynman rules for QED in light-front quantization were established as early as the 1970s in the works by Bjorken, Kogut and Soper [17, 23]. Nonetheless, a controversy concerning the explicit expression that one should adopt for the photon propagator in light-cone gauge has later emerged, as remarked e.g. in Refs. [34, 35, 39]. In the literature one can in

fact encounter two different expressions for the light-cone gauge propagator $\mathcal{D}^{\mu\nu}(q)$. The first expression contains the sum of two terms and reads [17, 40]:

$$\mathcal{D}^{\mu\nu}(q) = \frac{-i}{q^2}\left(g^{\mu\nu} - \frac{q^\mu n^\nu + q^\nu n^\mu}{q^+}\right) . \tag{3.1}$$

It can be recovered by adding to the Lagrangian density for the free electromagnetic field a gauge-fixing term of the form $(n_\mu A^\mu)^2$, as shown in Ref. [41]; but this is not enough to fix the gauge completely, and as a result both the longitudinal and the transverse photon degrees of freedom propagate.
The second expression contains instead the sum of three terms [42]:

$$\mathcal{D}_T^{\mu\nu}(q) = \frac{-i}{q^2}\left(g^{\mu\nu} - \frac{q^\mu n^\nu + q^\nu n^\mu}{q^+} + q^2\frac{n^\mu n^\nu}{(q^+)^2}\right) . \tag{3.2}$$

It can in turn be recovered by adding to the Lagrangian density a gauge-fixing term of the form $(n_\mu A^\mu)^2 + (\partial_\mu A^\mu)^2$ [41], which completely fixes the gauge; this is equivalent to considering only the transverse degrees of freedom as the propagating ones. However, the use of a non-covariant axial gauge, such as the light-cone gauge, generates a new contribution to the interaction Hamiltonian, corresponding to a four-fermion interaction with an instantaneous-photon propagator. The last term of Eq. (3.2), which comes from removing the longitudinal degree of freedom, compensates for the extra-term that describes the instantaneous interaction from the Hamiltonian [34, 35]. Therefore, it is possible to use either the three term expression of Eq. (3.2) together with the instantaneous interaction in the Hamiltonian, or the two-term expression of Eq. (3.1), omitting at the same time the instantaneous interaction.
This ambiguity is at the origin of the confusion about which form one should use for the propagator. As discussed in Ref. [35], the role of the propagator is crucial when proving the equivalence between the covariant perturbation theory and light-front TOPT, in particular when matching the contribution from instantaneous photons. We thus find it illustrative to repeat the proof of the equivalence, trying to clarify a few misleading results and statements in the literature. In particular, our findings partially differ from previous calculations [34–36].

Our approach to these issues is based on the two following considerations:

1. The form of the propagator must be deduced from the free-photon equations of motion in light-cone gauge.

2. The starting point of the calculation in the covariant theory does depend on the gauge choice; once this is fixed, one can decide whether to integrate over the light-front rather than the instant-form energy.

We stress that, although we perform our derivation in the QED framework and discuss the photon propagator, the results are not affected by the Abelian nature of the theory and are thus immediately transferable to the QCD case of the gluon propagator.

3.2 Light-front QED

Let us consider the gauge- and Lorentz-invariant QED Lagrangian density

$$\mathscr{L}_{\mathrm{QED}} = \bar{\psi}(i\partial\!\!\!/ - m)\psi - \frac{1}{4}F^{\mu\nu}F_{\mu\nu} + e\bar{\psi}\gamma^{\mu}\psi A_{\mu} \,, \tag{3.3}$$

where $e > 0$, m is the bare electron mass and $F^{\mu\nu} = \partial^{\mu}A^{\nu} - \partial^{\nu}A^{\mu}$ is the electromagnetic-field tensor. We first focus on the contribution from the free electromagnetic field, in order to recover an expression for the photon propagator. The photon polarization vectors $\varepsilon^{\mu}_{\lambda}(q)$ have four possible polarization states, but only two are actually physical. One can get rid of the redundant degrees of freedom via a proper transformation of the photon field $A^{\mu}(x) \mapsto A^{\mu}(x) + \partial^{\mu}\alpha(x)$, thus selecting a convenient gauge to work with.
In the Lorenz gauge, we assume

$$\partial_{\mu}A^{\mu} = 0 \tag{3.4}$$

and modify the free-photon Lagrangian by adding a gauge-fixing term, namely

$$\mathscr{L}_{\mathrm{elm}} = -\frac{1}{4}F^{\mu\nu}F_{\mu\nu} - \frac{1}{2\beta}\left(\partial_{\mu}A^{\mu}\right)^2 \,. \tag{3.5}$$

The Lorenz gauge leaves one residual degree of freedom. The covariant Feynman gauge, usually adopted in the Feynman diagram approach, coincides with the Lorenz gauge where we fix $\beta = 1/2$.
Alternatively, one can add a second gauge-fixing term: in a non-covariant axial gauge $n_{\mu}A^{\mu} = 0$, the electromagnetic-field Lagrangian becomes

$$\mathscr{L}_{\mathrm{elm}} = -\frac{1}{4}F^{\mu\nu}F_{\mu\nu} - \frac{1}{2\alpha}\left(n_{\mu}A^{\mu}\right)^2 - \frac{1}{2\beta}\left(\partial_{\mu}A^{\mu}\right)^2 \,. \tag{3.6}$$

We stress here that the axial-gauge condition, just like the Lorenz-gauge condition, is not by itself sufficient to fix the gauge completely. Once we have completely fixed the gauge, it is possible to reconstruct the propagator $\mathcal{D}^{\mu\lambda}(q)$ of the free photon with the Green's function method: more precisely, we solve, in momentum space,

$$\mathcal{O}_{\mu\nu}(q)\mathcal{D}^{\mu\lambda}(q) = \delta^{\lambda}_{\nu} \,, \tag{3.7}$$

where the operator $\mathcal{O}_{\mu\nu}$ satisfies $\mathcal{L}_{\mathrm{elm}} = A^{\mu}\mathcal{O}_{\mu\nu}A^{\nu}$. In Feynman gauge, one obtains the well-known result

$$\mathcal{D}^{\mu\nu}(q) = \frac{-ig^{\mu\nu}}{q^2} \,, \tag{3.8}$$

that is manifestly Lorentz-invariant and proportional to the sum of the polarization vectors over all the degrees of freedom:

$$d^{\mu\nu}(q) = \sum_{\lambda} \varepsilon^{\mu\,*}_{\lambda}(q)\varepsilon^{\nu}_{\lambda}(q) = -g^{\mu\nu} \,. \tag{3.9}$$

In light-cone gauge, instead, in the limit $\alpha, \beta \to 0$, one obtains [41]

$$\mathcal{D}_T^{\mu\nu}(q) = \frac{-i}{q^2}\left(g^{\mu\nu} - \frac{q^\mu n^\nu + q^\nu n^\mu}{q^+} + q^2\frac{n_\mu n_\nu}{(q^+)^2}\right), \tag{3.10}$$

which is proportional to the sum over the transverse-polarization degrees of freedom

$$d_T^{\mu\nu}(q) = \sum_{\lambda=1}^{2} \varepsilon_\lambda^{\mu\,*}(q)\varepsilon_\lambda^\nu(q) = -g^{\mu\nu} + \frac{q^\mu n^\nu + q^\nu n^\mu}{q^+} - q^2\frac{n^\mu n^\nu}{(q^+)^2}. \tag{3.11}$$

In light-front quantization an equivalent result can be recovered by imposing the light-cone gauge condition only. The reason is that the equations of motion for the free photon

$$\left(g^{\mu\nu}\partial^2 - \partial^\mu\partial^\nu\right)A_\nu = 0 \tag{3.12}$$

in light-front coordinates along with $A^+ = 0$, automatically imply the Lorenz-gauge condition (3.4). We can use the latter to write the transverse components of the gauge field as

$$\boldsymbol{\partial}_\perp \cdot \boldsymbol{A}_\perp = \partial^+ A^- \,. \tag{3.13}$$

It is then possible to evaluate the propagator through [43]

$$\langle 0|[A^\mu(x)A^\nu(0)]|0\rangle = \frac{i}{(2\pi)^4}\int \mathrm{d}^4q\, e^{-ix\cdot q}\,\frac{d_T^{\mu\nu}(q)}{q^2 + i\varepsilon}\,, \tag{3.14}$$

where $d_T^{\mu\nu}(q)$ coincides with the three-term sum given in Eq. (3.11).

Let us now go back to the full Lagrangian (3.3). In presence of an interaction term, the equations of motion of the photon become

$$\left(g^{\mu\nu}\partial^2 - \partial^\mu\partial^\nu\right)A_\nu = J^\mu\,, \tag{3.15}$$

with the electromagnetic current $J^\mu = e\bar{\psi}\gamma^\mu\psi$. Even though Eq. (3.15) does not lead to the Lorenz condition, we can still use it to rewrite the transverse components of the photon fields in terms of the other ones, by defining [42]

$$A^- = a^- + \chi\,, \tag{3.16}$$

with

$$\partial^+ a^- = \boldsymbol{\partial}_\perp \cdot \boldsymbol{A}_\perp\,, \qquad (\partial^+)^2\,\chi = -J^+\,. \tag{3.17}$$

Similarly, one can take advantage of the Dirac equation to isolate two independent (or "good") components of the fermion field [17, 42]

$$\psi_+ = \frac{1}{2}\gamma^-\gamma^+\psi\,. \tag{3.18}$$

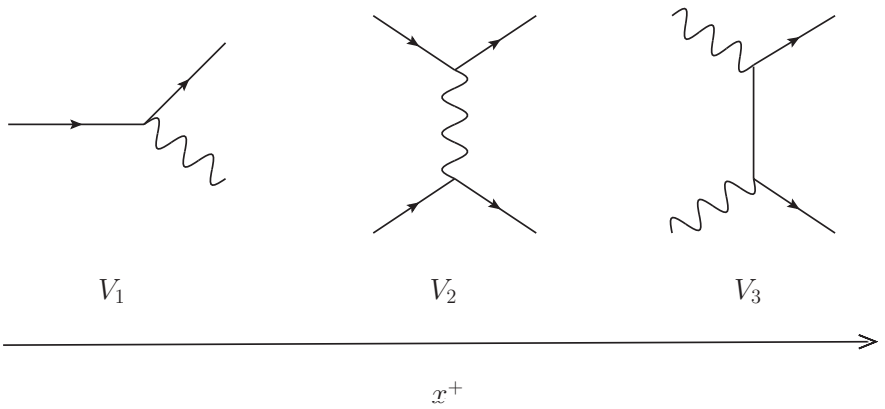

Figure 3.1: Time-ordered vertices corresponding to the interaction terms that appear in the light-front QED Hamiltonian. From left to right: three-point vertex in Eq. (3.21); four-fermion interaction with an instantaneous photon in Eq. (3.22); four point vertex with an instantaneous fermion in Eq. (3.23). Light-front time is supposed to flow from left to right.

We then take $\boldsymbol{a}_\perp = \boldsymbol{A}_\perp$ and ψ_+ as the dynamical fields of QED in light-front quantization, introducing for convenience the four vector $a^\mu = (0, a^-, \boldsymbol{a}_\perp)$.
We are now in position to describe the light-front dynamics of the fields. The QED Hamiltonian can be written in terms of the energy-momentum tensor $T^{\mu\nu}$, defined in Eq. (2.12), as [42]

$$H = \int \mathrm{d}^2\boldsymbol{x}_\perp \mathrm{d}x^- \, T^{+-}(x) = H_0 + V_1 + V_2 + V_3. \tag{3.19}$$

In Eq. (3.19), H_0 is the free Hamiltonian

$$H_0 = \int \mathrm{d}^2\boldsymbol{x}_\perp \mathrm{d}x^- \left[\frac{i}{2}\bar{\psi}_+\gamma^-\partial^+\psi_+ + \frac{1}{2}\left(F^{12}\right)^2 - \frac{1}{2}a^-\partial^+\boldsymbol{\partial}_\perp\cdot\boldsymbol{a}_\perp \right], \tag{3.20}$$

while the interaction terms read

$$V_1 = e\int \mathrm{d}^2\boldsymbol{x}_\perp \mathrm{d}x^- \, \bar{\psi}_+(x)\gamma^\mu\psi_+(x)a_\mu(x)\,, \tag{3.21}$$

$$V_2 = -\frac{ie^2}{4}\int \mathrm{d}^2\boldsymbol{x}_\perp \mathrm{d}x^-\mathrm{d}y^- \, \Theta\left(x^- - y^-\right)\bar{\psi}_+(x)\gamma^i a^i(x)\gamma^+\gamma^j a^j(y)\psi_+(y)\,, \tag{3.22}$$

$$V_3 = -\frac{e^2}{4}\int \mathrm{d}^2\boldsymbol{x}_\perp \mathrm{d}x^-\mathrm{d}y^- \, \bar{\psi}_+(x)\gamma^+\psi_+(x)\left|x^- - y^-\right|\bar{\psi}_+(y)\gamma^+\psi_+(y)\,, \tag{3.23}$$

with $y = (x^+, y^-, \boldsymbol{x}_\perp)$. The V_1 term in Eq. (3.21) describes a standard QED three-point vertex; V_2 in Eq. (3.22) and V_3 in Eq. (3.23), instead, are the non-local four-point vertices corresponding to the exchange of an instantaneous fermion and photon, respectively. The time-ordered diagrams of the three vertices are shown in Fig. 3.1. From the Hamiltonian (3.19), one can derive the light-front time-ordered contributions to one-loop processes in QED, as we will show in the following sections.

It is important to stress that the two instantaneous terms actually have different origins. The instantaneous-fermion interaction is ultimately due to the

fact that the fermions must have positive momenta [17], and hence it is a consequence of the choice of light-front coordinates. The instantaneous-photon interaction, on the other hand, is related to the fact that we are working in the non-covariant light-cone gauge. Its presence is in fact a property of any axial gauge $n_\mu A^\mu = 0$, as shown in Ref. [34] for the scalar QED case (which can be easily extended to the QED case as well). This situation is well known also in the case of the Coulomb gauge [44] and does not therefore depend on the use of light-front rather than instant-form coordinates.
In view of the considerations stated in the previous Section, we conclude that the natural starting point for the covariant calculation in light-cone gauge is the three-term propagator (3.10), recovered from the free electromagnetic-field Lagrangian with the proper gauge-fixing terms, including at the same time the diagrams containing both the standard triangle vertex *and* the instantaneous-photon interactions, which are consequence of the choice of the gauge. As we already mentioned, however, it can be proven that the contribution coming from the diagrams that contain an instantaneous photon is exactly canceled by an opposite contribution from the third term of the propagator (proportional to q^2) [34, 35, 43]. Therefore, one can alternatively drop the third term and consider only the ordinary three-point vertex. The diagrams with an instantaneous-fermion exchange, on the other hand, should not be included explicitly from the beginning, but rather recovered when we take the limit of light-front coordinates. In this way it is possible to connect one-by-one the diagrams arising in light-front TOPT with different terms from the covariant calculation, by applying the ordinary technique of integration by residues; we devote the rest of this Chapter to the proof of these statements for one-loop QED processes.

3.3 QED vertex correction

In this section we discuss the vertex correction at one-loop level in QED. We first revisit the calculation in light-front TOPT [12, 21, 42], then we present the results in covariant theory using light-front coordinates. We show how the contributions of light-front time-ordered diagrams can be recovered from a given Feynman diagram by integrating over the light-front energy. In proving the equivalence between the different formulations of the theory, we will discuss the form of the photon propagator.

3.3.1 Light-front TOPT

The vertex correction in light-front TOPT originates from contributions of the interaction terms in the form $(V_1)^3$, V_1V_2 and V_1V_3, see Eqs. (3.21)-(3.23). The $(V_1)^3$ contribution brings the two diagrams shown in Fig. 3.2, which are distinct for different ordering of the interaction vertexes with light-front time; note that in diagram (b) there appears a positron, labeled with an arrow of

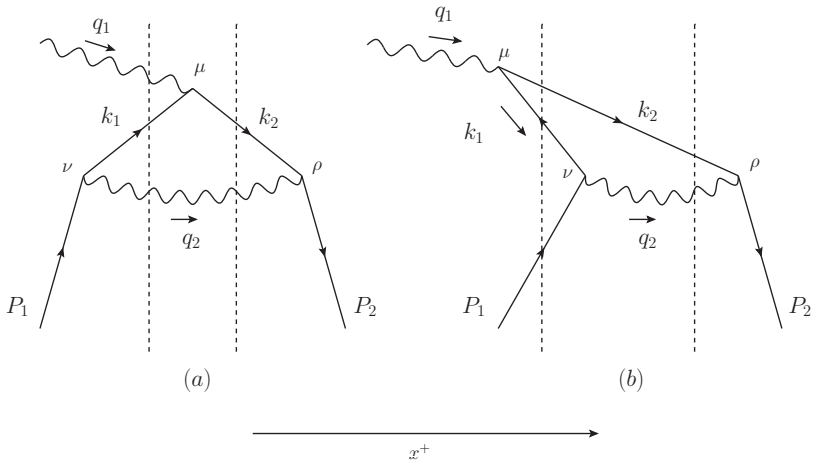

Figure 3.2: Diagrams for the vertex correction in light-front TOPT at one-loop order. The vertical dashed lines are at fixed light-front time.

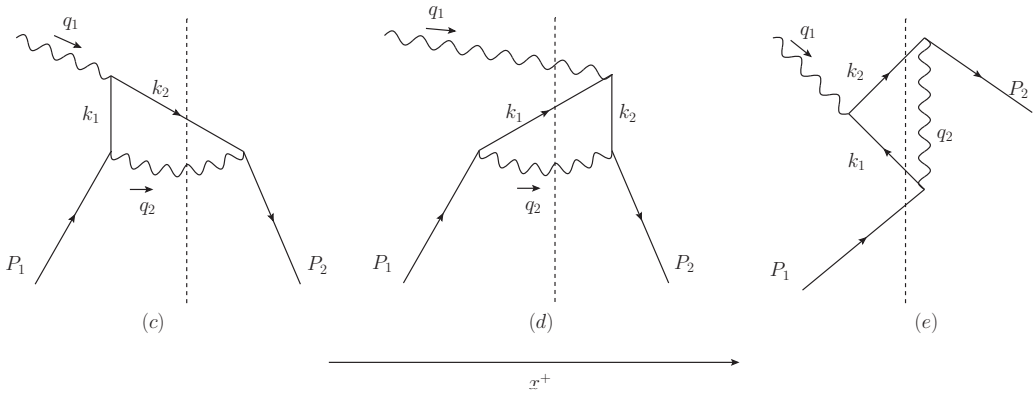

Figure 3.3: Diagrams for the vertex correction in light-front TOPT at one-loop order with instantaneous fermion exchange [(c) and (d)] and instantaneous photon exchange [(e)]. The vertical dashed lines are at fixed light-front time.

opposite direction with respect to its plus momentum. These diagrams are the analogue of the two diagrams that survive in the infinite-momentum frame in the scalar ϕ^3 theory, as explained in Section 2.2. Just like in the scalar case, all other possible time-ordered diagrams, with disconnected contributions of pair production or annihilation from the vacuum, vanish in the infinite-momentum frame. Here, however, the presence of the V_2 and V_3 interaction terms in the Hamiltonian leads to additional diagrams, shown in Fig. 3.3, which contain instantaneous fermions and photon propagators. It should be noticed that diagram (c) of Fig. 3.3 is peculiar, since it can be recovered from both diagram (a) and (b) of Fig. 3.2, by considering the propagator with momentum k_1 as instantaneous. Diagrams (d) and (e), on the contrary, can be drawn only as limits of diagrams (a) and (b), respectively.

In the calculation of the scattering amplitude we set the momenta of the particles as shown in the corresponding diagrams. As we aim to match the

terms derived from the evaluation of the light-front time-ordered diagrams with the corresponding current obtained in the covariant approach, it is convenient to decompose the momentum k^μ of a particle of mass m into an on-shell and an off-shell component, by defining

$$k^\mu_{\rm on-shell} \equiv \tilde{k}^\mu = \left(k^+, \frac{\boldsymbol{k}_\perp^2 + m^2}{2k^+}, \boldsymbol{k}_\perp\right), \tag{3.24a}$$

$$k^\mu_{\rm off-shell} \equiv \hat{k}^\mu = \left(0, \frac{k^2 - m^2}{2k^+}, \mathbf{0}_\perp\right) = \frac{k^2 - m^2}{2k^+} n^\mu \,, \tag{3.24b}$$

so that $k^\mu = \tilde{k}^\mu + \hat{k}^\mu$.
It is also useful to introduce the symmetric notation

$$q_1 \equiv \Delta \,, \quad P_{1,2} = P \mp \frac{\Delta}{2} \,, \quad k_{1,2} = k \mp \frac{\Delta}{2} \,, \quad q_2 = P - k \,. \tag{3.25}$$

As we already remarked, in the TOPT approach all particles are on shell but energy is not conserved at each vertex, contrarily to what happens in the covariant formulation. It is therefore understood that the last two identities in Eq. (3.25) are are valid only for the plus and transverse components, when working within light-front TOPT. We also define the longitudinal momentum fraction $x = k^+/P^+$ and the skewedness parameter[1] $\xi = \Delta^+/2P^+$. Furthermore, without loss of generality, we can fix $\xi > 0$, which means we are considering an incoming photon, and work in the reference frame where $\boldsymbol{P}_\perp = \mathbf{0}_\perp$. The on-shell conditions give:

$$P^- = \frac{1}{2P^+}\left(m^2 - \frac{t}{4}\right) \,, \quad \Delta^- = -2\xi P^- \,, \quad k^-_{1,2} = \frac{\mathbf{k}^2_{1,2,\perp} + m^2}{2k^+_{1,2}} \,, \quad q_2^- = \frac{\mathbf{q}^2_{2,\perp}}{2q_2^+} \,, \tag{3.26}$$

with $t \equiv \Delta^2$ and

$$k^+_{1,2} = k^+ \mp \frac{\Delta^+}{2} \,, \quad \mathbf{k}_{1,2,\perp} = \boldsymbol{k}_\perp \mp \frac{\boldsymbol{\Delta}_\perp}{2} \,, \quad q_2^+ = P^+ - k^+ \,, \quad \mathbf{q}_{2,\perp} = -\boldsymbol{k}_\perp \,. \tag{3.27}$$

Let us start from the contribution of order V_1^3 to the scattering amplitude. The corresponding matrix element of the transition matrix iT is:

$$\Lambda^{TOPT}_{(V_1^3)} = \langle e_{P_2}|iT|e_{P_1}\gamma_{q_1}\rangle = i\left\langle e_{P_2}\left|V_1\frac{1}{P_i^- - H_0}V_1\frac{1}{P_i^- - H_0}V_1\right|e_{P_1}\gamma_{q_1}\right\rangle \tag{3.28}$$

where $P_i^- = P_1^- + q_1^-$ is the total energy of the initial states. Spin indices are omitted as they are not relevant in the current discussion. By inserting the resolution of the identity with the complete set of eigenstates of the free

[1] This is the notation usually adopted in the treatment of Generalized Parton Distributions (GPD) and Generalized Transverse-Momentum Dependent (GTMD) distributions, see Sections 4.4 and 4.5. Note however that, in the GPD and GTMD notation, ξ is defined with an extra minus sign, see Eq. (4.37).

Hamiltonian, it is possible to identify the contributions $\Lambda^{TOPT}_{(a)}$ and $\Lambda^{TOPT}_{(b)}$ corresponding to diagrams (a) and (b) of Fig. 3.3, i.e.

$$\Lambda^{TOPT}_{(V_1^3)} = \Lambda^{TOPT}_{(a)} + \Lambda^{TOPT}_{(b)}. \tag{3.29}$$

The first contribution can be recast in the form

$$\Lambda^{TOPT}_{(a)} = (2\pi)^3 \delta\left(P_1^+ + q_1^+ - P_2^+\right) \delta^{(2)}\left(\boldsymbol{P}_{1,\perp} + \boldsymbol{q}_{1,\perp} - \boldsymbol{P}_{2,\perp}\right) (-ie)\, \varepsilon_\mu(q_1) J^\mu_{(a)} \,. \tag{3.30}$$

For later convenience , we isolate the energy denominator of the current $J^\mu_{(a)}$:

$$\begin{aligned} D_{(a)} =& \left\langle \gamma_{q_1} e_{k_1} \gamma_{q_2} \left| \frac{1}{P_1^- + q_1^- - H_0^-} \right| \gamma_{q_1} e_{k_1} \gamma_{q_2} \right\rangle \left\langle e_{k_2} \gamma_{q_2} \left| \frac{1}{P_1^- + q_1^- - H_0^-} \right| e_{k_2} \gamma_{q_2} \right\rangle \\ =& \frac{1}{P_1^- + q_1^- - \left(q_1^- + k_1^- + q_2^-\right)} \frac{1}{P_1^- + q_1^- - \left(k_2^- + q_2^-\right)} \,. \end{aligned} \tag{3.31}$$

By switching to the symmetric notation and using Eqs. (3.26) and (3.27), one can rewrite:

$$P_1^- + q_1^- - \left(q_1^- + k_1^- + q_2^-\right) = \kappa_3 - \kappa_1 \,, \tag{3.32}$$

$$P_1^- + q_1^- - \left(k_2^- + q_2^-\right) = \kappa_3 - \kappa_2 \,, \tag{3.33}$$

where we have defined

$$\kappa_{1,2} = \frac{\boldsymbol{k}_\perp^2 \mp \boldsymbol{k}_\perp \cdot \boldsymbol{\Delta}_\perp + (1 \mp \xi x)\left(m^2 - \frac{t}{4}\right)}{2P^+(x \mp \xi)} \,, \tag{3.34a}$$

$$\kappa_3 = \frac{\boldsymbol{k}_\perp^2 + (x-1)\left(m^2 - \frac{t}{4}\right)}{2(x-1)P^+}. \tag{3.34b}$$

The numerator of the current $J^\mu_{(a)}$ is given by

$$\begin{aligned} N^\mu_{(a)} =& -\frac{e^2 P^+}{(2\pi)^3} \int_\xi^1 \mathrm{d}x \int \mathrm{d}^2\boldsymbol{k}_\perp \frac{1}{(2P^+)^3 (1-x)\left(x^2 - \xi^2\right)} \\ & \times \bar{u}(P_2)\gamma^\rho \left(\tilde{\not{k}}_2 + m\right)\gamma^\mu \left(\tilde{\not{k}}_1 + m\right)\gamma^\nu d_{\nu\rho}(\tilde{q}_2)\, u(P_1) \,, \end{aligned} \tag{3.35}$$

where the limits of integration in the variable x are given by the constraint that all particles move along the positive light-front direction. In Eq. (3.35) the intermediate photon is on-shell, consistently with the rules of old-fashioned perturbation theory; accordingly, the sum $d^{\mu\nu}(q)$ over transversely-polarized states of the intermediate photon is given by Eq. (3.9) with $q^2 = 0$:

$$d^{\mu\nu}(q) = -g^{\mu\nu} + \frac{q^\mu n^\nu + q^\nu n^\mu}{q^+} \,. \tag{3.36}$$

This is at variance with respect to Ref. [34], which uses the three-term sum of Eq. (3.11) for the calculation of light-front time-ordered diagrams.

If we collect the results from Eqs. (3.31) and (3.35), we finally obtain the following contribution of the diagram (a) to the current

$$J^{\mu}_{(a)} = -\frac{e^2P^+}{(2\pi)^3}\int_{\xi}^{1}dx\int d^2\boldsymbol{k}_{\perp}\frac{1}{(2P^+)^3\,(1-x)\,(x^2-\xi^2)} \times \bar{u}(P_2)\gamma^{\rho}\frac{\left(\tilde{\not{k}}_2+m\right)}{\kappa_3-\kappa_1}\gamma^{\mu}\frac{\left(\tilde{\not{k}}_1+m\right)}{\kappa_3-\kappa_2}\gamma^{\nu}d_{\nu\rho}\left(\tilde{q}_2\right)u(P_1)\,. \tag{3.37}$$

A similar procedure can be followed also for diagram (b) in Fig. 3.2, corresponding to the contribution

$$\Lambda^{TOPT}_{(b)} = (2\pi)^3\delta\left(P_1^+ + q_1^+ - P_2^+\right)\delta^{(2)}\left(\boldsymbol{P}_{1,\perp}+\boldsymbol{q}_{1,\perp}-\boldsymbol{P}_{2,\perp}\right)(-ie)\,\varepsilon_{\mu}(q_1)J^{\mu}_{(b)}\,. \tag{3.38}$$

The current $J^{\mu}_{(b)}$ has an energy denominator given by

$$\begin{aligned} D_{(b)} &= \left\langle e_{P_1}e^+_{k_1}e_{k_2}\left|\frac{1}{P_1^- + q_1^- - H^-}\right|e_{P_1}e^+_{k_1}e_{k_2}\right\rangle\left\langle e_{k_2}\gamma_{q_2}\left|\frac{1}{P_1^- + q_1^- - H^-}\right|e_{k_2}\gamma_{q_2}\right\rangle \\ &= \frac{1}{P_1^- + q_1^- - \left(P_1^- - k_1^- + k_2^-\right)}\frac{1}{P_1^- + q_1^- - \left(k_2^- + q_2^-\right)}\,. \end{aligned} \tag{3.39}$$

We can rewrite:

$$P_1^- + q_1^- - \left(P_1^- - k_1^- + k_2^-\right) = \kappa_2 - \kappa_1\,, \tag{3.40}$$

while the energy denominator for the second intermediate state is again given by Eq. (3.33). If we evaluate also the numerator of $J^{\mu}_{(b)}$, we come up with the final result:

$$J^{\mu}_{(b)} = -\frac{e^2P^+}{(2\pi)^3}\int_{-\xi}^{\xi}\mathrm{d}x\int \mathrm{d}^2\boldsymbol{k}_{\perp}\frac{1}{(2P^+)^3\,(1-x)\,(x^2-\xi^2)} \times \bar{u}(P_2)\gamma^{\rho}\frac{\left(\tilde{\not{k}}_2+m\right)}{\kappa_3-\kappa_2}\gamma^{\mu}\frac{\left(\tilde{\not{k}}_1+m\right)}{\kappa_2-\kappa_1}\gamma^{\nu}d_{\nu\rho}\left(\tilde{q}_2\right)u(P_1)\,. \tag{3.41}$$

We now focus on the diagrams containing instantaneous propagators, which come from V_1V_2, V_2V_1 and V_1V_3 interaction terms in the matrix element. The result for the current $J^{\mu}_{(c)}$ of diagram (c) in Fig. 3.3 corresponds to the matrix element

$$\Lambda^{TOPT}_{(V_1V_2)} = i\left\langle e_{P_2}\left|V_1\frac{1}{P_i^- - H_0}V_2\right|e_{P_1}\gamma_{q_1}\right\rangle \tag{3.42}$$

$$= (2\pi)^3\delta\left(P_1^+ + q_1^+ - P_2^+\right)\delta^{(2)}\left(\boldsymbol{P}_{1,\perp}+\boldsymbol{q}_{1,\perp}-\boldsymbol{P}_{2,\perp}\right)(-ie)\,\varepsilon_{\mu}(q_1)J^{\mu}_{(c)}\,. \tag{3.43}$$

By following a procedure similar to the one described above, one finds that the current $J^{\mu}_{(c)}$ is given by

$$J^{\mu}_{(c)} = -\frac{e^2P^+}{(2\pi)^3}\int_{-\xi}^{1}\mathrm{d}x\int \mathrm{d}^2\boldsymbol{k}_{\perp}\,\frac{1}{(2P^+)^3\,(1-x)\,(x^2-\xi^2)}$$

$$\times\, \bar{u}(P_2)\gamma^\rho \frac{\left(\tilde{\not{k}}_2 + m\right)}{\kappa_3 - \kappa_2}\gamma^\mu\gamma^+\gamma^\nu d_{\nu\rho}\left(\tilde{q}_2\right) u(P_1)\,. \tag{3.44}$$

Note that this result can also be obtained by summing the contributions from diagrams (a) and (b), if we and make the replacement $(\not{k}_1 + m) \mapsto \gamma^+$ and remove from them the energy denominators (3.32) and (3.40), respectively. This is consistent with the light-front TOPT rules for an instantaneous fermion propagator [45]. Similarly, we obtain the following result for the contributions to the current from diagrams (d) in Fig. 3.3:

$$\begin{aligned} J^\mu_{(d)} = &-\frac{e^2P^+}{(2\pi)^3}\int_\xi^1 \mathrm{d}x \int \mathrm{d}^2\boldsymbol{k}_\perp \frac{1}{\left(2P^+\right)^3(1-x)\left(x^2-\xi^2\right)} \\ &\times \bar{u}(P_2)\gamma^\rho\gamma^+\gamma^\mu \frac{\left(\tilde{\not{k}}_1 + m\right)}{\kappa_3 - \kappa_1}\gamma^\nu d_{\nu\rho}\left(\tilde{q}_2\right) u(P_1)\,. \end{aligned} \tag{3.45}$$

Finally, diagram (e) in Fig. 3.3 with an instantaneous photon can be obtained from Eq. (3.41) with the substitution $d^{\mu\nu}(q)/q^+ \mapsto n^\mu n^\nu/(q^+)^2$ and removing the term $\kappa_2 - \kappa_1$ from the energy denominator (3.41). As a result, it reads

$$\begin{aligned} J^\mu_{(e)} = &-\frac{e^2P^+}{(2\pi)^3}\int_{-\xi}^{\xi} \mathrm{d}x \int \mathrm{d}^2\boldsymbol{k}_\perp \frac{1}{4\left(P^+\right)^3(1-x)\left(x^2-\xi^2\right)} \\ &\times \bar{u}(P_2)\gamma^\rho \frac{\left(\tilde{\not{k}}_2 + m\right)}{\kappa_3 - \kappa_1}\gamma^\mu\left(\tilde{\not{k}}_1 + m\right)\gamma^\nu \frac{n_\nu n_\rho}{(1-x)P^+} u(P_1)\,. \end{aligned} \tag{3.46}$$

3.3.2 Covariant approach

The one-loop vertex correction in the covariant approach with the light-cone-gauge condition $n_\mu A^\mu = 0$ is described in Fig. 3.4. Diagram (a) is the triangle diagram due to the term of the form $(V_1)^3$ in the interaction Hamiltonian (3.19) and diagram (b) is the so-called *swordfish diagram* due to the $V_1 V_3$ term that contains a four-fermion interaction. The matrix element of the triangle diagram reads

$$\Lambda = (2\pi)^4\delta^{(4)}\left(P_1 + q_1 - P_2\right)(-ie)\varepsilon_\mu(q_1)J^\mu_{\mathrm{Cov}}\,,$$

with the current J^μ_{Cov} given by

$$J^\mu_{\mathrm{Cov}} = \frac{e^2}{(2\pi)^4}\int \mathrm{d}^4k_1\,\bar{u}\left(P_2\right)\gamma_\rho \mathcal{S}_F(k_2)\gamma^\mu\mathcal{S}_F(k_1)\gamma_\nu\,\mathcal{D}_T^{\nu\rho}(q_2)u(p_1)\,, \tag{3.47}$$

where

$$\mathcal{S}_F(k) = \frac{i\left(\not{k} + m\right)}{k^2 - m^2 + i\epsilon} \tag{3.48}$$

is the electron propagator, and $\mathcal{D}_T^{\mu\nu}(q)$ is the photon propagator in the light-cone gauge from Eq. (3.10). As discussed in Sections 3.1 and 3.2, the third term in $\mathcal{D}_T^{\mu\nu}(q)$ generates a contribution which cancels out the one arising from the

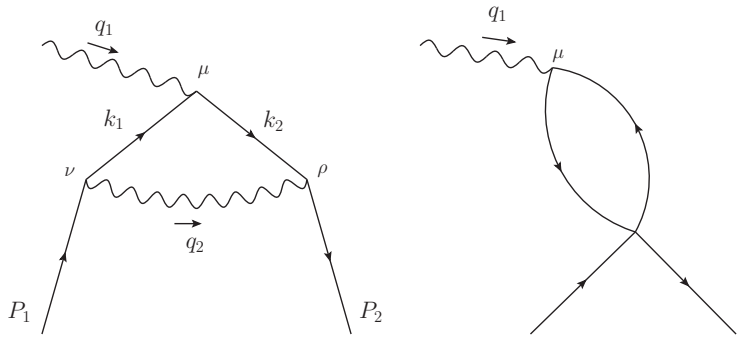

Figure 3.4: Vertex correction at one-loop order in covariant QED: (a) triangle diagram; (b) swordfish diagram containing the V_3 vertex.

four-fermion interaction, corresponding to diagram (b) in Fig. 3.4. As a result, the vertex correction in the covariant approach can effectively be obtained by taking into account the contribution from the triangle diagram in Fig. 3.4 (a) alone and replacing $\mathcal{D}_T^{\mu\nu}$ in (3.47) with the two-term expression $\mathcal{D}^{\mu\nu}$ of Eq. (3.1) for the photon propagator.
In the following we show the equivalence of the covariant approaches with the results of light-front TOPT discussed in the previous Section. In covariant theories, momentum is conserved at each vertex and we can write

$$q_2 = P_1 - k_1 \ , \quad k_2 = k_1 + q_1 \ , \quad P_2 = k_2 + q_2 \ . \tag{3.49}$$

If we apply again the splitting of the momenta in Eqs. (3.24a) and (3.24b), the fermion's and gauge boson's propagators get in turn decomposed into two parts, according to:

$$\mathcal{S}_F(k) = \frac{i\left(\not{k} + m\right)}{k^2 - m^2 + i\epsilon} = \frac{i\left(\tilde{\not{k}} + m\right)}{k^2 - m^2 + i\epsilon} + \frac{i\gamma^+}{2k^+}, \tag{3.50a}$$

$$\begin{aligned}\mathcal{D}^{\mu\nu}(q) =& \frac{-i}{q^2 + i\epsilon}\left(g^{\mu\nu} - \frac{q^\mu n^\nu + q^\nu n^\mu}{q^+}\right) \\ =& \frac{-i}{q^2 + i\epsilon}\left(g^{\mu\nu} - \frac{\tilde{q}^\mu n^\nu + \tilde{q}^\nu n^\mu}{q^+}\right) + \frac{in^\mu n^\nu}{\left(q^+\right)^2} = \frac{id^{\mu\nu}(\tilde{q})}{q^2 + i\epsilon} + \frac{in^\mu n^\nu}{\left(q^+\right)^2}.\end{aligned} \tag{3.50b}$$

The first terms in both decompositions depend on the light-front energy components k^- and q^-; therefore they yield the propagating part. The remaining terms, instead, do not depend on the minus component of the momenta and hence they correspond to the non-propagating instantaneous particles [33]. It should be noticed that, to some extent, in Eq. (3.50b) we recovered a three term propagator, but this time the numerator of the second term only depends on the on-shell component $\tilde{q}$ of the gauge-field momentum q.
As a consequence of the splitting in Eqs. (3.50a) and (3.50b), the current J^μ_{COV}

in Eq. (3.47) can be rewritten as:

$$J^{\mu}_{\mathrm{Cov}} = -\frac{ie^2}{(2\pi)^4}\int \mathrm{d}^4k_1\,\bar{u}\,(P_2)\,\gamma^{\rho}\left(\frac{\tilde{\not{k}}_2+m}{k_2^2-m^2+i\epsilon}+\frac{\gamma^+}{2k_2^+}\right) \times\gamma^{\mu}\left(\frac{\tilde{\not{k}}_1+m}{k_1^2-m^2+i\epsilon}+\frac{\gamma^+}{2k_1^+}\right)\gamma^{\nu}\left(\frac{d_{\nu\rho}\,(\tilde{q}_2)}{q_2^2+i\epsilon}+\frac{n_{\nu}n_{\rho}}{(q_2^+)^2}\right)u\,(P_1)\ . \tag{3.51}$$

We can hence separate J^{μ}_{Cov} into eight contributions, depending on different combinations of the propagating and instantaneous components of the propagators. Out of these eight contributions, four are non-vanishing[2]:

$$J^{\mu}_1\left[\tilde{k}_1,\tilde{k}_2,\tilde{q}_2\right] = -\frac{ie^2}{(2\pi)^4}\int \mathrm{d}^4k_1\,\bar{u}\,(P_2)\,\gamma^{\rho}\left(\frac{\tilde{\not{k}}_2+m}{k_2^2-m^2+i\epsilon}\right) \times\gamma^{\mu}\left(\frac{\tilde{\not{k}}_1+m}{k_1^2-m^2+i\epsilon}\right)\gamma^{\nu}\frac{d_{\nu\rho}\,(\tilde{q}_2)}{q_2^2+i\epsilon}u\,(P_1)\ , \tag{3.52a}$$

$$J^{\mu}_2\left[\tilde{k}_1,\tilde{k}_2,\tilde{q}_2\right] = -\frac{ie^2}{(2\pi)^4}\int \mathrm{d}^4k_1\,\bar{u}\,(P_2)\,\gamma^{\rho}\left(\frac{\tilde{\not{k}}_2+m}{k_2^2-m^2+i\epsilon}\right) \times\gamma^{\mu}\frac{\gamma^+}{2k_1^+}\gamma^{\nu}\frac{d_{\nu\rho}\,(\tilde{q}_2)}{q_2^2+i\epsilon}u\,(P_1)\ , \tag{3.52b}$$

$$J^{\mu}_3\left[\tilde{k}_1,\hat{k}_2,\tilde{q}_2\right] = -\frac{ie^2}{(2\pi)^4}\int \mathrm{d}^4k_1\,\bar{u}\,(P_2)\,\gamma^{\rho}\frac{\gamma^+}{2k_2^+} \times\gamma^{\mu}\left(\frac{\tilde{\not{k}}_1+m}{k_1^2-m^2+i\epsilon}\right)\gamma^{\nu}\frac{d_{\nu\rho}\,(\tilde{q}_2)}{q_2^2+i\epsilon}u\,(P_1)\ , \tag{3.52c}$$

$$J^{\mu}_4\left[\tilde{k}_1,\tilde{k}_2,\hat{q}_2\right] = -\frac{ie^2}{(2\pi)^4}\int \mathrm{d}^4k_1\,\bar{u}\,(P_2)\,\gamma^{\rho}\left(\frac{\tilde{\not{k}}_2+m}{k_2^2-m^2+i\epsilon}\right) \times\gamma^{\mu}\left(\frac{\tilde{\not{k}}_1+m}{k_1^2-m^2+i\epsilon}\right)\gamma^{\nu}\frac{n_{\nu}n_{\rho}}{(q_2^+)^2}u\,(P_1)\ , \tag{3.52d}$$

while three are vanishing because of their Dirac matrix structures:

$$J^{\mu}_5\left[\hat{k}_1,\tilde{k}_2,\hat{q}_2\right] \propto \gamma^{\rho}\left(\tilde{\not{k}}_2+m\right)\gamma^{\mu}\gamma^{+}\gamma^{\nu}n_{\nu}n_{\rho} = 0\ , \tag{3.53a}$$

$$J^{\mu}_6\left[\tilde{k}_1,\hat{k}_2,\hat{q}_2\right] \propto \gamma^{\rho}\gamma^{+}\gamma^{\mu}\left(\tilde{\not{k}}_1+m\right)\gamma^{\nu}n_{\nu}n_{\rho} = 0\ , \tag{3.53b}$$

$$J^{\mu}_7\left[\hat{k}_1,\hat{k}_2,\hat{q}_2\right] \propto \gamma^{\rho}\gamma^{+}\gamma^{\mu}\gamma^{+}\gamma^{\nu}n_{\nu}n_{\rho} = 0\ . \tag{3.53c}$$

There is one last term left, which is:

$$J^{\mu}_8\left[\hat{k}_1,\hat{k}_2,\tilde{q}\right] \propto \gamma^{\rho}\gamma^{+}\gamma^{\mu}\gamma^{+}\gamma^{\nu}\left(g_{\nu\rho}-\frac{n_{\nu}\tilde{q}_{2_{\rho}}+n_{\rho}\tilde{q}_{2_{\nu}}}{q_2^+}\right) = \gamma_{\nu}\gamma^{+}\gamma^{-}\gamma^{+}\gamma^{\nu}g^{\mu-}\ . \tag{3.54}$$

[2]We use the arguments in square brackets to specify which part (on-shell rather than off-shell) of the momenta enters in the numerator of the corresponding propagator.

	$x < -\xi$	$-\xi < x < \xi$	$\xi < x < 1$	$x > 1$
κ_{1_ϵ}	+	+	-	-
κ_{2_ϵ}	+	-	-	-
κ_{3_ϵ}	+	+	+	-

Table 3.1: Distribution of the poles in J_1^μ in the complex plane: the symbols $+, -$ denote whether the pole is located in the upper- or lower-half complex plane, respectively.

It is not vanishing by itself, but we notice that when we contract it with the polarization vector of the external photon, we obtain $\varepsilon^+(q)J_8^-$ which is zero in the light-cone gauge; therefore we can disregard this term as well.
The equivalence with the light-front TOPT approach can be established by applying the method of integration by residues over the light-front energy k^-. We focus on the contribution J_1^μ in Eq. (3.52a) as an example. We can use again the momentum parametrization (3.25), which is this time valid for all the components of the momenta. The denominator of J_1^μ is then

$$D_1\left[\tilde{k}_1, \tilde{k}_2, \tilde{q}_2\right] = \left[\left(k + \frac{\Delta}{2}\right)^2 - m^2 + i\epsilon\right]\left[\left(k - \frac{\Delta}{2}\right)^2 - m^2 + i\epsilon\right]\left[(P-k)^2 + i\epsilon\right] . \tag{3.55}$$

If we also take advantage of the on-shell conditions for both the initial- and final-state electron, i.e. the first two identities in Eq. (3.26), the zeros of the denominator (3.55) are:

$$\kappa_{1_\epsilon} = \kappa_1 - \frac{i\epsilon}{2(x-\xi)P^+} , \quad \kappa_{2_\epsilon} = \kappa_2 - \frac{i\epsilon}{2(x+\xi)P^+} , \quad \kappa_{3_\epsilon} = \kappa_3 - \frac{i\epsilon}{2(x-1)P^+} , \tag{3.56}$$

where κ_1, κ_2 and κ_3 are defined in Eqs. (3.34a)-(3.34b). By changing the variable of integration from k_1 to k according to the relations (3.25), we see that the poles of the integrand in J_1^μ are distributed in the complex k plane as shown in Table 3.1. The non-vanishing k^--integral in J_1^μ therefore comes from the region $-\xi < x < 1$: if we close the circuit of integration in the upper- or lower-half complex plane, the integral is obtained from the residue in κ_{1_ϵ}, with the result

$$\begin{aligned} J_1^\mu = &- \frac{e^2P^+}{(2\pi)^3}\int_{-\xi}^{\xi} \mathrm{d}x \int \mathrm{d}^2\boldsymbol{k}_\perp\, \bar{u}(P_2)\gamma^\rho \left(\frac{\tilde{\not{k}}_2 + m}{(2P^+)^3\,(x^2-\xi^2)\,(x-1)}\right) \\ &\times \gamma^\mu \left(\frac{\tilde{\not{k}}_1 + m}{\kappa_2^- - \kappa_1^-}\right)\gamma^\nu \left(\frac{d_{\nu\rho}(\tilde{q}_2)}{\kappa_2^- - \kappa_3^-}\right) u\,(P_1) \\ &+ \frac{e^2P^+}{(2\pi)^3}\int_{\xi}^{1} \mathrm{d}x \int \mathrm{d}^2\boldsymbol{k}_\perp\, \bar{u}(P_2)\gamma^\rho \left(\frac{\tilde{\not{k}}_2 + m}{\kappa_3^- - \kappa_2^-}\right) \\ &\times \gamma^\mu \left(\frac{\tilde{\not{k}}_1 + m}{\kappa_3^- - \kappa_1^-}\right)\gamma^\nu \left(\frac{d_{\nu\rho}(\tilde{q}_2)}{(2P^+)^3\,(x^2-\xi^2)\,(x-1)}\right) u\,(P_1) . \end{aligned} \tag{3.57}$$

We remark that the numerator remains unchanged after integration, since it does not depend on the minus component of k.
The same procedure can be applied to terms J_2^μ, J_3^μ and J_4^μ. The integrand in J_2^μ does not exhibit a pole in k_1^-; therefore, after integration, it still results into the sum of two terms

$$\begin{aligned} J_2^\mu =& -\frac{e^2P^+}{(2\pi)^3}\int_{-\xi}^{\xi}\mathrm{d}x\int\mathrm{d}^2\boldsymbol{k}_\perp\,\bar{u}(P_2)\gamma^\rho\left(\frac{\tilde{\not{k}}_2+m}{(2P^+)^3\,(x^2-\xi^2)\,(x-1)}\right)\\ &\times\gamma^\mu\,\gamma^+\gamma^\nu\left(\frac{d_{\nu\rho}(\tilde{q}_2)}{\kappa_2^- - \kappa_3^-}\right)u\,(P_1)\\ &+\frac{e^2P^+}{(2\pi)^3}\int_{\xi}^{1}\mathrm{d}x\int\mathrm{d}^2\boldsymbol{k}_\perp\,\bar{u}(P_2)\gamma^\rho\left(\frac{\tilde{\not{k}}_2+m}{\kappa_3^- - \kappa_2^-}\right)\\ &\times\gamma^\mu\,\gamma^+\gamma^\nu\left(\frac{d_{\nu\rho}(\tilde{q}_2)}{(2P^+)^3\,(x^2-\xi^2)\,(x-1)}\right)u\,(P_1)\ , \end{aligned} \tag{3.58}$$

yielding as a result

$$\begin{aligned} J_2^\mu =&\frac{e^2P^+}{(2\pi)^3}\int_{-\xi}^{1}\mathrm{d}x\int\mathrm{d}^2\boldsymbol{k}_\perp\,\bar{u}(P_2)\gamma^\rho\left(\frac{\tilde{\not{k}}_2+m}{\kappa_3^- - \kappa_2^-}\right)\\ &\times\gamma^\mu\,\gamma^+\gamma^\nu\left(\frac{d_{\nu\rho}(\tilde{q}_2)}{(2P^+)^3\,(x^2-\xi^2)\,(x-1)}\right)u\,(P_1)\,. \end{aligned} \tag{3.59}$$

The contributions J_3^μ and J_4^μ, instead, are non-vanishing only in the regions $\xi < x < 1$ and $-\xi < x < \xi$, respectively:

$$\begin{aligned} J_3^\mu =&\frac{e^2P^+}{(2\pi)^3}\int_{\xi}^{1}\mathrm{d}x\int\mathrm{d}^2\boldsymbol{k}_\perp\,\bar{u}(P_2)\gamma^\rho\,\gamma^+\gamma^\mu\left(\frac{\tilde{\not{k}}_1+m}{\kappa_3^- - \kappa_1^-}\right)\\ &\times\gamma^\nu\left(\frac{d_{\nu\rho}(\tilde{q}_2)}{(2P^+)^3\,(x^2-\xi^2)\,(x-1)}\right)u\,(P_1)\ , \end{aligned} \tag{3.60}$$

$$\begin{aligned} J_4^\mu =& -\frac{e^2}{(2\pi)^3}\int_{-\xi}^{\xi}\mathrm{d}x\int\mathrm{d}^2\boldsymbol{k}_\perp\,\bar{u}(P_2)\gamma^\rho\left(\frac{\tilde{\not{k}}_2+m}{4\,(P^+)^3\,(x^2-\xi^2)\,(1-x)^2}\right)\\ &\times\gamma^\mu\left(\frac{\tilde{\not{k}}_1+m}{\kappa_2^- - \kappa_1^-}\right)\gamma^\nu\,n_\nu n_\rho u\,(P_1)\ . \end{aligned} \tag{3.61}$$

We are now ready to discuss the equivalence between the covariant approach and the light-front TOPT approach. Let us consider J_1^μ in Eq. (3.57), which is the sum of two terms; if we compare them with the light-front TOPT results (3.37) and (3.41), we see that these contributions coincide with the sum of diagrams (a) and (b) in Fig. 3.2, where all particles in the intermediate states are propagating and we do not have instantaneous propagators.
The second contribution J_2^μ in covariant approach, Eq. (3.59), coincides instead with Eq. (3.44); notice that also in the covariant approach we can split

Light-Front TOPT	Covariant Approach
$J^\mu_{(a)} + J^\mu_{(b)}$	J^μ_1
$J^\mu_{(c)}$	J^μ_2
$J^\mu_{(d)}$	J^μ_3
$J^\mu_{(e)}$	J^μ_4

Table 3.2: Correspondence between the different contributions to the triangle diagram in light-front TOPT and covariant approach.

this term into two, according to the value of the plus momentum flowing in the instantaneous propagator, thus reproducing the situation in the light-front TOPT case.
Finally, the current terms J^μ_3 in (3.60) and J^μ_4 in (3.61) are exactly equivalent to their light-front TOPT counterparts, namely Eq. (3.45) and Eq. (3.46), respectively; the second term, in particular, refers to the diagram with the instantaneously-propagating photon.
The correspondence between the two approaches for the one-loop vertex correction is summarized in Table 3.2. Our result differs from the one found by Misra et al. in Ref. [35], where it is claimed that the three-term propagator is needed in order to obtain the equivalence. This is due to the fact that they do not evaluate $d^{\mu\nu}(q)$ at the pole in the calculation of the residue. By correctly accounting for this, one would automatically include the contribution from the instantaneous photon, with no need of adding it separately in the third term. Moreover, our results are more general as they apply to all the Lorentz components of the current, while the results in Ref. [35] refer only to the contribution from the plus component.

3.4 One-loop self-energy diagrams

In this section we complete the proof of the equivalence between light-front TOPT and covariant approaches in QED at one-loop order, by considering the self-energy diagrams for both the electron and the photon. We revisit the results in light-front TOPT which were also discussed in Refs. [35, 42], and we prove the equivalence with the covariant approaches, fixing some imprecisions in the calculation of Ref. [35].

3.4.1 Electron self-energy

We follow the derivation of Ref. [42] and consider the order-α amplitude

$$T_{PP} = \langle P, S'|T|P, S\rangle \tag{3.62}$$

of the transition matrix

$$T = V + V\frac{1}{P^- - H_0}V\,, \qquad V = V_1 + V_2 + V_3 \tag{3.63}$$

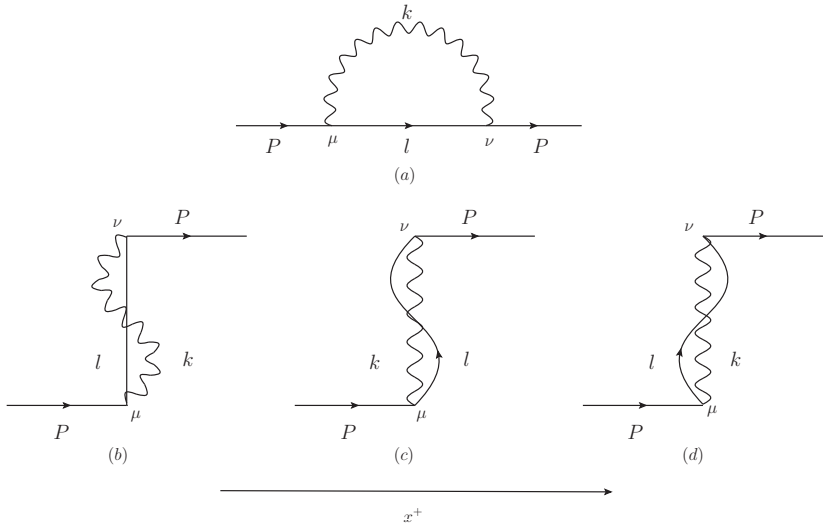

Figure 3.5: Diagrams for the electron self-energy in light-front TOPT at one-loop order, including the instantaneous exchange of fermions [(b)] and instantaneous exchange of photons [(c) and (d)].

between two electron states $|P,S\rangle$, and $|P,S'\rangle$. The latter are normalized as

$$\langle P',S'|P,S\rangle = 16\pi^3 P^+\delta(P^+-P'^+)\delta^{(2)}\left(\boldsymbol{P}_\perp-\boldsymbol{P}'_\perp\right)\delta_{S,S'}\ . \tag{3.64}$$

We can write

$$T_{PP}\equiv\delta_{S,S'}\,\delta T = \bar{u}(P,S')\Sigma(P)u(P,S)\ , \tag{3.65}$$

which defines the transition matrix $\Sigma(P)$ [3]. The order-α expansion of δT can be split into three contributions, arising from the different terms of the interaction Hamiltonian:

$$\begin{aligned}\delta T\delta_{S,S'} &= \left(\delta T_a+\delta T_b+\delta T_{c+d}\right)\delta_{S,S'}\\ &= \bar{u}(P,S')\left[\Sigma_a^{(2)}(P)+\Sigma_b^{(2)}(P)+\Sigma_{c+d}^{(2)}(P)\right]u(P,S)\ .\end{aligned} \tag{3.66}$$

The δT_a term corresponds to the contribution of second order in V_1, described by diagram (a) in Fig. 3.5. With the notation $k^+=xP^+$ and $(l^+,\boldsymbol{l}_\perp)=((1-x)P^+,-\boldsymbol{k}_\perp)$, one finds

$$\begin{aligned}&\delta T_a\delta_{S,S'} = \bar{u}_{S'}(P)\Sigma_a^{(2)}(P)u_S(P)\\ &= 2e^2P^+\int\frac{\mathrm{d}^2\boldsymbol{k}_\perp}{(4\pi)^3}\int_0^1\mathrm{d}x\,\frac{1}{x(1-x)\left(P^+\right)^2}\bar{u}_{S'}(P)\frac{\gamma^\nu\left(\tilde{l}+m\right)\gamma^\mu d_{\mu\nu}(\tilde{k})}{P^--k^--l^-}u_S(P)\ .\end{aligned} \tag{3.67}$$

[3] Our $\Sigma(P)$ has the dimension of a mass (consistently with the Peskin-Schroeder notation [46] where $\Sigma(P)$ represents the self-energy correction to the bare electron mass), at variance with the case of Ref. [42], where $\Sigma(P)$ is dimensionless.

The minus components can again be written from the on-shell conditions, i.e.

$$P^- = \frac{m^2}{2P^+}\,, \quad k^- = \frac{\boldsymbol{k}_\perp^2}{2xP^+}\,, \quad l^- = \frac{\boldsymbol{k}_\perp^2 + m^2}{2(1-x)P^+}\,. \tag{3.68}$$

The δT_b term, instead, refers to the contact interaction with an instantaneously-propagating fermion, due to the contribution in V_1V_2 in light-front TOPT and corresponds to diagram (b) in Fig. 3.5. It is given by

$$\begin{aligned}\delta T_b \delta_{S,S'} &= \bar{u}_{S'}(P)\Sigma_b^{(2)}(P)u_S(P)\\ &= e^2\left(P^+\right)^2\int\frac{\mathrm{d}^2\boldsymbol{k}_\perp}{(2\pi)^3}\int_0^\infty \mathrm{d}x\,\frac{1}{x(1-x)\left(P^+\right)^2}\,\delta_{S,S'}\,.\end{aligned} \tag{3.69}$$

Finally, the third term δT_{c+d} refers to the contact interaction with an instantaneously-propagating photon, due to the contribution in V_1V_3 in light-front TOPT and corresponds to the sum of diagrams (c) and (d) in Fig. 3.5. It results into

$$\begin{aligned}&\delta T_{c+d}\delta_{S,S'} = \bar{u}_{S'}(P)\Sigma_{c+d}^{(2)}(P)u_S(P)\\ &= e^2\left(P^+\right)^2\int\frac{\mathrm{d}^2\boldsymbol{k}_\perp}{(2\pi)^3}\int_0^\infty \mathrm{d}x\,\frac{1}{\left(P^+\right)^2}\left[\frac{1}{(1-x)^2}-\frac{1}{(1+x)^2}\right]\delta_{S,S'}\,.\end{aligned} \tag{3.70}$$

We now turn our attention to the covariant approach. As we discussed in the case of the vertex correction, the calculation in light-front quantization can effectively be performed by taking into account only diagram (a) in Fig. 3.5, disregarding the contributions from instantaneous interactions, and using the two-term expression for the photon propagator.
The Feynman rules for diagram (a) in Fig. 3.5 give

$$\begin{aligned}&-i\bar{u}_{S'}(P)\Sigma^{(2)}(P)\,u_S(P) = -\frac{e^2}{(2\pi)^4}\int \mathrm{d}^4k\,\bar{u}_{S'}(P)\gamma^\nu\frac{\not{l}+m}{l^2-m^2+i\epsilon}\gamma^\mu\frac{d_{\mu\nu}(k)}{k^2+i\epsilon}u_S(P)\\ &= -\frac{e^2}{(2\pi)^4}\int \mathrm{d}^4k\,\bar{u}_{S'}(P)\gamma^\nu\left(\frac{\tilde{\not{l}}+m}{l^2-m^2+i\epsilon}+\frac{\gamma^+}{2l^+}\right)\gamma^\mu\left[\frac{d_{\mu\nu}\left(\tilde{k}\right)}{k^2+i\epsilon}-\frac{n_\mu n_\nu}{\left(k^+\right)^2}\right]u_S(P)\,,\end{aligned} \tag{3.71}$$

where we split the momenta according to Eqs. (3.24a) and (3.24b); it is understood that $l = P - k$. One can rewrite $i\Sigma$ as the sum of the following four terms

$$\begin{aligned}&-i\bar{u}_{S'}(P)\Sigma_1^{(2)}(P)u_S(P)\left[\tilde{l},\tilde{k}\right]\\ &\qquad = -\frac{e^2}{(2\pi)^4}\int \mathrm{d}^4k\,\bar{u}_{S'}(P)\,\gamma^\nu\frac{\tilde{\not{l}}+m}{l^2-m^2+i\epsilon}\gamma^\mu\frac{d_{\mu\nu}\left(\tilde{k}\right)}{k^2+i\epsilon}u_S(P)\,,\end{aligned} \tag{3.72a}$$

$$-i\bar{u}_{S'}(P)\Sigma_2^{(2)}(P)u_S(P)\left[\hat{l},\tilde{k}\right] = -\frac{e^2}{(2\pi)^4}\int \mathrm{d}^4k\,\bar{u}_{S'}(P)\,\gamma^\nu\frac{\gamma^+}{2l^+}\gamma^\mu\frac{d_{\mu\nu}\left(\tilde{k}\right)}{k^2+i\epsilon}u_S(P)\,, \tag{3.72b}$$

$$-i\bar{u}_{S'}(P)\Sigma_3^{(2)}(P)u_S(P)\left[\tilde{l},\hat{k}\right] = \frac{e^2}{(2\pi)^4}\int \mathrm{d}^4k\,\bar{u}_{S'}(P)\,\gamma^\nu\frac{\tilde{\not{l}}+m}{l^2-m^2+i\epsilon}\gamma^\mu\frac{n_\mu n_\nu}{(k^+)^2}u_S(P)\ , \tag{3.72c}$$

$$i\bar{u}_{S'}(P)\Sigma_4^{(2)}(P)u_S(P)\left[\hat{l},\hat{k}\right] = \frac{e^2}{(2\pi)^4}\int \mathrm{d}^4k\,\bar{u}_{S'}(P)\,\gamma^\nu\gamma^+\gamma^\mu\frac{n_\mu n_\nu}{(k^+)^2}u_S(P)\ . \tag{3.72d}$$

The contribution from Σ_4 in Eq. (3.72d) is vanishing due to the structure of Dirac matrices. For the remaining contributions, we proceed as outlined in the previous section and perform the integration over k^- by residues. The first term in Eq. (3.72a) becomes

$$\begin{aligned}&-i\bar{u}_{S'}(P)\Sigma_1^{(2)}(P)u_S(P)\\ &= -P^+\frac{ie^2}{2(2\pi)^3}\int_0^1\mathrm{d}x\int\mathrm{d}^2\boldsymbol{k}_\perp\,\bar{u}_{S'}(P)\frac{\gamma^\nu(\tilde{\not{k}}+m)\gamma^\mu d_{\mu\nu}(\tilde{q})}{P^+\left[\boldsymbol{k}_\perp^2+x^2m^2\right]}u_S(P)\ .\end{aligned} \tag{3.73}$$

It exactly coincides with Eq. (3.67), via the conditions (3.68). The terms in Eqs. (3.72b) and (3.72c) are explicitly evaluated in Appendix A. Here we report only the final results given by

$$\bar{u}_{S'}(P)\Sigma_2^{(2)}(P)u_S(P) = \frac{e^2}{(2\pi)^3}\int\mathrm{d}^2\boldsymbol{k}_\perp\int_0^\infty\mathrm{d}x\,\frac{1}{x(1-x)}\delta_{S,S'}\ , \tag{3.74}$$

$$\bar{u}_{S'}(P)\Sigma_3^{(2)}(P)u_S(P) = \frac{e^2}{(2\pi)^3}\int\mathrm{d}^2\boldsymbol{k}_\perp\int_0^\infty\mathrm{d}x\left[\frac{1}{(1-x)^2}-\frac{1}{(1+x)^2}\right]\delta_{S,S'}\ . \tag{3.75}$$

By comparing these expressions with Eqs. (3.69) and (3.70), we can conclude that our calculation in the covariant approach perfectly reproduces the light-front TOPT results.

We remark again that this result is in contrast with what is claimed in Ref. [35], where the equivalence with the light-front TOPT result, however, is actually not achieved; this is again due to the fact that in Eq. (58) of Ref. [35] one should evaluate $d_{\mu\nu}(k)$ at the pole position.

3.4.2 Photon self-energy

We finally discuss the photon self-energy corrections, corresponding to the diagrams in Fig. 3.6 in light-front TOPT at order α. Again following Ref. [42], we denote with T'_{PP} the α-order amplitude of the transition matrix T in Eq. (3.63) between free-photon states with momentum and helicity (P,λ) and (P',λ'). We can define the self-energy correction to the fictitious photon mass as

$$\delta\mu^2\delta_{\lambda,\lambda'} = 2P^+T'_{PP}\ , \tag{3.76}$$

and identify a tensor $\Pi^{\mu\nu}$ through the identity

$$\delta\mu^2\delta_{\lambda,\lambda'} = \varepsilon^*_{\lambda',\mu}(P)\Pi^{\mu\nu}(P)\varepsilon_{\lambda,\nu}(P)\ . \tag{3.77}$$

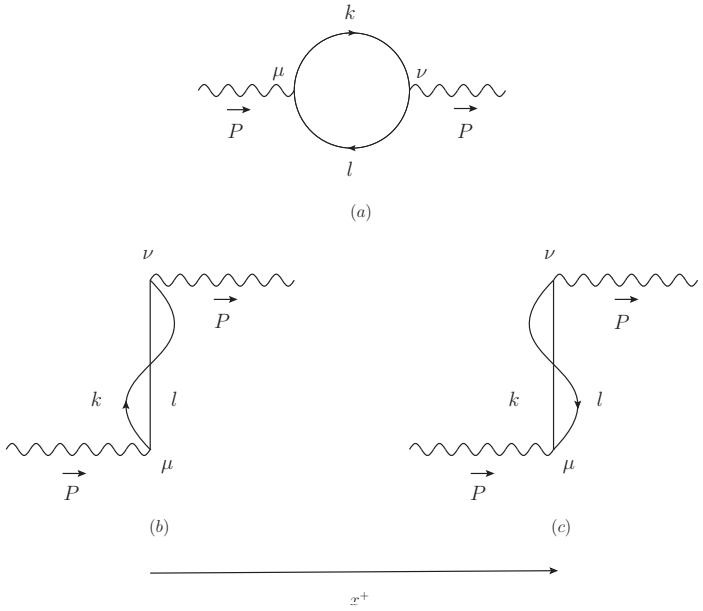

Figure 3.6: Diagrams for the photon self-energy in light-front TOPT at one-loop order, including the instantaneous exchange of electrons [(b)] and positrons [(c)].

It is important to notice that, in the above expressions, we need to consider only the physical degrees of freedom since both the incoming and the outgoing photons are real; therefore $\lambda, \lambda' = 1, 2$.
We are then able to separate $\delta\mu^2$ (and consequently $\Pi^{\mu\nu}$) into two contributions. The first one arises from a contribution in $(V_1)^2$ in the (light-front time-ordered) perturbative expansion, and corresponds to diagram (a) of Fig. 3.6:

$$\begin{aligned}\delta\mu_a^2\delta_{\lambda,\lambda'} &= \varepsilon^*_{\lambda',\mu}(P)\Pi_a^{\mu\nu}(P)\varepsilon_{\lambda,\nu}(P) \\ &= 2e^2P^+\int\frac{\mathrm{d}^2\boldsymbol{k}_\perp}{(4\pi)^3}\int_0^1\mathrm{d}x\,\frac{1}{x(1-x)\,(P^+)^2}\,\frac{\mathrm{Tr}\left[\not{\varepsilon}^*_{\lambda'}(P)(\tilde{\not{k}}+m)\not{\varepsilon}_\lambda(P)(\tilde{\not{l}}-m)\right]}{P^- - k^- - l^-}\,.\end{aligned} \tag{3.78}$$

The on-shell conditions now give

$$P^- = 0\,,\quad k^- = \frac{\boldsymbol{k}_\perp^2+m^2}{2xP^+}\,,\quad l^- = \frac{\boldsymbol{k}_\perp^2+m^2}{2(1-x)P^+}\,. \tag{3.79}$$

The second contribution is due to the V_1V_2 interaction terms, corresponding to the sum of diagram (b) and (c) in Fig. 3.6, and turns out to be [42]

$$\delta\mu^2_{b+c}\delta_{\lambda,\lambda'} = \varepsilon^*_{\lambda',\mu}(P)\Pi^{\mu\nu}_{b+c}(P)\varepsilon_{\lambda,\nu}(P) = e^2\int\frac{\mathrm{d}^2\boldsymbol{k}_\perp}{(2\pi)^3}\int_0^\infty\mathrm{d}x\left[\frac{1}{1-x}-\frac{1}{1+x}\right]\delta_{\lambda,\lambda'}\,. \tag{3.80}$$

In the covariant approach, we proceed as discussed in Sections 3.3.2 and 3.4.1 and apply the Feynman rules for the calculation of the diagram (a) in Fig. 3.6:

$$i\varepsilon^*_{\lambda',\nu}(P)\Pi^{\mu\nu}(P)\varepsilon_{\lambda,\mu}(P) = \frac{e^2}{(2\pi)^4}$$

$$\times \int \mathrm{d}^4k\, \varepsilon^*_{\lambda',\nu}(P) \frac{\mathrm{Tr}\left[\gamma^\nu(-\not{l}+m)\gamma^\mu(\not{k}+m)\right]}{\left(l^2-m^2+i\epsilon\right)\left(k^2-m^2+i\epsilon\right)} \varepsilon_{\lambda,\mu}(P)\,. \tag{3.81}$$

By using the decompositions for the momenta in Eqs. (3.24a) and (3.24b), we can identify the following four contributions to the self-energy:

$$i\varepsilon^*_{\lambda',\nu}(P)\Pi_1^{\mu\nu}(P)\varepsilon_{\lambda,\mu}(P)\left[\tilde{k},\tilde{l}\right] = -\frac{e^2}{(2\pi)^4}\int \mathrm{d}^4k_1\, \varepsilon^*_{\lambda',\nu}(P) \frac{\mathrm{Tr}\left[\gamma^\nu\left(\tilde{\not{l}}-m\right)\gamma^\mu\left(\tilde{\not{k}}+m\right)\right]}{\left(l^2-m^2+i\epsilon\right)\left(k^2-m^2+i\epsilon\right)} \varepsilon_{\lambda,\mu}(P)\,, \tag{3.82}$$

$$i\varepsilon^*_{\lambda',\nu}(P)\Pi_2^{\mu\nu}(P)\varepsilon_{\lambda,\mu}(P)\left[\hat{k},\tilde{l}\right] = -\frac{e^2}{(2\pi)^4}\int \mathrm{d}^4k\, \varepsilon^*_{\lambda',\nu}(P) \frac{\mathrm{Tr}\left[\gamma^\nu\left(\tilde{\not{l}}-m\right)\gamma^\mu\gamma^+\right]}{2k^+\left(l^2-m^2+i\epsilon\right)} \varepsilon_{\lambda,\mu}(P)\,, \tag{3.83}$$

$$i\varepsilon^*_{\lambda',\nu}(P)\Pi_3^{\mu\nu}(P)\varepsilon_{\lambda,\mu}(P)\left[\tilde{k},\hat{l}\right] = \frac{e^2}{(2\pi)^4}\int \mathrm{d}^4k\, \varepsilon^*_{\lambda',\nu}(P) \frac{\mathrm{Tr}\left[\gamma^\nu\gamma^+\gamma^\mu\left(\tilde{\not{k}}+m\right)\right]}{2l^+\left(k^2-m^2+i\epsilon\right)} \varepsilon_{\lambda,\mu}(P)\,, \tag{3.84}$$

$$i\varepsilon^*_{\lambda',\nu}(P)\Pi_4^{\mu\nu}(P)\varepsilon_{\lambda,\mu}(P)\left[\hat{k},\hat{l}\right] = \frac{e^2}{(2\pi)^4}\int \mathrm{d}^4k\, \frac{1}{2l^+}\frac{1}{2k^+}\varepsilon^*_{\lambda',\nu}(P)\mathrm{Tr}\left[\gamma^\nu\gamma^+\gamma^\mu\gamma^+\right]\varepsilon_{\lambda,\mu}(P)\,. \tag{3.85}$$

We can further evaluate $\Pi_1^{\mu\nu}$ in Eq. (3.82) by following the same procedure adopted for the electron self-energy, with the on-shell condition $P^2 = 0$; we obtain

$$i\varepsilon^*_{\lambda',\nu}(P)\Pi_1^{\mu\nu}(P)\varepsilon_{\lambda,\mu}(P)\left[\tilde{k},\tilde{l}\right] = -\frac{ie^2}{2(2\pi)^3}\int_0^1 \mathrm{d}x \int \mathrm{d}^2\boldsymbol{k}_\perp \frac{\mathrm{Tr}\left[\not{\varepsilon}_\lambda(P)\left(\tilde{\not{k}}+m\right)\not{\varepsilon}^*_{\lambda'}(P)\left(\tilde{\not{l}}-m\right)\right]}{\boldsymbol{k}_\perp^2+m^2}\,. \tag{3.86}$$

As we show explicitly in Appendix A, the contributions from $\Pi_2^{\mu\nu}$ and $\Pi_3^{\mu\nu}$ in Eqs. (3.83) and (3.84) can be rewritten as

$$i\varepsilon^*_{\lambda',\nu}(P)\Pi_2^{\mu\nu}(P)\varepsilon_{\lambda,\mu}(P)\left[\hat{k},\tilde{l}\right] = -\frac{ie^2}{2\left(2\pi\right)^3}\int \mathrm{d}^2\boldsymbol{k}_\perp \int \mathrm{d}x\, \frac{1}{x}\mathrm{sgn}\left(1-x\right)\delta_{\lambda,\lambda'}\,, \tag{3.87}$$

$$i\varepsilon^*_{\lambda',\nu}(P)\Pi_3^{\mu\nu}(P)\varepsilon_{\lambda,\mu}(P)\left[\tilde{k},\hat{l}\right] = \frac{ie^2}{2\left(2\pi\right)^3}\int \mathrm{d}^2\boldsymbol{k}_\perp \int dx\, \frac{1}{1-x}\mathrm{sgn}\left(x\right)\delta_{\lambda,\lambda'}\,. \tag{3.88}$$

Finally, the contribution from $\Pi_4^{\mu\nu}$ in (3.85) is vanishing. This follows from

$$\mathrm{Tr}\left[\gamma^\nu\gamma^+\gamma^\nu\gamma^+\right] = 2g^{\nu+}g^{\mu+} \tag{3.89}$$

and the contraction with the polarization vectors in light-cone gauge. If we use the substitution $x \to 1 - x'$ in Eq. (3.87) and then sum it with Eq. (3.88), it is straightforward to check that

$$i\varepsilon^*_{\lambda',\nu}(P)\left[\Pi_2^{\mu\nu} + \Pi_3^{\mu\nu}\right]\varepsilon_{\lambda,\mu}(P) = \frac{e^2}{(2\pi)^3}\int \mathrm{d}^2\boldsymbol{k}_\perp \left[\int_0^\infty \mathrm{d}x\,\frac{1}{1-x} - \int_{-\infty}^0 \mathrm{d}x\,\frac{1}{1-x}\right]$$
$$= \frac{e^2}{(2\pi)^3}\int \mathrm{d}^2\boldsymbol{k}_\perp \int_0^\infty \mathrm{d}x\left(\frac{1}{1-x} - \frac{1}{1+x}\right). \quad (3.90)$$

The final outcome of the covariant calculation is therefore given by Eqs. (3.82) and (3.90). If we compare them with the TOPT results (3.78) and (3.80), we once again find perfect agreement between the two approaches. This argument concludes the proof of the equivalence at one-loop level.

3.5 Summary

In this Chapter we addressed the controversy of which form should be used for the gauge-field propagator in light-cone gauge, due to the fact that in the literature two different expressions appear, namely Eqs. (3.1) and (3.2). This issue becomes particularly relevant when proving that the covariant formulation of quantum field theory in light-front coordinates can be matched with old-fashioned Time-Ordered Perturbation Theory in light-front quantization.
Our point of emphasis is that one should not wonder which of the two is the *correct* form, as done e.g. in Ref. [35, 41, 47]: the photon propagator obtained from the electromagnetic-field Lagrangian is the one given in Eq. (3.2) and contains the sum of three terms, but the third term is exactly canceled by the contribution from diagram containing instantaneous photons. Both forms, then, are actually correct, as long as one deals properly with the instantaneous interactions.
We proved the equivalence between covariant approach and light-front TOPT at one-loop level in QED by assuming that the covariant calculation must be performed with the two-term photon propagator and neglecting, at the same time, the contributions from diagrams with instantaneously-propagating particles. By applying the ordinary technique of integration by residues over the light-front energy, we were able to recover all the time-ordered diagrams that emerge in light-front QED, including the ones with instantaneous photon and fermions. This result is in contrast with the findings of Ref. [35], where it is claimed that the three-term propagator in the covariant approach is needed in order to match the contribution from instantaneously-propagating photons in TOPT.
A more general extension of this work could be achieved by interpolating the light-front and instant-form coordinates, as done in [12] for the scalar QED case, and working in a generic axial gauge $n_\mu A^\mu = 0$.

Chapter 4

QCD distribution functions

Our current knowledge of the internal structure of nucleons relies on the information encoded in partonic correlation functions, parametrized in terms of various types of distribution functions [48–52]. These objects provide a multidimensional description of the nucleon in terms of its elementary constituents both in momentum and position space. Although here we present them in the context of QCD, these distributions can be actually considered as instruments used to investigate the internal structure of any composite particle.

4.1 Generalized parton correlator

Let us consider a process in which a nucleon of mass M, with initial momentum p and light-front helicity Λ, interacts with a probe particle, ending up in a state with momentum p' and helicity Λ'. The following on-shell conditions must be satisfied:

$$p^2 = p'^2 = M^2 \,. \tag{4.1}$$

It is convenient to introduce two new kinematic variables

$$P = \frac{p + p'}{2} \,, \qquad \Delta = p' - p \,, \tag{4.2}$$

representing respectively the average momentum and the momentum transfer between the initial and final states. Notice that the on-shell conditions (4.1) for the initial and final states are equivalent to

$$P^2 = M^2 - \frac{\Delta^2}{4} \,, \tag{4.3}$$

$$P \cdot \Delta = 0 \,. \tag{4.4}$$

In the parton model assumption, the interaction takes place between the probe and one of the nucleon's partons, referred to as *active parton*. In this Chapter

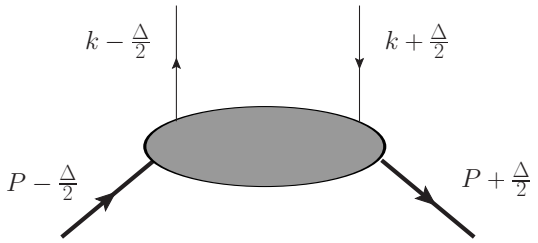

Figure 4.1: Kinematics for the Generalized Parton Correlator.

we focus on the case where the active parton is a quark. We denote its initial and final momenta with $k - \frac{\Delta}{2}$ and $k + \frac{\Delta}{2}$, respectively. The situation is represented schematically in Fig. 4.1.

Related to such processes is the most general, fully unintegrated quark-quark correlator function between hadron states in light-front helicity basis [49, 53]

$$[\Phi_{\Lambda,\Lambda'}]_{ij}(k,\Delta;P) = \int \frac{\mathrm{d}^4 z}{(2\pi)^4} e^{ik\cdot z} \langle p',\Lambda'|\bar{\psi}_j(0)\,\mathcal{U}_{(0,z)}\,\psi_i(z)|p,\Lambda\rangle \,. \tag{4.5}$$

Here $\psi_i(x)$ is a quark field carrying a Dirac index i, while $\mathcal{U}_{(0,z)}$ is a gauge link operator (see Section 4.1.1). The correlator (4.5) is a six-dimensional object depending on the variables k and Δ, whereas P, Λ and Λ' can be considered as parameters.
It is useful to introduce also the trace of the correlator (4.5) multiplied by an operator Γ generated by the Dirac space basis $\mathcal{D} = \{\mathbb{1}, \gamma^\mu, \gamma_5, \gamma^\mu\gamma_5, i\sigma^{\mu\nu}\}$:

$$\begin{aligned}\Phi^{[\Gamma]}_{\Lambda,\Lambda'}(k,\Delta;P) &= \frac{1}{2}\mathrm{Tr}\left[\Phi_{\Lambda,\Lambda'}(k,\Delta;P)\Gamma\right] \\ &= \frac{1}{2}\int \frac{\mathrm{d}^4 z}{(2\pi)^4} e^{ik\cdot z} \langle p',\Lambda'|\bar{\psi}_j(0)\,\mathcal{U}_{(0,z)}\,\Gamma_{ji}\psi_i(z)|p,\Lambda\rangle \,.\end{aligned} \tag{4.6}$$

In the following we will work in the leading-twist[1] approximation and consider only $\Gamma = \gamma^+, \gamma^+\gamma_5, i\sigma^{j+}\gamma_5$. These Dirac matrices project on different spin configurations of the active parton in the initial and final states, allowing one to account for contributions to the correlator from various helicity-transforming processes.
The quark-quark correlator in QCD cannot be calculated further analytically: this is due to the non-perturbative nature of strong interactions that is encoded in the hadron states. We can, however, parametrize the correlator in terms of measurable quantities and reconstruct its analytical structure adopting phenomenological methods. The most generic decomposition of the fully-unintegrated quark-quark correlator (4.6) in terms of complex-valued functions, called Generalized Parton Correlation Functions (GPCFs) $X(k,\Delta;P)$,

[1] In this work we adopt the working definition of *twist* t proposed by Jaffe [54]. The leading twist corresponds to $t = 2$.

was derived in Ref. [49] for all the elements of the Dirac basis $\mathcal{D}$. In a similar fashion, one can formally define different distribution functions by parametrizing proper limits of the so-called Generalized Transverse-Momentum Dependent (GTMD) correlator, namely the integral over k^- of the generalized parton correlator (4.5):

$$\begin{aligned}\Phi_{\Lambda,\Lambda'}(x,\boldsymbol{k}_\perp,\Delta;P) &= \int \mathrm{d}k^-\,\Phi_{\Lambda,\Lambda'}(k,\Delta;P) \\ &= \int \frac{\mathrm{d}z^-\mathrm{d}^2\boldsymbol{z}_\perp}{(2\pi)^3}\, e^{i(k^+z^- - \boldsymbol{z}_\perp\cdot\boldsymbol{k}_\perp)} \langle p',\Lambda'|\bar{\psi}(0)\,\mathcal{U}_{(0,z)}\,\psi(z)|p,\Lambda\rangle\Big|_{z^+=0}\,,\end{aligned} \tag{4.7}$$

where $x = k^+/P^+$ is the (average) longitudinal momentum fraction carried by the active parton. In the following sections we will show specific examples for cases of our interest.
We finally remark that, although the generalized correlator (4.7) is defined in six-dimensional momentum space, we can gain information also about the position of the partons inside the nucleon by Fourier transforming the momentum transfer to position space. In particular, for the interpretation of correlation functions in position space as quasi-probability distributions we will restrict to the impact-parameter space of coordinates $\boldsymbol{b}_\perp$, introduced in Section 2.3.1. We will come back to this point in Section 4.4.1.

4.1.1 Gauge link

A bi-local product of fermion-field operators at two different positions x and y in spacetime is not gauge-invariant: consider an Abelian, local transformation

$$\psi(x) \mapsto e^{-ig\alpha(x)}\psi(x)\,, \tag{4.8}$$

where g is the coupling constant between the fermion and the gauge field $A^\mu(x)$. Consequently, we have

$$\bar{\psi}(x)\psi(y) \mapsto \bar{\psi}(x)\psi(y)\, e^{ig[\alpha(x)-\alpha(y)]}\,. \tag{4.9}$$

In order to restore gauge-invariance, the following *gauge-link* (or *Wilson line*) operator is included in the definition of the correlator (4.5) [55–57]:

$$\mathcal{U}_{(x,y)} = \mathcal{P}\exp\left[ig\int_x^y \mathrm{d}\xi^\mu A_\mu(\xi)\right]. \tag{4.10}$$

The symbol $\mathcal{P}$ denotes path ordering of the integral from x to y and is actually needed only when we deal with non-Abelian gauge fields.
We will illustrate the physical interpretation of the gauge link in the QED case in Section 5.3.1. Here it is worth to stress, however, that the insertion of a Wilson line introduces a dependence of the correlator on the path chosen to perform the integration from $x = 0$ to $y = z$. We now briefly describe two

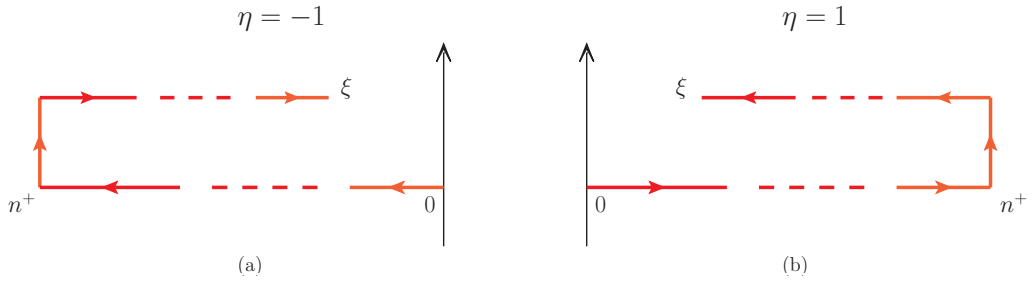

Figure 4.2: Different Wilson lines connecting the points 0 and z. Dashed lines indicate that integration along the n^+ direction is meant to be taken up to infinity. Path (a) [respectively, path (b)] is a past-pointing (future-pointing) Wilson line corresponding to the value $\eta = -1$ ($\eta = 1$).

possible path configurations associated to the processes of Semi-Inclusive Deep Inelastic Scattering (SIDIS) and Drell-Yan [48]. More complicated gauge-link structures arise for different processes (see Ref. [57]).
Let us consider the integrated correlator (4.7). Since we are working with $z^+ = 0$, we need to specify a path in the z^--$\boldsymbol{z}_\perp$ plane. By defining the *longitudinal gauge link*

$$\mathcal{U}^L(x^-, y^-; \boldsymbol{\xi}_\perp) = \mathcal{P} \exp\left[ig \int_{x^-}^{y^-} d\xi^- \, A^+(0, \xi^-, \boldsymbol{\xi}_\perp) \right] \tag{4.11}$$

and the *transverse gauge link*

$$\mathcal{U}^\perp(\boldsymbol{x}_\perp, \boldsymbol{y}_\perp; \xi^-) = \mathcal{P} \exp\left[-ig \int_{\boldsymbol{x}_\perp}^{\boldsymbol{y}_\perp} d^2\boldsymbol{\xi}_\perp \cdot \boldsymbol{A}_\perp(0, \xi^-, \boldsymbol{\xi}_\perp) \right] , \tag{4.12}$$

the physics of the SIDIS and Drell-Yan processes will lead us, respectively, to a *future-pointing* Wilson line $\mathcal{U}^{\eta=1}_{(0,z)}$ or a *past-pointing* Wilson line $\mathcal{U}^{\eta=-1}_{(0,z)}$. They are given by

$$\mathcal{U}^{\eta=\pm1}_{(0,z)} = \mathcal{U}_{(0,\pm\infty)} \mathcal{U}_{(\pm\infty,z)} \, , \tag{4.13}$$

where

$$\mathcal{U}_{(0,\pm\infty)} = \mathcal{U}^L(0^-, \pm\infty^-; \boldsymbol{0}_\perp) \mathcal{U}^\perp(\boldsymbol{0}_\perp, \boldsymbol{\infty}_\perp; \pm\infty^-) \, , \tag{4.14}$$

$$\mathcal{U}_{(\pm\infty,\xi)} = \mathcal{U}^\perp(\boldsymbol{\infty}_\perp, \boldsymbol{\xi}_\perp; \pm\infty^-) \mathcal{U}^L(\pm\infty^-, \xi^-; \boldsymbol{\xi}_\perp) \, . \tag{4.15}$$

The two possible choices possibilities are depicted in Fig. 4.2 and are related respectively to the SIDIS and Drell-Yan processes.
The variable $\eta = \pm 1$ has been introduced in order to explicitly keep track of the dependence of the correlator on the integration path, through the notation $\Phi_{\Lambda,\Lambda'}(k, \Delta; P|\eta)$ in light-front helicity basis. The GPCFs will in turn be denoted with $X(k, \Delta; P|\eta)$. Due to the properties of parity, hermiticity and time-reversal invariance of the correlator, the trace (4.6) must satisfy [49]:

$$\Phi^{[\Gamma]}_{\Lambda,\Lambda'}(k, \Delta; P|\eta) = \Phi^{[\gamma^0\Gamma\gamma^0]}_{\Lambda_P,\Lambda'_P}\left(\tilde{k}, \tilde{\Delta}; \tilde{P}\,|\eta\right) \tag{4.16}$$

$$\left[\Phi^{[\Gamma]}_{\Lambda,\Lambda'}(k,\Delta;P|\eta)\right]^* = \Phi^{[\gamma^0\Gamma^\dagger\gamma^0]}_{\Lambda',\Lambda}(k,-\Delta;P\,|\eta)\;, \tag{4.17}$$

$$\left[\Phi^{[\Gamma]}_{\Lambda',\Lambda}(k,\Delta;P|\eta)\right]^* = \Phi^{[(-i\gamma_5 C)\Gamma^*(-i\gamma_5 C)]}_{\Lambda_T,\Lambda'_T}\left(\tilde{k},\tilde{\Delta};\tilde{P}\,|-\eta\right)\;, \tag{4.18}$$

where $C = i\gamma^2\gamma^0$, $\tilde{P}^\mu = (P^0,-\boldsymbol{P})$ (and similarly for the other four-vectors), while Λ_P and Λ_T denote the parity-reversed and time-reversed helicities, respectively. In particular, the relations (4.17)-(4.18) imply for all GPCFs:

$$[X(k,\Delta;P,|\eta)]^* = \pm X(k,-\Delta;P|\eta)\;, \tag{4.19}$$

$$[X(k,\Delta;P,|\eta)]^* = X(k,\Delta;P|-\eta)\;. \tag{4.20}$$

Since η can only take the values ±1, it follows from Eqs. (4.19) and (4.20) that only the imaginary part of X depends on η, allowing us to write the decomposition:

$$X(k,\Delta;P|\eta) = X^e(k,\Delta;P) + iX^o(k,\Delta;P|\eta)\;, \tag{4.21}$$

with

$$X^o(k,\Delta;P|\eta) = -X^o(k,\Delta;P|-\eta)\;. \tag{4.22}$$

The real and imaginary parts of the GPCFs X are called respectively the *T-even* part X^e and the *T-odd* part X^o. Eq. (4.22), in particular, tells us that the T-odd part changes sign if we flip the direction of the Wilson line.

In the remaining of the present Chapter, for simplicity, it will always be assumed that the Wilson line is an identity, namely $U_{(0,z)} = \mathbb{1}$. This is, in fact, not a drastic requirement if we assume to work in the light-cone gauge: Eq. (4.11) implies that the longitudinal gauge link does not contribute when $A^+ = 0$, and consequently only the path in the transverse direction survives. Nevertheless, the transverse gauge link cannot be completely neglected as some subtleties concerning its contribution still arise, as we will discuss in Section 5.3.4.

4.2 Landscape of distribution functions

The landscape of the available distribution functions, as well as the links connecting them, is pictured in Fig. 4.3 [52].
As we mentioned at the end of Section 4.1, different distribution functions can be formally defined by parametrizing proper limits of the k^--integrated correlator (4.7); we will show specific examples in the following sections. It follows that the most general distributions that is possible to consider will show the full dependence on the six variables x, $\boldsymbol{k}_\perp$, Δ^+ and $\boldsymbol{\Delta}_\perp$. This is actually the case for the Generalized Transverse-Momentum Dependent Distribution functions (GTMDs) [28, 52, 58, 59]. For $\Delta^+ = 0$ they can be related, via Fourier transform from $\boldsymbol{\Delta}_\perp$ to $\boldsymbol{b}_\perp$, to the so-called Wigner distributions [60, 61], namely the quantum-mechanical analog of the classical phase-space distributions in five

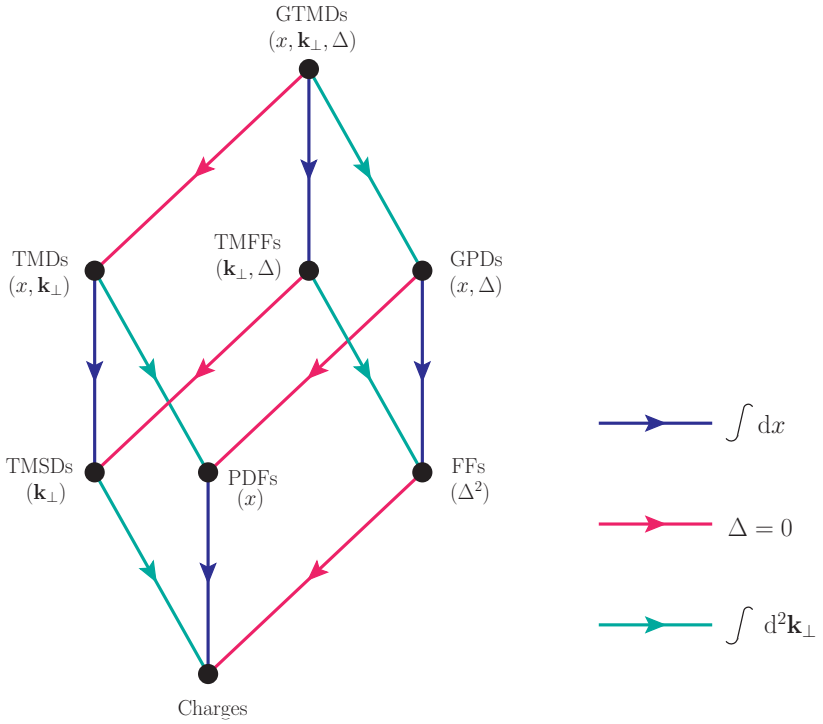

Figure 4.3: Links among different distribution functions. The blue, red and green lines indicate the limits in which we integrate over x, take $\Delta = 0$ and integrate over $\boldsymbol{k}_\perp$, respectively.

dimensions. We address GTMDs and Wigner distributions in greater detail in Section 4.5 and consider their application in QED in Chapter 5.

GTMDs are sometimes called "mother" distributions, since all the other functions can be recovered from them by taking proper limits, as one can see in Fig. 4.3. Of particular interest are the Transverse-Momentum Dependent distribution functions (TMDs), obtained from GTMDs in the limit $\Delta = 0$, and the Generalized Parton Distributions (GPDs) that correspond to the integral of GTMDs over the transverse momentum $\boldsymbol{k}_\perp$ of the active parton. TMDs [48, 62–64] depend on $(x, \boldsymbol{k}_\perp)$ and thus offer a three-dimensional picture of the nucleon in momentum space. We refer to Section 4.3 for more details and to Chapter 5 for their calculation in the QED case. GPDs [65–68] depend on (x, Δ) but can as well be Fourier-transformed to the $(x, \boldsymbol{b}_\perp)$ space (again with $\Delta^+ = 0$), providing a simultaneous description in momentum and position space (see Section 4.4). This allows one to gather information about the Angular Momentum of partons, as we will show in Chapter 6. It should be emphasized that there is no direct connection between TMDs and GPDs, as one can appreciate also from Fig. 4.3. Both TMDs and GPDs reduce to the well-known collinear Parton Distribution Functions (PDFs) in their respective limits of integration over $\boldsymbol{k}_\perp$ and $\Delta = 0$. Moreover, by integrating GPDs over the longitudinal momentum fraction x we end up with the electroweak Form Factors (FFs). PDFs and Form Factors in turn reduce to global properties of nucleons, labeled as "charges" in Fig. 4.3, which are the quantities that

one measures by looking at the proton as a whole. The remaining distributions that complete the landscape are the Transverse-Momentum Dependent Form Factors (TMFFs) and Transverse-Momentum Dependent Spin Densities (TMSDs); they are more of academic interest.

4.3 Transverse-Momentum Dependent parton distributions

We devote this Section to the theoretical definition of Transverse-Momentum Dependent parton distributions (TMDs); for the purpose of this work, we do not enter either experimental or phenomenological issues, for which we refer e.g. to Refs. [62, 63, 69].
Our starting point is the transverse-momentum dependent correlator [53, 62, 64]:

$$\begin{aligned}\Phi_{\Lambda,\Lambda'}(x,\boldsymbol{k}_\perp;P) &= \int \mathrm{d}k^-\,\Phi_{\Lambda,\Lambda'}(k;P) \\ &= \int \frac{\mathrm{d}z^-\mathrm{d}^2\boldsymbol{z}_\perp}{(2\pi)^3} e^{ik\cdot z}\langle P,\Lambda'|\bar\psi(0)\,\psi(z)|P,\Lambda\rangle\Big|_{z^+=0}\,. \end{aligned} \tag{4.23}$$

It can be obtained as the limit for $\Delta = 0$ of the k^--integrated Generalized Parton Correlator given in Eq. (4.7), namely

$$\Phi_{\Lambda,\Lambda'}(x,\boldsymbol{k}_\perp;P) = \Phi_{\Lambda,\Lambda'}(x,\boldsymbol{k}_\perp,\Delta=0;P)\,. \tag{4.24}$$

It is convenient to rewrite the correlator (4.24) in the spin basis as [70]

$$\Phi_S(x,\boldsymbol{k}_\perp;P) = \int \frac{\mathrm{d}z^-\mathrm{d}^2\boldsymbol{z}_\perp}{(2\pi)^3} e^{ik\cdot z}\langle P,S|\bar\psi(0)\,\psi(z)|P,S\rangle\Big|_{z^+=0}\,. \tag{4.25}$$

The four-momentum P and covariant spin four-vector S satisfy $P^2 = M^2$, $S^2 = -1$ and $P\cdot S = 0$. In the hadron frame, we have [71, 72]

$$S^\mu = \left(s_z\frac{P^+}{M}, -s_z\frac{M}{2P^+}, \boldsymbol{s}_\perp\right)\,, \tag{4.26}$$

where $(\boldsymbol{s}_\perp, s_z)$ is the spin three-vector in the rest frame and $\boldsymbol{s}^2 = 1$. The relation between the correlators in the spin and light-front helicity basis is:

$$\begin{aligned}\Phi_S(x,\boldsymbol{k}_\perp;P) = &\frac{1+s_z}{2}\Phi_{+,+}(x,\boldsymbol{k}_\perp;P) + \frac{1-s_z}{2}\Phi_{-,-}(x,\boldsymbol{k}_\perp;P) \\ &+ \frac{s_x - is_y}{2}\Phi_{+,-}(x,\boldsymbol{k}_\perp;P) + \frac{s_x+is_y}{2}\Phi_{-,+}(x,\boldsymbol{k}_\perp;P)\,. \end{aligned} \tag{4.27}$$

The diagrammatic representation of the correlator (4.27) is shown in Fig. 4.4. It corresponds to the QCD handbag diagram (see Appendix B.1), "amputated" of the virtual photon lines. We will see in Section 5.3.2 how the correlator can

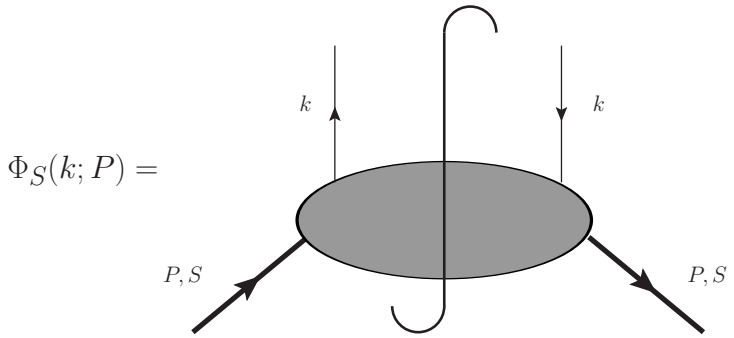

Figure 4.4: Diagrammatic representation of the quark-quark correlator for $\Delta = 0$.

be evaluated in the framework of QED, by applying the usual Feynman rules.

The leading-twist parametrization of the TMD correlator (4.23), written in the Dirac basis $\mathcal{D}$, is then [53, 70]

$$\begin{aligned}\Phi =&\frac{1}{2}\Bigg[\not{n}_+ f_1 - \frac{\epsilon^{ij}k_\perp^i s_\perp^j}{M}\not{n}_+ f_{1T}^\perp + s_z\gamma^5\not{n}_+ g_{1L} + \frac{\boldsymbol{k}_\perp\cdot\boldsymbol{s}_\perp}{M}\gamma^5\not{n}_+ g_{1T} + \frac{[\not{s}_\perp,\not{n}_+]}{2}\gamma^5 h_{1T}\\ &+\Lambda\frac{[\not{k}_\perp,\not{n}_+]}{2M}\gamma^5 h_{1L}^\perp + \frac{\boldsymbol{k}_\perp\cdot\boldsymbol{s}_\perp[\not{k}_\perp,\not{n}_+]}{2M^2}\gamma^5 h_{1T}^\perp + \frac{i[\not{k}_\perp,\not{n}_+]}{2M}h_1^\perp\Bigg],\end{aligned} \tag{4.28}$$

where $n_+ = (1, 0, \mathbf{0}_\perp)$. Eq. (4.28) introduces the leading-twist TMDs f_1, $f_{1T}^\perp$, g_{1L}, g_{1T}, h_{1T}, $h_{1L}^\perp$, $h_{1T}^\perp$, $h_1^\perp$ depending on $(x, \boldsymbol{k}_\perp^2)$. The notation used for labeling the TMDs is related to the polarizations of the parent hadron and of the active quark. Here we adopt the convention proposed in Ref. [62]: letters L and T refer, respectively, to the situation where the spin of the hadron is along the longitudinal direction [$\boldsymbol{s} = (\mathbf{0}_\perp, s_z)$] and in the transverse plane [$\boldsymbol{s} = (\boldsymbol{s}_\perp, 0)$]. Similarly, letters f, g and h refer to unpolarized (i.e. averaged over all polarizations), longitudinally-polarized and transversely-polarized active quark. The "$\perp$" symbols stands for an explicit dependence on transverse momenta with an uncontracted index.
The leading-twist Dirac-space projections of the TMD correlator, obtained by integrating Eq. (4.6), are rewritten in terms of combinations of TMDs as [62,64]

$$\Phi_S^{[\gamma^+]}(x,\boldsymbol{k}_\perp) = f_1(x,\boldsymbol{k}_\perp^2) - \frac{\epsilon^{ij}k_\perp^i s_\perp^j}{M}f_{1T}^\perp(x,\boldsymbol{k}_\perp^2)\,, \tag{4.29}$$

$$\Phi_S^{[\gamma^+\gamma_5]}(x,\boldsymbol{k}_\perp) = s_z g_{1L}(x,\boldsymbol{k}_\perp^2) + \frac{\boldsymbol{k}_\perp\cdot\boldsymbol{s}_\perp}{M}g_{1T}(x,\boldsymbol{k}_\perp^2)\,, \tag{4.30}$$

$$\begin{aligned}\Phi_S^{[i\sigma^{j+}\gamma_5]}(x,\boldsymbol{k}_\perp) =& s_\perp^j h_1(x,\boldsymbol{k}_\perp^2) + s_z\frac{k_\perp^j}{M}h_{1L}^\perp(x,\boldsymbol{k}_\perp^2)\\ &+ s_\perp^i\frac{2k_\perp^i k_\perp^j - \boldsymbol{k}_\perp^2\delta^{ij}}{2M^2}h_{1T}^\perp(x,\boldsymbol{k}_\perp^2) + \frac{\epsilon^{ji}k_\perp^i}{M}h_1^\perp(x,\boldsymbol{k}_\perp^2)\,,\end{aligned} \tag{4.31}$$

where

$$h_1(x,\boldsymbol{k}_\perp^2) = h_{1T}(x,\boldsymbol{k}_\perp^2) + \frac{\boldsymbol{k}_\perp^2}{2M^2}h_{1T}^\perp(x,\boldsymbol{k}_\perp^2)\,. \tag{4.32}$$

A final remark concerns the behavior of TMDs under time-reversal. According to the definition that we gave in Section 4.1, it is possible to identify two T-odd TMDs, namely the Boer-Mulders [73] function $h_1^\perp$ and the Sivers [74] function $f_{1T}^\perp$. The six remaining leading-twist TMDs are T-even.

4.4 Generalized Parton Distributions

In this section we address the definition of Generalized Parton Distributions (GPDs). Also in this case we focus only on the theoretical side; detailed reviews covering experimental issues can be found e.g. in Refs. [65, 67].
The relevant correlator for the GPD case is obtained by integrating the generalized parton correlator (4.5) over k^-, $\boldsymbol{k}_\perp$:

$$\begin{aligned}\Phi_{\Lambda,\Lambda'}(x,\Delta;P) &= \int \mathrm{d}k^-\,\mathrm{d}^2\boldsymbol{k}_\perp\,\Phi_{\Lambda,\Lambda'}(k,\Delta;P) \\ &= \int \frac{\mathrm{d}z^-}{2\pi}\,e^{ik^+z^-}\langle p',\Lambda'|\bar\psi(0)\,\psi(z)|p,\Lambda\rangle\Big|_{z^+=0,\,\boldsymbol{z}_\perp=\boldsymbol{0}_\perp}\,. \end{aligned} \tag{4.33}$$

Notice that in the above Equation we are taking the fermion fields at the same transverse position. This means that the previous expression remains valid as long as we work in the light-cone gauge (where the gauge link along the longitudinal direction coincides with the identity), whereas a Wilson line still needs to be inserted for different gauge choices.
Similarly to the TMD case, we consider the projection $\Phi^{[\Gamma]}$ of the correlator over the space of Dirac matrices. The leading-twist contribution to its parametrization turns out to be [65, 71]

$$\Phi^{[\gamma^+]}_{\Lambda,\Lambda'}(x,\Delta) = \frac{1}{2P^+}\bar u_{\Lambda'}(p')\left[\gamma^+\,H(x,\xi,t) + \frac{i\sigma^{+\mu}\Delta_\mu}{2M}E(x,\xi,t)\right]u_\Lambda(p)\,, \tag{4.34}$$

$$\Phi^{[\gamma^+\gamma_5]}_{\Lambda,\Lambda'}(x,\Delta) = \frac{1}{2P^+}\bar u_{\Lambda'}(p')\left[\gamma^+\gamma_5\,\tilde H(x,\xi,t) + \frac{\Delta^+\gamma_5}{2M}\tilde E(x,\xi,t)\right]u_\Lambda(p)\,, \tag{4.35}$$

$$\begin{aligned}\Phi^{[i\sigma^{j+}\gamma_5]}_{\Lambda,\Lambda'}(x,\Delta) &= -\frac{i\varepsilon^{ij}}{2P^+}\bar u_{\Lambda'}(p')\Big[i\sigma^{+i}H_T(x,\xi,t) + \frac{\gamma^+\Delta^i_\perp - \Delta^+\gamma^i_\perp}{2M}E_T(x,\xi,t) \\ &+ \frac{P^+\Delta^i_\perp - \Delta^+P^i_\perp}{M^2}\tilde H_T(x,\xi,t) + \frac{\gamma^+P^i_\perp - P^+\gamma^i_\perp}{M}\tilde E_T(x,\xi,t)\Big]u_\Lambda(p)\,. \end{aligned} \tag{4.36}$$

The relations (4.34)-(4.36) define the leading-twist GPDs H, E, $\tilde H$, $\tilde E$, H_T, E_T, $\tilde H_T$ and $\tilde E_T$ depending on the three variables

$$x = \frac{k^+}{P^+}\,, \qquad \xi = -\frac{\Delta^+}{2P^+}\,, \qquad t = \Delta^2\,, \tag{4.37}$$

already introduced in Section 3.3.1. As shown in Fig. 4.3, GPDs reduce to ordinary form factors via integration over x. More precisely, we are interested

in the following sum rules[2] [65]:

$$\int_{-1}^{1} \mathrm{d}x\, H(x,\xi,t) = F_1(t)\,, \qquad \int_{-1}^{1} \mathrm{d}x\, E(x,\xi,t) = F_2(t)\,, \tag{4.38}$$

$$\int_{-1}^{1} \mathrm{d}x\, \tilde{H}(x,\xi,t) = G_A(t)\,, \qquad \int_{-1}^{1} \mathrm{d}x\, \tilde{E}(x,\xi,t) = G_P(t)\,, \tag{4.39}$$

where $F_1(t)$ and $F_2(t)$ are, respectively, the Dirac and Pauli form factors defined by the relation

$$\langle p',\Lambda'|\bar{\psi}(0)\gamma^\mu\psi(0)|p,\Lambda\rangle = \bar{u}_{\Lambda'}(p')\left[\gamma^\mu F_1(t) + \frac{i\sigma^{\mu\nu}\Delta_\nu}{2M}F_2(t)\right]u_\Lambda(p)\,, \tag{4.40}$$

while $G_A(t)$ and $G_P(t)$ are, respectively, the axial-vector and induced-pseudoscalar form factors defined through

$$\langle p',\Lambda'|\bar{\psi}(0)\gamma^\mu\gamma_5\psi(0)|p,\Lambda\rangle = \bar{u}_{\Lambda'}(p')\left[\gamma^\mu\gamma_5 G_A(t) + \frac{\gamma_5\Delta^\mu}{2M}G_P(t)\right]u_\Lambda(p)\,. \tag{4.41}$$

We anticipate that fundamental relations exist between moments of the GPDs with respect to the x variable and form factors of the QCD energy-momentum tensor, see Section 6.4.

4.4.1 GPDs in the impact parameter space

GPDs provide the possibility of accessing simultaneously information about the partons' longitudinal momentum and position in the transverse plane. This is achieved through a Fourier transform from the transverse component $\boldsymbol{\Delta}_\perp$ of the momentum transferred to the impact parameter space of coordinates $\boldsymbol{b}_\perp$. We devote this section to the interpretation of the impact-parameter variable (and of the distributions that depend on it) in light-front quantization, mainly following Refs. [25, 75].

Form factors [recovered as averages of the GPDs over x, according to Eqs. (4.38) and (4.39)] parametrize off-forward matrix element of a given current, as one can see from Eqs. (4.40) and (4.41). Nonetheless, they can be generally related, via Fourier transform, to position-space distributions of charges, that correspond in turn to diagonal matrix element of the same current in position space. Actually, this is true only if we disregard relativistic corrections that eventually arise from the boost transformations needed to connect states with different momenta: these are purely kinematic only in the non-relavistic limit of Galilean boosts, whereas they become dynamical in the relativistic case (see the discussion in Section 2.3).
A qualitative proof of the above statements was carried out explicitly in Ref. [75];

[2]Note that integration over the longitudinal momentum fraction x runs from -1 to 1 to account for contributions from antiquarks.

here we simply report a sketch of the derivation. Consider the charge distribution in position space $\rho(\boldsymbol{x})$ associated to the form factor $F_1(t)$ and satisfying

$$\langle p'|\rho(\mathbf{0})|p\rangle = \left(p'^0 - p^0\right) F_1(t) \,, \tag{4.42}$$

with $p^0 = \sqrt{M^2 + \boldsymbol{p}^2}$, $p'^0 = \sqrt{M^2 + (\boldsymbol{p}+\boldsymbol{\Delta})^2}$. Given a wave packet

$$|\Psi\rangle = \int \frac{\mathrm{d}^3\boldsymbol{p}}{\sqrt{2(2\pi)^3 p_0}}\, \psi(\boldsymbol{p})|\boldsymbol{p}\rangle \tag{4.43}$$

with a certain distribution $\psi(\boldsymbol{p})$ in momentum space, we take as Fourier transform of the charge distribution:

$$\mathcal{F}_\Psi(\boldsymbol{\Delta}) = \int \mathrm{d}^3x\, e^{-i\boldsymbol{\Delta}\cdot\boldsymbol{x}} \langle\Psi|\rho(\boldsymbol{x})|\Psi\rangle \,. \tag{4.44}$$

It can be shown that Eq. (4.44) coincides with $F_1(t = -\boldsymbol{\Delta}^2)$ only in the non-relativistic limit $M^2 \gg \boldsymbol{q}^2, \boldsymbol{p}\cdot\boldsymbol{\Delta}$ (where $p^0 = p'^0$ and therefore $\Delta^0 = 0$) and assuming that the wave packet is arbitrarily broad in momentum space (i.e. localized in an arbitrarily small region in position space), so that

$$\int \mathrm{d}^3\boldsymbol{p}\, \psi^*(\boldsymbol{p}+\boldsymbol{\Delta})\psi(\boldsymbol{p}) \sim \int \mathrm{d}^3\boldsymbol{p}\, |\psi(\boldsymbol{p})|^2 \,. \tag{4.45}$$

On the other hand, if we include terms up to order $\mathcal{O}(\boldsymbol{\Delta}^2)$ in the expansion of $F_\Psi(\boldsymbol{\Delta})$, the equivalence is spoiled by corrections scaling with $(\boldsymbol{p}\cdot\boldsymbol{\Delta})/\left(p^0\right)^2$ and $\boldsymbol{\Delta}^2/\left(p^0\right)^2$, which are not negligible in the assumption of a wave packet localized in an arbitrarily small region. A natural way to get rid of these relativistic corrections is to work in the infinite-momentum frame with $\Delta^0 = 0$, so as to keep $\boldsymbol{p}\cdot\boldsymbol{\Delta}$, $\boldsymbol{\Delta}^2$ constant while sending $p^0 \to \infty$. We call *elastic frames* the class of reference frames where the energy transfer vanishes. Thanks to Eq. (4.4), in instant-form coordinates elastic frames are defined by the condition $\boldsymbol{P}\cdot\boldsymbol{\Delta} = 0$; we then pick $P = (0, 0, P_z)$, $\boldsymbol{\Delta} = (\boldsymbol{\Delta}_\perp, 0)$ and let $P_z \to \infty$. By doing so, one comes up with the result that in the IMF the form factor $F(-\boldsymbol{\Delta}_\perp^2)$ can be identified with Fourier transform of a charge distribution in two-dimensional position space, without being affected by relativistic corrections.

From the above discussion, it is evident that light-front quantization offers the best framework to describe distributions functions in position space. The kinematic property of transverse boosts in the light-front formalism, pointed out in Section 2.3, is the underlying reason why we need to restrict ourselves to the transverse plane in order to avoid relativistic corrections to our distributions [25].
The physical interpretation of two-dimensional spatial distributions relies on the definition (2.55) of the center of transverse momentum, which allows us to localize the nucleon in the transverse plane; we can then naturally infer how

partons are distributed around it. To this purpose, we consider light-front-helicity eigenstates $|p^+, \boldsymbol{p}_\perp, \Lambda\rangle$ and Fourier-transform them to position space according to:

$$|p^+, \boldsymbol{R}_\perp = \boldsymbol{0}_\perp, \Lambda\rangle = \mathcal{N} \int \frac{\mathrm{d}^2\boldsymbol{p}_\perp}{(2\pi)^2} |p^+, \boldsymbol{p}_\perp, \Lambda\rangle \,, \tag{4.46}$$

where $\mathcal{N}$ satisfies

$$|\mathcal{N}|^2 \int \frac{\mathrm{d}^2\boldsymbol{p}_\perp}{(2\pi)^2} = 1 \,. \tag{4.47}$$

The states defined in (4.46) are simultaneously eigenstates of the operators P^+, $\boldsymbol{R}_\perp = -\boldsymbol{B}_\perp/p^+$ and J_z with eigenvalues p^+, $\boldsymbol{0}_\perp$ and λ, respectively.
Let us rewrite the Dirac-space projection of the GPD correlator as

$$\begin{aligned}\Phi^{[\Gamma]}_{\Lambda,\Lambda'}(x,\Delta) &= \frac{1}{2}\int \frac{\mathrm{d}z^-}{2\pi}\, e^{ik^+z^-} \left\langle p', \Lambda'|\bar\psi(0,0,\boldsymbol{0}_\perp)\Gamma\psi(0,z^-,\boldsymbol{0}_\perp)|p,\Lambda\right\rangle \\ &= \left\langle p', \Lambda'|\mathcal{O}^{[\Gamma]}(x,\boldsymbol{0}_\perp)|p,\Lambda\right\rangle \,,\end{aligned} \tag{4.48}$$

so as to emphasize its definition in terms of the off-forward matrix element of the operator

$$\mathcal{O}^{[\Gamma]}(x,\boldsymbol{b}_\perp) = \frac{1}{2}\int \frac{\mathrm{d}z^-}{2\pi}\, e^{ik^+z^-}\, \bar\psi(0,0,\boldsymbol{b}_\perp)\Gamma\psi(0,z^-,\boldsymbol{b}_\perp) \tag{4.49}$$

with $\boldsymbol{b}_\perp = \boldsymbol{0}_\perp$. As we previously mentioned, in order to get rid of probabilistic corrections one must reduce himself to the frame where the energy transfer is vanishing. In light-front coordinates, this condition is equivalent to the requirement $\xi = 0$, which we will assume from now on. This consequently results into $t = -\boldsymbol{\Delta}_\perp^2$, meaning that GPDs will eventually depend only on $(x, \boldsymbol{\Delta}_\perp)$. We also take, as an example, the case $\Gamma = \gamma^+$ with $\Lambda = \Lambda'$, so that Eq. (4.34) becomes

$$\Phi^{[\gamma^+]}_{\Lambda,\Lambda}(x,0,t=-\boldsymbol{\Delta}_\perp^2) = H(x,0,t=-\boldsymbol{\Delta}_\perp^2) \equiv H(x,-\boldsymbol{\Delta}_\perp^2) \,. \tag{4.50}$$

Let us now consider the following *forward* matrix element of the operator (4.49) at generic $\boldsymbol{b}_\perp \neq \boldsymbol{0}_\perp$:

$$\rho(x,\boldsymbol{b}_\perp) = \langle p^+, \boldsymbol{R}_\perp = \boldsymbol{0}_\perp, \Lambda|\mathcal{O}^{[\gamma^+]}(x,\boldsymbol{b}_\perp)|p^+, \boldsymbol{R}_\perp = \boldsymbol{0}_\perp, \Lambda\rangle \,. \tag{4.51}$$

It is possible to show that Eq. (4.51) represents the probability distributions of finding a parton with longitudinal momentum x at a position $\boldsymbol{b}_\perp$ in the transverse plane with respect to the center of transverse momentum, that we identify with the origin of the xy-plane. According to the discussion at the end of Section 2.3, we hence identify $\boldsymbol{b}_\perp$ with the impact parameter of the parton. Using Eqs. (4.46), (4.47) and (4.50) along with the translation property of the field $\psi(x)$, we have

$$\rho(x,\boldsymbol{b}_\perp) = |\mathcal{N}|^2 \int \frac{\mathrm{d}^2\boldsymbol{p}_\perp}{(2\pi)^2} \int \frac{\mathrm{d}^2\boldsymbol{p}'_\perp}{(2\pi)^2}\, H\left(x, -(\boldsymbol{p}_\perp - \boldsymbol{p}'_\perp)^2\right) e^{i\boldsymbol{b}_\perp\cdot(\boldsymbol{p}_\perp - \boldsymbol{p}'_\perp)}$$

$$= \int \frac{\mathrm{d}^2\boldsymbol{\Delta}_\perp}{(2\pi)^2} H(x, -\boldsymbol{\Delta}_\perp^2) e^{-i\boldsymbol{b}_\perp\cdot\boldsymbol{\Delta}_\perp} \,. \tag{4.52}$$

In the last step we changed the integration variables according to $\int \mathrm{d}^2\boldsymbol{p}_\perp \int \mathrm{d}^2\boldsymbol{p}'_\perp = \int \mathrm{d}^2\boldsymbol{P}_\perp \int \mathrm{d}^2\boldsymbol{\Delta}_\perp$ and used the fact that the distributions which parametrize the correlator, as already emphasized, do not in fact depend on $\boldsymbol{P}_\perp$.
Eq. (4.52) shows that the density (4.51) is nothing but the Fourier transform with respect to $\boldsymbol{\Delta}_\perp$ of the GPD H, taken at $\xi = 0$. It follows that, thanks to the relations (4.38) and (4.39), by integrating both sides of Eq. (4.52) over x we can relate the Fourier conjugate of form factors with charge distributions in the transverse plane, without suffering from relativistic corrections. GPDs in the transverse plane therefore give us information about the contributions to two-dimensional charge distributions from different regions of x. This is a crucial result that can be simply illustrated in the language of light-front quantization. We dedicate Chapter 6 to an application of these considerations in QCD.

4.5 GTMDs and Wigner distributions

So far we have focused on specific regions of phase space, both in momentum and position space. It is natural to wonder whether it is possible to explore the whole six-dimensional phase space of a composite system in Quantum Field Theory. The study of Wigner distributions is motivated by the attempt to answer this question.

The evolution of a point-like particle at the classical level is fully described by a trajectory $f(\boldsymbol{r}, \boldsymbol{p}, t)$ in six-dimensional phase space. At any time t, we can interpret $f(\boldsymbol{r}, \boldsymbol{p})\,\mathrm{d}^3r\,\mathrm{d}^3p$ as the probability of finding the particle in an infinitesimal volume $\mathrm{d}^3r\,\mathrm{d}^3p$ around the point $(\boldsymbol{r}, \boldsymbol{p})$, which specifies the state of the particle. In principle, nothing limits the precision with which we can access the values of position and momentum at the same time.
In the context of non-relativistic Quantum Mechanics, on the other hand, Heisenberg uncertainty principle prescribes $\Delta\boldsymbol{p}\Delta\boldsymbol{r} \gtrsim \hbar^3$ and does not allow one to access simultaneously position and momentum of the system with arbitrary precision. Still one can define a six-dimensional *Wigner distribution* [60, 76]

$$\rho_W(\boldsymbol{r}, \boldsymbol{p}) = \int \frac{\mathrm{d}^3\boldsymbol{z}}{(2\pi)^3} e^{-\frac{i}{\hbar}\boldsymbol{p}\cdot\boldsymbol{z}} \psi^*(\boldsymbol{r})\psi\left(\boldsymbol{r} + \boldsymbol{z}\right) \,, \tag{4.53}$$

where $\psi(\boldsymbol{r})$ is the wave function describing the system.
Because of Heisenberg's principle, the distribution (4.53) is not positive-definite: this prevents us from interpreting it as a probability density. Nonetheless, in the classical limit $\hbar \to 0$ we have:

$$\rho_W(\boldsymbol{r}, \boldsymbol{p}) \xrightarrow{\hbar\to 0} f(\boldsymbol{r}, \boldsymbol{p}) \,. \tag{4.54}$$

In this sense, we can state that the Wigner distribution has a *quasi-probabilistic* (or *semi-classical*) interpretation: the regions of space-time where $\rho_W(\boldsymbol{r},\boldsymbol{p})$ is negative are volumes of order $\hbar^3$ and we hence recover the probabilistic interpretation in the classical limit.

The first attempt to transpose this formalism to the framework of Quantum Field Theory is due to Ji *et al.* [60,61]. They introduced a Wigner operator

$$\mathcal{W}^{[\Gamma]}(r,k) = \frac{1}{2}\int \frac{\mathrm{d}^4 z}{(2\pi)^4}\, e^{ik\cdot z}\, \bar{\psi}\,(r)\,\Gamma\psi\,(r+z)\ , \tag{4.55}$$

which resembles the non-relativistic distribution (4.53), but where $\psi(r)$ is now a fermionic field operator. In Eq. (4.55) the matrix Γ is again an element generated by the basis $\mathcal{D}$ of Dirac operators and $r = (0,\boldsymbol{r})$. Observe that the Wigner operator reduces, for $\boldsymbol{r} = \boldsymbol{0}$, to the operator appearing in the Dirac projection of the generalized parton correlator (4.6), analogously to the situation discussed for the operator (4.49) in the GPD case. This consideration suggests to follow the same procedure adopted in the previous section, in order to relate Wigner distributions to Fourier transform of off-forward matrix elements of the Wigner operator.
To this aim, Ji and collaborators proposed to consider, in instant-form coordinates, the elastic frame $\Delta^0 = 0$ and introduced the distribution

$$\begin{aligned} W^{[\Gamma]}_{S,S'}(\boldsymbol{r},k) &= \int \frac{d^3\boldsymbol{\Delta}}{(2\pi)^3} \left\langle P+\frac{\Delta}{2}, S' \left| \mathcal{W}^{[\Gamma]}(\boldsymbol{r},k) \right| P-\frac{\Delta}{2}, S \right\rangle \\ &= \int \frac{d^3\boldsymbol{\Delta}}{(2\pi)^3} e^{-i\boldsymbol{r}\cdot\boldsymbol{\Delta}} \left\langle P+\frac{\Delta}{2}, S' \left| \mathcal{W}^{[\Gamma]}(\boldsymbol{0},k) \right| P-\frac{\Delta}{2}, S \right\rangle\ , \end{aligned} \tag{4.56}$$

where $\Delta = (0,\boldsymbol{\Delta})$. Integrating the previous expression over $k^- = (k^0 - k_z)/\sqrt{2}$, we obtain the six-dimensional Wigner distribution

$$W^{[\Gamma]}_{S,S'}(\boldsymbol{r},\boldsymbol{k}) = \int \mathrm{d}k^-\, W^{[\Gamma]}_{S,S'}(\boldsymbol{r},k)\ . \tag{4.57}$$

In consideration of what we discussed in Section 4.4.1, however, the distribution defined in Eq. (4.57) presents problems for its interpretation as a quasi-probability density, since it it is spoilt by relativistic corrections. There is, in fact, no way to avoid them as long as we want to have a picture of the system in three-dimensions in position space, due to the impossibility to connect states with different three-momenta with only kinematic boosts.
It is therefore necessary to give up information about one direction in position space and restrict ourselves to the description in the transverse plane, as was first proposed by Lorcé and Pasquini [28, 58, 77]. To this end, we switch to light-front coordinates and re-define the Wigner operator as

$$\mathcal{W}^{[\Gamma]}(x,\boldsymbol{b}_\perp,\boldsymbol{k}_\perp) = \frac{1}{2}\int \frac{\mathrm{d}z^+\mathrm{d}^2\boldsymbol{z}_\perp}{(2\pi)^3}\, e^{i(k^+z^- - \boldsymbol{k}_\perp\cdot\boldsymbol{z}_\perp)}\, \bar{\psi}\,(r)\,\Gamma\psi\,(r+z)\Big|_{z^+=0}\ , \tag{4.58}$$

where now $r = (0, 0, \boldsymbol{b}_\perp)$. By taking matrix elements of Eq. (4.58) at $\xi = 0$, so as to get rid of relativistic corrections, we come up with the Wigner distributions

$$W^{[\Gamma]}_{\Lambda,\Lambda'}(x, \boldsymbol{k}_\perp, \boldsymbol{b}_\perp) = \int \frac{d^2\boldsymbol{\Delta}_\perp}{(2\pi)^2} \left\langle p^+, \boldsymbol{P}_\perp + \frac{\boldsymbol{\Delta}_\perp}{2}, \Lambda' \middle| \mathcal{W}^{[\Gamma]}(x, \boldsymbol{k}_\perp, \boldsymbol{b}_\perp) \middle| p^+, \boldsymbol{P}_\perp - \frac{\boldsymbol{\Delta}_\perp}{2}, \Lambda \right\rangle . \tag{4.59}$$

These distributions (yet still not-positive-definite) do have a quasi-probabilistic interpretation in the sense given by Eq. (4.54), i.e. they are no longer affected by relativistic correction, unlike the six-dimensional functions (4.57).
Let us consider again the GTMD correlator (4.7): we report here the leading-twist decomposition of its projection over Dirac space [49]

$$\begin{aligned}\Phi^{[\gamma^+]}_{\Lambda,\Lambda'}(x, \boldsymbol{k}_\perp, \Delta) =& \frac{1}{2M} \bar{u}_{\Lambda'}(p') \left[F_{1,1} + \frac{i\sigma^{i+} k^i_\perp}{P^+} F_{1,2} + \frac{i\sigma^{i+} \Delta^i_\perp}{P^+} F_{1,3} \right. \\ &\left. + \frac{i\sigma^{ij} k^i_\perp \Delta^j_\perp}{M^2} F_{1,4} \right] u_\Lambda(p) , \end{aligned} \tag{4.60}$$

$$\begin{aligned}\Phi^{[\gamma^+\gamma_5]}_{\Lambda,\Lambda'}(x, \boldsymbol{k}_\perp, \Delta) =& \frac{1}{2M} \bar{u}_{\Lambda'}(p') \left[- \frac{i\varepsilon^{ij} k^i_\perp \Delta^j_\perp}{M^2} G_{1,1} + \frac{i\sigma^{i+}\gamma_5 k^i_\perp}{P^+} G_{1,2} + \frac{i\sigma^{i+}\gamma_5 \Delta^i_\perp}{P^+} G_{1,3} \right. \\ &\left. + i\sigma^{+-}\gamma_5 G_{1,4} \right] u_\Lambda(p) , \end{aligned} \tag{4.61}$$

$$\begin{aligned}\Phi^{[i\sigma^{j+}\gamma_5]}_{\Lambda,\Lambda'}(x, \boldsymbol{k}_\perp, \Delta) =& \frac{1}{2M} \bar{u}_{\Lambda'}(p') \left[- \frac{i\varepsilon^{ij} k^i_\perp}{M} H_{1,1} - \frac{i\varepsilon^{ij} \Delta^i_\perp}{M} H_{1,2} + \frac{M i\sigma^{j+}\gamma_5}{P^+} H_{1,3} \right. \\ &+ \frac{k^j_\perp i\sigma^{i+}\gamma_5 k^i_\perp}{MP^+} H_{1,4} + \frac{\Delta^j_\perp i\sigma^{i+}\gamma_5 k^i_\perp}{MP^+} H_{1,5} + \frac{\Delta^j_\perp i\sigma^{i+}\gamma_5 \Delta^i_\perp}{MP^+} H_{1,6} \\ &\left. + \frac{k^j_\perp i\sigma^{+-}\gamma_5}{M} H_{1,7} + \frac{\Delta^j_\perp i\sigma^{+-}\gamma_5}{M} H_{1,8} \right] u_\Lambda(p) . \end{aligned} \tag{4.62}$$

The 16 leading-twist Generalized Transverse-Momentum Dependent distribution functions $F_{1,i}$, $G_{1,i}$ and $H_{1,i}$ appearing on the right-hand sides of Eqs. (4.60) to (4.62) depend in general on x, $\boldsymbol{k}_\perp$, ξ and $\boldsymbol{\Delta}_\perp$. Proper limits of the GTMDs link them to GPDs and TMDs, as shown in detail in Ref. [49].
By following the same procedure described in the case of GPDs in Section 4.4.1, one can show that Wigner distributions are related to Fourier transforms of GTMDs at $\xi = 0$ according to:

$$W^{[\Gamma]}_{\Lambda,\Lambda'}(x, \boldsymbol{k}_\perp, \boldsymbol{b}_\perp) = \int \frac{d^2\boldsymbol{\Delta}_\perp}{(2\pi)^2} e^{-i\boldsymbol{b}_\perp \cdot \boldsymbol{\Delta}_\perp} \Phi^{[\Gamma]}_{\Lambda,\Lambda'}(x, \boldsymbol{k}_\perp, \boldsymbol{\Delta}_\perp) , \tag{4.63}$$

where

$$\Phi^{[\Gamma]}_{\Lambda,\Lambda'}(x, \boldsymbol{k}_\perp, \boldsymbol{\Delta}_\perp) = \frac{1}{2} \int \frac{\mathrm{d}z^- \mathrm{d}^2\boldsymbol{z}_\perp}{(2\pi)^3} e^{i(k^+ z^- - \boldsymbol{k}_\perp \cdot \boldsymbol{z}_\perp)}$$

$$\times \left\langle P^+, \boldsymbol{P}_\perp + \frac{\boldsymbol{\Delta}_\perp}{2}, \Lambda' | \bar{\psi}(0)\, \Gamma \psi(z) | P^+, \boldsymbol{P}_\perp - \frac{\boldsymbol{\Delta}_\perp}{2}, \Lambda \right\rangle \Big|_{z^+=0} \tag{4.64}$$

is the projection in Dirac space of the GTMD correlator (4.7) for $\xi = 0$.
As they provide information simultaneously on position and momentum of partons in the transverse plane, Wigner distributions are valuable instruments for the the investigation of Orbital Angular Momentum contributions from both quarks [78–82] and gluons [83–85].
At variance with the cases relative to the other distributions functions, discussed in the previous sections, there is no universal agreement concerning a process that can be used to obtain experimental measures of either GTMDs or Wigner distributions, although in the recent years it has been argued that measurements are possible both in the gluon [86–88] and in the quark [89] sectors of GTMDs. These proposals are, at the present time, still waiting for an experimental validation.

4.6 LFWF overlap representation of distribution functions

Light-front quantization does not only offer a suitable language for the description of distribution functions in the impact-parameter space, but provides also an effective tool for performing practical calculations with the language of Light-Front Wave Functions (LFWFs), introduced in Section 2.4. Indeed it is easy to realize that we can use the Fock-state expansion (2.64) to rewrite the hadron states appearing in the correlators, which will eventually be expressed as overlap of LFWFs. Thanks to the properties of LFWFs, this leads to an intuitive parton interpretation of the content of a given parton distribution.
In this section, we briefly illustrate how this procedure can be applied by considering, as an example, the case of GTMDs; detailed derivations can be found in Ref. [52, 90–92]. It is then immediate to transpose the results to the case of other parton distributions.
We first rewrite the Fock-state expansion of an hadron state $|P, \Lambda\rangle$ in the light-front helicity basis and in light-cone gauge $A^+ = 0$ as

$$|P, \Lambda\rangle = \sum_{n,\lambda_i} \int [\mathrm{d}x]_n [\mathrm{d}^2\boldsymbol{k}_\perp]_n \, \Psi^\Lambda_{n,\lambda_i}(x_i, \boldsymbol{k}_{\perp,i}) |\mu_n(x_i, \boldsymbol{k}_{\perp,i}, \lambda_i)\rangle \,, \tag{4.65}$$

where the integration measures

$$[\mathrm{d}x]_n = \left[\prod_{i=1}^n \mathrm{d}x_i\right] \delta\left(1 - \sum_{j=1}^n x_j\right) \,, \tag{4.66}$$

$$[\mathrm{d}^2\boldsymbol{k}_\perp]_n = \frac{1}{(16\pi^3)^{n-1}} \left[\prod_{i=1}^n \mathrm{d}^2\boldsymbol{k}_{\perp,i}\right] \delta^{(2)}\left(\sum_{j=1}^n \boldsymbol{k}_{\perp,j}\right) \tag{4.67}$$

take into account the conditions (2.67)-(2.68). In practical calculations, one has to truncate the sum at a finite value of n, which represents the number of particles to be included in the description (the typical choice is $n = 3$ for the nucleon). The hadron states are normalized according to Eq. (3.64) and the LFWFs satisfy

$$\sum_{n,\lambda_i} \int [\mathrm{d}x]_n [\mathrm{d}^2\boldsymbol{k}_\perp]_n \left|\Psi^\Lambda_{n,\lambda_i}(x_i, \boldsymbol{k}_{\perp,i})\right|^2 = 1 \,. \tag{4.68}$$

In order to rewrite the correlator, we also need the following Fourier expansion of the "good' components of the quark field [see Eq. (3.18)] at fixed light-front time $z^+ = 0$:

$$\begin{aligned}\psi_+(z^-, \boldsymbol{z}_\perp) = \int \frac{\mathrm{d}k^+ \mathrm{d}^2\boldsymbol{k}_\perp}{2(2\pi)^3 k^+}\, \Theta(k^+) \\ \times \sum_\lambda \left[b_\lambda(k) u_{+,\lambda}(k) e^{-i(k^+ z^- - \boldsymbol{z}_\perp\cdot\boldsymbol{k}_\perp)} + d^\dagger_\lambda(k) v_{+,\lambda}(k) e^{i(k^+ z^- - \boldsymbol{z}_\perp\cdot\boldsymbol{k}_\perp)} \right] ,\end{aligned} \tag{4.69}$$

where $b, b^\dagger$ and $d, d^\dagger$ are the ladder operators that create and annihilate quarks and antiquarks, respectively, and $u_{+,\lambda} = \frac{1}{2}\gamma^-\gamma^+ u_\lambda$, $v_{+,\lambda} = \frac{1}{2}\gamma^-\gamma^+ v_\lambda$. For the gluon field one similarly has (omitting color indices for better readability):

$$\begin{aligned}A^\mu(z^-, \boldsymbol{z}_\perp) = \int \frac{\mathrm{d}q^+ \mathrm{d}^2\boldsymbol{q}_\perp}{2(2\pi)^3 q^+}\, \Theta(q^+) \\ \times \sum_{\lambda_\gamma} \left[a_{\lambda_\gamma}(q) \varepsilon^\mu_{\lambda_\gamma}(q) e^{-i(q^+ z^- - \boldsymbol{z}_\perp\cdot\boldsymbol{q}_\perp)} + a^\dagger_{\lambda_\gamma}(q) \varepsilon^{\mu\,*}_{\lambda_\gamma}(q) e^{i(q^+ z^- - \boldsymbol{z}_\perp\cdot\boldsymbol{q}_\perp)} \right] ,\end{aligned} \tag{4.70}$$

a,$a^\dagger$ being the gluon creation and annihilation operators. The usual commutation and anti-commutation relations are assumed:

$$\left\{ b_\lambda(k), b^\dagger_{\lambda'}(k') \right\} = \left\{ d_\lambda(k), d^\dagger_{\lambda'}(k') \right\} = 2(2\pi)^3 k^+ \delta\left(k^+ - k'^+\right) \delta^{(2)}\left(\boldsymbol{k}_\perp - \boldsymbol{k}'_\perp\right) \delta_{\lambda,\lambda'} \,, \tag{4.71}$$

$$\left[a_\lambda(q), a^\dagger_{\lambda'}(q') \right] = 2(2\pi)^3 q^+ \delta\left(q^+ - q'^+\right) \delta^{(2)}\left(\boldsymbol{q}_\perp - \boldsymbol{q}'_\perp\right) \delta_{\lambda,\lambda'} \,. \tag{4.72}$$

We take for simplicity the $\xi = 0$ case and obtain for the 3-particle contribution to the projection (4.64) of the GTMD correlator in Dirac space [52]

$$\begin{aligned}\Phi^{[\Gamma]}_{\Lambda,\Lambda'}(x, \boldsymbol{k}_\perp, \boldsymbol{\Delta}_\perp) =& 3 \sum_{\lambda_i,\lambda'_i} \int [\mathrm{d}x]_3 [\mathrm{d}^2\boldsymbol{k}_\perp]_3\, \Theta(x) \delta(x - x_1) \delta^{(2)}\left(\boldsymbol{k}_\perp - \boldsymbol{k}_{1,\perp}\right) \\ & \times M^{[\Gamma]}_{\lambda_1,\lambda'_1} \delta_{\lambda_2,\lambda'_2} \delta_{\lambda_3,\lambda'_3} \left[\Psi^{\Lambda'}_{3,\lambda'_i}(x'_i, \boldsymbol{k}'_{i,\perp})\right]^* \Psi^\Lambda_{3,\lambda_i}(x_i, \boldsymbol{k}_{i,\perp}) \,.\end{aligned} \tag{4.73}$$

In Eq. (4.73) the index $i = 1$ refers to the active quark, whereas $i = 2$ and $i = 3$ to the spectators. The final-state momenta appearing as arguments of the LFWFs are

$$x'_i = x_i \,, \qquad\qquad i = 1, 2, 3 \,,$$

$$\boldsymbol{k}'_{1,\perp} = \boldsymbol{k}_{1,\perp} + (1 - x_1)\frac{\boldsymbol{\Delta}_\perp}{2}$$
$$\boldsymbol{k}'_{i,\perp} = \boldsymbol{k}_{i,\perp} - x_i\frac{\boldsymbol{\Delta}_\perp}{2}\ , \qquad i = 2, 3\ .$$

One can select different configurations of both initial-state and final-state polarizations of the active quark via proper projections in Dirac space, described by the operator $M^{[\Gamma]}_{\lambda,\lambda'}$. More precisely, denoting the Pauli matrices with σ_i ($i = 1, 2, 3$), for the Dirac operators that contribute at leading twist we have

$$M^{[\gamma^+]}_{\lambda,\lambda'} = \delta_{\lambda,\lambda'}\ , \quad M^{[i\sigma^{j+}\gamma_5]}_{\lambda,\lambda'} = (\sigma_j)_{\lambda,\lambda'}\ , \quad M^{[\gamma^+\gamma_5]}_{\lambda,\lambda'} = (\sigma_3)_{\lambda,\lambda'}\ . \tag{4.74}$$

Since LFWFs are eigenstates of light-front helicity, the overlap representation (4.73) helps to have an immediate perception of which helicity transformations of the active quark are involved in a given distribution. Moreover, thanks to the probabilistic interpretation of the square modulus of LFWFs, mentioned at the end of Section 2.4, in this language it is easy to recognize the correlators depending on diagonal matrix elements as a probability density.
We will show examples of LFWFs overlap representations of GTMDs and TMDs in the framework of QED in Chapter 5 and of GPDs in the context of QCD in Chapter 6.

Chapter 5

The electron structure in light-front QED

We are now going to apply the formalism of correlation functions, introduced in Chapter 4 in the framework of QCD, to the field of Quantum Electrodynamics (QED). Due to its perturbative nature, QED serves as an ideal proving ground for the test of novel techniques to be applied in Quantum Field Theory; as such it has been studied e.g. in Ref. [26, 93–96].

The electron, unlike hadrons, is a point-like particle. Nonetheless, due to Heisenberg uncertainty principle, in the QFT picture the electron field encounters quantum fluctuations that cause the emission and re-absorption of photons; these can, in turn, break into virtual electron-positron pairs, consistently with the quantum numbers of the parent electron. As a result, the latter effectively becomes a dressed particle consisting of a cloud of photons, electrons and positrons. To this extent, it is legitimate to think of the electron as an object with a three-dimensional structure, both in momentum and position space, and to give it an interpretation as a composite particle. One can then probe the inner content of the electron cloud and describe it in terms of its partons with the language of distribution functions, in analogy with the QCD case. In this perspective, it is possible to define the notion of "shape" of the electron [93, 94] and analyze how its spin arises form the contribution of Orbital Angular Momentum (OAM) and spin of the constituents [26, 93–95]. The purpose of the present Chapter is to address these issues with the language of GTMDs and TMDs (introduced in Chapter 4) in light-cone quantization. This approach allows for a description of the dressed electron in three-dimensional momentum space, along with an assessment of non-trivial relations between position, momentum and spin of the partons. We also focus on the comparison between QED and QCD, with particular emphasis on their Abelian rather than non-Abelian nature. To this aim, we provide a detailed treatment of the role of Wilson lines in the context of gauge-invariance, enlightening differences and similarities of the two theories. For our purposes, it

will be sufficient to consider the electron at order α as a composite two-body system, consisting of an electron-photon pair.

5.1 Fock-state decomposition of the electron cloud

Let $|e_D\rangle \equiv |e_D; p, \Lambda\rangle$ denote the state of a "dressed" (or "physical", or "parent") electron with mass M, light-cone helicity Λ and momentum $p = (p^+, p^-, \mathbf{0}_\perp)$ in the reference frame that we denote as *electron frame*, in analogy with the hadron frame in QCD. In view of the above discussion, it is justified to decompose the state $|e_D\rangle$ through the Fock-space expansion

$$|e_D\rangle = |e\rangle + |e\gamma\rangle + |e\gamma\gamma\rangle \ + \dots \ . \tag{5.1}$$

Each term in the right-hand side of Eq. (5.1) represents a bound state containing a given number n of particles, compatibly with the quantum numbers of the dressed electron in the left-hand side. In particular, we denote with e the bare electron inside the physical electron and consider it as a constituent parton, within the analogy between the electron cloud and the nucleon as composite systems. We label the three momentum of the internal electron in the electron frame as

$$\boldsymbol{p}_e = (xp^+, \boldsymbol{k}_\perp)$$

and its light-cone helicity with λ_e. One can recognize that Eq. (5.1) corresponds to a perturbative expansion of the parent-electron state in powers of the QED coupling constant e. In the present discussion, we truncate the sum up to order e and, accordingly, study the dressed electron as a composite two-body system consisting of an electron-photon pair:

$$|e_D\rangle = \sqrt{Z}|e\rangle + |e\gamma\rangle \ , \tag{5.2}$$

where we also introduced the renormalization constant Z, that one can properly evaluate by fixing a convenient regularization scheme (e.g. Pauli-Villars regularization, see Ref. [26]).
The one-particle, bare-electron state in the first term is given by

$$|e\rangle = b^\dagger_\Lambda(p)|0\rangle \ , \tag{5.3}$$

where in this context b and $b^\dagger$ are the electron ladder operators. The second term in Eq. (5.2) indicates the electron-photon state, written in terms of the two-particle LFWF $\Psi^\Lambda_{\lambda_e,\lambda_\gamma}(x, \boldsymbol{k}_\perp)$ as[1]

$$|e\gamma\rangle = \sum_{\lambda_e,\lambda_\gamma} \int \frac{\mathrm{d}x\, \mathrm{d}^2\boldsymbol{k}_\perp}{2(2\pi)^3\sqrt{x(1-x)}} \Psi^\Lambda_{\lambda_e,\lambda_\gamma}(x, \boldsymbol{k}_\perp)|p_e, \lambda_e; p_\gamma, \lambda_\gamma\rangle \ , \tag{5.4}$$

[1] One should pay attention not to confuse the *bound* state $|e\gamma\rangle$ with the state of *free particles*

$$|p_e, \lambda_e; p_\gamma, \lambda_\gamma\rangle = b^\dagger_{\lambda_e}(p_e)a^\dagger_{\lambda_\gamma}(p_\gamma)|0\rangle \ .$$

where λ_γ is the photon polarization. We emphasize that in Eq. (5.4), in view of the conditions (2.67)-(2.68), it is assumed that the photon three-momentum is written as

$$\boldsymbol{p}_\gamma = ((1-x)p^+, -\boldsymbol{k}_\perp) \ . \tag{5.5}$$

In the framework of QED it is possible to obtain an explicit expression for the LFWFs by carrying out the perturbative expansion of the bound states up to the desired perturbative order. This fact marks a crucial difference with respect to the QCD case, where LFWFs inherit the non-perturbative nature of strong interactions binding nucleon states. For the electron-photon bound state, light-front perturbation theory yields[2]

$$|e\gamma; p, \Lambda\rangle = \sum_{\lambda_e,\lambda_\gamma} \int \frac{\mathrm{d}p_e^+ \, \mathrm{d}^2\boldsymbol{p}_{e,\perp}}{2(2\pi)^3 p_e^+} \int \frac{\mathrm{d}p_\gamma^+ \, \mathrm{d}^2\boldsymbol{p}_{\gamma,\perp}}{2(2\pi)^3 p_\gamma^+} \frac{\langle p_e, \lambda_e; p_\gamma, \lambda_\gamma | V | e; p, \Lambda\rangle}{p^- - p_e^- - p_\gamma^-} |p_e, \lambda_e; p_\gamma, \lambda_\gamma\rangle \ , \tag{5.6}$$

with the QED potential V given by

$$V = -e \int \mathrm{d}x^- \mathrm{d}^2\boldsymbol{x}_\perp \, \bar{\psi}(x^-, \boldsymbol{x}_\perp) \gamma^\mu \psi(x^-, \boldsymbol{x}_\perp) A_\mu(x^-, \boldsymbol{x}_\perp) \ . \tag{5.7}$$

The energy denominator in Eq. (5.6) can be conveniently expressed via the on-shell conditions

$$p^2 = M^2 \ , \qquad p_e^2 = m^2 \ , \qquad p_\gamma^2 = \mu^2 \ , \tag{5.8}$$

where m is the bare electron mass appearing in the QED Lagrangian and μ is a fictitious photon mass that we keep different from zero for regularization issues. We recall that, even in the limit $\mu = 0$, the physical mass M does not coincide with the bare mass m, due to self-energy corrections.
If we compare Eqs. (5.4) and (5.6), and use the expansions (4.69)-(4.70) along with the (anti)commutation relations (4.71)-(4.72), we find

$$\Psi^\Lambda_{\lambda_e,\lambda_\gamma}(x, \boldsymbol{k}_\perp^2) = \phi(x, \boldsymbol{k}_\perp^2) \bar{u}_{\lambda_e}(p_e) \gamma_\mu \varepsilon^{\mu\,*}_{\lambda_\gamma}(p_\gamma) u_\Lambda(p) \ , \tag{5.9}$$

with

$$\phi(x, \boldsymbol{k}_\perp^2) = \frac{e\sqrt{x(1-x)}}{\boldsymbol{k}_\perp^2 + u(x, \mu^2)} \tag{5.10}$$

and

$$u(x, \mu^2) = x\mu^2 + (1-x)m^2 - x(1-x)M^2 \ . \tag{5.11}$$

[2]For better clarity, here we explicitly denote momentum and spin of the states appearing in the expansion Eq. (5.1).

The free light-front spinors and antispinors for a fermion of mass m read [97]:

$$u_{1/2}(k) = \frac{1}{\sqrt{2^{3/2}k^+}}\begin{pmatrix}\sqrt{2}k^+ + m\\ k_R\\ \sqrt{2}k^+ - m\\ k_R\end{pmatrix}, \qquad u_{-1/2}(k) = \frac{1}{\sqrt{2^{3/2}k^+}}\begin{pmatrix}-k_L\\ \sqrt{2}k^+ + m\\ k_L\\ -\sqrt{2}k^+ + m\end{pmatrix}, \tag{5.12}$$

$$v_{1/2}(k) = -\frac{1}{\sqrt{2^{3/2}k^+}}\begin{pmatrix}-k_L\\ \sqrt{2}k^+ - m\\ k_L\\ -\sqrt{2}k^+ - m\end{pmatrix}, \qquad v_{-1/2}(k) = -\frac{1}{\sqrt{2^{3/2}k^+}}\begin{pmatrix}\sqrt{2}k^+ - m\\ k_R\\ \sqrt{2}k^+ + m\\ k_R\end{pmatrix}, \tag{5.13}$$

where

$$k_{R,L} = k_x \pm ik_y\,, \qquad \Delta_{R,L} = \Delta_x \pm i\Delta_y\,. \tag{5.14}$$

If we insert them into Eq. (5.9), the dressed electron LFWFs read

$$\Psi^+_{+,+1}(x,\mathbf{k}_\perp) = -\left[\Psi^-_{-,-1}(x,\mathbf{k}_\perp)\right]^* = \sqrt{\frac{2}{x}}\frac{(k_x - ik_y)}{(1-x)}\,\phi(x,\mathbf{k}_\perp^2)\,, \tag{5.15}$$

$$\Psi^+_{+,-1}(x,\mathbf{k}_\perp) = -\left[\Psi^-_{-,+1}(x,\mathbf{k}_\perp)\right]^* = -\sqrt{2x}\frac{(k_x + ik_y)}{(1-x)}\,\phi(x,\mathbf{k}_\perp^2)\,, \tag{5.16}$$

$$\Psi^+_{-,+1}(x,\mathbf{k}_\perp) = \Psi^-_{+,-1}(x,\mathbf{k}_\perp) = \sqrt{\frac{2}{x}}(m - xM)\,\phi(x,\mathbf{k}_\perp^2)\,, \tag{5.17}$$

$$\Psi^+_{-,-1}(x,\mathbf{k}_\perp) = \Psi^-_{+,+1}(x,\mathbf{k}_\perp) = 0\,. \tag{5.18}$$

Here and throughout this Chapter the $\pm$ sign indicates $\Lambda, \lambda_e = \pm 1/2$ for the light-front helicities of the dressed and bare electrons, whereas $\lambda_\gamma = \pm 1$ is the light-front polarization of the internal photon. Notice that the LFWFs in Eqs. (5.15) to (5.18) are related by

$$\Psi^{\Lambda}_{\lambda_e,\lambda_\gamma}(x,\boldsymbol{k}_\perp) = (-1)^{\Lambda-\lambda_e+\lambda_\gamma}\left[\Psi^{-\Lambda}_{-\lambda_e,-\lambda_\gamma}(x,\boldsymbol{k}_\perp)\right]^*\,. \tag{5.19}$$

5.2 Wigner distributions for the dressed electron

5.2.1 Analytical evaluation in the b_x-k_y space

Let us now consider the GTMD correlator for the physical electron

$$\Phi^{[\Gamma]}_{\Lambda,\Lambda'}(x,\boldsymbol{k}_\perp,\Delta;P) = \int \frac{\mathrm{d}z^-\mathrm{d}^2\boldsymbol{z}_\perp}{(2\pi)^3}\,e^{i(k^+z^- - \boldsymbol{k}_\perp\cdot\boldsymbol{z}_\perp)} \times \langle e_D;\,p',\Lambda'|\bar\psi(0)\,\Gamma\,\psi(z)|e_D;\,p,\Lambda\rangle\Big|_{z^+=0}\,, \tag{5.20}$$

where $|e_D; p, \Lambda\rangle$ is a dressed electron state, as introduced in the previous section. For the moment we still neglect the gauge-link contribution. We can use the Fock state decomposition (5.2) in order to obtain the LFWF overlap representation of the correlator (5.20). We restrict to the case $\xi = 0$ and work in the so-called "average frame" where $\boldsymbol{P}_\perp = \boldsymbol{0}_\perp$. We denote the three-momenta of the incoming and outgoing partons as

$$\boldsymbol{p}_e = \left(xP^+, \boldsymbol{k}_\perp - \frac{\boldsymbol{\Delta}_\perp}{2}\right) , \qquad \boldsymbol{p}_\gamma = ((1-x)P^+, -\boldsymbol{k}_\perp) , \tag{5.21}$$

$$\boldsymbol{p}'_e = \left(xP^+, \boldsymbol{k}_\perp + \frac{\boldsymbol{\Delta}_\perp}{2}\right) , \qquad \boldsymbol{p}'_\gamma = ((1-x)P^+, -\boldsymbol{k}_\perp) , \tag{5.22}$$

so that

$$\boldsymbol{p} = \left(P^+, -\frac{\boldsymbol{\Delta}_\perp}{2}\right) , \qquad \boldsymbol{p}' = \left(P^+, \frac{\boldsymbol{\Delta}_\perp}{2}\right) . \tag{5.23}$$

We recall, however, that the momenta appearing in the arguments of the LFWFs in the two-particle state (5.4) are to be taken in the respective electron frames; one can resort to the light-front boost (2.69) so as to recover them. Taking this into account, one obtains the following overlap representation of the correlator for $\Gamma = \gamma^+$ and $\Gamma = \gamma^+\gamma_5$

$$\begin{aligned}\Phi^{[\gamma^+]}_{\Lambda,\Lambda'}(x, \boldsymbol{k}_\perp, \boldsymbol{\Delta}_\perp) =& Z\delta_{\Lambda,\Lambda'}\delta(1-x)\delta^{(2)}(\boldsymbol{k}_\perp) \\ &+ \frac{1}{2(2\pi)^3}\sum_{\lambda_e,\lambda_\gamma} \Psi^{\Lambda' \,*}_{\lambda_e,\lambda_\gamma}(x, \tilde{\boldsymbol{k}}_\perp)\Psi^{\Lambda}_{\lambda_e,\lambda_\gamma}(x, \hat{\boldsymbol{k}}_\perp) ,\end{aligned} \tag{5.24}$$

$$\begin{aligned}\Phi^{[\gamma^+\gamma_5]}_{\Lambda,\Lambda'}(x, \boldsymbol{k}_\perp, \boldsymbol{\Delta}_\perp) =& Z\delta_{\Lambda,\Lambda'}\delta(1-x)\delta^{(2)}(\boldsymbol{k}_\perp) \\ &+ \frac{1}{2(2\pi)^3}\sum_{\lambda_\gamma}\Big[\Psi^{\Lambda' \,*}_{+,\lambda_\gamma}(x, \tilde{\boldsymbol{k}}_\perp)\Psi^{\Lambda}_{+,\lambda_\gamma}(x, \hat{\boldsymbol{k}}_\perp) \\ &- \Psi^{\Lambda' \,*}_{-,\lambda_\gamma}(x, \tilde{\boldsymbol{k}}_\perp)\Psi^{\Lambda}_{-,\lambda_\gamma}(x, \hat{\boldsymbol{k}}_\perp)\Big] ,\end{aligned} \tag{5.25}$$

where

$$\tilde{\boldsymbol{k}}_\perp = \boldsymbol{k}_\perp + (1-x)\frac{\boldsymbol{\Delta}_\perp}{2} , \qquad \hat{\boldsymbol{k}}_\perp = \boldsymbol{k}_\perp - (1-x)\frac{\boldsymbol{\Delta}_\perp}{2} .$$

The bare-particle contribution proportional to Z becomes relevant only at the end-point $x = 1$, $\boldsymbol{k}_\perp = \boldsymbol{0}_\perp$. We will exclude the end-point from our results since its inclusion would require a proper renormalization procedure which is beyond the scope of the present work. By inverting Eqs. (4.60) and (4.61), we recover the following expressions of GTMDs in terms of the correlators (5.24) and (5.25):

$$F_{1,1} = \frac{1}{2}\left[\Phi^{[\gamma^+]}_{+,+} + \Phi^{[\gamma^+]}_{-,-}\right] , \tag{5.26}$$

$$F_{1,4} = \frac{M^2}{(k_L\Delta_R - k_R\Delta_L)}\left[\Phi^{[\gamma^+]}_{+,+} - \Phi^{[\gamma^+]}_{-,-}\right] , \tag{5.27}$$

$$G_{1,1} = \frac{M^2}{(k_R\Delta_L - k_L\Delta_R)}\left[\Phi^{[\gamma^+\gamma_5]}_{+,+} + \Phi^{[\gamma^+\gamma_5]}_{-,-}\right] , \tag{5.28}$$

$$G_{1,4} = \frac{1}{2}\left[\Phi^{[\gamma^+\gamma_5]}_{+,+} - \Phi^{[\gamma^+\gamma_5]}_{-,-}\right] , \tag{5.29}$$

$k_{R,L}$ and $\Delta_{R,L}$ being defined in Eq. (5.14). If we insert the explicit expressions of the LFWFs given in Eqs. (5.15) to (5.18) in the overlap representations Eqs. (5.24) and (5.25), we obtain the following expressions for the GTMDs at $x \neq 1$, $\boldsymbol{k}_\perp \neq \boldsymbol{0}_\perp$:

$$\begin{aligned} F_{1,1}(x, \boldsymbol{k}_\perp, \boldsymbol{\Delta}_\perp) =& \frac{\alpha}{2\pi^2(1-x)f(x, \boldsymbol{k}_\perp, \boldsymbol{\Delta}_\perp)} \\ & \times \left\{(1+x^2)\left[\boldsymbol{k}_\perp^2 - (1-x)^2\frac{\boldsymbol{\Delta}_\perp^2}{4}\right] + M^2(1-x)^4\right\} , \end{aligned} \tag{5.30}$$

$$F_{1,4}(x, \boldsymbol{k}_\perp, \boldsymbol{\Delta}_\perp) = -G_{1,1}(x, \boldsymbol{k}_\perp, \boldsymbol{\Delta}_\perp) = \frac{\alpha(1-x^2)M^2}{2\pi^2 f(x, \boldsymbol{k}_\perp, \boldsymbol{\Delta}_\perp)} , \tag{5.31}$$

$$\begin{aligned} G_{1,4}(x, \boldsymbol{k}_\perp, \boldsymbol{\Delta}_\perp) =& \frac{\alpha}{2\pi^2(1-x)f(x, \boldsymbol{k}_\perp, \boldsymbol{\Delta}_\perp)} \\ & \times \left\{(1+x^2)\left[\boldsymbol{k}_\perp^2 - (1-x)^2\frac{\boldsymbol{\Delta}_\perp^2}{4}\right] - M^2(1-x)^4\right\} , \end{aligned} \tag{5.32}$$

where

$$f(x, \boldsymbol{k}_\perp, \boldsymbol{\Delta}_\perp) = \left[\left(\boldsymbol{k}_\perp + (1-x)\frac{\boldsymbol{\Delta}_\perp}{2}\right)^2 + \mathcal{M}^2(x)\right]\left[\left(\boldsymbol{k}_\perp - (1-x)\frac{\boldsymbol{\Delta}_\perp}{2}\right)^2 + \mathcal{M}^2(x)\right]$$

and

$$\mathcal{M}^2(x) = \mu^2 x + M^2(1-x)^2 .$$

As we mentioned in Section 4.5, Wigner distributions are related to Fourier transforms of the GTMDs. One can distinguish different Wigner distributions according to the possible spin configurations assumed by the active parton and the parent particle. In particular, the GTMDs in (5.26)-(5.29) are connected to the distributions describing the situation where either the bare electron or the dressed electron are either unpolarized or polarized in the longitudinal direction: this is achieved through the definition [28]

$$\rho_{\Lambda,\lambda_e}(x, \boldsymbol{k}_\perp, \boldsymbol{b}_\perp) = \frac{1}{2}\left[\mathcal{W}^{[\gamma^+]}_{\Lambda,\Lambda}(x, \boldsymbol{k}_\perp, \boldsymbol{b}_\perp) + \lambda_e \mathcal{W}^{[\gamma^+\gamma_5]}_{\Lambda,\Lambda}(x, \boldsymbol{k}_\perp, \boldsymbol{b}_\perp)\right] , \tag{5.33}$$

where $\mathcal{W}^{[\Gamma]}_{\Lambda,\Lambda}(x, \boldsymbol{k}_\perp, \boldsymbol{b}_\perp)$ is given in Eq. (4.63). It is possible to decompose the distribution in Eq. (5.33) as

$$\rho_{\Lambda,\lambda_e} = \frac{1}{2}\left[\rho_{UU} + \Lambda\rho_{LU} + \lambda_e\rho_{UL} + \Lambda\lambda_e\rho_{LL}\right] , \tag{5.34}$$

where the dependence of both sides on the argument $(x, \boldsymbol{k}_\perp, \boldsymbol{b}_\perp)$ is understood. In the notation used in Eq. (5.34), suffixes U and L indicate respectively unpolarized and longitudinally polarized dressed electron (first entry) and internal

electron (second entry). The distributions ρ_{UL}, ρ_{LU} and ρ_{LL} actually represent the distortion caused by longitudinal polarization with respect to the unpolarized case ρ_{UU}. The following relations hold:

$$\rho_{UU}(x,\boldsymbol{k}_\perp,\boldsymbol{b}_\perp) = \int \frac{\mathrm{d}^2\boldsymbol{\Delta}_\perp}{(2\pi)^2}\, e^{-i\boldsymbol{b}_\perp\cdot\boldsymbol{\Delta}_\perp}\, F_{1,1}(x,\boldsymbol{k}_\perp,\boldsymbol{\Delta}_\perp)\,, \tag{5.35}$$

$$\rho_{LU}(x,\boldsymbol{k}_\perp,\boldsymbol{b}_\perp) = -\frac{1}{M^2}\left(\boldsymbol{k}_\perp\times\frac{\partial}{\partial\boldsymbol{b}_\perp}\right)_z \int \frac{\mathrm{d}^2\boldsymbol{\Delta}_\perp}{(2\pi)^2} e^{-i\boldsymbol{b}_\perp\cdot\boldsymbol{\Delta}_\perp}\, F_{1,4}(x,\boldsymbol{k}_\perp,\boldsymbol{\Delta}_\perp)\,, \tag{5.36}$$

$$\rho_{UL}(x,\boldsymbol{k}_\perp,\boldsymbol{b}_\perp) = \frac{1}{M^2}\left(\boldsymbol{k}_\perp\times\frac{\partial}{\partial\boldsymbol{b}_\perp}\right)_z \int \frac{\mathrm{d}^2\boldsymbol{\Delta}_\perp}{(2\pi)^2} e^{-i\boldsymbol{b}_\perp\cdot\boldsymbol{\Delta}_\perp}\, G_{1,1}(x,\boldsymbol{k}_\perp,\boldsymbol{\Delta}_\perp)\,, \tag{5.37}$$

$$\rho_{LL}(x,\boldsymbol{k}_\perp,\boldsymbol{b}_\perp) = \int \frac{\mathrm{d}^2\boldsymbol{\Delta}_\perp}{(2\pi)^2}\, e^{-i\boldsymbol{b}_\perp\cdot\boldsymbol{\Delta}_\perp}\, G_{1,4}(x,\boldsymbol{k}_\perp,\boldsymbol{\Delta}_\perp)\,. \tag{5.38}$$

It can be readily checked that $\rho_{LU}(x,\boldsymbol{k}_\perp,\boldsymbol{b}_\perp) = \rho_{UL}(x,\boldsymbol{k}_\perp,\boldsymbol{b}_\perp)$ for the dressed electron.

From a practical point of view, it turns out to be impossible to carry out the integration analytically and obtain a closed-form expression for any of the Wigner distributions in Eqs. (5.35) to (5.38). Nonetheless, if we further integrate over k_x and b_y, we obtain [28, 94, 96]

$$\rho(x,k_y,b_x) = \int \mathrm{d}b_y \mathrm{d}k_x\, \rho(x,\boldsymbol{k}_\perp,\boldsymbol{b}_\perp)\,, \tag{5.39}$$

whose analytical expressions can be derived explicitly. One obtains

$$\begin{aligned}\rho_{UU}(x,k_y,b_x) =& \frac{\alpha}{4\pi(1-x)^2}\exp\left[-2\frac{|b_x|}{1-x}\sqrt{k_y^2+\mathcal{M}^2(x)}\right]\\ &\times\frac{2M^2(1-x)^2(x^2-x+1)+(1+x^2)(2k_y^2+x\mu^2)}{k_y^2+\mathcal{M}^2(x)}\,,\end{aligned} \tag{5.40}$$

$$\begin{aligned}\rho_{LU}(x,k_y,b_x) =& \rho_{UL}(x,k_y,b_x)\\ =& -\frac{\alpha(1+x)}{2\pi(1-x)}\exp\left[-2\frac{|b_x|}{1-x}\sqrt{k_y^2+\mathcal{M}^2(x)}\right]\frac{k_y\,\mathrm{sign}(b_x)}{\sqrt{k_y^2+\mathcal{M}^2(x)}}\,,\end{aligned} \tag{5.41}$$

$$\begin{aligned}\rho_{LL}(x,k_y,b_x) =& \frac{\alpha}{4\pi(1-x)^2}\exp\left[-2\frac{|b_x|}{1-x}\sqrt{k_y^2+\mathcal{M}^2(x)}\right]\\ &\times\frac{2k_y^2(1+x^2)+x\left[2M^2(1-x)^2+\mu^2(1+x^2)\right]}{k_y^2+\mathcal{M}^2}\,.\end{aligned} \tag{5.42}$$

The k_y and b_x variables are orthogonal in the transverse plane and thus not constrained by Heisenberg uncertainty principle; consequently, (combinations of) the integrated distributions (5.40)-(5.42) have the interpretation of three-dimensional probability densities. It is clear from the analytical expressions Eqs. (5.30) to (5.32) of the GTMDs that one can obtain $\rho(x,k_x,b_y)$ from $\rho(x,k_y,b_x)$ simply through the exchange $(k_y,b_x)\to(k_x,b_y)$.

5.2.2 Numerical results

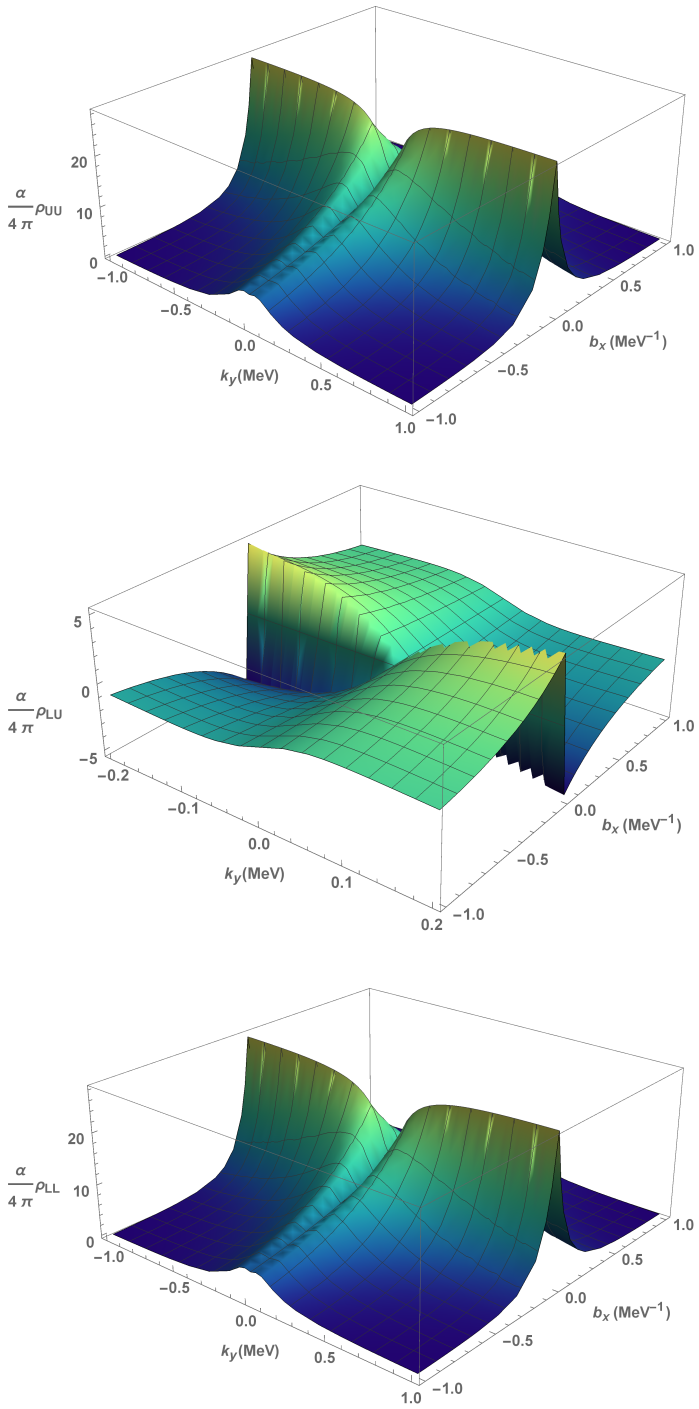

Figure 5.1: 3D-plots of the Wigner distributions ρ_{UU}, $\rho_{LU} = \rho_{UL}$ and ρ_{LL} (top to bottom), integrated over the longitudinal momentum fraction from $x = 0$ to $x = 0.9$, in the b_x-k_y space. The plots are in units of $\frac{\alpha}{4\pi}$ and the value of the masses are $M = m = 0.5$ MeV and $\mu = 0$.

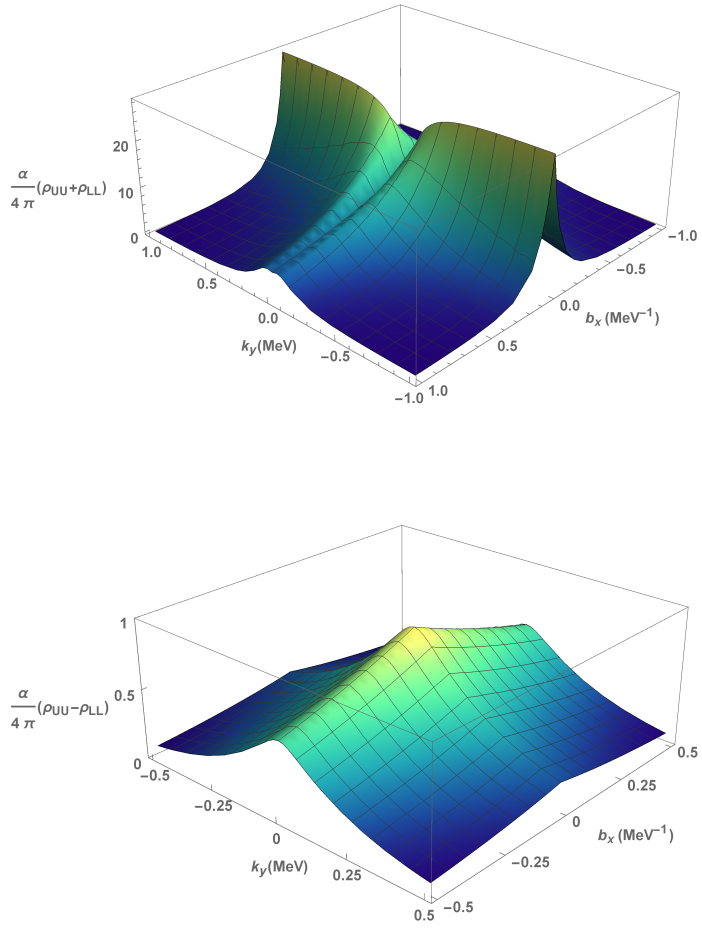

Figure 5.2: 3D-plots of the combinations of Wigner distributions $(\rho_{UU} \pm \rho_{LL})/2$ (top to bottom), integrated over the longitudinal momentum fraction from $x = 0$ to $x = 0.9$, in the b_x-k_y space. The plots are in units of $\frac{\alpha}{4\pi}$ and the value of the masses are $M = m = 0.5$ MeV and $\mu = 0$.

In Figs. 5.1 and 5.2 we report the 3D-plots plots in the k_y-b_x plane relative to the Wigner distributions ρ_{UU}, $\rho_{LU} = \rho_{UL}$, ρ_{LL} and to the combinations $(\rho_{UU} \pm \rho_{LL})/2$. Since in our treatment we have excluded the end-point, we integrate over the longitudinal momentum fraction from $x = 0$ to $x = 0.9$ to draw the plots. Accordingly, we take $\mu = 0$ for the photon mass.

We notice that the distribution ρ_{UU} is always positive, consistently with its interpretation as a probability density. At a fixed value of the impact parameter, the distribution appears even in the k_y variable and, for $b_x \neq 0$, the probability of finding the bare electron with momentum k_y inside the dressed electron has a maximum at a certain value of $|k_y|$. As $|b_x|$ grows, the value of the maximum decreases in magnitude and its position shifts from from $|k_y| = \infty$ to $k_y = 0$. At $b_x = 0$, the k_y profile exhibits a minimum for $k_y = 0$ and then reaches an

asymptotic limit for growing $|b_x|$. On the other hand, at a fixed value k_y of momentum, the probability of finding the unpolarized bare electron inside the unpolarized dressed electron at a distance b_x from the center of transverse momentum has a maximum in $b_x = 0$ and goes monotonically to zero as we move towards the periphery of the electron cloud, the fall-off becoming steeper as $|k_y|$ grows. The same behavior is observed also for ρ_{LL} as a function of (k_y, b_x); the difference between the two is in fact too small to be appreciated by eye.
Contrary to ρ_{UU} and ρ_{LL}, the distribution $\rho_{LU} = \rho_{UL}$ assumes also negative values. We stress again, however, that ρ_{LU}, as well as ρ_{UL} and ρ_{LL}, represent only the distortions with respect to ρ_{UU} caused by longitudinal polarization; therefore only the combinations $(\rho_{UU} \pm \rho_{LU})/2$ and $(\rho_{UU} \pm \rho_{LL})/2$ must be positive, in agreement with their interpretation as probability densities. This is indeed what we find, as one can readily recognize by comparing the scales of the two plots in Fig. 5.1.
The combinations $(\rho_{UU} \pm \rho_{LL})/2$ describe the probability distributions relative to the cases where the spin of the internal electron is, respectively, aligned and antialigned with the spin of the dressed electron. We note that the probability of having the spins antialigned shows an opposite behavior with respect to the aligned case, reaching a maximum for $b_x = k_y = 0$ and decreasing monotonically in both directions. By comparing the scales of the two plots we also see that the antialigned configuration is suppressed with respect to the aligned one.

Distributions in mixed position and momentum space in the x-y plane provide us information about orbital angular momentum of the dressed electron polarized in the z-direction. More precisely, the average contribution of the internal electron to OAM is given by [28]

$$l_z = \int \mathrm{d}x\, \mathrm{d}^2\boldsymbol{k}_\perp\, \mathrm{d}^2\boldsymbol{b}_\perp\, (\boldsymbol{b}_\perp \times \boldsymbol{k}_\perp)\, [\rho_{UU}(x, \boldsymbol{k}_\perp, \boldsymbol{b}_\perp) + \rho_{LU}(x, \boldsymbol{k}_\perp, \boldsymbol{b}_\perp)] \ . \tag{5.43}$$

Symmetry of ρ_{UU} with respect to the origin, both in the b_x and in the k_y direction, implies that the bare electron's contribution to OAM is zero in the unpolarized case:

$$\int \mathrm{d}x\, \mathrm{d}^2\boldsymbol{k}_\perp\, \mathrm{d}^2\boldsymbol{b}_\perp\, (\boldsymbol{b}_\perp \times \boldsymbol{k}_\perp)\, \rho_{UU}(x, \boldsymbol{k}_\perp, \boldsymbol{b}_\perp) = 0 \ . \tag{5.44}$$

On the contrary, the distribution $\rho_{LU}(k_y, b_x)$ is an odd function with respect to both variables and thus gives a non-vanishing contribution to the parent electron's OAM, that can be evaluated as [28, 98]:

$$l_z = -\int \mathrm{d}x\, \mathrm{d}^2\boldsymbol{k}_\perp \frac{\boldsymbol{k}_\perp^2}{M^2} F_{1,4}(x, \boldsymbol{k}_\perp, \boldsymbol{0}_\perp) \ . \tag{5.45}$$

Finally, we compare our results with the existing literature. We find that the analytical expression for $\rho_{UU}(x, b_x, k_y)$ in Eq. (5.40) does not match the one reported by Miller in Ref. [94], although they show a similar behavior. The reason is that in Ref. [94] a longitudinal-polarization degree of freedom for the

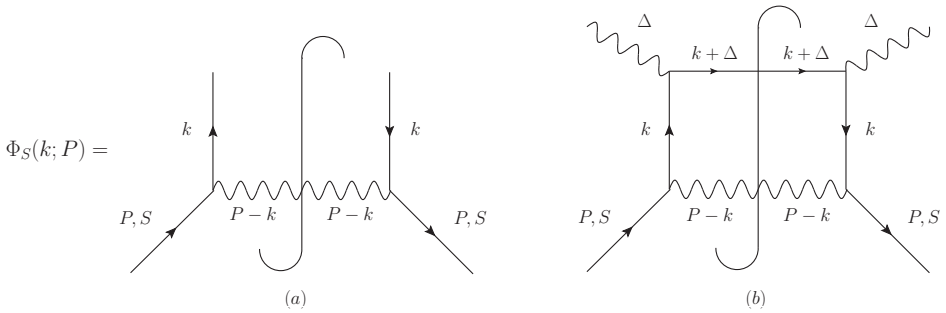

Figure 5.3: Diagrammatic representation of the correlator for the dressed electron $\Phi_S(k;P)$ (a) and QED handbag diagram (b).

massive photon is also included, giving origin to an additional contribution from the corresponding LFWFs. More recently, Kumar and Mondal [96] also produced plots of the Wigner distributions for the electron in the mixed space. Their results do not seem to be compatible with ours, as for the behavior of the considered distributions is concerned. We refrain from guessing the possible source of the discrepancies, as Ref. [96] does not provide enough details about the derivation of the plots that are necessary for a proper comparison.

5.3 TMDs for the dressed electron

In this Section we present the leading-twist Transverse-Momentum Dependent distribution functions for the electron-photon system. In an effort to provide a treatment that is as complete as possible, we derive analytical expressions for the TMDs by means of two different techniques: the diagrammatic approach with QED Feynman rules, both in light-cone gauge and Feynman gauge, and the Light-Front Wave Function overlap representation. The contribution coming from the Wilson line becomes crucial as we compare two different gauges. We thus illustrate in details how to account for it, with particular emphasis on the role of the transverse gauge link, defined in Eq. (4.12). Finally, we give a brief description of the TMDs relative to the internal photon. Our discussion mainly follows Refs. [99, 100].

5.3.1 General framework

As shown in Section 4.3, TMDs parametrize the transverse-momentum dependent correlator (4.23), that we report here in the spin basis for the dressed electron[3]:

$$\begin{aligned}\Phi_S(x,\boldsymbol{k}_\perp;P) &= \int \frac{\mathrm{d}z^-\mathrm{d}^2\boldsymbol{z}_\perp}{(2\pi)^3} e^{ik\cdot z}\langle e_D;P,S|\bar{\psi}(0)\,\psi(z)|e_D;P,S\rangle\Big|_{z^+=0} \\ &= \int \mathrm{d}k^-\Phi_S(k;P)\;. \end{aligned} \tag{5.46}$$

[3]Here we denote the momentum of the states appearing in the correlator with $p = p' = P$.

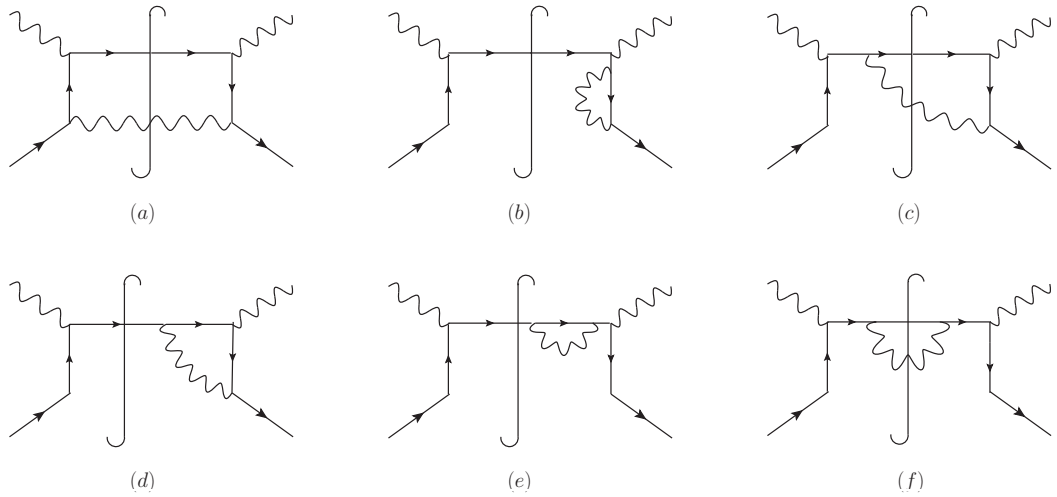

Figure 5.4: Contributions to the correlator at order α and up to second order in the gauge link. Notice that also the Hermitian conjugates of each diagram should be taken into account.

In analogy with the QCD case, the correlator (5.46) has the diagrammatic representation shown in Fig. 5.3 (a), corresponding to the "lower part" of the handbag diagram in Fig. 5.3 (b).
The QED Lagrangian (3.3) is invariant under the following local transformation of the fields:

$$\psi(z) \to e^{ie\alpha(z)}\psi(z)\,, \quad A^\mu(z) \to A^\mu(z) + \partial^\mu\alpha(z)\,. \tag{5.47}$$

Gauge-invariance of the correlator is therefore guaranteed by the insertion of a guage-link operator $\mathcal{U}_{(0,z)}$, as defined in Eq. (4.10) with $g = -e$; accordingly, we rewrite

$$\Phi_S(x, \boldsymbol{k}_\perp; P) = \int \frac{\mathrm{d}z^-\mathrm{d}^2\boldsymbol{z}_\perp}{(2\pi)^3} e^{ik\cdot z}\langle e_D; P, S|\bar{\psi}(0)\,\mathcal{U}_{(0,z)}\psi(z)|e_D; P, S\rangle\Big|_{z^+=0}\,. \tag{5.48}$$

Hereafter we will consider a future-pointing Wilson line $\mathcal{U}_{(0,z)} = \mathcal{U}_{(0,+\infty)}\mathcal{U}_{(+\infty,z)}$ [see Eqs. (4.14) and (4.15)]. From a physical point of view, this choice allows one to take into account the so-called *final-state interactions*, i.e. the (infinitely many, in principle) photons that can be emitted and re-absorbed by the outgoing particles in a SIDIS process [57, 101, 102]. The situation is represented diagrammatically in Fig. 5.4, where we show the order-α contributions to the handbag diagram (and consequently to the correlator) in presence of the gauge link. Similarly, a past-pointing Wilson line would be needed when considering a Drell-Yan process, so as to account for the *initial-state interactions* involving the incoming particles.
Diagrams (a) and (b) in Fig. 5.4 are actually of zeroth order in the gauge link, as they refer, respectively, to the handbag diagram already shown in Fig. 5.3 and to the correction due to the self-energy of the internal electron; diagrams

(c) and (d) contain one gauge photon and they are hence described using the first-order approximation of the Wilson line in the coupling constant e, while (e) and (f) are of second order in the expansion of the gauge link. Diagram (d), in particular, accounts for the virtual vertex correction; along with diagram (b) it will hence contribute only at the end point $x = 1$, $\boldsymbol{k}_\perp = \mathbf{0}_\perp$. Consistently with what we did in the case of GTMDs, we exclude the end-point from our analysis and hence neglect diagrams (b) and (d). Diagrams (e) and (f) are proportional to n_-^2 [with $n_-^\mu = (0, 1, \mathbf{0}_\perp)$] and can thus be discarded as well, as long as we take the direction of the gauge link off the light front. Nevertheless, we remark here that a proper definition of TMDs must deal also with the end points and the occurrence of infrared and rapidity divergences, which can be regularized, e.g., by taking n_- to be off the light cone. These are critical issues in proving factorization theorems and introducing well-defined TMDs, both for QCD and for QED. Careful investigations of these issues can be found in several papers and books (see e.g. [48, 103–109]).
Note that, contrarily to QCD, we can evaluate the correlator analytically either by adopting the usual Feynman rules obtained in standard perturbation theory, or via the overlap representation in terms of the QED LFWFs (5.15) to (5.18).

5.3.2 TMDs in Feynman gauge

We derive analytical expressions for the TMDs of the bare electron inside the dressed electron by working in the covariant Feynman gauge (see Section 3.2). Hereafter we assume, for simplicity, $M = m$ for the masses of the physical and bare electron and $\mu = 0$ for the internal photon.
We first focus on the gauge-link structure. In Feynman gauge the boundary condition $\boldsymbol{A}_\perp(\infty) = \mathbf{0}_\perp$ is assumed for the transverse components of the gauge field at infinity, implying that the transverse gauge link reduces to the identity in this gauge. On the other hand, the longitudinal gauge link is non-trivial, unlike in the light-cone gauge case: this means that we need to add also the contribution from diagram (c) in Fig. 5.4 (along with its Hermitian conjugate) to our calculation. The situation is summarized in Fig. 5.5.

Let us focus first on the contribution of diagram (a) in Fig. 5.5, whose amplitude can be written as

$$|\mathcal{M}|^2 = \frac{1}{(2\pi)^3}\delta\left((P-k)^2\right)\delta\left((k+\Delta)^2 - m^2\right) M_{ij}^{\text{low}} M_{ji}^{\text{up}} \,. \tag{5.49}$$

The notation used in Eq. (5.49), where we re-introduced Dirac indices explicitly, indicates that we can factor out the transition matrix corresponding to

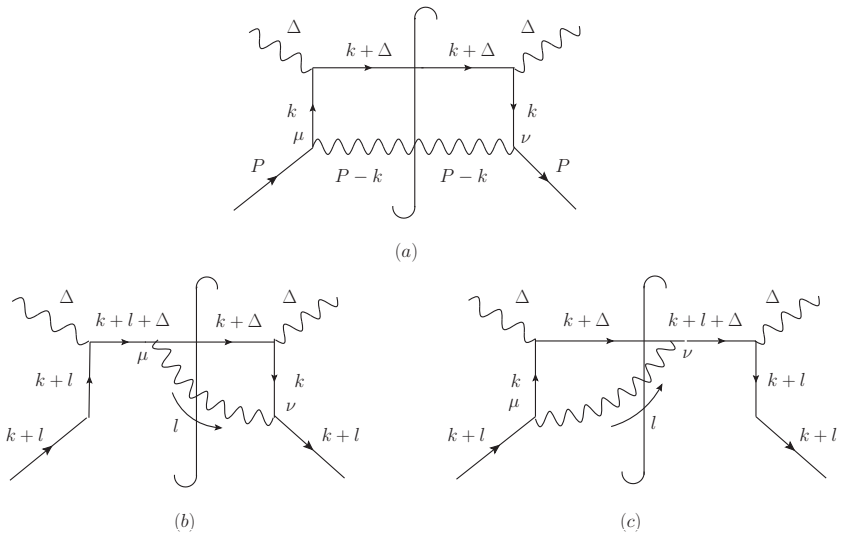

Figure 5.5: Handbag diagrams contributing to TMDs in Feynman gauge at order α and for $x \neq 1$, $\boldsymbol{k}_\perp \neq \boldsymbol{0}_\perp$.

the "upper part" of the handbag diagram[4], given by

$$\mathcal{M}^{\text{up}}_{ij} = e^2 \Big(\not{\epsilon}^*_{\lambda_v}(\Delta)(\not{k} + \not{\Delta} + m)\not{\epsilon}_{\lambda_v}(\Delta) \Big)_{ij} , \tag{5.50}$$

λ_v being the polarization of the virtual photon, from the one corresponding to the "lower part", namely

$$\mathcal{M}^{\text{low}}_{ij} = e^2 \bar{u}_{S,k}(P) \left(\gamma_\nu \frac{\not{k} + m}{k^2 - m^2 - i\epsilon} \right)_{kj} d^{\mu\nu}(P-k) \left(\frac{\not{k} + m}{k^2 - m^2 + i\epsilon} \gamma_\mu \right)_{il} u_{S,l}(P) . \tag{5.51}$$

In Eq. (5.51) we take

$$d^{\mu\nu}(p) = \sum_{\lambda_\gamma} \varepsilon^{\mu *}_{\lambda_\gamma}(p) \varepsilon^{\nu}_{\lambda_\gamma}(p) = -g^{\mu\nu} \tag{5.52}$$

in Feynman gauge, as in Eq. (3.9). The unintegrated correlator appearing in the second line of Eq. (5.46) is then related to the transition matrix of the lower part through

$$\left[\Phi_S\right]_{ij}(k;P) = \frac{1}{(2\pi)^3} \delta\left((P-k)^2\right) \mathcal{M}^{\text{low}}_{ij} . \tag{5.53}$$

The on-shell condition is equivalent to

$$\delta\left((P-k)^2\right) = \frac{1}{2(P-k)^+} \delta\left(k^- - P^- + \frac{\boldsymbol{k}_\perp^2}{2(P-k)^+} \right) , \tag{5.54}$$

[4]In the context of QED we refrain from using the QCD nomenclature of "hard" and "soft" parts of the scattering process, since it is not possible to distinguish between a perturbative and non-perturbative part.

with $P^- = m^2/(2P^+)$ in the reference frame where $\boldsymbol{P}_\perp = \boldsymbol{0}_\perp$. By integrating over k^- and projecting with different Dirac matrices Γ, we finally recover the contribution of diagram (a) in Fig. 5.5 for all TMDs. Here we take as an example the distribution $f_1^e(x, \boldsymbol{k}_\perp)$ relative to an unpolarized bare electron in an unpolarized dressed electron[5]; accordingly, we consider the trace of the correlator (5.53) multiplied by $\Gamma = \gamma^+$ (with a factor 1/2) and average over the initial-state (respectively, sum over the final-state) spin configurations. As a result, we obtain:

$$\begin{aligned} f_1^a(x, \boldsymbol{k}_\perp^2) &= \sum_S \int \mathrm{d}k^- \frac{1}{8(2\pi)^3 (P-k)^+} \delta\left(k^- - P^- + \frac{\boldsymbol{k}_\perp^2}{2(P-k)^+}\right) \\ &\quad \times \frac{(-e^2)}{(k^2-m^2)^2} \left[\bar{u}_S(P)\gamma_\mu(\not{k}+m)\gamma^+(\not{k}+m)\gamma^\mu u_S(P)\right] \\ &= \frac{1}{(2\pi)^3}\left[\frac{\boldsymbol{k}_\perp^2 + m^2(1-4x+x^2)}{x}\right]\phi^2(x, \boldsymbol{k}_\perp^2) \,, \end{aligned} \tag{5.55}$$

where $\phi(x, \boldsymbol{k}_\perp)$ is the same as in Eq. (5.10) with $M = m$ and $\mu = 0$. In Eq. (5.55) we dropped the imaginary part of the fermion propagator since the internal electron cannot be on-shell.

The evaluation of the contribution from diagrams (b) and (c) of Fig. 5.5 can be performed in a similar fashion, except for what concerns the separation of the handbag diagram into its upper and lower part.
The amplitude of diagram (b) is

$$\begin{aligned} |\mathcal{M}|^2 = &- e^4\, \delta\left(l^2\right) \delta\left((k+\Delta)^2 - m^2\right)\, \bar{u}_S(k+l)\gamma_\nu g^{\mu\nu} \frac{\not{k}+m}{k^2-m^2-i\epsilon} \\ &\times \not{\epsilon}^*_{\lambda_v}(\Delta)(\not{k}+\not{\Delta}+m)\gamma_\mu \frac{\not{k}+\not{\Delta}+\not{l}+m}{(k+\Delta+l)^2-m^2+i\epsilon} \not{\epsilon}_{\lambda_v}(\Delta) u_S(k+l) \,. \end{aligned} \tag{5.56}$$

Notice that the transition-matrix term in Eq. (5.50) cannot be factored out, due to the presence of a Dirac structure in the propagator of the electron with momentum $k + l + \Delta$. We can overcome this issue by applying the so-called *eikonal approximation* [55, 103], which consists in considering as relevant only the "-" component of the momentum of the electron after interaction with the virtual photon; moreover, it is assumed that the emission or the absorption of a "soft" photon, with small momentum l, does not alter the fermion momentum. This requirements are summarized in the following conditions:

$$\begin{aligned} &(k+\Delta+l)^- \gg (k+\Delta+l)^+ \,, \qquad &&(k+\Delta+l)^- \gg k_{i,\perp} + \Delta_{i,\perp} + l_{i,\perp} \,, \\ &(k+\Delta+l)^- \gg m \,, &&(k+\Delta)^- \gg l^- \,. \end{aligned} \tag{5.57}$$

[5]Here and in the following, we append the superscript "e" to indicate the TMDs of the internal electron.

Along with the on-shell relations $(k+\Delta)^2 = m^2$ and $l^2 = 0$, Eq. (5.57) allow us to rewrite the propagator of the struck electron as

$$\frac{\not{k} + \not{\Delta} + \not{l} + m}{(k+\Delta+l)^2 - m^2 + i\epsilon} \simeq \frac{(k+\Delta)^- \gamma^+}{2(k+\Delta)^- l^+ + i\epsilon} = \frac{\gamma^+}{2l^+ + i\epsilon'} \,, \tag{5.58}$$

where

$$\epsilon' = \frac{\epsilon}{(k+\Delta)^-}$$

is still positive, since $k + \Delta$ is the momentum of the outgoing electron. The sign of the imaginary part in the *eikonal propagator* (5.58) actually depends on the considered processes; we refer to Appendix B.3 for a brief treatment of the Drell-Yan case. The numerator of the amplitude (5.56) now contains the Dirac structure

$$\gamma_\mu(\not{k} + \not{\Delta} + m)\gamma^\mu\gamma^+ \simeq (k+\Delta)^-\gamma_\mu\gamma^+\gamma^\mu\gamma^+ = 2\gamma_\mu g^{\mu-}(k+\Delta)^-\gamma^+ \simeq 2\gamma^+(\not{k} + \not{\Delta} + m) \,, \tag{5.59}$$

where in the first and last steps we applied the eikonal approximation. As a result, the amplitude (5.56) finally becomes

$$\begin{aligned} |\mathcal{M}|^2 = &- e^4\delta\left(l^2\right)\delta\left((k+\Delta)^2 - m^2\right) \\ &\times \bar{u}_S(P) g^{\mu-} \frac{\gamma_\mu}{l^+ + i\epsilon} \frac{\not{k} + m}{k^2 - m^2 - i\epsilon} \not{\epsilon}^*_\lambda(\Delta)(\not{k} + \not{\Delta} + m)\not{\epsilon}_\lambda(\Delta) u_S(P) \,, \end{aligned} \tag{5.60}$$

and we can factor out the transition matrix related to the correlator, that reads

$$\mathcal{M}^{\text{low}}_{ij} = -\frac{e^2}{l^+ + i\epsilon} g^{\mu\nu} n_{-\mu}\, \bar{u}_{S,k}(P) \left(\gamma_\nu \frac{\not{k} + m}{k^2 - m^2 - i\epsilon}\right)_{kj} u_{S,i}(P) \,. \tag{5.61}$$

The imaginary part in the fermion propagator can be discarded with the same argument discussed for the contribution of diagram (a). As far as the denominator of the photon propagator is concerned, we have

$$\frac{1}{l^+ + i\epsilon} = \frac{1}{l^+} - i\pi\delta(l^+) \,. \tag{5.62}$$

The second term on the right-hand side is however canceled by an opposite contribution coming from diagram (c), where the photon vertex appears on the other side of the cut.

The separation of the handbag diagram into its upper and lower parts through the eikonal approximation has the diagrammatic representation shown in Fig. 5.6, where we introduce a new representation for the Feynman rules related to the eikonal propagator, illustrated in Fig. 5.7. It is easy to check that the lower diagram on the right-hand side of Fig. 5.6 yields the transition matrix (5.61).

The resulting contributions from diagrams (b) and (c) to the TMD $f_1(x, \boldsymbol{k}_\perp)$ turn out to be:

$$f_1^b(x, \boldsymbol{k}_\perp) = f_1^c(x, \boldsymbol{k}_\perp) = \frac{1}{(2\pi)^3}\left[\frac{\boldsymbol{k}_\perp^2 + m^2(1-x)^2}{(1-x)^2}\right]\varphi^2(x, \boldsymbol{k}_\perp) \,. \tag{5.63}$$

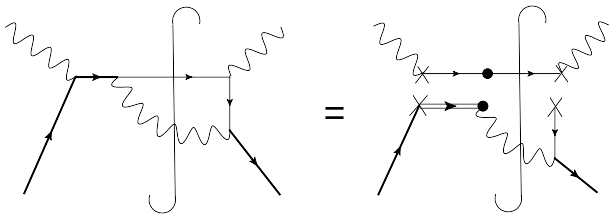

Figure 5.6: Handbag diagram with a photon loop separated into its upper and lower part, the latter corresponding to the correlator. The two factorized subdiagrams are meant to be "attached" by joining crosses with crosses and circles with circles.

Figure 5.7: Feynman rules for the eikonal propagator (left) and vertex (right), when appearing on the left-hand side of cut diagrams. Notice that the momentum flowing in the propagator is equal to the momentum of the photon attached to vertex.

If we sum the contributions in Eqs. (5.55) and (5.63), the final expression for the TMD $f_1^e(x, \boldsymbol{k}_\perp)$ is:

$$f_1^e(x, \boldsymbol{k}_\perp) = \frac{\phi^2(x, \boldsymbol{k}_\perp)}{(2\pi)^3} \left[\frac{(1+x^2)\boldsymbol{k}_\perp^2 + m^2(1-x)^4}{x(1-x)^2} \right] . \tag{5.64}$$

One can readily check that $f_1^e(x, \boldsymbol{k}_\perp) = F_{1,1}(x, \boldsymbol{k}_\perp, \boldsymbol{0}_\perp)$ by comparison of Eqs. (5.30) and (5.64), in agreement with the $\Delta \to 0$ limit of GTMDs pictured in Fig. 4.3. The same procedure yields for the remaining leading-twist TMDs[6]:

$$g_{1L}^e(x, \mathbf{k}_\perp) = \frac{1}{(2\pi)^3} \left[\frac{\mathbf{k}_\perp^2(1+x^2) - m^2(1-x)^4}{x(1-x)^2} \right] \varphi^2(x, \mathbf{k}_\perp^2), \tag{5.65}$$

$$g_{1T}^e(x, \boldsymbol{k}_\perp^2) = -\frac{2m^2}{(2\pi)^3}\, \varphi^2(x, \mathbf{k}_\perp^2) \, , \tag{5.66}$$

$$h_{1L}^{\perp e}(x, \boldsymbol{k}_\perp^2) = \frac{2m^2}{(2\pi)^3 x}\, \varphi^2(x, \mathbf{k}_\perp^2) \, , \tag{5.67}$$

$$h_{1T}^{\perp e}(x, \boldsymbol{k}_\perp^2) = 0 \, , \tag{5.68}$$

$$h_1^e(x, \boldsymbol{k}_\perp^2) = \frac{2}{(2\pi)^3} \frac{\mathbf{k}_\perp^2}{(1-x)^2}\, \varphi^2(x, \mathbf{k}_\perp^2) \, , \tag{5.69}$$

$$h_1^{\perp e}(x, \boldsymbol{k}_\perp^2) = f_{1T}^{\perp e}(x, \boldsymbol{k}_\perp^2) = 0 \, . \tag{5.70}$$

Note, in particular, that the T-odd TMDs $f_{1T}^{\perp e}$ and $h_1^{\perp e}$ are identically vanishing. This is in contrast with respect to what happens in QCD, where the Sivers [74] and Boer-Mulders [73] effects occur. This discrepancy between the

[6] In Appendix B.2 we report also, for each leading-twist TMD, the separated contributions from the three diagrams in Fig. 5.5.

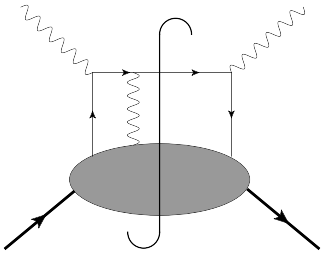

Figure 5.8: QCD handbag diagram with a gauge-photon loop at one side of the cut.

two theories is due to the fact that only diagrams with a gauge-boson loop at one side of the cut can potentially give a non-zero contribution to T-odd TMDs [101], as shown in Fig. 5.8 for the QCD handbag diagram. In our model for the electron, since the gauge photon cannot couple to the the "remnant" (that is a photon itself), only diagrams (b) and (d) of Fig. 5.4 contain such loops, but they vanish for $x \neq 1$, $\boldsymbol{k}_\perp \neq \boldsymbol{0}_\perp$. This holds true at least up to order α^2, whereas at higher orders it could be possible, in principle, to link the gauge photon by inserting fermion loops in the remnant. We will further comment on this in Section 5.4

5.3.3 TMDs in light-cone gauge

We now check that the same results that we found in the Feynman gauge are recovered also in the light-cone gauge. We will adopt both the diagrammatic approach and the formalism of light-front quantization, thus obtaining an overlap representation of TMDs in terms of LFWFs.

We already remarked that the longitudinal gauge link is trivial in the light-cone gauge. For the moment we also neglect the contribution coming from the transverse gauge link, that we will study separately later. Therefore, the expression we should start with is the correlator in Eq. (5.46). An effective way to derive explicit expressions for the TMDs is to represent the correlator in the basis where we consider the light-front helicity of both the dressed and the internal electron, and we treat them symmetrically. We can therefore define the light-front helicity amplitudes [70]:

$$\Phi_{\Lambda',\lambda'_e;\Lambda,\lambda_e}(x,\boldsymbol{k}_\perp) = \frac{1}{N}\langle e_D; P,\Lambda'|b^\dagger_{\lambda'_e}(x,\boldsymbol{k}_\perp)b_{\lambda_e}(x,\boldsymbol{k}_\perp)|e_D; P,\Lambda\rangle \,, \tag{5.71}$$

where λ_e, λ'_e are the light-front helicities of the internal electron in the initial and final state, respectively and

$$N = [2(2\pi)^3]^2 x\delta^{(3)}(\boldsymbol{0}) \,.$$

By inserting in Eq. (5.71) the Fock-state expansion (5.2), we obtain the following overlap representation of the correlator:

$$\Phi_{\Lambda',\lambda'_e;\Lambda,\lambda_e}(x,\boldsymbol{k}_\perp) = \frac{1}{2(2\pi)^3}\sum_{\lambda_\gamma}\Psi^{\Lambda'\,*}_{\lambda'_e,\lambda_\gamma}(x,\boldsymbol{k}_\perp)\Psi^{\Lambda}_{\lambda_e,\lambda_\gamma}(x,\boldsymbol{k}_\perp) \,. \tag{5.72}$$

The light-front helicity amplitudes are parametrized by the following combinations of TMDs [70, 110]:

$$\Phi = \begin{pmatrix} \frac{1}{2}(f_1^e + g_{1L}^e) & -\frac{k_R}{2m}(ih_1^{\perp e} - h_{1L}^{\perp e}) & \frac{k_L}{2m}(if_{1T}^{\perp e} + g_{1T}^e) & h_1^e \\ \frac{k_L}{2m}(ih_1^{\perp e} + h_{1L}^{\perp e}) & \frac{1}{2}(f_1^e - g_{1L}^e) & \frac{k_L^2}{2m^2}h_{1T}^{\perp e} & \frac{k_L}{2m}(if_{1T}^{\perp e} - g_{1T}^e) \\ -\frac{k_R}{2m}(if_{1T}^{\perp e} - g_{1T}^e) & \frac{k_R^2}{2m^2}h_{1T}^{\perp e} & \frac{1}{2}(f_1^e - g_{1L}^e) & -\frac{k_R}{2m}(ih_1^{\perp e} + h_{1L}^{\perp e}) \\ h_1^e & -\frac{k_R}{2m}(if_{1T}^{\perp e} + g_{1T}^e) & \frac{k_L}{2m}(ih_1^{\perp e} - h_{1L}^{\perp e}) & \frac{1}{2}(f_1^e + g_{1L}^e) \end{pmatrix}, \tag{5.73}$$

where the row entries are $(\Lambda', \lambda_e') = (++), (+-), (-+), (--)$, while the column entries are $(\Lambda, \lambda_e) = (++), (+-), (-+), (--)$. The resulting LFWF overlap representation of the T-even TMDs is:

$$\begin{aligned} f_1^e(x, \boldsymbol{k}_\perp^2) =& \frac{1}{4(2\pi)^3} \sum_{\Lambda, \lambda_e, \lambda_\gamma} |\Psi^\Lambda_{\lambda_e, \lambda_\gamma}(x, \boldsymbol{k}_\perp)|^2 \\ =& \frac{1}{2(2\pi)^3} \left[|\Psi^+_{+,+1}(x, \boldsymbol{k}_\perp)|^2 + |\Psi^+_{+,-1}(x, \boldsymbol{k}_\perp)|^2 + |\Psi^+_{-,+1}(x, \boldsymbol{k}_\perp)|^2 \right], \end{aligned} \tag{5.74}$$

$$g_{1L}^e(x, \boldsymbol{k}_\perp^2) = \frac{1}{2(2\pi)^3} \left[|\Psi^+_{+,+1}(x, \boldsymbol{k}_\perp)|^2 + |\Psi^+_{+,-1}(x, \boldsymbol{k}_\perp)|^2 - |\Psi^+_{-,+1}(x, \boldsymbol{k}_\perp)|^2 \right], \tag{5.75}$$

$$\begin{aligned} g_{1T}^e(x, \boldsymbol{k}_\perp^2) =& \frac{m}{4(2\pi)^3 \boldsymbol{k}_\perp^2} \sum_{\lambda_\gamma} \Big[k_R \, \Psi^{+\,*}_{+,\lambda_\gamma}(x, \boldsymbol{k}_\perp) \Psi^-_{+,\lambda_\gamma}(x, \boldsymbol{k}_\perp) \\ & + k_L \, \Psi^{-\,*}_{+,\lambda_\gamma}(x, \boldsymbol{k}_\perp) \Psi^+_{+,\lambda_\gamma}(x, \boldsymbol{k}_\perp) \Big], \end{aligned} \tag{5.76}$$

$$\begin{aligned} h_{1L}^{\perp e}(x, \boldsymbol{k}_\perp^2) =& \frac{m}{2(2\pi)^3 \boldsymbol{k}_\perp^2} \sum_{\lambda_\gamma} \Big[k_R \, \Psi^{+\,*}_{-,\lambda_\gamma}(x, \boldsymbol{k}_\perp) \Psi^+_{+,\lambda_\gamma}(x, \boldsymbol{k}_\perp) \\ & + k_L \, \Psi^{+\,*}_{+,\lambda_\gamma}(x, \boldsymbol{k}_\perp) \Psi^+_{-,\lambda_\gamma}(x, \boldsymbol{k}_\perp) \Big], \end{aligned} \tag{5.77}$$

$$\begin{aligned} h_{1T}^{\perp e}(x, \boldsymbol{k}_\perp^2) =& \frac{m^2}{2(2\pi)^3 \boldsymbol{k}_\perp^2} \sum_{\lambda_\gamma} \Big[k_R^2 \, \Psi^{+\,*}_{-,\lambda_\gamma}(x, \boldsymbol{k}_\perp) \Psi^-_{+,\lambda_\gamma}(x, \boldsymbol{k}_\perp) \\ & + k_L^2 \, \Psi^{-\,*}_{+,\lambda_\gamma}(x, \boldsymbol{k}_\perp) \Psi^+_{-,\lambda_\gamma}(x, \boldsymbol{k}_\perp) \Big], \end{aligned} \tag{5.78}$$

$$h_1^e(x, \boldsymbol{k}_\perp^2) = \frac{1}{2(2\pi)^3} \left[\Psi^{+\,*}_{+,+1}(x, \boldsymbol{k}_\perp) \Psi^-_{-,+1}(x, \boldsymbol{k}_\perp) + \Psi^{+\,*}_{+,-1}(x, \boldsymbol{k}_\perp) \Psi^-_{-,-1}(x, \boldsymbol{k}_\perp) \right]. \tag{5.79}$$

The analytic results found by inserting the explicit expressions (5.15)-(5.18) of the LFWFs indeed coincide with the results (5.64)-(5.70) obtained in Feynman gauge.

As already mentioned in Section 2.4.3, the LFWFs are eigenstates of the total light-front helicity of the partons $\Lambda^{e\gamma} = \lambda_e + \lambda_\gamma$ and of the total OAM $L_z = \Lambda - \Lambda^{e\gamma}$. For the two-body LFWFs of the electron, one can have only $L_z = 0$, and $L_z = \pm 1$. They are commonly labeled as S and P waves, respectively, although this is an abuse of language as partial waves should refer to L and not L_z. The LFWF overlap representation in Eqs. (5.74) to (5.79) allows one to disclose the different contributions to the TMDs from the spin and OAM configurations of the partons. In particular, f_1^e, g_{1L}^e and h_1^e are all

diagonal in the OAM, while the remaining TMDs contain different interference terms between S and P waves, and therefore involve a transfer of OAM between the initial and final electron states. The interplay between the different partial waves in the TMDs will be discussed in more detail in Section 5.3.6.

It is useful to analyze the diagrammatic approach in light-cone gauge also, in order to explicitly enlighten the gauge invariance of TMDs. Since we are disregarding the contributions from the gauge link, we need to take into account only diagram (a) in Fig. 5.5. Instead of the photon propagator (5.52) in Feynman gauge, however, we have to use the two-term propagator (3.36) that we already introduced in Section 3.3.1 and that we report here[7]:

$$d^{\mu\nu}(p) = \sum_{\lambda_\gamma=1,2} \varepsilon^{\mu *}_{\lambda_\gamma}(p)\varepsilon^{\nu}_{\lambda_\gamma}(p) = -g^{\mu\nu} + \frac{1}{p^+}\left(p^\nu n_-^\mu + p^\mu n_-^\nu\right) . \tag{5.80}$$

If we insert Eq. (5.80) into Eq. (5.51), we get three contributions for the lower part of the diagram:

$$\mathcal{M}^{\text{low}} \equiv A + B + C ,$$

with

$$A = -e^2 \bar{u}_S(P)\gamma_\mu \frac{\not{k} + m}{k^2 - m^2 - i\epsilon}\frac{\not{k} + m}{k^2 - m^2 + i\epsilon}\gamma^\mu u_S(P) , \tag{5.81}$$

$$B = \frac{e^2}{(P-k)^+}\bar{u}_S(P)\gamma^+ \frac{\not{k} + m}{k^2 - m^2 - i\epsilon}\frac{\not{k} + m}{k^2 - m^2 + i\epsilon}(\not{P} - \not{k})u_S(P) , \tag{5.82}$$

$$C = \frac{e^2}{(P-k)^+}\bar{u}_S(P)(\not{P} - \not{k})\frac{\not{k} + m}{k^2 - m^2 - i\epsilon}\frac{\not{k} + m}{k^2 - m^2 + i\epsilon}\gamma^+ u_S(P) . \tag{5.83}$$

It is now easy to recognize that the term A is equivalent to the contribution of Eq. (5.51) evaluated in the Feynman gauge. Let us focus on the B term: by using the Dirac equation $(\not{P} - m)u_S(P) = 0$, we can rewrite

$$\frac{\not{k} + m}{k^2 - m^2}(\not{P} - \not{k})u_S(P) = \frac{\not{k} + m}{k^2 - m^2}(m - \not{k})u_S(P) = -u_S(P) .$$

Hence we find that term B, which comes from the extra term in the polarization sum in light-cone gauge, actually coincides with the contribution of Eq. (5.61), treated with the eikonal approximation. The same applies also to term C, which in turn corresponds to diagram (c) of Fig. 5.5 in Feynman gauge after eikonal approximation. We can also easily check that the term of the correlator that is related to diagram (b) and (c) of Fig. 5.5 are actually vanishing in the light-cone gauge. If we still use the eikonal approximation, but substitute the polarization-vector sum in light-cone gauge in (5.61), the latter becomes:

$$\mathcal{M}^{\text{low}} = -\frac{e^2}{(P-k)^+ + i\epsilon}\bar{u}_S(P)\gamma_\nu\left[-g^{\mu\nu} + \frac{(P-k)^\mu n_-^\nu + (P-k)^\nu n_-^\mu}{(P-k)^+}\right]$$

[7] In this case we are considering a real, on-shell photon; we hence sum over the transverse degrees of freedom, omitting the term proportional to $p^2 = 0$, like we did in (3.36).

$$\times \frac{\not{k} + m}{k^2 - m^2 - i\epsilon} n_{-\mu} u_S(P) \,, \tag{5.84}$$

which contains the Dirac structure

$$-\gamma^+ + \frac{1}{(P-k)^+} \gamma_\mu n_-^\mu (P-k)^\nu n_{-\nu} + \frac{1}{(P-k)^+} (\not{P} - \not{k}) n_-^2 = 0 \,.$$

5.3.4 Transverse gauge link

In the previous sections we performed the derivation of the TMDs for the electron, first in Feynman gauge including the contribution from the longitudinal gauge link, then in light-cone gauge but neglecting the Wilson line. As a result, we found perfect agreement between the two gauges, as expected in a gauge-invariant theory; however, we did not include the transverse gauge link in the the light-cone gauge evaluation. The latter does have an important role in taking into account the final-state interactions when working in light-cone gauge, as it was noticed by Ji *et al.* in Refs. [102, 111]. The reason why the equivalence still holds is that the contribution of the transverse gauge link shows up only at $x = 1$. Even though we have so far excluded the end-point from our analysis, we find it illustrative to discuss the role of the transverse gauge link in the context of QED.

Let us go back to the diagrams contributing to the TMD correlator, shown in Fig. 5.5. We observe that, according to the cut-diagram rules, the four-momentum of the intermediate photon must be integrated over. When we use the sum over the polarization vectors in light-cone gauge given in Eq. (5.80), then, we should actually regularize the singularity due to the p^+ factor in the denominator. In practice, this can be done in three different ways, i.e. by choosing among the following prescriptions for the regularization:

$$\text{Retarded}: \quad \frac{1}{p^+} \longrightarrow \frac{1}{p^+ + i\epsilon} \,, \tag{5.85}$$

$$\text{Advanced}: \quad \frac{1}{p^+} \longrightarrow \frac{1}{p^+ - i\epsilon} \,, \tag{5.86}$$

$$\text{Principal value}: \quad \frac{1}{p^+} \longrightarrow \frac{1}{2}\left[\frac{1}{p^+ + i\epsilon} + \frac{1}{p^+ - i\epsilon}\right] \,. \tag{5.87}$$

Physical results must not depend on the choice of a specific prescription and must also coincide with their counterparts in Feynman gauge, where the problem of regularizing the denominators does not arise and the transverse gauge link does not contribute. Nonetheless, if we come back to our evaluation of the TMD $f_1^e(x, \boldsymbol{k}_\perp^2)$ from Feynman diagrams, we can quickly check that it is not the case if we do not include the contribution from the transverse gauge link at infinity.
Let us first take the retarded prescription as an example: if we make the replacement (5.85) in Eq. (5.80) and then put the latter in the amplitude

Eq. (5.51), term A in Eq. (5.81) would be unchanged, whereas terms B and C in (5.82) and (5.83) would be modified into

$$B = \frac{e^2}{(P-k)^+ + i\epsilon}\bar{u}_S(P)\gamma^+\frac{\not{k}+m}{k^2-m^2-i\epsilon}\frac{\not{k}+m}{k^2-m^2+i\epsilon}(\not{P}-\not{k})u_S(P)\,, \tag{5.88}$$

and similarly for C. We rewrite

$$\frac{1}{(P-k)^+ + i\epsilon} = \text{P.V.}\left(\frac{1}{(P-k)^+}\right) - i\pi\delta\left((P-k)^+\right)\,. \tag{5.89}$$

This leads us to the final result for the TMD f_1^e (including all three terms):

$$\begin{aligned} f_1^{\text{ret}}(x,\boldsymbol{k}_\perp^2) =& \frac{1}{(2\pi)^3}\left[\mathbf{k}_\perp^2\frac{(1+x^2)}{x(1-x)^2} + m^2\frac{(1-x)^2}{x}\right]\varphi^2(x,\mathbf{k}_\perp^2) \\ & - \frac{i}{(2\pi)^2}\left[\frac{\boldsymbol{k}_\perp^2}{1-x} + m^2(1-x)\right]\varphi^2(x,\boldsymbol{k}_\perp^2)\,\delta(1-x) \\ =& f_1^e(x,\boldsymbol{k}_\perp^2) - i\frac{e^2}{(2\pi)^2}\frac{1}{\boldsymbol{k}_\perp^2}\,\delta(1-x)\,. \end{aligned} \tag{5.90}$$

Similarly, we obtain for the advanced prescription:

$$f_1^{\text{adv}}(x,\boldsymbol{k}_\perp^2) = f_1^e(x,\boldsymbol{k}_\perp^2) + i\frac{e^2}{(2\pi)^2}\frac{1}{\boldsymbol{k}_\perp^2}\,\delta(1-x)\,. \tag{5.91}$$

In the principal-value prescription, instead, the denominators of B and C remain unchanged since

$$\frac{1}{2}\left[\frac{1}{p^+ + i\epsilon} + \frac{1}{p^+ - i\epsilon}\right] = \frac{1}{2}\left[\text{P.V.}\left(\frac{1}{p^+}\right) - i\pi\delta(p^+) + \text{P.V.}\left(\frac{1}{p^+}\right) + i\pi\delta(p^+)\right] = \frac{1}{p^+}$$

and hence the final result coincides with the one found in Feynman gauge:

$$f_1^{\text{pv}}(x,\boldsymbol{k}_\perp^2) = f_1^e(x,\boldsymbol{k}_\perp^2)\,. \tag{5.92}$$

We expect all results to be the same when adding also the transverse gauge-link contribution. In order to prove it, we perform a straightforward evaluation of the correlator (5.48) in light-cone gauge, by means of the Fock-state expansion (5.2). We can restrict immediately to the case of $f_1^e(x,\boldsymbol{k}_\perp)$ and consider the diagonal matrix element of the electron current between light-front helicity states in the correlator:

$$\Phi_\Lambda^{[\gamma^+]}(x,\boldsymbol{k}_\perp) = \int\frac{\mathrm{d}z^-\mathrm{d}^2\boldsymbol{z}_\perp}{2(2\pi)^3}\,e^{ik\cdot z}\,\langle P,\Lambda|\bar{\psi}(0)\gamma^+\mathcal{U}_{(0,\infty)}\mathcal{U}_{(\infty,z)}\psi(z)|P,\Lambda\rangle\Big|_{z^+=0}\,. \tag{5.93}$$

We approximate the Wilson line at first order in e as

$$\mathcal{U}_{(0,\infty)}\mathcal{U}_{(\infty,z)} \simeq \mathbb{1} + ie\int_{\mathbf{0}_\perp}^{\boldsymbol{z}_\perp}\mathrm{d}\boldsymbol{\xi}_\perp\cdot\boldsymbol{A}_\perp(0,\infty,\boldsymbol{\xi}_\perp) = \mathbb{1} + ie\int_0^1\mathrm{d}t\,\boldsymbol{A}_\perp(0,\infty,t\boldsymbol{z}_\perp)\cdot\boldsymbol{z}_\perp\,. \tag{5.94}$$

We neglect the identity in (5.94) and focus on the gauge-link terms. If we insert the Fock expansion (5.2), the correlator splits into the sum of four contributions. However, the term containing the gauge link between two $|e\gamma\rangle$ states is vanishing, because the photon coming from the final- (or initial-) state interaction cannot couple to the spectator photon. The term with the gauge link between one-particle states, instead, accounts for the virtual-vertex and self-energy corrections. The only relevant contributions will then come from the terms where the matrix element is between the states $|e\rangle$ and $|e\gamma\rangle$; in this situation, the gauge photon which interacts with the bare particle in the initial (or final) state coincides with the photon in the dressed electron. Therefore, we are left with the following two terms, contributing to the correlator:

$$I = ie \int \frac{\mathrm{d}z^- \mathrm{d}^2\boldsymbol{z}_\perp}{2(2\pi)^3}\, e^{ik\cdot z}\, \langle e|\bar{\psi}(0)\gamma^+ \left(\int_0^1 \mathrm{d}t\, \boldsymbol{A}_\perp(0,\infty,t\boldsymbol{z}_\perp)\cdot\boldsymbol{z}_\perp\right)\psi(z)|e\gamma\rangle\Big|_{z^+=0}, \tag{5.95}$$

$$II = ie \int \frac{\mathrm{d}z^- \mathrm{d}^2\boldsymbol{z}_\perp}{2(2\pi)^3}\, e^{ik\cdot z}\, \langle e\gamma|\bar{\psi}(0)\gamma^+ \left(\int_0^1 \mathrm{d}t\, \boldsymbol{A}_\perp(0,\infty,t\boldsymbol{z}_\perp)\cdot\boldsymbol{z}_\perp\right)\psi(z)|e\rangle\Big|_{z^+=0}. \tag{5.96}$$

After some manipulations and by resolving the integral over t, the contribution of I to f_1^e can be split into two terms, $I = I_A + I_B$, with

$$\begin{aligned} I_A =& -\frac{e}{2}\int \frac{\mathrm{d}z^- \mathrm{d}^2\boldsymbol{z}_\perp}{2(2\pi)^3}\int \frac{\mathrm{d}x' \mathrm{d}^2\boldsymbol{k}'_\perp}{2(2\pi)^3\sqrt{x'(1-x')}} e^{i(k-p_e)\cdot z} e^{-ip_\gamma^+\infty} \\ &\times \sum_{\Lambda,\lambda_e,\lambda_\gamma} \frac{\boldsymbol{\varepsilon}_{\lambda_\gamma,\perp}(p_\gamma)\cdot\boldsymbol{z}_\perp}{\boldsymbol{p}_{\gamma,\perp}\cdot\boldsymbol{z}_\perp}\, \bar{u}_\Lambda(P)\gamma^+ u_{\lambda_e}(p_e)\Psi^\Lambda_{\lambda_e,\lambda_\gamma}(x',\boldsymbol{k}'_\perp)\Big|_{z^+=0}, \end{aligned} \tag{5.97}$$

$$\begin{aligned} I_B =& \frac{e}{2}\int \frac{\mathrm{d}z^- \mathrm{d}^2\boldsymbol{z}_\perp}{2(2\pi)^3}\int \frac{\mathrm{d}x' \mathrm{d}^2\boldsymbol{k}'_\perp}{2(2\pi)^3\sqrt{x'(1-x')}} e^{i(k-p_e)\cdot z} e^{-ip_\gamma^+\infty} e^{i\boldsymbol{p}_\gamma\cdot\boldsymbol{z}_\perp} \\ &\times \sum_{\Lambda,\lambda_e,\lambda_\gamma} \frac{\boldsymbol{\varepsilon}_{\lambda_\gamma,\perp}(p_\gamma)\cdot\boldsymbol{z}_\perp}{\boldsymbol{p}_{\gamma,\perp}\cdot\boldsymbol{z}_\perp}\, \bar{u}_\Lambda(P)\gamma^+ u_{\lambda_e}(p_e)\Psi^\Lambda_{\lambda_e,\lambda_\gamma}(x',\boldsymbol{k}'_\perp)\Big|_{z^+=0}, \end{aligned} \tag{5.98}$$

where $\mathbf{p}_e = (x'P^+, \mathbf{k}'_\perp)$ and $\mathbf{p}_\gamma = ((1-x')P^+, -\mathbf{k}'_\perp)$. The sum appearing in the second line of Eqs. (5.97) and (5.98) is

$$\sum_{\Lambda,\lambda,\lambda_\gamma} \bar{u}_\Lambda(P)\gamma^+ u_{\lambda_e}(p_e)\Psi^\Lambda_{\lambda_e,\lambda_\gamma}(x',\boldsymbol{k}'_\perp)\frac{\boldsymbol{\varepsilon}_{\lambda_\gamma,\perp}(p_\gamma)\cdot\boldsymbol{z}_\perp}{\boldsymbol{p}_{\gamma,\perp}\cdot\boldsymbol{z}_\perp} = 4P^+\left(1+2\frac{x'}{1-x'}\right). \tag{5.99}$$

Equation (5.97) consequently becomes

$$\begin{aligned} I_A =& -2eP^+\int \frac{\mathrm{d}z^- \mathrm{d}^2\boldsymbol{z}_\perp}{2(2\pi)^3}\int \frac{\mathrm{d}x' \mathrm{d}^2\boldsymbol{k}'_\perp}{2(2\pi)^3\sqrt{x'(1-x')}} e^{i(k-p_e)\cdot z} \\ &\times \left(e^{-i\infty p_\gamma^+} + 2x'P^+\frac{e^{-i\infty p_\gamma^+}}{p_\gamma^+}\right)\varphi(x',\boldsymbol{k}'^2_\perp)\Big|_{z^+=0}. \end{aligned} \tag{5.100}$$

We can handle the exponential at infinity appearing in the term in brackets in Eq. (5.100) in the sense of principal-value distributions [102, 111], and write

$$\frac{e^{-i\infty p_\gamma^+}}{p_\gamma^+} \equiv \lim_{L\to\infty} \frac{e^{-iLp_\gamma^+}}{p_\gamma^+} = 2\pi i\chi\delta(p_\gamma^+) \,, \tag{5.101}$$

where χ is a constant that takes different values, according to the prescription that we adopt for the denominator:

$$\chi = \begin{cases} -1 & \text{Retarded} \,, \\ 0 & \text{Advanced} \,, \\ -\frac{1}{2} & \text{Principal value} \,. \end{cases} \tag{5.102}$$

Still in the sense of principal-value distribution, we have

$$e^{-i\infty p_\gamma^+} = 0 \,, \tag{5.103}$$

which allows us to drop the first term in the bracket of (5.100). Note that this term comes from the $-g^{\mu\nu}$ in the polarization sum, which appears in Feynman gauge also; Eq. (5.103) is then consistent with the fact that the transverse gauge link does not contribute in the Feynman gauge.

Now we can easily perform the integration over z^-, $\boldsymbol{z}_\perp$, x' and $\boldsymbol{k}'_\perp$; we finally obtain

$$I_A = -\frac{i\chi e^2}{(2\pi)^2} \frac{x}{[(1-x)m^2 + \boldsymbol{k}_\perp^2]} \delta(1-x) = \frac{ie^2}{(2\pi)^2} \frac{\chi}{\boldsymbol{k}_\perp^2} \delta(1-x) \,. \tag{5.104}$$

Let us now focus on term I_B, which is rewritten as

$$I_B = -eP^{+2} \int \frac{\mathrm{d}z^- \mathrm{d}^2\boldsymbol{z}_\perp}{(2\pi)^3} \int \frac{\mathrm{d}x' \mathrm{d}^2\boldsymbol{k}'_\perp}{(2\pi)^3\sqrt{x'(1-x')}} e^{i(k-p_e)\cdot z} \frac{e^{-i\infty p_\gamma^+}}{p_\gamma^+} \, x' \varphi(x', \boldsymbol{k}_\perp'^2) \Big|_{z^+=0} \,. \tag{5.105}$$

We notice that in any prescription (except for the advanced, where it is vanishing), it would become proportional to $\delta(1-x)$, thanks to Eq. (5.101); furthermore, the integral over $\boldsymbol{\xi}_\perp^2$ would now yield a $\delta^{(2)}(\boldsymbol{k}_\perp)$. We can henceforth conclude that this term would be relevant only at the end point ($x = 1, \boldsymbol{k}_\perp = \boldsymbol{0}_\perp$), and for this reason we neglect it in our discussion.

Term II in Eq. (5.96) can be handled in a similar fashion: it can in turn be split into the sum of two contributions, of which the first one becomes relevant only at the end point, while the second one reads

$$II_A = -\frac{eP^+}{(2\pi)^3} \int \mathrm{d}x' \frac{x'}{\sqrt{x'(1-x')}} \frac{e^{i\infty p_\gamma^+}}{p_\gamma^+} \varphi(x', \boldsymbol{k}_\perp^2) \delta(1-x) \,. \tag{5.106}$$

In the sense of principal-value distribution, also in the above equation we can write

$$\frac{e^{i\infty p_\gamma^+}}{p_\gamma^+} = 2\pi i\zeta\delta(p_\gamma^+) \,, \tag{5.107}$$

where in this case, according to the different prescriptions, the constant ζ takes the values

$$\zeta = \begin{cases} 0 & \text{Retarded ,} \\ 1 & \text{Advanced ,} \\ \frac{1}{2} & \text{Principal value .} \end{cases} \tag{5.108}$$

We now need to fix a prescription in order to proceed further. In the retarded prescription, II_A is vanishing while I_A becomes, from (5.104),

$$I_A = \frac{ie^2}{(2\pi)^2}\frac{1}{\boldsymbol{k}_\perp^2}\delta(1-x) \,. \tag{5.109}$$

If we were to fix the advanced prescription, instead, we would find that I_A is zero, while II_A would read

$$II_A = \frac{-ieP^+}{(2\pi)^2}\int \mathrm{d}x' \frac{x'}{[(1-x')^2m^2+\boldsymbol{k}_\perp^2]}\frac{\delta(1-x')}{P^+}\delta(1-x) = -\frac{ie}{(2\pi)^2}\frac{1}{\boldsymbol{k}_\perp^2}\delta(1-x) \,. \tag{5.110}$$

Finally, in the principal-value prescription the sum of I_A and II_A gives zero.

We may summarize our results by stating that the contribution of the transverse gauge link to the TMD $f_1^e(x,\boldsymbol{k}_\perp^2)$, in the different prescriptions, is

$$\begin{aligned} &\text{Retarded:} \quad \frac{ie^2}{(2\pi)^2}\frac{1}{\boldsymbol{k}_\perp^2}\delta(1-x) \,, \\ &\text{Advanced:} \quad -\frac{ie^2}{(2\pi)^2}\frac{1}{\boldsymbol{k}_\perp^2}\delta(1-x) \,, \\ &\text{Principal value:} \quad 0 \,. \end{aligned} \tag{5.111}$$

We remark that this is not what one usually finds in the case of the nucleon (see e.g. [12]), since the retarded prescription is the one corresponding to having $\boldsymbol{A}_\perp(\infty) = \boldsymbol{0}_\perp$ and hence the transverse gauge link should vanish in that prescription. However, we stress that in the present discussion we have not taken into account all the corrections to the distributions at the end point $x = 1$, and this might explain the discrepancy with the existing calculations in QCD.

If we compare the contributions in Eq. (5.111) to the values (5.90), (5.91) and (5.92) of the TMD f_1^e in the corresponding prescriptions, we see that the transverse gauge link allows one to compensate exactly for the extra terms that come from specific choices for the regularization of the pole. We thus recover the same results obtained in the Feynman gauge.

5.3.5 Photon TMDs

Although in the present work we have been focusing only on the distribution functions relative to quarks inside the nucleon (and, accordingly, to the bare

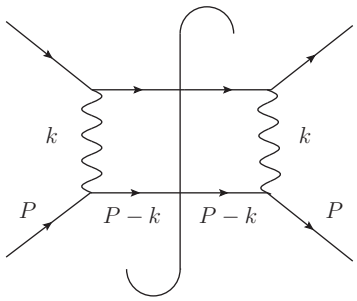

Figure 5.9: Handbag diagrams related to the photon TMDs.

electron inside the dressed electron), it is interesting to study also the contribution of the photon to the TMDs of the physical electron. This is done in analogy with the gluon distributions in QCD (see e.g. [71, 112–115]).

We still consider the scattering of the physical electron off a lepton, with the situation this time described by the handbag diagram in Fig. 5.9, where the internal photon acts as the active parton; we indicate its four-momentum with $k = (xP^+, k^-, \boldsymbol{k}_\perp)$. In this section, we add the superscript "γ" both to the correlator and to the photon TMDs to distinguish them from the ones relative to the internal electron.

The relevant correlator between initial and final electron states for photon TMDs is[8]

$$\Phi_S^{\gamma[ij]}(k;P) = \frac{1}{xP^+}\int \frac{\mathrm{d}z^-\mathrm{d}^2\boldsymbol{z}_\perp}{(2\pi)^3}\, e^{ik\cdot z}\langle P,S|F^{+j}(0)F^{+i}(z)|P,S\rangle\Big|_{z^+=0}. \tag{5.112}$$

The field tensor $F^{\mu\nu}$ in QED is already invariant under the gauge transformation (5.47); therefore in this case a Wilson line is not required. The situation is different in QCD, where the field tensor is not gauge invariant and gluon self-interactions are present.

In order to obtain the parametrization of the correlator (5.112), we introduce the symmetry operator in the transverse plane $\hat{\mathbf{S}}$, whose action on given object O^{ij} is defined by

$$\hat{\mathbf{S}}O^{ij} = \frac{1}{2}\left(O^{ij} + O^{ji} - \delta_{i,j}\sum_m O^{mm}\right). \tag{5.113}$$

The leading-twist TMDs of a photon inside the dressed electron are defined by the following decomposition of the correlator [71]:

$$\sum_{i=1}^{2}\Phi^{\gamma[ii]}(x,\boldsymbol{k}_\perp) = f_1^\gamma - \frac{\epsilon_\perp^{ij}k_\perp^i s_\perp^j}{m}f_{1T}^{\perp\gamma}, \tag{5.114}$$

$$i\epsilon^{ij}\Phi^{\gamma[ij]}(x,\boldsymbol{k}_\perp) = s_z g_{1L}^\gamma + \frac{\boldsymbol{k}_\perp\cdot\boldsymbol{s}_\perp}{m}g_{1T}^\gamma, \tag{5.115}$$

$$-\hat{\mathbf{S}}\Phi^{\gamma[ij]}(x,\boldsymbol{k}_\perp) = -\frac{\hat{\mathbf{S}}k_\perp^i k_\perp^j}{2m^2}h_1^{\perp\gamma} + s_z\frac{\hat{\mathbf{S}}\epsilon^{jk}k_\perp^i k_\perp^k}{2m^2}h_{1L}^{\perp\gamma} + \frac{\hat{\mathbf{S}}\epsilon^{jk}k_\perp^i s_\perp^k}{2m}\left(h_{1T}^\gamma + \frac{\boldsymbol{k}_\perp^2}{2m^2}h_{1T}^{\perp\gamma}\right)$$

[8] Indices i and j here refer to transverse Lorentz components.

$$+\frac{\hat{\mathbf{S}}k_\perp^i\epsilon^{jk}(2k_\perp^k\boldsymbol{k}_\perp\cdot\boldsymbol{s}_\perp-s_\perp^k\boldsymbol{k}_\perp^2)}{4m^3}h_{1T}^{\perp\gamma}\,, \tag{5.116}$$

where on the right-hand side we omitted the dependence of the TMDs on $(x,\boldsymbol{k}_\perp^2)$. For the photon TMDs we adopt the nomenclature of Ref. [71]: letters f, g and h refer,respectively, to an unpolarized, circularly polarized or linearly polarized photon, while L and T still indicate the polarization of the dressed electron in the longitudinal rather than transverse direction. Out of the eight photon TMDs implicitly defined in Eqs. (5.114) to (5.116), four are T-even ($f_1^\gamma, g_{1L}^\gamma, g_{1T}^\gamma$ and $h_1^{\perp\gamma}$) and four T-odd ($f_{1T}^{\perp\gamma}, h_{1L}^{\perp\gamma}, h_{1T}^\gamma$ and $h_{1T}^{\perp\gamma}$). If we work in the light-cone gauge, the components of the field tensor entering the correlator (5.112) reduce to $F^{+i}=\partial^+A^i$. In light-front helicity basis, the LFWF overlap representation of the correlator reads

$$\begin{aligned}\Phi^{\gamma[ij]}_{\Lambda,\Lambda'}(x,\boldsymbol{k}_\perp)=&\frac{1}{2(2\pi)^3}\sum_{\lambda_e,\lambda_\gamma,\lambda_e',\lambda_\gamma'}\Psi^{\Lambda'\,*}_{\lambda_e',\lambda_\gamma'}\left((1-x),-\boldsymbol{k}_\perp\right)\\&\times\Psi^{\Lambda}_{\lambda_e,\lambda_\gamma}\left((1-x),-\boldsymbol{k}_\perp\right)\varepsilon^{j\,*}_{\lambda_\gamma'}(k)\varepsilon^i_{\lambda_\gamma}(k)\,.\end{aligned} \tag{5.117}$$

Further development of (5.117) yields[9]

$$\begin{aligned}\Phi^{\gamma[ij]}_{\Lambda,\Lambda'}(x,\boldsymbol{k}_\perp)=&\frac{|\varphi\left((1-x),\boldsymbol{k}_\perp^2\right)|^2}{2(2\pi)^3}\bar{u}_{\Lambda'}(P)\left(-\gamma^j+\frac{k_\perp^j}{xP^+}\gamma^+\right)\\&\times(\not{p}_e+m)\left(-\gamma^i+\frac{k_\perp^i}{xP^+}\gamma^+\right)u_\Lambda(P)\,,\end{aligned} \tag{5.118}$$

where the three-momentum of the inner electron is now $\mathbf{p}_e=((1-x)P^+,-\boldsymbol{k}_\perp)$. The Feynman-gauge result is completely equivalent, the difference in the polarization vectors being compensated by the extra ∂^iA^+ term in the field tensor.

If one takes the proper combinations of helicities for the dressed electron and transverse indices, it is easy to recover from Eqs. (5.114) to (5.116) the following results for the leading-twist photon TMDs:

$$f_1^\gamma(x,\boldsymbol{k}_\perp^2)=\frac{e^2}{(2\pi)^3}\frac{\boldsymbol{k}_\perp^2\left[1+(1-x)^2\right]+m^2x^4}{x\left[\boldsymbol{k}_\perp^2+m^2x^2\right]^2}\,, \tag{5.119}$$

$$g_{1L}^\gamma(x,\boldsymbol{k}_\perp^2)=\frac{e^2}{(2\pi)^3}\frac{\boldsymbol{k}_\perp^2(2-x)+m^2x^3}{\left[\boldsymbol{k}_\perp^2+m^2x^2\right]^2}\,, \tag{5.120}$$

$$g_{1T}^\gamma(x,\boldsymbol{k}_\perp^2)=-\frac{2e^2}{(2\pi)^3}m^2\frac{x(1-x)}{\left[\boldsymbol{k}_\perp^2+m^2x^2\right]^2}\,, \tag{5.121}$$

$$h_1^{\perp\gamma}(x,\boldsymbol{k}_\perp^2)=\frac{2e^2}{(2\pi)^3}m^2\frac{(1-x)}{x\left[\boldsymbol{k}_\perp^2+m^2x^2\right]^2}\,, \tag{5.122}$$

$$f_{1T}^{\perp\gamma}(x,\boldsymbol{k}_\perp^2)=h_{1L}^{\perp\gamma}(x,\boldsymbol{k}_\perp^2)=h_{1T}^{\perp\gamma}(x,\boldsymbol{k}_\perp^2)=h_{1T}^\gamma(x,\boldsymbol{k}_\perp^2)=0\,. \tag{5.123}$$

[9]Notice that the denominator from the photon propagator does not need to be regularized, since we are not integrating over the photon momentum.

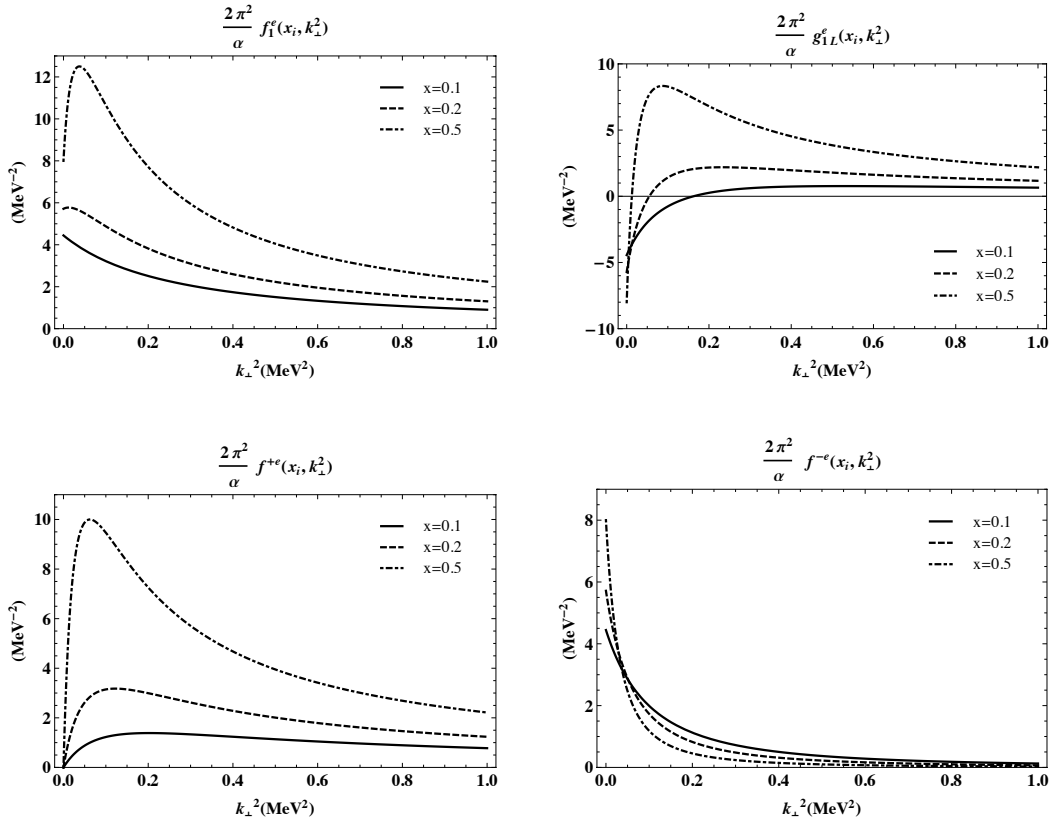

Figure 5.10: TMDs $f_1^e(x, \boldsymbol{k}_\perp^2)$ (upper-left panel), $g_{1L}^e(x, \boldsymbol{k}_\perp^2)$ (upper-right panel), along with their sum (lower-left panel) and their difference (lower-right panel). All distributions are rescaled by a factor $2\pi^2/\alpha$, and shown as function of $\boldsymbol{k}_\perp^2$, and for different values of the longitudinal momentum fraction x: $x = 0.1$ (solid lines); $x = 0.2$ (dashed lines), and $x = 0.5$ (dashed-dotted lines).

Notice that the T-odd functions are vanishing: this is not surprising, since there are no contributions that can be interpreted as final-state interactions. Even if we go up to order α^2, we can check explicitly that T-odd photon TMDs still vanish. This is probably true to all orders, since it is related to the absence of a gauge link in the correlator. The vanishing of the Sivers function up to order α^2 is also consistent with the sum rule derived by Burkardt [113,116,117], since we found that the Sivers effect for the electron vanishes both at order α and α^2.

5.3.6 Numerical results

In this section we discuss the results of our calculations for the electron and photon TMDs at $\mathcal{O}(\alpha)$, which are strictly valid at $(x, \boldsymbol{k}_\perp) \neq (1, \boldsymbol{0})$. In Fig. 5.10, we present the unpolarized TMD f_1^e (upper-left panel), and the TMD g_{1L}^e (upper-right panel) for a longitudinally polarized electron in a longitudinally polarized dressed electron, as functions of $\boldsymbol{k}_\perp^2$ and for different values of x. In the lower panels of Fig. 5.10, we show the combinations $f^{+e} = (f_1^e + g_{1L}^e)/2$ and

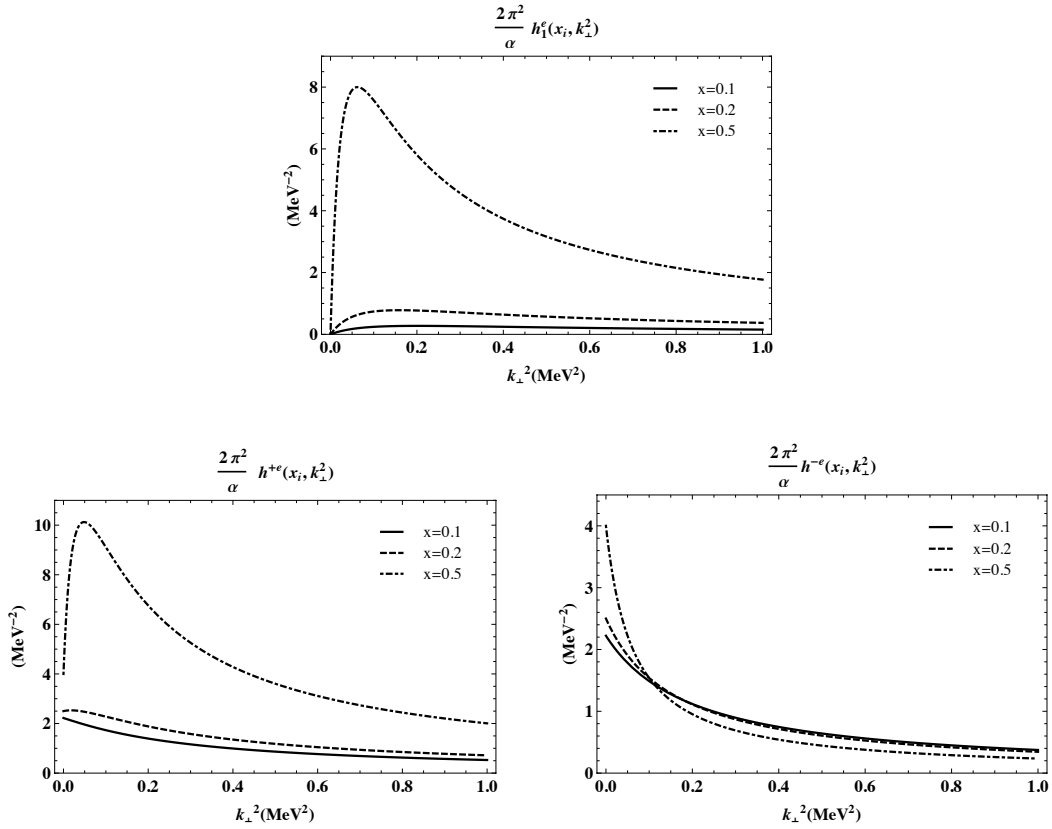

Figure 5.11: TMDs $h_1^e(x, \boldsymbol{k}_\perp^2)$ (upper panel), $h^{+e}(x, \boldsymbol{k}_\perp^2)$ (lower left panel) and $h^{-e}(x, \boldsymbol{k}_\perp^2)$ (lower right panel), rescaled by a factor $2\pi^2/\alpha$, as function of $\boldsymbol{k}_\perp^2$, and for different values of the longitudinal momentum fraction x: $x = 0.1$ (solid lines); $x = 0.2$ (dashed lines), and $x = 0.5$ (dashed-dotted lines).

$f^{-e} = (f_1^e - g_{1L}^e)/2$, describing the probability to find the internal electron with spin aligned and antialigned to the spin of the parent electron, respectively. As discussed in Section 5.3.3, f_1^e and g_{1L}^e are given by different combinations of the squares of S- and P-wave components. In particular, f_1^e is obtained from the sum of the contribution from the two partial waves, while in g_{1L}^e one has the difference between the S- and P-wave contributions. Correspondingly, with the combination f^{+e} we isolate the contribution from P waves to both f_1^e and g_{1L}^e, while f^{-e} gives the S-wave contribution which enters with a positive sign in f_1^e and a negative sign in g_{1L}^e. We notice that for $\boldsymbol{k}_\perp^2 \to 0$, the P-wave contribution is vanishing, while the S-wave contribution reaches its maximum, with larger values at increasing x. On the other side, the falloff in $\boldsymbol{k}_\perp^2$ of the S-wave contribution is very steep, and the contribution of the P wave takes over at increasing transverse momentum. This also means that, for vanishing transverse momentum, the configuration with the spin of the internal electron being antialigned with the spin of the target electron and the spin of the photon being aligned with the spin of the target electron is favored, and at larger $\boldsymbol{k}_\perp^2$ the spin of the internal electron is most likely to flip in the direction of the spin of the parent electron. The spin-flip of the active parton at low transverse

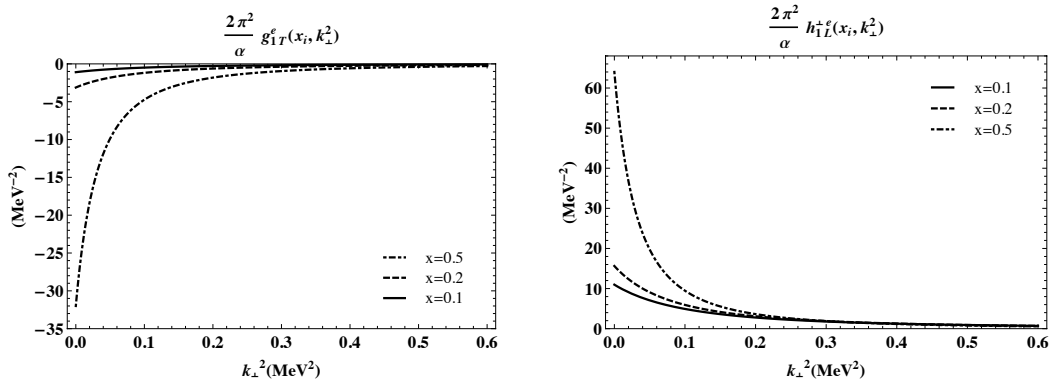

Figure 5.12: TMDs $g_{1T}^e(x, \boldsymbol{k}_\perp^2)$ (left panel), $h_{1L}^e(x, \boldsymbol{k}_\perp^2)$ (right panel), rescaled by a factor $2\pi^2/\alpha$, as function of $\boldsymbol{k}_\perp^2$, and for different values of the longitudinal momentum fraction x: $x = 0.1$ (solid lines); $x = 0.2$ (dashed lines), and $x = 0.5$ (dashed-dotted lines).

momentum is also responsible for the sign change in g_{1L}^e, which occurs faster in $\boldsymbol{k}_\perp^2$ at larger values of x.

In Fig. 5.11 we show the results for the transversity TMD h_1^e, and the combinations $h^{+e} = (f_1^e + h_1^e)/2$ and $h^{-e} = (f_1^e - h_1^e)/2$, describing the probability of finding the internal electron with transverse spin aligned and antialigned to the transverse spin of the parent electron, respectively. Being chiral odd, h_1^e involves a helicity-flip of the internal electron from the initial to the final state, which is compensated by a helicity flip of the parent electron in the same direction. Since total helicity is the same in initial and final states, h_1^e is diagonal in OAM, and, from the LFWF overlap representation in Eq. (5.79), we note that it is given in terms of the partial waves with $L_z = \pm 1$ only, without contributions from the S-wave components. The P-waves enter in h_1^e with different combinations with respect to the contribution in f_1^e and g_{1L}^e, as given by f^{+e}. In particular, from the LFWF overlap representation in Eqs. (5.74), (5.75), and (5.79), we find that f^{+e} contains the sum of the square of the $L_z = +1$ and $L_z = -1$ components, while h_1^e is given by the interference between the two P waves, i.e.

$$f^{+e}(x, \boldsymbol{k}_\perp^2) = \frac{1}{2(2\pi)^3}\left[|\Psi^+_{+,+1}(x, \boldsymbol{k}_\perp)|^2 + |\Psi^+_{+,-1}(x, \boldsymbol{k}_\perp)|^2\right] , \tag{5.124}$$

$$h_1^e(x, \boldsymbol{k}_\perp^2) = \frac{1}{(2\pi)^3}\mathrm{Re}\left[\Psi^{+\,*}_{+,+1}(x, \boldsymbol{k}_\perp)\Psi^-_{-,+1}(x, \boldsymbol{k}_\perp)\right] , \tag{5.125}$$

where we used the property (5.19) of the two-body component of the electron LFWFs. From the analytical expressions in Eqs. (5.64), (5.65) and (5.69), one also finds

$$h_1^e(x, \boldsymbol{k}_\perp^2) = \frac{2x}{1+x^2} f^{+e}(x, \boldsymbol{k}_\perp^2) . \tag{5.126}$$

As a result, h_1^e has the same dependence on $\boldsymbol{k}_\perp^2$ as f^{+e}, but its overall size is always smaller, particularly at smaller values of x. In the combination h^{+e}, the positive contribution from the S-wave components of f_1^e is evident at vanishing

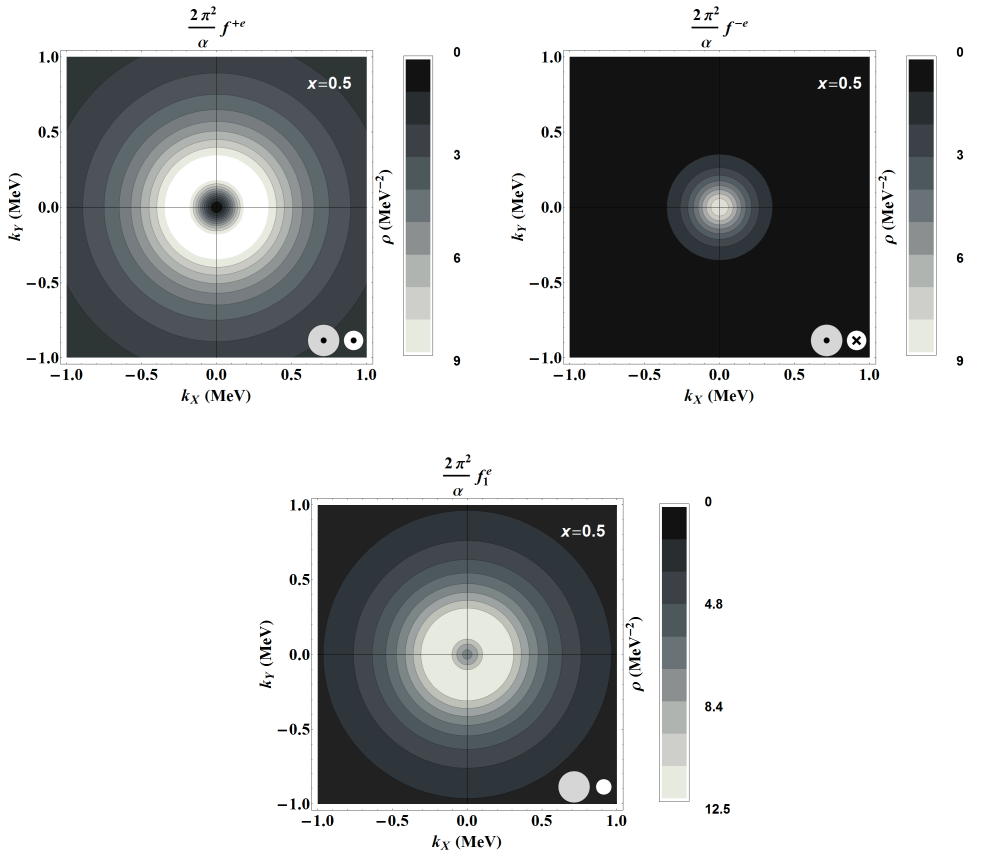

Figure 5.13: Density plots in the transverse momentum plane $k_x - k_y$ and at fixed value of $x = 0.5$ for f^{+e} (upper left panel), f^{-e} (upper right panel) and f_1^e (lower panel), rescaled by a factor $2\pi^2/\alpha$. The legend in the bottom-right corner of each panel indicates the corresponding spin configurations: the grey and white empty discs refer to the unpolarized dressed and unpolarized bare electron, respectively; the circle and cross inside the discs stand for polarization along the longitudinal axes, in opposite directions.

transverse momentum, while at higher values of $\boldsymbol{k}_\perp^2$ the contributions of the P waves from f_1^e and h_1^e become dominant. In the case of h^{-e} the P-wave contributions from f_1^e and h_1^e partially cancel, especially at higher values of x, and we find that the low-$\boldsymbol{k}_\perp^2$ behavior is dominated by the S-wave contribution of f_1^e, while the P waves still control the tail at higher transverse momentum. As a consequence, at $x = 0.5$ the transverse spin of the internal electron tends to be aligned with the transverse spin of the parent electron in the full $\boldsymbol{k}_\perp^2$ range, while for smaller values of x there is no marked preference between the parallel or antiparallel configuration of the two transverse spins. In Fig. 5.12 we show the TMD g_{1T}^e for longitudinally polarized electrons in a transversely-polarized electron target in comparison with $h_{1L}^{\perp e}$, describing the momentum distribution for transversely polarized electron in a longitudinally polarized electron target. These distributions are characteristic effects due to transverse momentum, since they are the only ones which have no analog in the spin densities related to the GPDs in the impact parameter space [118], and vanish

after integration over $\boldsymbol{k}_\perp$. Since the LFWFs $\Psi^+_{-,-}$ and $\Psi^-_{+,+}$ vanish, the LFWF overlap representation in Eqs. (5.76) and (5.77) can be rewritten as

$$g^e_{1T}(x,\boldsymbol{k}_\perp^2) = \frac{m}{2(2\pi)^3\boldsymbol{k}_\perp^2}\mathrm{Re}\left[k_R\,\Psi^{+\,*}_{+,-1}(x,\boldsymbol{k}_\perp)\Psi^-_{+,-1}(x,\boldsymbol{k}_\perp)\right], \tag{5.127}$$

$$h^{\perp e}_{1L}(x,\boldsymbol{k}_\perp^2) = \frac{m}{(2\pi)^3\boldsymbol{k}_\perp^2}\mathrm{Re}\left[k_R\,\Psi^{+\,*}_{-,+1}(x,\boldsymbol{k}_\perp)\Psi^+_{+,+1}(x,\boldsymbol{k}_\perp)\right]. \tag{5.128}$$

We notice that g^e_{1T} requires a helicity flip of the electron target that is not compensated by a change of the helicity of the internal electron, and vice versa $h^{\perp e}_{1L}$ involves a helicity flip of the internal electron, but is diagonal in the helicity of the electron target. As a result, the two distributions require a transfer of OAM between the initial and final states: in the case of g^e_{1T}, this comes from the interference of the S wave and the P wave with $L_z = +1$, while for $h^{\perp e}_{1L}$ it is driven from the S wave and the P wave with $L_z = -1$. The difference between the two P waves in Eqs. (5.15) and (5.16) leads to the following relations for the TMDs:

$$g^e_{1T}(x,\boldsymbol{k}_\perp^2) = -x h^{\perp e}_{1L}(x,\boldsymbol{k}_\perp^2), \tag{5.129}$$

which explains the suppression of g^e_{1T}, in absolute value, with respect to $h^{\perp e}_{1L}$, especially at lower values of x. From Eqs. (4.29)-(4.31) and omitting the contributions of $f^{\perp e}_{1T}$, $h^{\perp e}_1$ and $h^{\perp e}_{1T}$, which are vanishing at leading order in α, we can form the following densities for electrons of definite longitudinal or transverse polarization:

$$\rho_{\lambda_e,\boldsymbol{s}^e_\perp,\Lambda,\boldsymbol{S}_\perp}(x,\boldsymbol{k}_\perp) = \frac{1}{2}\left[f^e_1 + \lambda_e\Lambda\, g^e_{1L} + \frac{\lambda_e\,\boldsymbol{s}_\perp\cdot\boldsymbol{k}_\perp}{m}\, g^e_{1T} + \frac{\Lambda\,\boldsymbol{s}^e_\perp\cdot\boldsymbol{k}_\perp}{m}\, h^{\perp e}_{1L} + \boldsymbol{s}^e_\perp\cdot\boldsymbol{S}_\perp\, h^e_1\right], \tag{5.130}$$

where we denote the transverse spin of the internal electron with $\boldsymbol{s}^e_\perp$. In Fig. 5.13 we show the densities in the transverse momentum plane and at fixed $x = 0.5$ for a longitudinally polarized electron target and longitudinally polarized internal electron, with helicity in the same (f^{+e}) or opposite (f^{-e}) direction, along with the corresponding results for f^e_1. As discussed above, the behavior of f^{+e} is determined from the P waves, which rapidly increase starting from the dip in the center, reach a maximum at $|\boldsymbol{k}_\perp| \approx 200$ keV and smoothly decrease at larger values. On the other hand, the S-wave contribution to f^{-e} is maximum at the centre and rapidly falls off towards the periphery of the k_x-k_y plane. The interplay between the P-and S-wave contributions determines the pattern of $f^e_1 = f^{+e} + f^{-e}$ from the center to higher values of $\boldsymbol{k}_\perp$. In summary, the density of electrons in a dressed electron in momentum space, averaged over all polarizations, at $x = 0.5$, looks like a ring-shaped image, with a radius of about 200 keV. In Fig. 5.14 we show the transverse polarization densities h^{+e} and h^{-e}. Qualitatively, they look similar to their longitudinal counterparts, but they are different in the details. The P-wave contribution is more pronounced in h^{+e}, but the S wave is also present, and the density at $\boldsymbol{k}_\perp^2 = 0$ is not zero. The S wave dominates in h^{-e}, but a P-wave contribution is also present, even

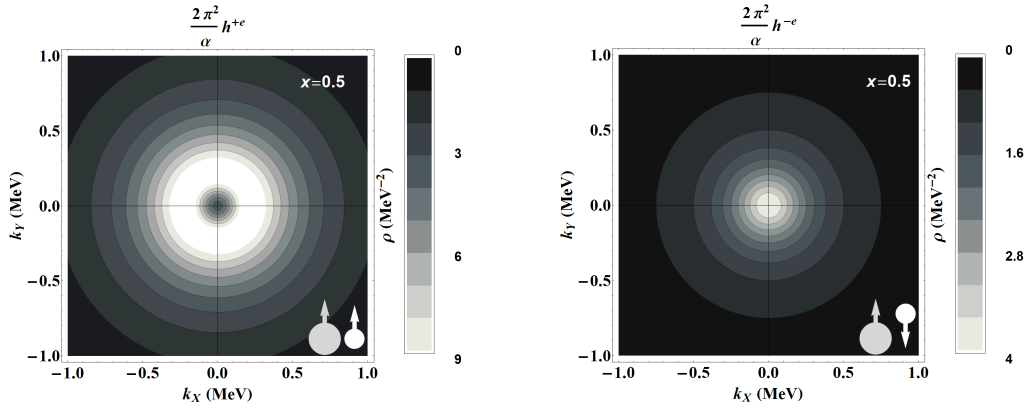

Figure 5.14: Density plots in the transverse momentum plane $k_x - k_y$ and at fixed value of $x = 0.5$ for h^{+e} (left panel) and h^{-e} (right panel), rescaled by a factor $2\pi^2/\alpha$. The legend in the bottom-right corner of each panel indicates the corresponding spin configurations: the grey and white discs refer to the dressed and bare electron, respectively; the arrows indicate polarization along the y direction.

though it is suppressed. Note that the transverse polarization density could in principle be not cylindrically symmetric. However, the fact that $h_{1T}^{\perp e}$ and $h_1^{\perp e}$ vanish in QED at this order makes the density symmetric.

In Fig. 5.15 the distorting effect induced by the polarization is shown. In the left panel, we present the density in the transverse momentum plane and at fixed $x = 0.5$ for longitudinally polarized electrons in an electron target transversely polarized along the y direction. This is obtained by adding the dipole deformation due to the term $(k_y/m)\, g_{1T}^e$ in Eq. (5.130) to the monopole distribution of f_1^e. The term in g_{1T}^e features a significant dipole deformation along the direction of the spin of the parent electron, and is responsible for the sizable downward shift along y. An analogous observation can be made for transversely polarized electrons in a longitudinally polarized electron target, as displayed in the right panel of Fig. 5.15. In this case, the effect of the distortion is even more pronounced and in the opposite direction, since the strength of the deformation is due to the term $(k_y/m)\, h_{1L}^{\perp e}$, with $h_{1L}^{\perp e} = -2g_{1T}^e$ at $x = 0.5$. We avoid showing plots of all the photon TMDs, but we take the chance to make a few observations. The functions f_1^γ and g_{1T}^γ are similar to their electron counterparts with the replacement $x \leftrightarrow (1-x)$. The helicity distribution has no straightforward relation to the electron helicity distribution. At variance with the electron case, the combination $f^{-\gamma}$ contains contributions only from P waves, while $f^{+\gamma}$ contains contributions from both P and S waves. The other nonvanishing photon TMD is the so-called Boer-Mulders function $h_1^{\perp\gamma}$, describing linearly polarized photons in an unpolarized electron [71, 73, 112]. We plot it in Fig. 5.16 (left panel), where we observe that it is very large, especially at low x. The corresponding function for gluons in a proton has been the topic of a few articles in the last years [119–121], mainly because it does not require polarized targets and it can be generated through perturbative QCD corrections [122], similarly to what happens in our QED calculation. In

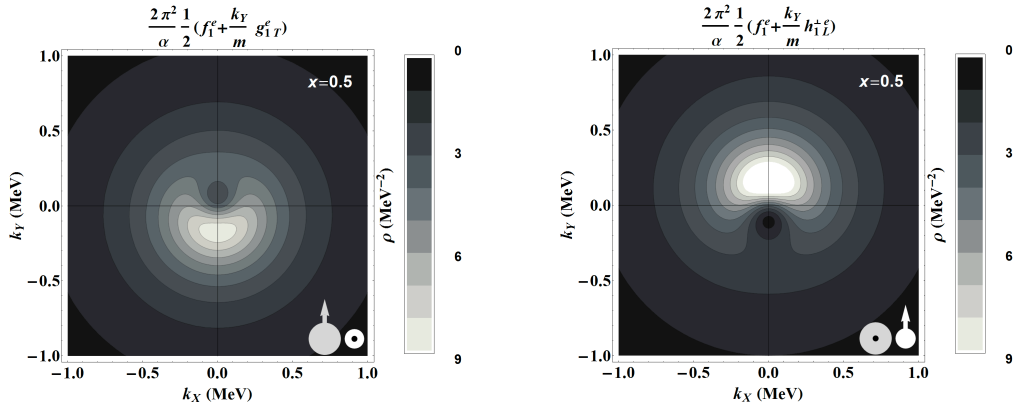

Figure 5.15: Density plots in the transverse momentum plane $k_x - k_y$ and at fixed value of $x = 0.5$ for the sum $(f_1^e + (k_y/m)\, g_{1T}^e)/2$ (left panel) and $(f_1^e + (k_y/m)\, h_{1L}^{\perp e})/2$ (right panel), rescaled by a factor $2\pi^2/\alpha$. The legend in the bottom-right corner of each panel indicates the corresponding spin configurations: the grey and white discs refer to the dressed and bare electron, respectively; the circle inside the discs stands for polarization along the longitudinal axes; the arrows indicate polarization along the y direction.

Fig. 5.16 (right panel), we plot the combination $\left[f_1^\gamma + (k_y^2 - k_x^2)/(2m^2) h_1^{\perp\gamma}\right]/2$ corresponding to the density of photons with linear polarization along the y direction in an unpolarized dressed electron. The distribution has two peaks, shifted along the polarization direction by approximately ±200 keV at $x = 0.5$.

5.4 Summary

In this Chapter we applied the formalisms of Wigner distributions and Transverse-Momentum Dependent distributions, described in Chapter 4, to the electron cloud, imagined as a electron-photon bound system. The goal was to obtain a description of the point-like electron in a new perspective, by taking into account its quantum fluctuations that give it an extended structure both in position and momentum space. To this end, we applied methods that are usually addressed to the study of nucleons in the context of QCD.
We first derived the exact (up to order α) expressions of the Light-Front Wave Functions of the dressed electron as a two-body system. As for the Wigner distributions is concerned, we provided analytical expressions for their projection in the mixed space of coordinates b_x-k_y.
We recovered analytical expressions also for the leading-twist TMDs, related both to internal electron and to the internal photon. Furthermore, in our treatment we have put particular emphasis on the issue of gauge-invariance, by explicitly checking that the results obtained in Feynman gauge coincide with those in light-cone gauge. In particular, we proved that the transverse gauge link makes the evaluation of TMDs prescription independent in light-cone gauge.
A comment is in order about the T-odd TMDs of the bare electron. We showed

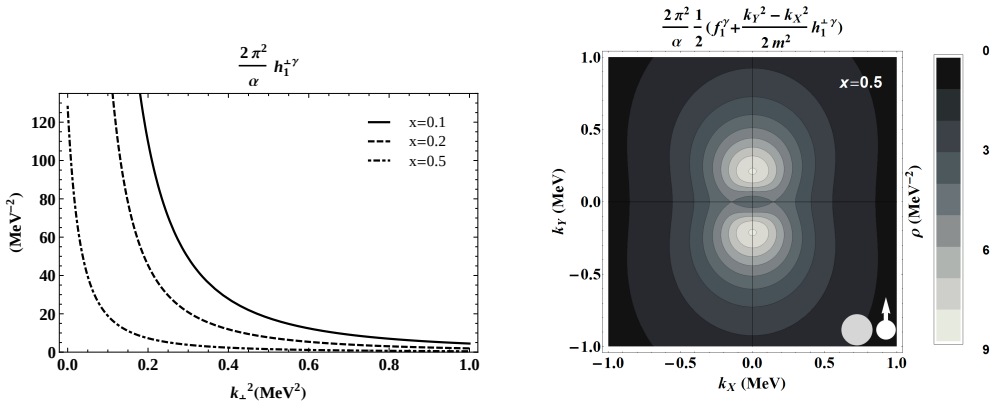

Figure 5.16: Left panel: photon TMD $h_1^{\perp\gamma}(x, \boldsymbol{k}_\perp^2)$, rescaled by a factor $2\pi^2/\alpha$, as function of $\boldsymbol{k}_\perp^2$, and for different values of the longitudinal momentum fraction x: $x = 0.1$ (solid lines); $x = 0.2$ (dashed lines), and $x = 0.5$ (dashed-dotted lines). Right panel: density plot in the transverse momentum plane $k_x - k_y$ and at fixed value of $x = 0.5$ for the combination $\left[(f_1^\gamma + (k_y^2 - k_x^2)/(2m^2)h_1^{\perp\gamma}\right]/2$, rescaled by a factor $2\pi^2/\alpha$. The legend in the bottom-right corner of indicates the corresponding spin configurations: the grey empty disc refers to the unpolarized dressed electron, the white disc with arrow indicate a photon with linear polarization along the y direction.

that they are vanishing in our model up to order α^2, at variance with the QCD case; however, the Sivers and Boer-Mulders effects should be a general property of a gauge theory, irrespectively of its Abelian rather than non-Abelian nature. This suggests that T-odd TMDs should be non-zero also in QED. One reason why we did not find this behavior in our derivation may be due to the fact that, as we already stressed, up to order α^2 it is not possible to draw a diagram with a photon loop at one side of the cut (at least as far as we exclude the end-point). However, we cannot exclude that the effects show up at higher order.

We mention that another source of investigation of the Sivers and Boer-Mulders effects in QED could be the analysis of the positronium system[10]: in this case, both the active parton and the remnant are fermions and therefore we can easily obtain a diagram that could in principle give contribution to T-odd TMDs. The situation is described in Fig. 5.17, both for the SIDIS and the Drell-Yan cases. If the T-odd TMDs of the positron in fact turn out to be non-zero, one should also observe a sign difference in the TMDs calculated in these two processes, as it is in QCD [123].

[10]One has to take into account that the positron is a spin-0 or spin-1 boson, at variance with the spin-1/2 nucleon, and modify the TMD formalism accordingly.

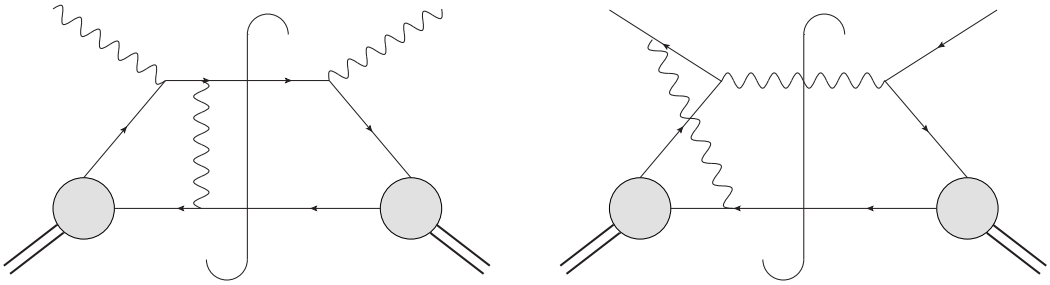

Figure 5.17: Diagrams for the SIDIS (a) and Drell-Yan (b) processes involving a positronium bound state, with a gauge-photon loop at one side of the cut.

Chapter 6

Angular-momentum density inside the nucleon

We are finally going to apply the formalism of light-front quantization to the analysis of the nucleon's structure. In particular, we will study the form factors of the QCD energy-momentum tensor, that can be connected with the Generalized Parton Distributions introduced in Chapter 4 and provide information about the quark's angular momentum density inside the nucleon.

As we mentioned in the Introduction of the present work, the ultimate goal of Hadronic Physics is to explain how global properties of protons and neutrons emerge from different contributions of their constituents. A typical example is given by the proton's spin, whose decomposition in terms of spin and Orbital Angular Momentum (OAM) of quarks and gluons has been a puzzle over the last few decades and still represents one of the key open questions in the field. Many conceptual issues concerning gauge-symmetry, relativity and non-perturbative aspects make this problem far from trivial to address, both from the theoretical and the experimental point of view. One of the most relevant issues is that the nucleon spin decomposition is not unique [7, 124–126], since it is possible to give various gauge-invariant definitions of the different contributions.
Generalized Parton Distributions help us in the investigation of the problem, as they are measurable quantities that can be related to the (kinetic) total angular momentum of quarks and gluons [66,127]. As we showed in Section 4.4.1, GPDs contain information about the spatial distribution of quarks and gluons inside the nucleon; it is therefore conceivable that they encode also information about the spatial distribution of their angular momentum. However, the relation between GPD and total angular momentum has been clearly established only at the level of quantities integrated over all space; it remains an open question how to precisely interpret the corresponding densities. The description at the density level is nonetheless relevant if we want to understand

the global properties of nucleons as arising from those of their elementary constituents.
Polyakov *et al.* provided in Refs. [128–131] an attempt to answer this question by defining angular momentum densities in terms of form factors of the QCD energy-momentum tensor in the instant-form formalism. They considered three-dimensional densities and took the limit of infinite nucleon mass, so as to avoid the relativistic corrections that we discussed in Section 4.4.1. More recently, Adhikari and Burkardt mentioned in Ref. [132] the possibility to study impact-parameter densities in the light-front quantization framework, where, as we saw, relativistic corrections are automatically avoided. In addition, they compared different definitions of the angular momentum density and reached the conclusion that none of the them agree at the density level. They attributed some of the discrepancies to missing total divergence terms, as it had been pointed out earlier in Refs. [128, 129].
In this Chapter we revisit the works of Polyakov and collaborators and discuss in detail how to connect three-dimensional densities in the instant-form and impact-parameter densities in the front-form. At variance with Ref. [128], where the Belinfante's version of the energy-momentum tensor is considered, here we take as a starting point a non-symmetric energy-momentum tensor. The comparison of the two possibilities also help us to explain the apparent inconsistencies pointed out in Ref. [132]. We follow the discussion of Ref. [133].

6.1 Canonical and Belinfante's energy-momentum tensors

In Section 2.3 we introduced the generalized angular momentum tensor at the density level

$$J^{\mu\alpha\beta}(x) = L^{\mu\alpha\beta}(x) + S^{\mu\alpha\beta}(x) \,, \tag{6.1}$$

sum of a spin-density contribution $S^{\mu\nu\rho}(x)$ and of an OAM-density contribution

$$L^{\mu\alpha\beta}(x) = x^{\alpha} T^{\mu\beta}(x) - x^{\beta} T^{\mu\alpha}(x) \,. \tag{6.2}$$

We remark that each one of these tensors is antisymmetric under $\alpha \leftrightarrow \beta$.
The Energy-Momentum Tensor (EMT) density $T^{\mu\nu}(x)$ appearing in Eq. (6.2) is referred to as *canonical* EMT and is obtained via Noether's theorem from Eq. (2.12) with the QCD Lagrangian [1]

$$\mathscr{L}_{\rm QCD} = \sum_{q}^{N_f} \bar{\psi}_q (i \not{D} - m_q) \psi_q - \frac{1}{4} G_{\mu\nu} G^{\mu\nu} \,. \tag{6.3}$$

Here N_f is the number of quark flavors, the covariant derivative reads $D^{\mu} = \partial^{\mu} - i g_s A^{\mu}$, g_s is the strong coupling constant and the field-strength tensor is

[1] Both quark and gluon fields should carry a color index. We omit them in the present discussion.

$G_{\mu\nu}(x) = \partial_\mu A_\nu(x) - \partial_\nu A_\mu(x) - ig_s\,[A_\mu(x), A_\nu(x)]$, A^μ denoting now the gluon field.
The canonical EMT it is in general neither gauge invariant nor symmetric. In particular, it follows from the conservation of both $T^{\mu\nu}$ and $J^{\mu\nu\rho}$ that the antisymmetric part is given by the divergence of the spin density:

$$T^{[\alpha\beta]}(x) = -\partial_\mu S^{\mu\alpha\beta}(x), \tag{6.4}$$

where $a^{[\mu}b^{\nu]} = a^\mu b^\nu - a^\nu b^\mu$.
Belinfante and Rosenfeld [134–136] proposed to add a so-called *superpotential* term to the definition of both the energy-momentum and generalized angular momentum tensors, defining the Belinfante-improved tensors as

$$T^{\mu\nu}_{\rm Bel}(x) = T^{\mu\nu}(x) + \partial_\lambda G^{\lambda\mu\nu}(x), \tag{6.5}$$

$$J^{\mu\alpha\beta}_{\rm Bel}(x) = J^{\mu\alpha\beta}(x) + \partial_\lambda\big[x^\alpha G^{\lambda\mu\beta}(x) - x^\beta G^{\lambda\mu\alpha}(x)\big]\ , \tag{6.6}$$

where the superpotential $G^{\lambda\mu\nu}$ is given by the combination

$$G^{\lambda\mu\nu}(x) = \frac{1}{2}\big[S^{\lambda\mu\nu}(x) + S^{\mu\nu\lambda}(x) + S^{\nu\mu\lambda}(x)\big] = -G^{\mu\lambda\nu}(x)\ . \tag{6.7}$$

In the usual hypothesis that surface terms vanish after integration, the effect of such addition is to modify the definition of the local density, without changing the total charge. The Belinfante-improved tensors (6.5)-(6.6) are conserved and usually turn out to be gauge invariant. Moreover, the particular choice (6.7) allows us to write the total AM in a purely orbital form

$$J^{\mu\alpha\beta}_{\rm Bel}(x) = x^\alpha T^{\mu\beta}_{\rm Bel}(x) - x^\beta T^{\mu\alpha}_{\rm Bel}(x). \tag{6.8}$$

Since the new tensors are conserved, it follows from this expression that the Belinfante-improved EMT is symmetric.
As discussed in Refs. [7, 137], the requirement of a symmetric EMT is usually motivated in the context of General Relativity, where the notion of spin is not accounted for from the beginning and it is natural to consider AM as purely orbital. From a Particle Physics perspective, however, one naturally includes a spin contribution to the total AM as in Eq. (6.1). In the Belinfante-improved tensors, instead, spin and angular momentum are reshuffled and the effects of spin is hidden in a new contribution to momentum that has a rather obscure interpretation. Nevertheless, the choice of the Belinfante's version seems to be the most typical in the Hadronic Physics literature.

6.1.1 Kinetic tensor

Instead of the Belinfante-improved tensors, Ji [66] proposed to use in the context of QCD the kinetic EMT

$$T^{\mu\nu}_{\rm kin}(x) = T^{\mu\nu}_{{\rm kin},q}(x) + T^{\mu\nu}_{{\rm kin},g}(x), \tag{6.9}$$

where the gauge-invariant quark and gluon contributions are given by [7, 137]

$$T^{\mu\nu}_{\text{kin},q}(x) = \frac{1}{2}\,\overline{\psi}(x)\gamma^{\mu} i\overleftrightarrow{D}^{\nu}\psi(x)\,, \tag{6.10}$$

$$T^{\mu\nu}_{\text{kin},g}(x) = -2\,\text{Tr}\left[G^{\mu\lambda}(x)G^{\nu}{}_{\lambda}(x)\right] + \frac{1}{2}\,g^{\mu\nu}\,\text{Tr}[G^{\rho\sigma}(x)G_{\rho\sigma}(x)]\,. \tag{6.11}$$

Here $\overleftrightarrow{D}^{\mu} = \overleftrightarrow{\partial}^{\mu} - ig_s A^{\mu}$, with $\overleftrightarrow{\partial}^{\mu} = \overrightarrow{\partial}^{\mu} - \overleftarrow{\partial}^{\mu}$. The kinetic generalized AM tensor is

$$J^{\mu\alpha\beta}_{\text{kin}}(x) = L^{\mu\alpha\beta}_{\text{kin},q}(x) + S^{\mu\alpha\beta}_{q}(x) + J^{\mu\alpha\beta}_{\text{kin},g}(x) \tag{6.12}$$

with

$$L^{\mu\alpha\beta}_{\text{kin},q}(x) = x^{\alpha}T^{\mu\beta}_{\text{kin},q}(x) - x^{\beta}T^{\mu\alpha}_{\text{kin},q}(x)\,, \tag{6.13}$$

$$S^{\mu\alpha\beta}_{q}(x) = \frac{1}{2}\,\varepsilon^{\mu\alpha\beta\lambda}\,\overline{\psi}(x)\gamma_{\lambda}\gamma_{5}\psi(x)\,, \tag{6.14}$$

$$J^{\mu\alpha\beta}_{\text{kin},g}(x) = x^{\alpha}T^{\mu\beta}_{\text{kin},g}(x) - x^{\beta}T^{\mu\alpha}_{\text{kin},g}(x)\,. \tag{6.15}$$

Contrary to the quark total AM, the gluon total AM cannot be split into orbital and spin contributions which are at the same time gauge-invariant and local [138, 139]. The kinetic and Belinfante-improved tensors in QCD are related as follows

$$T^{\mu\nu}_{\text{kin},q}(x) = T^{\mu\nu}_{\text{Bel},q}(x) - \frac{1}{2}\,\partial_{\lambda}S^{\lambda\mu\nu}_{q}(x)\,, \tag{6.16}$$

$$L^{\mu\alpha\beta}_{\text{kin},q}(x) + S^{\mu\alpha\beta}_{q}(x) = J^{\mu\alpha\beta}_{\text{Bel},q}(x) - \frac{1}{2}\,\partial_{\lambda}\left[x^{\alpha}S^{\lambda\mu\beta}_{q}(x) - x^{\beta}S^{\lambda\mu\alpha}_{q}(x)\right]\,, \tag{6.17}$$

while the gluon contributions are the same in both cases, namely $T^{\mu\nu}_{\text{kin},g}(x) = T^{\mu\nu}_{\text{Bel},g}(x)$ and $J^{\mu\alpha\beta}_{\text{kin},g}(x) = J^{\mu\alpha\beta}_{\text{Bel},g}(x)$. By using the conservation of the total AM $J^{\mu\alpha\beta}_{\text{kin}}(x)$ and the symmetry of $T^{\mu\nu}_{\text{kin},g}(x)$, one can relate the antisymmetric part of the quark kinetic EMT to the quark spin divergence

$$T^{[\alpha\beta]}_{\text{kin},q}(x) = -\partial_{\mu}S^{\mu\alpha\beta}_{q}(x), \tag{6.18}$$

similarly to Eq. (6.4). More explicitly, by means of the QCD equations of motion, it is possible to show that

$$\overline{\psi}(x)\gamma^{[\alpha}i\overleftrightarrow{D}^{\beta]}\psi(x) = -\varepsilon^{\alpha\beta\mu\lambda}\,\partial_{\mu}\left[\overline{\psi}(x)\gamma_{\lambda}\gamma_{5}\psi(x)\right]\,. \tag{6.19}$$

It then follows that the Belinfante-improved EMT simply coincides with the symmetric part of the kinetic EMT:

$$\frac{1}{2}\,T^{\{\mu\nu\}}_{\text{kin},a}(x) = T^{\mu\nu}_{\text{Bel},a}(x)\,, \qquad\qquad a = q, g \tag{6.20}$$

where $a^{\{\mu}b^{\nu\}} = a^{\mu}b^{\nu} + a^{\nu}b^{\mu}$. This relation is eventually due only to the total antisymmetry of the spin contribution.

Since kinetic and Belinfante-improved tensors differ by superpotential terms, they lead to the same charges. For this reason, the superpotentials are often dropped from the discussions in the literature. However, it is crucial to pay attention to these terms when discussing quantities at the density level, as we will show explicitly in the next Sections.

6.1.2 Energy-Momentum Tensor parametrization

We are interested in the matrix elements of the above-mentioned density operators. It will be sufficient to consider the operators evaluated at $x = 0$, since the general case is recovered simply through a translation of fields. Moreover, since the average position is the Fourier conjugate of the momentum transfer Δ, we need to consider off-forward matrix elements. As shown in Ref. [140], the matrix elements of the general local asymmetric Energy-Momentum Tensor for a spin-1/2 target are parametrized in terms of five form factors[2]:

$$\langle p', \boldsymbol{s}'|T^{\mu\nu}(0)|p, \boldsymbol{s}\rangle = \overline{u}(p', \boldsymbol{s}')\left[\frac{P^\mu P^\nu}{M}A(t) + \frac{P^\mu i\sigma^{\nu\lambda}\Delta_\lambda}{4M}(A+B+D)(t) + \frac{\Delta^\mu\Delta^\nu - g^{\mu\nu}\Delta^2}{M}C(t) + Mg^{\mu\nu}\bar{C}(t) + \frac{P^\nu i\sigma^{\mu\lambda}\Delta_\lambda}{4M}(A+B-D)(t)\right]u(p, \boldsymbol{s}) \,. \tag{6.21}$$

Here M denotes the nucleon mass and the three-vectors $\boldsymbol{s}$ and $\boldsymbol{s}'$ (with $\boldsymbol{s}^2 = \boldsymbol{s}'^2 = 1$) indicate the three-dimensional rest-frame polarization of the initial and final states, respectively. As for the momentum four-vector, we follow the GPD notation in Chapter 4. It is important to stress the presence of the $D(t)$ form factor, that is due to antisymmetry of the generic EMT and thus vanishes in the parametrization of the corresponding Belinfante's version.
Beside the EMT, we also need a parametrization of the matrix elements of the quark spin operator $S_q^{\mu\alpha\beta}(0)$. Owing to Eq. (6.14), we can write

$$\langle p', \boldsymbol{s}'|S_q^{\mu\alpha\beta}(0)|p, \boldsymbol{s}\rangle = \frac{1}{2}\varepsilon^{\mu\alpha\beta\lambda}\,\overline{u}(p', \boldsymbol{s}')\left[\gamma_\lambda\gamma_5\,G_A^q(t) + \frac{\Delta_\lambda\gamma_5}{2M}\,G_P^q(t)\right]u(p, \boldsymbol{s}), \tag{6.22}$$

where $G_A^q(t)$ and $G_P^q(t)$ are, respectively, the axial-vector and induced pseudoscalar form factors already introduced in Eq. (4.39). It then follows from the QCD identity (6.19) that the form factor associated with the antisymmetric part of the quark EMT is related to the axial-vector form factor according to [7, 140]

$$D_q(t) = -G_A^q(t) \,. \tag{6.23}$$

6.2 Three-dimensional densities in the instant form

Inspired by Sachs' interpretation of the electromagnetic form factors in the Breit frame [141], Polyakov and collaborators discussed the spatial distribution of angular momentum in instant form based on the Belinfante form of the EMT [128–131]. Here we revisit their discussion in more detail by using, this

[2]Several notations can be found in the literature to denote the form factors; here we use the convention of Ref. [7]. See Ref. [130] for more details.

time, the more general asymmetric EMT.
In the following we will consider the kinetic version (6.9) of the EMT. As we aim to discuss how OAM and spin contribute to the total angular momentum, emphasizing at the same time the role of the antisymmetric part of the EMT, from now on we will disregard the gluon term of the kinetic EMT, in view of the considerations that we made after Eqs. (6.15) and (6.17). It will therefore be understood that $T^{\mu\nu} = T^{\mu\nu}_{\mathrm{kin},q}$, the latter being given in Eq. (6.10).

Let us start with the definition of kinetic OAM distribution in four-dimensional position space

$$\langle L^i \rangle(x) = \varepsilon^{ijk}\, x^j \int \frac{\mathrm{d}^3\boldsymbol{\Delta}}{(2\pi)^3}\, e^{i\Delta\cdot x}\, \langle T^{0k} \rangle, \tag{6.24}$$

where we introduced for convenience

$$\langle T^{\mu\nu} \rangle \equiv \frac{\langle p', \boldsymbol{s}|T^{\mu\nu}(0)|p, \boldsymbol{s}\rangle}{2\sqrt{p'^0 p^0}}\ . \tag{6.25}$$

Notice that the energy transfer Δ^0 is not an independent variable but a function of the three-momentum transfer $\boldsymbol{\Delta}$ through the on-shell conditions (4.4); more precisely, we have

$$\Delta^0 = \frac{\boldsymbol{P}\cdot\boldsymbol{\Delta}}{P^0}, \qquad P^0 = \frac{1}{2}\left[\sqrt{\left(\boldsymbol{P}+\frac{\boldsymbol{\Delta}}{2}\right)^2 + M^2} + \sqrt{\left(\boldsymbol{P}-\frac{\boldsymbol{\Delta}}{2}\right)^2 + M^2}\right]. \tag{6.26}$$

By using integration by parts, and disregarding as usual the surface term, we rewrite Eq. (6.24) as

$$\langle L^i \rangle(x) = \varepsilon^{ijk} \int \frac{\mathrm{d}^3\boldsymbol{\Delta}}{(2\pi)^3}\, e^{i\Delta\cdot x}\left[-i\frac{\partial\langle T^{0k}\rangle}{\partial\Delta^j} + \frac{x^0}{2}\left(\frac{p'^j}{p'^0} + \frac{p^j}{p^0}\right)\langle T^{0k}\rangle\right]. \tag{6.27}$$

The second term in square brackets is in general different from zero. Its explicit time dependence comes from the non-conservation of the individual contributions to the total AM of the system. We can give it an interpretation as a distortion that changes the OAM distribution about the center of energy of the system, whit respect to the situation at rest (i.e. $\boldsymbol{P} = \boldsymbol{0}$). Accordingly, this term goes to zero if we take $\boldsymbol{L}$ and $\boldsymbol{P}$ parallel. It is interesting to notice that the total OAM remains nonetheless unvaried, as the distortion vanishes upon integration over space:

$$\varepsilon^{ijk}\int \mathrm{d}^3\boldsymbol{x} \int \frac{\mathrm{d}^3\boldsymbol{\Delta}}{(2\pi)^3} e^{-i\Delta\cdot x}\, \frac{x^0}{2}\left(\frac{p'^j}{p'^0} + \frac{p^j}{p^0}\right)\langle T^{0k}\rangle = \varepsilon^{ijk} x^0 \frac{P^j}{P^0}\langle T^{0k}\rangle\Big|_{\Delta=0} = 0\ , \tag{6.28}$$

where we used $\langle T^{0k}\rangle \xrightarrow{\Delta=0} 2P^0P^k$.
A simple way to get rid of the distortion term, along with the x^0 dependence in Eq. (6.27), is to restrict ourselves to the Breit (or "brick-wall") frame (BF),

defined by the condition $\boldsymbol{P} = \boldsymbol{0}$. This implies in particular $\Delta^0 = 0$ and $P^0 = \sqrt{\frac{\boldsymbol{\Delta}^2}{4} + M^2}$. We can then define the spatial density of kinetic OAM as[3]

$$\langle L^i \rangle(\boldsymbol{x}) = -i\varepsilon^{ijk} \int \frac{\mathrm{d}^3\boldsymbol{\Delta}}{(2\pi)^3}\, e^{-i\boldsymbol{\Delta}\cdot\boldsymbol{x}}\, \frac{\partial \langle T^{0k} \rangle}{\partial \Delta^j}\bigg|_{\mathrm{BF}} , \tag{6.29}$$

where the notation indicates that we need to take the Breit-frame limit *after* derivation. Eq. (6.29) is indeed consistent with a density interpretation since $\boldsymbol{p}' = -\boldsymbol{p}$ implies that the initial and final wave functions undergo the same Lorentz contraction.
We use the general parametrization (6.21) with the same rest-frame polarization three-vector $\boldsymbol{s}$ for both the initial and final states. If we insert the following relations involving Dirac bilinears [142]:

$$\overline{u}\left(\tfrac{\boldsymbol{\Delta}}{2}, \boldsymbol{s}\right) \gamma_5 u\left(-\tfrac{\boldsymbol{\Delta}}{2}, \boldsymbol{s}\right) = -(\boldsymbol{\Delta}\cdot\boldsymbol{s}) , \tag{6.30}$$

$$\overline{u}\left(\tfrac{\boldsymbol{\Delta}}{2}, \boldsymbol{s}\right) \gamma^k \gamma_5 u\left(-\tfrac{\boldsymbol{\Delta}}{2}, \boldsymbol{s}\right) = 2P^0 s^k - \frac{\Delta^k(\boldsymbol{\Delta}\cdot\boldsymbol{s})}{2(P^0 + M)} , \tag{6.31}$$

$$\overline{u}\left(\tfrac{\boldsymbol{\Delta}}{2}, \boldsymbol{s}\right) i\sigma^{k\lambda}\Delta_\lambda u\left(-\tfrac{\boldsymbol{\Delta}}{2}, \boldsymbol{s}\right) = -2M\, i\epsilon^{klm}\Delta^l s^m , \tag{6.32}$$

we find that the kinetic OAM density reads

$$\langle L^i \rangle(\boldsymbol{x}) = \int \frac{\mathrm{d}^3\boldsymbol{\Delta}}{(2\pi)^3}\, e^{-i\boldsymbol{\Delta}\cdot\boldsymbol{x}} \left[s^i\, L(t) + \left[(\boldsymbol{\Delta}\cdot\boldsymbol{s})\Delta^i - \boldsymbol{\Delta}^2 s^i\right] \frac{\mathrm{d}L(t)}{\mathrm{d}t} \right]_{t=-\boldsymbol{\Delta}^2} , \tag{6.33}$$

where we introduced for convenience the combination of energy-momentum form factors

$$L(t) = \frac{1}{2}\left[A(t) + B(t) + D(t)\right] . \tag{6.34}$$

Similarly, for the spin density we find that

$$\begin{aligned} \langle S^i \rangle(\boldsymbol{x}) &= \frac{1}{2}\,\varepsilon^{ijk} \int \frac{\mathrm{d}^3\boldsymbol{\Delta}}{(2\pi)^3}\, e^{-i\boldsymbol{\Delta}\cdot\boldsymbol{x}}\, \langle S^{0jk} \rangle\big|_{\mathrm{BF}} \\ &= \int \frac{\mathrm{d}^3\boldsymbol{\Delta}}{(2\pi)^3}\, e^{-i\boldsymbol{\Delta}\cdot\boldsymbol{x}} \left[\frac{s^i}{2}\, G_A(t) - \frac{(\boldsymbol{\Delta}\cdot\boldsymbol{s})\,\Delta^i}{4}\, \frac{\mathrm{d}G(t)}{\mathrm{d}t} \right]_{t=-\boldsymbol{\Delta}^2} , \end{aligned} \tag{6.35}$$

where we introduced for better readability

$$\frac{\mathrm{d}G(t)}{\mathrm{d}t} = \frac{1}{2P^0}\left[\frac{G_A(t)}{P^0 + M} + \frac{G_P(t)}{M} \right] . \tag{6.36}$$

As we previously mentioned, Polyakov and collaborators [128–131] considered the Belinfante-improved form of the EMT. Recalling that $T^{\mu\nu}_{\mathrm{Bel}} = \frac{1}{2}T^{\{\mu\nu\}}$, it is

[3] We note in passing that the incorrect sign for the Fourier transform was used in [128–131].

easy to see that the density of Belinfante-improved total AM assumes the same structure as in Eq. (6.33), but now without the $D(t)$ contribution:

$$\langle J^i_{\rm Bel}\rangle(\boldsymbol{x}) = \int \frac{\mathrm{d}^3\boldsymbol{\Delta}}{(2\pi)^3}\, e^{-i\boldsymbol{\Delta}\cdot\boldsymbol{x}} \left[s^i\, J(t) + \left[(\boldsymbol{\Delta}\cdot\boldsymbol{s})\Delta^i - \boldsymbol{\Delta}^2 s^i\right] \frac{\mathrm{d}J(t)}{\mathrm{d}t} \right]_{t=-\boldsymbol{\Delta}^2}, \quad (6.37)$$

where we used Polyakov's form factor

$$J(t) = \frac{1}{2}\left[A(t) + B(t)\right]. \quad (6.38)$$

We can compare this expression with the kinetic total AM density $\langle J^i\rangle(\boldsymbol{x}) = \langle L^i\rangle(\boldsymbol{x}) + \langle S^i\rangle(\boldsymbol{x})$. From Eqs. (6.33) and (6.35) and taking into account that $D(t) = -G_A(t)$, we find

$$\begin{aligned}\left\langle J^i\right\rangle(\boldsymbol{x}) &= \int \frac{\mathrm{d}^3\boldsymbol{\Delta}}{(2\pi)^3}\, e^{-i\boldsymbol{\Delta}\cdot\boldsymbol{x}} \\ &\times \left[s^i\, J(t) + \left[(\boldsymbol{\Delta}\cdot\boldsymbol{s})\Delta^i - \boldsymbol{\Delta}^2 s^i\right] \frac{\mathrm{d}L(t)}{\mathrm{d}t} - \frac{(\boldsymbol{\Delta}\cdot\boldsymbol{s})\,\Delta^i}{4}\, \frac{\mathrm{d}G(t)}{\mathrm{d}t} \right]_{t=-\boldsymbol{\Delta}^2}. \end{aligned} \quad (6.39)$$

Therefore we have at the density level

$$\langle J^i\rangle(\boldsymbol{x}) \neq \langle J^i_{\rm Bel}\rangle(\boldsymbol{x}), \quad (6.40)$$

while

$$\left\langle J^i\right\rangle = \int \mathrm{d}^3\boldsymbol{x}\, \langle J^i\rangle(\boldsymbol{x}) = \int \mathrm{d}^3\boldsymbol{x}\, \langle J^i_{\rm Bel}\rangle(\boldsymbol{x}) = s^i J(0), \quad (6.41)$$

which is nothing but the Ji relation [66] in the rest frame of the target. The reason for this mismatch is the total divergence in Eq. (6.17). We obtain for the corresponding density

$$\begin{aligned}\langle M^i\rangle(\boldsymbol{x}) &= \frac{1}{2}\,\varepsilon^{ijk} \int \frac{\mathrm{d}^3\boldsymbol{\Delta}}{(2\pi)^3}\, e^{-i\boldsymbol{\Delta}\cdot\boldsymbol{x}}\, \Delta^l\, \frac{\partial\langle S^{l0k}\rangle}{\partial\Delta^j}\bigg|_{\rm BF} \\ &= -\int \frac{\mathrm{d}^3\boldsymbol{\Delta}}{(2\pi)^3}\, e^{-i\boldsymbol{\Delta}\cdot\boldsymbol{x}} \left[\frac{\left[(\boldsymbol{\Delta}\cdot\boldsymbol{s})\Delta^i - \boldsymbol{\Delta}^2 s^i\right]}{2}\, \frac{\mathrm{d}G_A(t)}{\mathrm{d}t} + \frac{(\boldsymbol{\Delta}\cdot\boldsymbol{s})\,\Delta^i}{4} \frac{\mathrm{d}G(t)}{\mathrm{d}t} \right]_{t=-\boldsymbol{\Delta}^2}, \end{aligned} \quad (6.42)$$

leading then to

$$\langle J^i\rangle(\boldsymbol{x}) = \langle J^i_{\rm Bel}\rangle(\boldsymbol{x}) + \langle M^i\rangle(\boldsymbol{x}), \quad (6.43)$$

as expected.
Notice that, since integrating over $\boldsymbol{x}$ is equivalent to setting $\boldsymbol{\Delta} = \boldsymbol{0}$, from Eqs. (6.37), (6.39) and (6.41) we can also write

$$J^i = s^i \int \mathrm{d}^3\boldsymbol{x} \int \frac{\mathrm{d}^3\boldsymbol{\Delta}}{(2\pi)^3}\, e^{-i\boldsymbol{\Delta}\cdot\boldsymbol{x}}\, J(-\boldsymbol{\Delta}^2). \quad (6.44)$$

It may therefore be tempting to interpret the Fourier transform of the form factor $J(t)$ as the density of total angular momentum. We see however from

Eqs. (6.37) and (6.39) that, in both the Belinfante's and in the kinetic case, other terms explicitly depending on $\boldsymbol{\Delta}$ do also contribute at the density level. More precisely, for the kinetic total AM we can introduce the following decomposition:

$$\left\langle J^i \right\rangle(\boldsymbol{x}) = \left\langle J^i \right\rangle_{\text{naive}}(\boldsymbol{x}) + \left\langle J^i \right\rangle_{\text{corr}}(\boldsymbol{x}) \tag{6.45}$$

into a "naive" contribution

$$\left\langle J^i \right\rangle_{\text{naive}}(\boldsymbol{x}) = \int \frac{\mathrm{d}^3\boldsymbol{\Delta}}{(2\pi)^3}\, e^{-i\boldsymbol{\Delta}\cdot\boldsymbol{x}}\, s^i J(-\boldsymbol{\Delta}^2) \tag{6.46}$$

and a correction

$$\begin{aligned}\left\langle J^i \right\rangle_{\text{corr}}(\boldsymbol{x}) = \int \frac{\mathrm{d}^3\boldsymbol{\Delta}}{(2\pi)^3}\, e^{-i\boldsymbol{\Delta}\cdot\boldsymbol{x}} \\ \times \left[\left[(\boldsymbol{\Delta}\cdot\boldsymbol{s})\Delta^i - \boldsymbol{\Delta}^2 s^i \right] \frac{\mathrm{d}L(t)}{\mathrm{d}t} - \frac{(\boldsymbol{\Delta}\cdot\boldsymbol{s})\,\Delta^i}{4} \frac{\mathrm{d}G(t)}{\mathrm{d}t} \right]_{t=-\boldsymbol{\Delta}^2},\end{aligned} \tag{6.47}$$

satisfying

$$\int \mathrm{d}^3\boldsymbol{x} \left\langle J^i \right\rangle_{\text{naive}}(\boldsymbol{x}) = \left\langle J^i \right\rangle, \qquad \int \mathrm{d}^3\boldsymbol{x} \left\langle J^i \right\rangle_{\text{corr}}(\boldsymbol{x}) = 0\,. \tag{6.48}$$

Finally, in order to establish the connection with the results of [128–131], we decompose Eq. (6.37)

$$\langle J^i_{\text{Bel}} \rangle(\boldsymbol{x}) = \langle J^i_{\text{Bel}} \rangle_{\text{mono}}(\boldsymbol{x}) + \langle J^i_{\text{Bel}} \rangle_{\text{quad}}(\boldsymbol{x}), \tag{6.49}$$

into monopole and quadrupole contributions

$$\langle J^i_{\text{Bel}} \rangle_{\text{mono}}(\boldsymbol{x}) = s^i \int \frac{\mathrm{d}^3\boldsymbol{\Delta}}{(2\pi)^3}\, e^{-i\boldsymbol{\Delta}\cdot\boldsymbol{x}} \left[J(t) + \frac{2t}{3} \frac{\mathrm{d}J(t)}{\mathrm{d}t} \right]_{t=-\boldsymbol{\Delta}^2}, \tag{6.50}$$

$$\langle J^i_{\text{Bel}} \rangle_{\text{quad}}(\boldsymbol{x}) = s^j \int \frac{\mathrm{d}^3\boldsymbol{\Delta}}{(2\pi)^3}\, e^{-i\boldsymbol{\Delta}\cdot\boldsymbol{x}} \left[\Delta^i\Delta^j - \frac{1}{3}\,\delta^{ij}\boldsymbol{\Delta}^2 \right] \frac{\mathrm{d}J(t)}{\mathrm{d}t}\bigg|_{t=-\boldsymbol{\Delta}^2}. \tag{6.51}$$

6.3 Densities in the impact-parameter space

The density interpretation in the Breit frame is valid only when relativistic effects associated with the motion of the target can be neglected. For this reason, we considered $\boldsymbol{P} = \boldsymbol{0}$ to define 3D densities in the previous Section.
As argued in Section 4.4.1, the front-form dynamics represents an elegant way of getting rid of these relativistic corrections. Here we first consider, in the instant form, the two-dimensional limit of the Breit-frame densities introduced in Section 6.2, then the 2D densities in the elastic frame with $\boldsymbol{P} \neq \boldsymbol{0}$; finally we show how these are connected with the light-front densities in the impact-parameter space. In order to comply with the notation adopted in the rest of this work, we will denote the Fourier conjugate variable to $\boldsymbol{\Delta}_\perp$ by $\boldsymbol{b}_\perp$ instead of $\boldsymbol{x}_\perp$.

6.3.1 2D densities in the Breit frame

We first consider two-dimensional densities in the Breit frame $\boldsymbol{P} = \boldsymbol{0}$, obtained as projections on the transverse plane of the 3D distributions in Eqs. (6.33), (6.35), (6.37) and (6.42), namely

$$\langle j^i \rangle(\boldsymbol{b}_\perp) = \int \mathrm{d}x^3 \, \langle j^i \rangle(\boldsymbol{x})\big|_{\boldsymbol{x}=(\boldsymbol{b}_\perp, x^3)} \tag{6.52}$$

with $j^i = L^i, S^i, J^i_{\mathrm{Bel}}, M^i$ and $i = 1, 2, 3$. Note that since $\boldsymbol{x}$ is Fourier conjugate to $\boldsymbol{\Delta}$, integrating over x^3 amounts to set $\Delta^3 = 0$.
As we integrate out a specific direction, spherical symmetry is broken and it is hence convenient to distinguish between longitudinal and transverse components of the considered angular momentum densities. As far as the longitudinal components is concerned, we find

$$\langle L^z \rangle(\boldsymbol{b}_\perp) = s^z \int \frac{\mathrm{d}^2\boldsymbol{\Delta}_\perp}{(2\pi)^2} \, e^{-i\boldsymbol{\Delta}_\perp \cdot \boldsymbol{b}_\perp} \left[L(t) + t \, \frac{\mathrm{d}L(t)}{\mathrm{d}t} \right]_{t=-\boldsymbol{\Delta}_\perp^2} , \tag{6.53}$$

$$\langle S^z \rangle(\boldsymbol{b}_\perp) = \frac{s^z}{2} \int \frac{\mathrm{d}^2\boldsymbol{\Delta}_\perp}{(2\pi)^2} \, e^{-i\boldsymbol{\Delta}_\perp \cdot \boldsymbol{b}_\perp} \, G_A(-\boldsymbol{\Delta}_\perp^2) , \tag{6.54}$$

$$\langle J^z_{\mathrm{Bel}} \rangle(\boldsymbol{b}_\perp) = s^z \int \frac{\mathrm{d}^2\boldsymbol{\Delta}_\perp}{(2\pi)^2} \, e^{-i\boldsymbol{\Delta}_\perp \cdot \boldsymbol{b}_\perp} \left[J(t) + t \, \frac{\mathrm{d}J(t)}{\mathrm{d}t} \right]_{t=-\boldsymbol{\Delta}_\perp^2} , \tag{6.55}$$

$$\langle M^z \rangle(\boldsymbol{b}_\perp) = -\frac{s^z}{2} \int \frac{\mathrm{d}^2\boldsymbol{\Delta}_\perp}{(2\pi)^2} \, e^{-i\boldsymbol{\Delta}_\perp \cdot \boldsymbol{b}_\perp} \left[t \, \frac{\mathrm{d}G_A(t)}{\mathrm{d}t} \right]_{t=-\boldsymbol{\Delta}_\perp^2} . \tag{6.56}$$

The distributions are axially symmetric and satisfy once again

$$\langle J^z \rangle(b_\perp) = \langle L^z \rangle(b_\perp) + \langle S^z \rangle(b_\perp) = \langle J^z_{\mathrm{Bel}} \rangle(b_\perp) + \langle M^z \rangle(b_\perp) . \tag{6.57}$$

Note also that the dependence on the induced pseudoscalar form factor $G_P(t)$ has disappeared because the latter is multiplied by $\Delta^3 = 0$.
As for the transverse components, instead, we obtain

$$\left\langle L^i_\perp \right\rangle(\boldsymbol{b}_\perp) = \int \frac{\mathrm{d}^2\boldsymbol{\Delta}_\perp}{(2\pi)^2} \, e^{-i\boldsymbol{\Delta}_\perp \cdot \boldsymbol{b}_\perp} \left[s^i_\perp \, L(t) + \left[(\boldsymbol{\Delta}_\perp \cdot \boldsymbol{s}_\perp)\Delta^i_\perp - \boldsymbol{\Delta}^2_\perp s^i_\perp \right] \frac{\mathrm{d}L(t)}{\mathrm{d}t} \right]_{t=-\boldsymbol{\Delta}_\perp^2} , \tag{6.58}$$

$$\langle S^i_\perp \rangle(\boldsymbol{b}_\perp) = \int \frac{\mathrm{d}^2\boldsymbol{\Delta}_\perp}{(2\pi)^2} \, e^{-i\boldsymbol{\Delta}_\perp \cdot \boldsymbol{b}_\perp} \left[\frac{s^i_\perp}{2} \, G_A(t) - \frac{(\boldsymbol{\Delta}_\perp \cdot \boldsymbol{s}_\perp)\, \Delta^i_\perp}{4} \, \frac{\mathrm{d}G(t)}{\mathrm{d}t} \right]_{t=-\boldsymbol{\Delta}_\perp^2} , \tag{6.59}$$

$$\langle J^i_{\mathrm{Bel},\perp} \rangle(\boldsymbol{b}_\perp) = \int \frac{\mathrm{d}^2\boldsymbol{\Delta}_\perp}{(2\pi)^2} \, e^{-i\boldsymbol{\Delta}_\perp \cdot \boldsymbol{b}_\perp} \left[s^i_\perp \, J(t) + \left[(\boldsymbol{\Delta}_\perp \cdot \boldsymbol{s}_\perp)\Delta^i_\perp - \boldsymbol{\Delta}^2_\perp s^i_\perp \right] \frac{\mathrm{d}J(t)}{\mathrm{d}t} \right]_{t=-\boldsymbol{\Delta}_\perp^2} , \tag{6.60}$$

$$\begin{aligned} \langle M^i_\perp \rangle(\boldsymbol{b}_\perp) = -\int \frac{\mathrm{d}^2\boldsymbol{\Delta}_\perp}{(2\pi)^2} \, e^{-i\boldsymbol{\Delta}_\perp \cdot \boldsymbol{b}_\perp} \Bigg[& \frac{\left[(\boldsymbol{\Delta}_\perp \cdot \boldsymbol{s}_\perp)\Delta^i_\perp - \boldsymbol{\Delta}^2_\perp s^i_\perp \right]}{2} \, \frac{\mathrm{d}G_A(t)}{\mathrm{d}t} \\ & + \frac{(\boldsymbol{\Delta}_\perp \cdot \boldsymbol{s}_\perp)\, \Delta^i_\perp}{4} \, \frac{\mathrm{d}G(t)}{\mathrm{d}t} \Bigg]_{t=-\boldsymbol{\Delta}_\perp^2} , \end{aligned} \tag{6.61}$$

with $i = 1, 2$.

6.3.2 2D densities in the elastic frame

Let us now consider the case where $\boldsymbol{P} \neq \boldsymbol{0}$. The only densities we can define are necessarily two-dimensional: in order to preserve the condition $\Delta^0 = 0$, which ensures that both the initial and final states are affected by the same Lorentz contraction factor, we have to restrict $\boldsymbol{\Delta}$ to the subspace orthogonal to $\boldsymbol{P}$.
In Section 4.4.1 we defined the elastic frames (EF) by the condition $\boldsymbol{P} \cdot \boldsymbol{\Delta} = 0$. They constitute a class of frames characterized by the fact that there is no energy transferred to the system, i.e. $\Delta^0 = 0$; the energy of the system is then given by

$$P^0 = \sqrt{\boldsymbol{P}^2 + \frac{\boldsymbol{\Delta}^2}{4} + M^2} \, .$$

The Breit frame appears as a particular element of this class.
Also in this case, $\boldsymbol{P}$ distinguishes a particular spatial direction; it is thus convenient to write three-vectors in terms of longitudinal and transverse components. Without loss of generality, we choose the spatial axes so that $\boldsymbol{P}$ lies along the z axis

$$\boldsymbol{P} = (\boldsymbol{0}_\perp, P) \, , \qquad \boldsymbol{\Delta} = (\boldsymbol{\Delta}_\perp, 0) \, . \tag{6.62}$$

Accordingly, we treat longitudinal and transverse components of the considered densities separately. Since the transverse ones involve complicated dependencies on the P variable, that are not relevant for our discussion, here it is sufficient to focus on the longitudinal components only. Note that this choice allows us to automatically get rid of the time-dependence in Eq. (6.27).
We define the impact-parameter densities of kinetic OAM and spin as

$$\begin{aligned}
\langle L^z \rangle(\boldsymbol{b}_\perp) &= -i\varepsilon^{3jk} \int \frac{\mathrm{d}^2\boldsymbol{\Delta}_\perp}{(2\pi)^2} \, e^{-i\boldsymbol{\Delta}_\perp \cdot \boldsymbol{b}_\perp} \, \frac{\partial \langle T^{0k} \rangle}{\partial \Delta_\perp^j} \bigg|_{\mathrm{EF}} \\
&= s^z \int \frac{\mathrm{d}^2\boldsymbol{\Delta}_\perp}{(2\pi)^2} \, e^{-i\boldsymbol{\Delta}_\perp \cdot \boldsymbol{b}_\perp} \left[L(t) + t \, \frac{\mathrm{d}L(t)}{\mathrm{d}t} \right]_{t=-\boldsymbol{\Delta}_\perp^2} \, , \qquad (6.63) \\
\langle S^z \rangle(\boldsymbol{b}_\perp) &= \frac{1}{2} \, \varepsilon^{3jk} \int \frac{\mathrm{d}^2\boldsymbol{\Delta}_\perp}{(2\pi)^2} \, e^{-i\boldsymbol{\Delta}_\perp \cdot \boldsymbol{b}_\perp} \, \langle S^{0jk} \rangle \big|_{\mathrm{EF}} \\
&= \frac{s^z}{2} \int \frac{\mathrm{d}^2\boldsymbol{\Delta}_\perp}{(2\pi)^2} \, e^{-i\boldsymbol{\Delta}_\perp \cdot \boldsymbol{b}_\perp} \, G_A(-\boldsymbol{\Delta}_\perp^2) \, . \qquad (6.64)
\end{aligned}$$

Similarly, for the impact-parameter densities of Belinfante-improved total AM and total divergence, we find

$$\begin{aligned}
\langle J^z_{\mathrm{Bel}} \rangle(\boldsymbol{b}_\perp) &= -i\varepsilon^{3jk} \int \frac{\mathrm{d}^2\boldsymbol{\Delta}_\perp}{(2\pi)^2} \, e^{-i\boldsymbol{\Delta}_\perp \cdot \boldsymbol{b}_\perp} \, \frac{\partial \langle T^{0k}_{\mathrm{Bel}} \rangle}{\partial \Delta_\perp^j} \bigg|_{\mathrm{EF}} \\
&= s^z \int \frac{\mathrm{d}^2\boldsymbol{\Delta}_\perp}{(2\pi)^2} \, e^{-i\boldsymbol{\Delta}_\perp \cdot \boldsymbol{b}_\perp} \left[J(t) + t \, \frac{\mathrm{d}J(t)}{\mathrm{d}t} \right]_{t=-\boldsymbol{\Delta}_\perp^2} \, , \qquad (6.65) \\
\langle M^z \rangle(\boldsymbol{b}_\perp) &= \frac{1}{2} \, \varepsilon^{3jk} \int \frac{\mathrm{d}^2\boldsymbol{\Delta}_\perp}{(2\pi)^2} \, e^{-i\boldsymbol{\Delta}_\perp \cdot \boldsymbol{b}_\perp} \, \Delta_\perp^l \, \frac{\partial \langle S^{l0k} \rangle}{\partial \Delta_\perp^j} \bigg|_{\mathrm{EF}}
\end{aligned}$$

$$= -\frac{s^z}{2} \int \frac{\mathrm{d}^2\boldsymbol{\Delta}_\perp}{(2\pi)^2}\, e^{-i\boldsymbol{\Delta}_\perp\cdot\boldsymbol{b}_\perp} \left[t\, \frac{\mathrm{d}G_A(t)}{\mathrm{d}t} \right]_{t=-\boldsymbol{\Delta}_\perp^2} . \tag{6.66}$$

The following Dirac bilinears in the elastic frame have been used:

$$\overline{u}\left(P_z, \tfrac{\boldsymbol{\Delta}_\perp}{2}, \boldsymbol{s}\right) \gamma^3\gamma_5 u(P_z, -\tfrac{\boldsymbol{\Delta}_\perp}{2}, \boldsymbol{s}) = 2P^0\, s^z \,, \tag{6.67}$$

$$\overline{u}\left(P_z, \tfrac{\boldsymbol{\Delta}_\perp}{2}, \boldsymbol{s}\right) i\sigma^{k\lambda}\Delta_\lambda u(P_z, -\tfrac{\boldsymbol{\Delta}_\perp}{2}, \boldsymbol{s}) = -2M\, i\epsilon^{kl3}\Delta^l s^z \,, \qquad k = 1, 2 \,. \tag{6.68}$$

Note that, remarkably, the 2D distributions (6.53)-(6.56) appear to be independent of $\boldsymbol{P}$. The reason is that longitudinal boosts do not mix longitudinal components of angular momentum. As a consequence, as long as we restrict to the longitudinal direction, 2D distributions in the elastic frame coincide with the projections onto the transverse plane of the 3D distributions in the Breit frame, namely Eqs. (6.53) to (6.56).

6.3.3 2D densities in the front form

Let us now switch to light-front coordinates. Similarly to the instant-form case, we start with the definition of kinetic OAM distribution in four-dimensional position space. Once again we focus on the longitudinal component only, and write

$$\langle L^z\rangle(x) = \varepsilon^{3jk}\, x_\perp^j \int \frac{\mathrm{d}^2\boldsymbol{\Delta}_\perp\, \mathrm{d}\Delta^+}{(2\pi)^3}\, e^{i\Delta\cdot x}\, \langle T^{+k}\rangle_{\mathrm{LF}}, \tag{6.69}$$

where[4]

$$\langle T^{\mu\nu}\rangle_{\mathrm{LF}} \equiv \frac{\langle p', \boldsymbol{s}|T^{\mu\nu}(0)|p, \boldsymbol{s}\rangle}{2\sqrt{p'^+ p^+}}. \tag{6.70}$$

Via the onshell conditions, we can express the light-front energy transfer Δ^- in terms of the three-momentum transfer $(\Delta^+, \boldsymbol{\Delta}_\perp)$ as

$$\Delta^- = \frac{\boldsymbol{P}_\perp\cdot\boldsymbol{\Delta}_\perp - P^-\Delta^+}{P^+}, \tag{6.71}$$

$$P^- = \frac{1}{2}\left[\frac{(\boldsymbol{P}_\perp + \frac{\boldsymbol{\Delta}_\perp}{2})^2 + M^2}{2(P^+ + \frac{\Delta^+}{2})} + \frac{(\boldsymbol{P}_\perp - \frac{\boldsymbol{\Delta}_\perp}{2})^2 + M^2}{2(P^+ - \frac{\Delta^+}{2})} \right]. \tag{6.72}$$

If we use integration by parts and disregard the surface term, we can rewrite Eq. (6.69) as

$$\langle L^z\rangle(x) = \varepsilon^{3jk} \int \frac{\mathrm{d}^2\boldsymbol{\Delta}_\perp\, \mathrm{d}\Delta^+}{(2\pi)^3}\, e^{i\Delta\cdot x} \left[-i\frac{\partial\langle T^{+k}\rangle_{\mathrm{LF}}}{\partial\Delta_\perp^j} + \frac{x^+}{2}\left(\frac{p'^j_\perp}{p'^+} + \frac{p^j_\perp}{p^+} \right) \langle T^{+k}\rangle_{\mathrm{LF}} \right]. \tag{6.73}$$

Densities in the light-front formalism are defined in the Drell-Yan (DY) frame where $\Delta^+ = 0$ and $\boldsymbol{P}_\perp = \boldsymbol{0}_\perp$; this amounts to integrating the four-dimensional

[4] In this context, we indicate the spin-dependence of the states with the rest-frame spin $\boldsymbol{s}$.

distributions over the longitudinal light-front coordinate x^-. In such a frame, analogously to the situation in the Breit frame in instant form, the dependence on the light-front time x^+ in Eq. (6.73) drops out. We can use the following Dirac bilinears involving light-front spinors u_{LF}:

$$\overline{u}_{\mathrm{LF}}\left(P^+, \tfrac{\boldsymbol{\Delta}_\perp}{2}, \boldsymbol{s}\right)\gamma^+\gamma_5 u_{\mathrm{LF}}(P^+, -\tfrac{\boldsymbol{\Delta}_\perp}{2}, \boldsymbol{s}) = 2P^+ s^z \,, \tag{6.74}$$

$$\overline{u}_{\mathrm{LF}}\left(P^+, \tfrac{\boldsymbol{\Delta}_\perp}{2}, \boldsymbol{s}\right) i\sigma^{k\lambda}\Delta_\lambda u_{\mathrm{LF}}\left(P^+, -\tfrac{\boldsymbol{\Delta}_\perp}{2}, \boldsymbol{s}\right) = -2M\, i\epsilon^{kl3}\Delta_\perp^l s^z \,, \qquad k = 1, 2 \,. \tag{6.75}$$

The impact-parameter densities of kinetic OAM and spin in the light-front formalism are then given by

$$\begin{aligned}\langle L^z\rangle(\boldsymbol{b}_\perp) &= -i\varepsilon^{3jk}\int \frac{\mathrm{d}^2\boldsymbol{\Delta}_\perp}{(2\pi)^2}\, e^{-i\boldsymbol{\Delta}_\perp\cdot\boldsymbol{b}_\perp}\, \frac{\partial\langle T^{+k}\rangle_{\mathrm{LF}}}{\partial\Delta_\perp^j}\bigg|_{\mathrm{DY}} \\ &= s^z\int \frac{\mathrm{d}^2\boldsymbol{\Delta}_\perp}{(2\pi)^2}\, e^{-i\boldsymbol{\Delta}_\perp\cdot\boldsymbol{b}_\perp}\left[L(t) + t\,\frac{\mathrm{d}L(t)}{\mathrm{d}t}\right]_{t=-\boldsymbol{\Delta}_\perp^2}, \end{aligned} \tag{6.76}$$

$$\begin{aligned}\langle S^z\rangle(\boldsymbol{b}_\perp) &= \frac{1}{2}\,\varepsilon^{3jk}\int \frac{\mathrm{d}^2\boldsymbol{\Delta}_\perp}{(2\pi)^2}\, e^{-i\boldsymbol{\Delta}_\perp\cdot\boldsymbol{b}_\perp}\, \langle S^{+jk}\rangle_{\mathrm{LF}}\big|_{\mathrm{DY}} \\ &= \frac{s^z}{2}\int \frac{\mathrm{d}^2\boldsymbol{\Delta}_\perp}{(2\pi)^2}\, e^{-i\boldsymbol{\Delta}_\perp\cdot\boldsymbol{b}_\perp} G_A(-\boldsymbol{\Delta}_\perp^2) \,. \end{aligned} \tag{6.77}$$

Similarly, for the impact-parameter densities of Belinfante-improved total angular momentum and total divergence, we find

$$\begin{aligned}\langle J^z_{\mathrm{Bel}}\rangle(\boldsymbol{b}_\perp) &= -i\varepsilon^{3jk}\int \frac{\mathrm{d}^2\boldsymbol{\Delta}_\perp}{(2\pi)^2}\, e^{-i\boldsymbol{\Delta}_\perp\cdot\boldsymbol{b}_\perp}\, \frac{\partial\langle T^{+k}_{\mathrm{Bel}}\rangle_{\mathrm{LF}}}{\partial\Delta_\perp^j}\bigg|_{\mathrm{DY}} \\ &= s^z\int \frac{\mathrm{d}^2\boldsymbol{\Delta}_\perp}{(2\pi)^2}\, e^{-i\boldsymbol{\Delta}_\perp\cdot\boldsymbol{b}_\perp}\left[J(t) + t\,\frac{\mathrm{d}J(t)}{\mathrm{d}t}\right]_{t=-\boldsymbol{\Delta}_\perp^2}, \end{aligned} \tag{6.78}$$

$$\begin{aligned}\langle M^z\rangle(\boldsymbol{b}_\perp) &= \frac{1}{2}\,\varepsilon^{3jk}\int \frac{\mathrm{d}^2\boldsymbol{\Delta}_\perp}{(2\pi)^2}\, e^{-i\boldsymbol{\Delta}_\perp\cdot\boldsymbol{b}_\perp}\, \Delta_\perp^l\, \frac{\partial\langle S^{l+k}\rangle_{\mathrm{LF}}}{\partial\Delta_\perp^j}\bigg|_{\mathrm{DY}} \\ &= -\frac{s^z}{2}\int \frac{\mathrm{d}^2\boldsymbol{\Delta}_\perp}{(2\pi)^2}\, e^{-i\boldsymbol{\Delta}_\perp\cdot\boldsymbol{b}_\perp}\left[t\,\frac{\mathrm{d}G_A(t)}{\mathrm{d}t}\right]_{t=-\boldsymbol{\Delta}_\perp^2}. \end{aligned} \tag{6.79}$$

We observe that these light-front densities in the Drell-Yan frame coincide with the corresponding instant-form densities in the elastic frame in Eqs. (6.63) to (6.66). This should not be too surprising, since the Drell-Yan frame is nothing but the elastic frame with $\boldsymbol{P}$ defining the light-front direction. Moreover, instant-form and front-form definitions of the longitudinal angular momentum coincide in the infinite-momentum frame limit[5] $P_z \to \infty$. Since the 2D densities that we considered do not depend on P_z, they should be the same in both instant form and front form.

[5]We mention here that the link between instant-form and light-front form is not so straightforward for the transverse components, see e.g. Ref. [143–145] for the related issues.

6.3.4 Impact-parameter dependent form factors

By inspection of Eqs. (6.58) to (6.61) and (6.76) to (6.79), we recognize that the impact-parameter densities can be expressed with combinations of 2D Fourier transform of the form factors, defined as

$$\tilde{F}(b_\perp) = \int \frac{\mathrm{d}^2\boldsymbol{\Delta}_\perp}{(2\pi)^2}\, e^{-i\boldsymbol{\Delta}_\perp\cdot\boldsymbol{b}_\perp}\, F(-\boldsymbol{\Delta}_\perp^2)\,. \tag{6.80}$$

Let us consider the longitudinal components first. One finds

$$\langle L^z\rangle(b_\perp) = -\frac{s^z}{2}\, b_\perp\, \frac{\mathrm{d}\tilde{L}(b_\perp)}{\mathrm{d}b_\perp}\,, \tag{6.81}$$

$$\langle S^z\rangle(b_\perp) = \frac{s^z}{2}\, \tilde{G}_A(b_\perp)\,, \tag{6.82}$$

$$\langle J^z_{\mathrm{Bel}}\rangle(b_\perp) = -\frac{s^z}{2}\, b_\perp\, \frac{\mathrm{d}\tilde{J}(b_\perp)}{\mathrm{d}b_\perp}\,, \tag{6.83}$$

$$\langle M^z\rangle(b_\perp) = \frac{s^z}{2}\left[\tilde{G}_A(b_\perp) + \frac{1}{2}\, b_\perp \frac{\mathrm{d}\tilde{G}_A(b_\perp)}{\mathrm{d}b_\perp}\right]. \tag{6.84}$$

where again we integrated by parts and used

$$-2\boldsymbol{\Delta}_\perp^2 \frac{\mathrm{d}F}{\mathrm{d}t} = \boldsymbol{\Delta}_\perp\cdot(\boldsymbol{\nabla}_{\boldsymbol{\Delta}_\perp} F)\,, \qquad \boldsymbol{\nabla}_{\boldsymbol{b}_\perp}\tilde{F} = \frac{\boldsymbol{b}_\perp}{b_\perp}\frac{\mathrm{d}\tilde{F}}{\mathrm{d}b_\perp}\,.$$

The impact-parameter density of kinetic total AM $\langle J^z\rangle(b_\perp) = \langle L^z\rangle(b_\perp) + \langle S^z\rangle(b_\perp)$ will differ from the "naive" density

$$\langle J^z\rangle_{\mathrm{naive}}(b_\perp) = s^z \tilde{J}(b_\perp) \tag{6.85}$$

by a correction term

$$\langle J^z\rangle_{\mathrm{corr}}(b_\perp) = -s^z\left[\tilde{L}(b_\perp) + \frac{1}{2}\, b_\perp\, \frac{\mathrm{d}\tilde{L}(b_\perp)}{\mathrm{d}b_\perp}\right]. \tag{6.86}$$

We can also project the 3D monopole and quadrupole contributions to the Belinfante-improved total AM (6.50) and (6.51) onto the transverse plane. This gives

$$\langle J^z_{\mathrm{Bel}}\rangle_{\mathrm{mono}}(b_\perp) = \frac{s^z}{3}\left[\tilde{J}(b_\perp) - b_\perp\, \frac{\mathrm{d}\tilde{J}(b_\perp)}{\mathrm{d}b_\perp}\right], \tag{6.87}$$

$$\langle J^z_{\mathrm{Bel}}\rangle_{\mathrm{quad}}(b_\perp) = -\frac{s^z}{3}\left[\tilde{J}(b_\perp) + \frac{1}{2}\, b_\perp\, \frac{\mathrm{d}\tilde{J}(b_\perp)}{\mathrm{d}b_\perp}\right]. \tag{6.88}$$

Clearly, the total divergence (6.84), the correction (6.86) and the quadrupole (6.88) terms vanish once integrated over $\boldsymbol{b}_\perp$

$$2\pi \int \mathrm{d}b_\perp\, b_\perp\, \langle M^z\rangle(b_\perp) = 2\pi \int \mathrm{d}b_\perp\, b_\perp\, \langle J^z\rangle_{\mathrm{corr}}(b_\perp)$$

$$= 2\pi \int \mathrm{d}b_\perp \, b_\perp \, \langle J^z_{\mathrm{Bel}} \rangle_{\mathrm{quad}}(b_\perp) = 0, \tag{6.89}$$

as one can see using integration by parts. This explains why the naive $\tilde{J}(b_\perp)$, the Polyakov-Goeke $\rho_J^{\mathrm{PG}}(b_\perp)$ and the infinite-momentum frame $\rho_J^{\mathrm{IMF}}(b_\perp)$ definitions considered by Adhikari and Burkardt [132] (corresponding in our notations to $\langle J^z \rangle_{\mathrm{naive}}(b_\perp)$, $\langle J^z_{\mathrm{Bel}} \rangle_{\mathrm{mono}}(b_\perp)$ and $\langle J^z_{\mathrm{Bel}} \rangle(b_\perp)$, respectively) are different, even though they lead to the same integrated total angular momentum.

As for the transverse components is concerned, from Eqs. (6.58) to (6.61) we obtain

$$\left\langle L^i_\perp \right\rangle (\boldsymbol{b}_\perp) = \frac{s^i_\perp}{2} \tilde{L}\,(b_\perp) + \frac{1}{2}\left[\frac{(\boldsymbol{s}_\perp \cdot \boldsymbol{b}_\perp)}{b_\perp} b^i_\perp - s^i_\perp b_\perp \right] \frac{\mathrm{d}\tilde{L}}{db_\perp} \,, \tag{6.90}$$

$$\left\langle S^i_\perp \right\rangle (\boldsymbol{b}_\perp) = \frac{s^i_\perp}{2} \tilde{G}_A(b_\perp) - \frac{1}{8}\left[\frac{s^i_\perp}{2} \tilde{G}(b_\perp) + \frac{1}{2} \frac{(\boldsymbol{s}_\perp \cdot \boldsymbol{b}_\perp)}{b_\perp} b^i_\perp \frac{\mathrm{d}\tilde{G}}{db_\perp} \right] , \tag{6.91}$$

$$\left\langle J^i_{\mathrm{Bel},\perp} \right\rangle (\boldsymbol{b}_\perp) = \frac{s^i_\perp}{2} \tilde{J}\,(b_\perp) + \frac{1}{2}\left[\frac{(\boldsymbol{s}_\perp \cdot \boldsymbol{b}_\perp)}{b_\perp} b^i_\perp - s^i_\perp b_\perp \right] \frac{\mathrm{d}\tilde{J}}{db_\perp} \,, \tag{6.92}$$

$$\begin{aligned} \left\langle M^i_\perp \right\rangle (\boldsymbol{b}_\perp) = &- \frac{s^i_\perp}{4} \tilde{G}_A(b_\perp) + \frac{1}{4} \frac{(\boldsymbol{s}_\perp \cdot \boldsymbol{b}_\perp)}{b_\perp} b^i_\perp \frac{\mathrm{d}\tilde{G}_A}{db_\perp} - \frac{s^i}{4} b_\perp \frac{\mathrm{d}\tilde{G}_A}{db_\perp} \\ &+ \frac{1}{8}\left[\frac{s^i_\perp}{2} \tilde{G}(b_\perp) + \frac{1}{2} \frac{(\boldsymbol{s}_\perp \cdot \boldsymbol{b}_\perp)}{b_\perp} b^i_\perp \frac{\mathrm{d}\tilde{G}}{db_\perp} \right] . \end{aligned} \tag{6.93}$$

Finally, we comment on the decomposition of the transverse components of the Belinfante total AM $\left\langle J^i_{\mathrm{Bel},\perp} \right\rangle$ into quadrupole and monopole contributions. If we first separate the corresponding three-dimensional density according to Eq. (6.49), we find

$$\left\langle J^i_{\mathrm{Bel},\perp} \right\rangle_{\mathrm{quad}} (\boldsymbol{b}_\perp) = \frac{s^i_\perp}{6} \tilde{J}\,(b_\perp) - \frac{1}{2}\left[\frac{b_\perp}{3} s^i_\perp - \frac{(\boldsymbol{s}_\perp \cdot \boldsymbol{b}_\perp)}{b_\perp} b^i_\perp \right] \frac{\mathrm{d}\tilde{J}}{db_\perp} \,, \tag{6.94}$$

$$\left\langle J^i_{\mathrm{Bel},\perp} \right\rangle_{\mathrm{mono}} (\boldsymbol{b}_\perp) = s^i \left[\frac{1}{3} \tilde{J}\,(b_\perp) - \frac{1}{3} b_\perp \frac{\mathrm{d}\tilde{J}}{db_\perp} \right] , \tag{6.95}$$

whose sum correctly yields Eq. (6.92). Nonetheless, we could proceed the other way around, by going to 2-dimensional space first, via integration over x^3, and then separating the two contributions. The latter would of course differ from the previous case, yielding

$$\left\langle J^i_{\mathrm{Bel},\perp} \right\rangle_{\mathrm{quad}} (\boldsymbol{b}_\perp) = \left[-\frac{b_\perp}{4} s^i_\perp + \frac{1}{2} \frac{(\boldsymbol{s}_\perp \cdot \boldsymbol{b}_\perp)}{b_\perp} b^i_\perp \right] \frac{\mathrm{d}\tilde{J}}{db_\perp} \,, \tag{6.96}$$

$$\left\langle J^i_{\mathrm{Bel},\perp} \right\rangle_{\mathrm{mono}} (\boldsymbol{b}_\perp) = s^i_\perp \left[\frac{1}{2} \tilde{J}\,(b_\perp) - \frac{1}{4} b_\perp \frac{\mathrm{d}\tilde{J}}{db_\perp} \right] , \tag{6.97}$$

but their sum would still give Eq. (6.92). The two operations are therefore commuting.

6.4 Illustration within the scalar-diquark model

In this Section we provide explicit calculations for the impact-parameter densities in the framework of the scalar-diquark model [9, 91, 146]. This simple model depicts the nucleon as a two-body system formed by an active quark of mass m and a spectator system described by a scalar diquark of mass m_D. We suppose the interaction to be ruled by a Yukawa potential with coupling constant g. We stress that, strictly speaking, this is not a QCD model of the nucleon, as there are no gluon fields involved. Nonetheless, we consider this model for illustrative purposes and in order to establish a direct comparison with the results of Ref. [132].

Similarly to what we did for the dressed electron, we can reconstruct the quark Light-Front Wave Functions $\Psi^\Lambda_\lambda(x, \boldsymbol{k}_\perp)$ in the scalar-diquark model by applying perturbation theory up to first order in the Yukawa coupling. Here $\Lambda = \pm$ and $\lambda = \pm$ denote the light-front helicities of the nucleon and of the quark, respectively. One finds:

$$\Psi^+_+(x, \boldsymbol{k}_\perp) = \Psi^-_-(x, \boldsymbol{k}_\perp) = \left(M + \frac{m}{x}\right)\phi(x, \boldsymbol{k}_\perp^2), \tag{6.98}$$

$$\Psi^+_-(x, \boldsymbol{k}_\perp) = -\left[\Psi^-_+(x, \boldsymbol{k}_\perp)\right]^* = -\frac{k^x + ik^y}{x}\,\phi(x, \boldsymbol{k}_\perp^2), \tag{6.99}$$

where

$$\phi(x, \boldsymbol{k}_\perp^2) = -\frac{g\,x\sqrt{1-x}}{\boldsymbol{k}_\perp^2 + u(x, m_D^2)} \tag{6.100}$$

and $u(x, \mu^2)$ is the same defined in Eq. (5.11). We define the 2-dimensional Fourier transform of LFWFs from momentum to impact-parameter space as [132, 147, 148]

$$\Psi^\Lambda_\lambda(x, \boldsymbol{b}_\perp) = \frac{1}{1-x}\int \frac{\mathrm{d}^2\boldsymbol{k}_\perp}{(2\pi)^2}\, e^{i\boldsymbol{k}_\perp\cdot\boldsymbol{b}_\perp/(1-x)}\,\Psi^\Lambda_\lambda(x, \boldsymbol{k}_\perp). \tag{6.101}$$

As remarked in Ref. [132], the quark's momentum in the transverse plane $\boldsymbol{k}_\perp$ is not Fourier conjugate to the impact parameter $\boldsymbol{b}_\perp$, but rather to the displacement $\boldsymbol{r}_\perp = \boldsymbol{r}_{1,\perp} - \boldsymbol{r}_{2,\perp}$ between the active quark and the spectator; in order to account for that, a factor $\frac{1}{1-x}$ appears in the exponent of Eq. (6.101). The overall prefactor of $\frac{1}{1-x}$ is instead needed to guarantee proper normalization of the wave functions.
Writing $\boldsymbol{b}_\perp = b_\perp\,(\cos\phi_b, \sin\phi_b)$, we obtain (see Appendix C.1 for details)

$$\Psi^+_+(x, \boldsymbol{b}_\perp) = \Psi^-_-(x, \boldsymbol{b}_\perp) = -\frac{g\,(xM+m)}{2\pi\sqrt{1-x}}\,K_0(Z), \tag{6.102}$$

$$\Psi^+_-(x, \boldsymbol{b}_\perp) = \left[\Psi^-_+(x, \boldsymbol{b}_\perp)\right]^* = \frac{ig\sqrt{u(x, m_D^2)}\,e^{i\phi_b}}{2\pi\sqrt{1-x}}\,K_1(Z), \tag{6.103}$$

where K_n is the n-th order modified Bessel function of the second kind and $Z = \sqrt{u(x, m_D^2)}\, b_\perp/(1-x)$.

In Sections 4.4 and 4.4.1 we introduced Generalized Distribution Functions in momentum space first, then showed how their Fourier transform in the impact-parameter space can be interpreted as probability distribution. As we will briefly illustrate in the following, it is possible to establish a connection between the leading-twist GPDs and the form factors of the energy-momentum tensor in $\boldsymbol{b}_\perp$-space and eventually to the angular-momentum densities (6.81)-(6.84). As a final result, we obtain overlap representations of the impact-parameter densities in terms of LFWFs.
We denote the Fourier transforms of GPDs as

$$\mathcal{F}(x, b_\perp) = \int \frac{\mathrm{d}^2\boldsymbol{\Delta}_\perp}{(2\pi)^2}\, e^{-i\boldsymbol{\Delta}_\perp\cdot\boldsymbol{b}_\perp}\, F(x, 0, -\boldsymbol{\Delta}_\perp^2)\,.$$

The following LFWF overlap representation in impact-parameter space holds[6] [132] :

$$\mathcal{H}(x, b_\perp) = \frac{1}{2(2\pi)(1-x)^2}\left[|\Psi_+^+(x, \boldsymbol{b}_\perp)|^2 + |\Psi_-^+(x, \boldsymbol{b}_\perp)|^2\right], \tag{6.104}$$

$$-\frac{1}{2M}\left(i\frac{\partial}{\partial b_x} + \frac{\partial}{\partial b_y}\right)\mathcal{E}(x, b_\perp) = \frac{1}{2(2\pi)(1-x)^2}\left[\Psi_+^{+\,*}(x, \boldsymbol{b}_\perp)\Psi_+^-(x, \boldsymbol{b}_\perp) + \Psi_-^{+\,*}(x, \boldsymbol{b}_\perp)\Psi_-^-(x, \boldsymbol{b}_\perp)\right], \tag{6.105}$$

$$\tilde{\mathcal{H}}(x, b_\perp) = \frac{1}{2(2\pi)(1-x)^2}\left[|\Psi_+^+(x, \boldsymbol{b}_\perp)|^2 - |\Psi_-^+(x, \boldsymbol{b}_\perp)|^2\right]. \tag{6.106}$$

In the scalar-diquark model, by using Eqs. (6.102)-(6.103), we find

$$\mathcal{H}(x, b_\perp) = \frac{g^2}{2(2\pi)^3(1-x)}\left\{(xM+m)^2\left[K_0(Z)\right]^2 + u(x, m_D^2)\left[K_1(Z)\right]^2\right\}, \tag{6.107}$$

$$\mathcal{E}(x, b_\perp) = \frac{g^2}{2(2\pi)^3}\, 2M(xM+m)\left[K_0(Z)\right]^2, \tag{6.108}$$

$$\tilde{\mathcal{H}}(x, b_\perp) = \frac{g^2}{2(2\pi)^3(1-x)}\left\{(xM+m)^2\left[K_0(Z)\right]^2 - u(x, m_D^2)\left[K_1(Z)\right]^2\right\}. \tag{6.109}$$

Taking the second Mellin moment of these expression, we obtain the EMT form factors in impact-parameter space [65]:

$$\int_0^1 dx\, x\left[\mathcal{H}(x, b_\perp) + \mathcal{E}(x, b_\perp)\right] = \tilde{A}(b_\perp) + \tilde{B}(b_\perp), \tag{6.110}$$

[6] We provide a derivation in Appendix C.1

$$\int_0^1 dx\, \tilde{\mathcal{H}}(x, b_\perp) = \tilde{G}_A(b_\perp) = -\tilde{D}(b_\perp)\ , \tag{6.111}$$

which can then be inserted in Eqs (6.81)-(6.88) to get the various contributions to the density of AM in the longitudinal direction.

In Fig. 6.1 we plot the above-mentioned densities as functions of the modulus $b_\perp$ of the impact parameter for a longitudinally polarized target. We choose the same mass parameters as Adhikari and Burkardt [132], namely $M = m = m_D = 1$ fm^{-1}. In order to regulate the ultraviolet divergences $b_\perp \to 0$, we adopt the Pauli-Villars regularization, using the diquark mass m_D as a regulator. More precisely, for each one of the functions $\langle j^z\rangle(b_\perp; m_D^2)$ considered, we plot

$$b_\perp \left[\langle j^z\rangle(b_\perp; m_D^2) - \langle j^z\rangle(b_\perp; M_D^2)\right], \tag{6.112}$$

with $M_D^2 = 10\, m_D^2$. The extra factor of $b_\perp$ comes from the Jacobian of the transformation to polar coordinates.
Going from top to bottom, in the first plot we present the kinetic total AM $\langle J^z\rangle$ (solid line) resulting from the sum of kinetic orbital angular momentum $\langle L^z\rangle$ in Eq. (6.76) (dashed line) and spin $\langle S^z\rangle$ in Eq. (6.77) (dashed line). In the scalar diquark model both contributions appear to be positive.
In the second plot we compare the kinetic total angular momentum $\langle J^z\rangle$ (solid line) with the Belinfante-improved total AM $\langle J^z_{\rm Bel}\rangle(b_\perp)$ in Eq. (6.78) (dashed line), the difference being attributed to the $\langle M^z\rangle(b_\perp)$ term in Eq. (6.79) (dotted line), which originates from the total-divergence term in Eq. (6.17).
In the third plot, we compare the kinetic total angular momentum $\langle J^z\rangle(b_\perp)$ (solid line) with the naive density $\tilde{J}(b_\perp)$ in Eq. (6.85) (dashed line). Their difference is given by the correction term $\langle J^z\rangle_{\rm corr}(b_\perp)$ in Eq. (6.86) (dotted line).
In the fourth and last plot, we decomposed the Belinfante-improved total AM $\langle J^z_{\rm Bel}\rangle(b_\perp)$ (dashed line) into the sum of the monopole contribution $\left\langle J^z_{\rm Bel}\right\rangle_{\rm mono}$ in Eq. (6.87) (dashed line) and the quadrupole contribution $\left\langle J^z_{\rm Bel}\right\rangle_{\rm quad}$ in Eq. (6.88) (dotted line).

The monopole term is what Adhikari and Burkardt called the Polyakov-Goeke definition [132]. Once again, although the total divergence term $\langle M^z\rangle(b_\perp)$, the correction term $\langle J^z\rangle_{\rm corr}(b_\perp)$ and the quadrupole contribution $\langle J^z_{\rm Bel}\rangle_{\rm quad}(b_\perp)$ integrate to zero, they need to be taken into account when comparing different definitions for the density of angular momentum.
Since there is no gauge field in the scalar diquark model we considered, we expect the kinetic OAM to coincide with the canonical (or Jaffe-Manohar) OAM [7]. The latter can be expressed in terms of the following LFWF overlap representation in impact-parameter space:

$$\mathcal{L}^z(b_\perp) = \frac{1}{2(2\pi)} \int_0^1 \mathrm{d}x\, (1-x)\, |\Psi^+_-(x, \boldsymbol{b}_\perp)|^2\ . \tag{6.113}$$

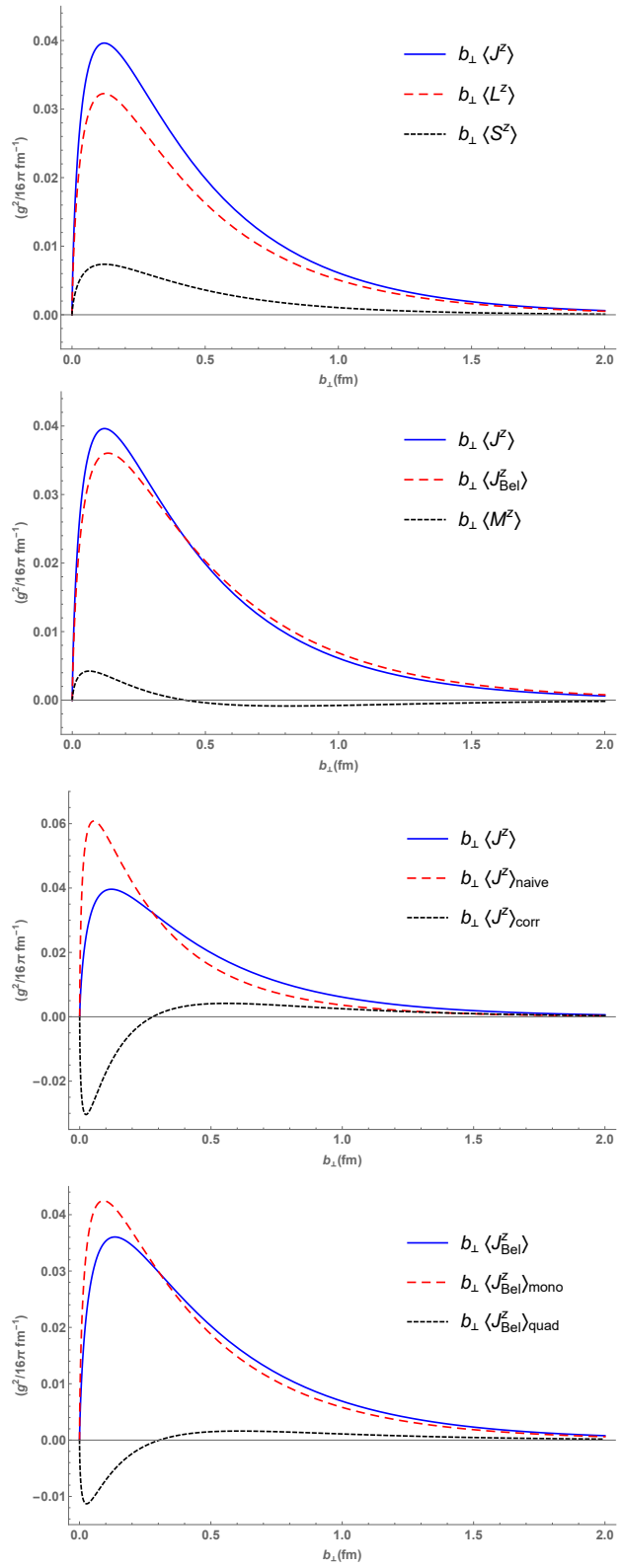

Figure 6.1: Plots of the densities of longitudinal angular momentum in units of $\frac{g^2}{16\pi}$ fm^{-1} as functions of $b_\perp = |\boldsymbol{b}_\perp|$. See the body of the text for a more detailed description.

By inserting Eq. (6.103), we find

$$\mathcal{L}^z(b_\perp) = \frac{g^2}{2(2\pi)^3}\int_0^1 \mathrm{d}x\, u(x,m_D^2)\left[K_1(Z)\right]^2 \ . \tag{6.114}$$

Note that the canonical OAM can alternatively be defined in terms of GTMDs according to Eq. (5.45)[7] leading to the same expression as in Eq. (6.113) in the scalar diquark model [149]. This has to be compared with the expression for the kinetic OAM $\langle L^z\rangle(b_\perp)$ that we obtain from Eq. (6.81), using (6.107)-(6.111):

$$\begin{aligned}\langle L^z\rangle(b_\perp) =& \frac{g^2}{2(2\pi)^3}\frac{1}{2}\int_0^1 \mathrm{d}x\,\frac{1}{1-x}\Big\{\left[(1-x)(x^2M^2-m^2)+(1+x)\,u(x,m_D^2)\right]\\ &\times ZK_0(Z)K_1(Z)(1+x)\,u(x,m_D^2)\left[K_1(Z)\right]^2\Big\}\,.\end{aligned} \tag{6.115}$$

As we prove in Appendix C.3, we find that $\langle L^z\rangle(b_\perp) = \mathcal{L}^z(b_\perp)$ for $b_\perp > 0$. To the best of our knowledge, this is the first time that the equality between kinetic and canonical OAM is checked explicitly at the density level. We also understand the failure to observe the equality in Ref. [132] as coming from the fact that the authors incorrectly defined the density of kinetic OAM as

$$L^z_{\mathrm{IMF}}(b_\perp) \equiv \langle J^z_{\mathrm{Bel}}\rangle(b_\perp) - \langle S^z\rangle(b_\perp)\,, \tag{6.116}$$

which misses the total divergence term $\langle M^z\rangle(b_\perp)$ as one can see from Eq. (6.57).

6.5 Summary

In this Chapter we addressed the question of the definition of angular momentum at the density level. Our point of emphasis is that in the context of Particle Physics, where spin densities play a fundamental role, one should consider the canonical, non-symmetric version of the Energy-Momentum Tensor. While superpotential terms do not play any role at the level of integrated quantities, it is of crucial importance to keep track of them at the density level. In particular, we showed that for a spin-1/2 target the form factor accounting for the antisymmetric part of the energy-momentum tensor coincides (up to a sign) with the axial-vector form factor. This provides an interesting new way of calculating the latter on the lattice.

We revisited and extended Polyakov's work on the three-dimensional distribution of angular momentum in instant form and in the Breit frame. Working with an asymmetric energy-momentum tensor allowed us to derive directly the correct density of orbital angular momentum. Densities in the Breit frame can be extended to the more general class of the elastic frame, provided one

[7] To be precise, Eq. (5.45) coincides with the Jaffe-Manohar definition of the OAM only when the Wilson line has the staple shape given by Eq. (4.13). In light-cone gauge, however, the residual transverse gauge link does not contribute to the OAM and can thus be ignored [7].

projects onto a two-dimensional plane. Thanks to this generalization, we were able to establish a simple connection between instant-form densities defined in the Breit frame and light-front densities defined in the Drell-Yan frame for the longitudinal components of angular momentum.

We used the scalar diquark model to illustrate our results. We showed explicitly that when all the terms integrating to zero are included in the expressions, no discrepancies are found between the different definitions of angular momentum. In particular, we checked for the first time explicitly that the canonical and kinetic angular momentum do coincide at the density level, as expected in a system without gauge bosons.

Chapter 7

Summary and conclusions

The Standard Model (SM) has encountered invaluable success over the last few years in classifying and describing elementary particles that build the visible universe. Despite these tremendous achievements, however, it still misses to explain some fundamental properties of subatomic particles. This is true, in particular, for what concerns the QCD sector of the SM, which accounts for the strong interactions: the non-Abelian nature of the theory makes it impossible to solve it mathematically with the ordinary perturbative approaches and introduces difficulties in the interpretation of experiments. As a result, we are currently not able to see the global properties of nucleons, such as its mass and spin, as deriving from the properties of their elementary constituents, namely quarks and gluons. The ultimate goal of Hadronic Physics is to provide a solution to these problems.

The Standard Model is formulated in the framework of Quantum Field Theory (QFT). In this thesis we considered the formalism of light-front quantization, a QFT language which turns out to be particularly effective to reveal the internal structure of composite particles, and we applied it to the cases of QCD and QED.

We showed how light-front quantization helps us to rewrite and interpret the partonic distribution functions, which map quarks and gluons inside nucleons. We focused in particular on Generalized Transverse-Momentum Dependent (GTMD) and Transverse-Momentum Dependent (TMD) distribution functions, which we analyzed in the QED context. This procedure allowed us to obtain a order-α description, both in momentum and position space, of the dressed electron, thought as a two-body system composed of a bare electron and a photon.

Since light-front quantization prescribes the choice of the non-covariant light-cone gauge, we took the opportunity to discuss gauge invariance of QED in many facets. More precisely, we addressed the issue of which gauge-field propagator should be used in light-cone gauge in order to match light-front Time-Ordered Perturbation Theory and covariant approach with Feynamn diagrams; we also emphasized the role of the gauge link in preserving gauge invariance

when dealing with the calculation of TMDs. These are examples of results that are immediately transferable from QED to QCD, as they depend only on the common nature of the two as gauge theories.
We finally focused on the problem of properly defining quark's angular momentum densities in position space inside the nucleon. This is a relevant issue concerning the spin-decomposition puzzle. Light-front quantization again provides a beautiful solution aimed to avoid relativistic corrections in the two-dimensional impact-parameter space, thus making it possible to interpret the considered densities as probability distributions.

In the following we summarize the results and possible outlooks of this work, referring to Sections 3.5, 5.4 and 6.5 for a more extended discussion.

7.1 Results

In this thesis we first gave an overview of light-front quantization methods for QCD, with particular emphasis on partonic distribution functions, then showed possible applications of this formalism in QED and QCD.
In Chapter 2 we introduced light-front quantization, mainly by adopting an historical point of view. We discussed several advantages of this formalism compared to the usual equal-time quantization, focusing especially on the simplification of the time-order perturbation theory (TOPT) approach, as well as on the effects related to the dynamics in the impact-parameter space.
In Chapter 3 we addressed the question of which form should be used for the gauge-field propagator in light-cone gauge, for the purpose of clarifying some inconsistencies and misleading results in the literature. To this end we reviewed the proof of the equivalence between light-front TOPT and Feynman-diagram approach in light-cone gauge at one-loop level in QED. Our conclusion is that the photon propagator should contain the sum of three terms, but the third can be dropped if one ignores at the same time the contributions from four-fermion interactions with instantaneous photons (which appear whenever we work in an axial gauge) in the covariant theory. We showed explicitly how light-front time-ordered diagrams containing instantaneous photons can be matched starting from the two-term propagator, by correctly applying integration by residues of Feynman diagrams; this result is in contrast with what had been previously stated in the literature.
In Chapter 4 we recalled the definitions of the various distribution functions of partons inside the nucleon, adopting the light-front language. We focused in particular on the Fourier transforms of GPDs and GTMDs to the impact-parameter space. The definitions of these objects are actually valid for any spin-1/2 composite system, thus making it possible to apply them also in the QED case of the electron.
In Chapter 5 we derived analytical expressions for the three-dimensional Wigner distributions in mixed momentum and position space and for the TMDs rel-

ative to the bare electron and to the photon inside the dressed electron. The latter appears as a ring-shaped object in momentum space, with a radius of about 200 keV. Remarkably, the electron's T-odd TMDs are vanishing at order α if we do not include vertex-correction and self-energy contributions. This fact represents a difference with respect to quark's TMDs in the QCD scenario. We argue, however, that this should not be the case, since the Sivers effect is supposed to show up in any gauge theory, regardless of its Abelian nature. The mismatch could then be due to the approximations we assumed; namely, our results are valid only up to order α and excluding the end-point $x = 0$, $\boldsymbol{k}_\perp = \boldsymbol{0}_\perp$. We showed how the formalism of LFWF overlap representation gives a clear and simple interpretation of spin-spin and spin-orbit correlations encoded in TMDs. We also discussed the role of the transverse-gauge link in restoring gauge invariance of the theory, finding similar (yet not exactly equivalent) results compared to what happens in QCD.
Finally, in Chapter 6 we studied angular-momentum densities of quarks inside the nucleon in terms of form factors of the QCD energy-momentum tensor. In this regard, our work marks a step forward with respect to the preexisting literature, as it clarifies which definitions should be taken for the orbital angular momentum and spin density contributions to the total angular momentum density. We also stressed the importance of using the non-symmetric version of the energy-momentum tensor in the context of Particle Physics: in our derivation it is indeed crucial to take into account superpotential terms at the density level, although they vanish after integration. We evaluated the impact-parameter densities in the scalar-diquark model of the nucleon, by means of the Light-Front Wave Function representation of GPDs, thus explaining the discrepancies between different definitions of (total) angular momentum found in previous works Ref. [132].

7.2 Outlooks

This thesis offers several opportunities for future perspectives, including both straightforward extensions of this work and applications in original projects.
First, it is natural to wonder whether the results related to the distribution functions in the QED context could be verified experimentally. Although we cannot provide an answer to this question, a couple of comments are in order. As for the GTMDs is concerned, we remark that the identification of a QED process that could (at least in principle) allow for their measurement would be of great theoretical importance, since GTMDs are currently not accessible experimentally even in QCD[1]. Some proposals have been advanced for measurement of Wigner distributions with Quantum Optics methods [150,151], that may be connected to Wigner distributions of the photon inside the dressed electron. The dressed electron TMDs, instead, could be used to evaluate ra-

[1]Actually, as we mentioned in Section 4.5, there have recently been new suggestions for measurements of GTMDs in QCD, which are currently awaiting experimental validation.

diative correction relevant in high-precision experiments involving a leptonic probe, with a procedure similar to the evaluation of proton-proton collisions (i.e. via a convolution of the TMDs of the electron and that of the target). Before embarking in such tasks, however, it would be necessary to provide a proper regularization and renormalization procedure so as to make sure that all physical contributions are taken into account. It would be interesting also to check whether the Sivers and Boer-Mulders effects are present in the QED context, either by extending the calculations presented in this thesis to higher perturbative orders, or by considering the analogous case of the positronium system.
For what concerns the quark's angular momentum densities, an interesting extension consists in considering also the transverse components of the operators studied in Chapter 6. We expect these to show a non-trivial dependence on the average momentum $\boldsymbol{P}$ of the system. In this case, then, it would be interesting to establish a connection between instant-form and light-front form results. We finally mention that also the other components of the QCD Energy-Momentum Tensor (EMT) could be analyzed in terms of form factors with a procedure similar to ours. As discussed in Ref. [128], these are related to fundamental quantities such as the nucleon mass and shear forces and pressures inside the nucleon. We stress again the importance, as our derivation makes evident, of adopting the non-symmetric EMT in this context. In particular, the $D(t)$ form factor related to the antisymmetric part of the EMT could be investigated on the lattice, by taking advantage of its simple relation with the axial-vector form factor, as we have derived from the QCD equations of motion.

Appendix A

Electron self-energies

In this Appendix we explicitly derive the results (3.74) and (3.75) which give, respectively, the contributions Σ_2 and Σ_3 to the electron self-energy in covariant approach.

We start from the contribution Σ_2. The matrix element in the numerator of the integrand in Eq. (3.72b) can be rewritten as

$$\bar{u}_{s'}(P)\gamma^\nu\gamma^+\gamma^\mu d_{\mu\nu}(\tilde{k})u_s(P) = 2\bar{u}_{s'}(P)\gamma^+u_s(P) = 4P^+\delta_{s,s'}, \tag{A.1}$$

where we used the relations

$$\gamma_\mu\gamma^\nu\gamma^\mu = -2\gamma^\nu\ , \quad \bar{u}_{s'}(P)\gamma^+u_s(P) = 2P^+\delta_{s,s'}\ .$$

As a result we can write

$$-i\bar{u}_{s'}(P)\Sigma_2(P)u_s(P) = -\frac{e^2P^+}{2m(2\pi)^3}\delta_{s,s'}\int \mathrm{d}^2\boldsymbol{k}_\perp \int \mathrm{d}x\,\frac{4P^+}{2(1-x)P^+}I_1\ , \tag{A.2}$$

where in the I_1 term we have isolated the integral over k^-, i.e.

$$I_1 = \int \frac{\mathrm{d}k^-}{2\pi}\frac{1}{k^2+i\epsilon}\ .$$

By introducing the new variable

$$u = \frac{1}{k^-}\ , \tag{A.3}$$

we can rewrite I_1 as

$$I_1 = -\frac{1}{2xP^+}\int \frac{\mathrm{d}u}{2\pi}\frac{1}{u}\frac{1}{\left[1-u\left(\frac{\boldsymbol{k}_\perp^2-i\epsilon}{2xP^+}\right)\right]}\ , \tag{A.4}$$

which shows poles for $u=0$ (i.e. $k^-=\infty$) and $u=\frac{2xP^+}{\boldsymbol{k}_\perp^2-i\epsilon}\equiv u_x$. We regularize the first singularity by substituting

$$\frac{1}{u} \to \frac{1}{2}\left(\frac{1}{u+i\delta}+\frac{1}{u-i\delta}\right)\ . \tag{A.5}$$

As a result, we have

$$I_1 = -\frac{1}{4xP^+}\int \frac{\mathrm{d}u}{2\pi}\frac{1}{\left[1-u\left(\frac{\boldsymbol{k}_\perp^2-i\epsilon}{2xP^+}\right)\right]}\left(\frac{1}{u+i\delta}+\frac{1}{u-i\delta}\right). \tag{A.6}$$

When considering the first term in round brackets, the first singularity now falls into the lower half-plane (at $u = -i\delta$); therefore we will obtain a nonzero result when u_x is in the upper half-plane, which means for $x > 0$. The specular situation holds for the second term in round brackets, which will then contribute only for $x < 0$.
If we choose the contour of integration for the first and second term enclosing the $-i\delta$ and $+i\delta$ poles, respectively, and then take the limit $\delta \to 0$, it is easy to see that we come up with the following result

$$I_1 = \frac{i}{4xP^+}\left[\theta(x)-\theta(-x)\right] = \frac{i}{4xP^+}\mathrm{sgn}(x)\,. \tag{A.7}$$

As we insert Eq. (A.7) into (A.2), we finally get

$$\begin{aligned}-i\bar{u}_{s'}(P)\Sigma_2(P)u_s(P) &= -\frac{ie^2}{4m(2\pi)^3}\delta_{s,s'}\int \mathrm{d}^2\boldsymbol{k}_\perp \int \mathrm{d}x\,\frac{1}{x(1-x)}\mathrm{sgn}(x)\\ &= -\frac{ie^2}{2m(2\pi)^3}\int \mathrm{d}^2\boldsymbol{k}_\perp \int_0^\infty \mathrm{d}x\,\frac{1}{x(1-x)}\delta_{s,s'}\,,\end{aligned} \tag{A.8}$$

as reported in Eq. (3.74).
For the calculation of the contribution Σ_3, we start from Eq. (3.72c) and rewrite the matrix element in the numerator of the integrand as

$$\begin{aligned}\bar{u}_{s'}(P)\gamma^+(\tilde{\not{l}}+m)\gamma^+u_s(P) &= l^+\bar{u}_{s'}(P)\gamma^+\gamma^-\gamma^+u_s(P)\\ &= 2(1-x)P^+\bar{u}_{s'}(P)\gamma^+u_s(P) = 4(1-x)\left(P^+\right)^2\delta_{s,s'}\,.\end{aligned} \tag{A.9}$$

As a result, we have

$$-i\bar{u}_{s'}(P)\Sigma_3(P)u_s(P) = \frac{e^2P^+}{2m(2\pi)^3}\delta_{s,s'}\int \mathrm{d}^2\boldsymbol{k}_\perp \int \mathrm{d}x\,\frac{4(1-x)\left(P^+\right)^2}{\left(xP^+\right)^2}I_2\,, \tag{A.10}$$

where the integral I_2 over k^- is given by

$$I_2 = \int \frac{\mathrm{d}k^-}{2\pi}\frac{1}{(P-k)^2-m^2+i\epsilon}\,. \tag{A.11}$$

By changing the variable of integration as in (A.3), and using the on-shell condition $P^2 = m^2$, one obtains

$$I_2 = -\frac{1}{2(1-x)P^+}\int \frac{\mathrm{d}u}{2\pi}\frac{1}{u}\frac{1}{\left[1-u\,\frac{xm^2+\boldsymbol{k}_\perp^2-i\epsilon}{2(x-1)P^+}\right]}\,. \tag{A.12}$$

We can henceforth proceed as before, replacing $1/u$ according to (A.5); the integration around the pole at $u = -i\delta$ will now give a nonzero result only when $x - 1 > 0$, while the integration around the pole at $u = i\delta$ contributes when $x - 1 < 0$. By taking the limit $\delta \to 0$, one finds

$$I_2 = \frac{i}{4(x-1)P^+}\left[\theta(x-1) - \theta(1-x)\right] = -\frac{i}{4(x-1)P^+}\mathrm{sgn}(1-x)\,. \tag{A.13}$$

Inserting this back in (A.10), one comes up with

$$-i\bar{u}_{s'}(P)\Sigma_3(P)u_s(P) = \frac{ie^2}{2m\,(2\pi)^3}\delta_{s,s'}\int \mathrm{d}^2\boldsymbol{k}_\perp \int \mathrm{d}x\,\frac{1}{x^2}\,\mathrm{sgn}(1-x)\,. \tag{A.14}$$

Note that, since $1/x^2$ is an even function of x, we have:

$$\begin{aligned}\int \mathrm{d}x\,\frac{1}{x^2}\,\mathrm{sgn}(1-x) &= -\int_{-\infty}^{1}\mathrm{d}x\,\frac{1}{x^2} + \int_1^\infty \mathrm{d}x\,\frac{1}{x^2} = -\int_{-1}^{\infty}\mathrm{d}x\,\frac{1}{x^2} + \int_1^\infty \mathrm{d}x\,\frac{1}{x^2} \\ &= -\int_0^\infty \mathrm{d}x\,\frac{1}{(1-x)^2} + \int_0^\infty \mathrm{d}x\,\frac{1}{(1+x)^2}\,. \end{aligned}\tag{A.15}$$

We therefore conclude that Eq. (A.14) becomes

$$\bar{u}_{s'}(P)\Sigma_3(P)u_s(P) = \frac{e^2}{2m(2\pi)^3}\delta_{s,s'}\int \mathrm{d}^2\boldsymbol{k}_\perp \int_0^\infty \mathrm{d}x\left[\frac{1}{(1-x)^2} - \frac{1}{(1+x)^2}\right], \tag{A.16}$$

which coincides with Eq. (3.75).

Let us now prove the derivation of Eqs. (3.87) and (3.88) from (3.83) and (3.84), respectively. Notice that (thanks to the invariance of the trace under cyclic permutations), Eqs. (3.83) and (3.84) can be obtained one from the other via the exchange $k \leftrightarrow l$, up to a minus sign; we hence evaluate only one of the two equations. The numerator of (3.83) is

$$\mathrm{Tr}\left[\gamma^\nu \tilde{\not{l}}\gamma^\mu\gamma^+\right] = l^+\mathrm{Tr}\left[\gamma^\nu\gamma^-\gamma^\mu\gamma^+\right] + l^-\mathrm{Tr}\left[\gamma^\nu\gamma^+\gamma^\mu\gamma^+\right] - l_i\mathrm{Tr}\left[\gamma^\nu\gamma^i\gamma^\mu\gamma^+\right]\,. \tag{A.17}$$

Out of these three terms, the second one can be neglected with the same argument made for (3.85), while the third one can be dropped since $l_i = -k_i$ ($i = 1, 2$) and we are integrating over $\boldsymbol{k}_\perp$. Consequently, we are left with

$$\varepsilon^*_{\lambda',\nu}(P)\mathrm{Tr}\left[\gamma^\nu\gamma^-\gamma^\mu\gamma^+\right]\varepsilon_{\lambda,\mu}(P) = 4\delta_{\lambda,\lambda'}\,, \tag{A.18}$$

where we used

$$\varepsilon^*_{\lambda',\mu}(P)\varepsilon^\mu_\lambda(P) = g_{\lambda,\lambda'} = -\delta_{\lambda,\lambda'}\,, \qquad \text{for } \lambda,\lambda' = 1,2\,.$$

Therefore we can rewrite

$$i\varepsilon^*_{\lambda',\nu}(P)\Pi_2^{\mu\nu}(P)\varepsilon_{\lambda,\mu}(P) = -\frac{4e^2P^+}{(2\pi)^3}\int \mathrm{d}^2\boldsymbol{k}_\perp\int \mathrm{d}x\,\frac{(1-x)P^+}{xP^+}\delta_{\lambda,\lambda'}I_2\,, \tag{A.19}$$

where the integral I_2 coincides with (A.11) and yields the result (A.13); if we put the latter into (A.19), we finally get Eq. (3.87). The substitution $k \to l$ now reduces to the exchange $x \to 1 - x$; if we also put an extra minus sign, we recover Eq. (3.88).

Appendix B

On the TMD calculation

B.1 Handbag diagram and Deep Inelastic Scattering

It is useful to revisit how the correlator (4.27) is linked to the cross section of the simplest process involving a diagonal matrix element of the quark current between initial and final states with zero momentum transfer, namely inclusive Deep Inelastic Scattering (DIS) [62, 63, 152]. We eventually recover that the diagrammatic representation of the correlator is given by the handbag diagram Fig. 4.4. It should be emphasized, however, that DIS cannot be used to experimentally access TMDs, since in this process we are not sensitive to the transverse momentum of the active parton.
DIS is illustrated in Fig. B.1: a leptonic probe with momentum l and spin s scatters off an hadron with momentum P, mass M and spin S via the exchange of a virtual photon with momentum q. The process is said to be *inclusive* when we detect only the lepton with momentum $l' = l - q$ and spin s' in the final state, while the final hadronic states, which we denote as X, are unobserved. We define the virtuality of the photon as $Q^2 = -q^2$, which is referred to also as the *hard* scale of the process. The scattering is considered *deep* in the limit $Q^2 \gg M^2$ along with $P \cdot q \gg M^2$, while the ratio

$$x_B = \frac{Q^2}{2P \cdot q} \,, \tag{B.1}$$

which defines the Bjorken variable x_B, is assumed to remain constant as $Q, P \cdot q \to \infty$. In this approximation, the parton-model approach where the scattering takes place only between the lepton probe and one of the quarks inside the nucleon, while the other are considered as non-interacting spectators, is a good assumption.
The differential cross section of the inclusive DIS process can be expressed as

$$l' \frac{\mathrm{d}\sigma}{d^3 l'} = \frac{1}{l \cdot P} \frac{\alpha^2}{Q^4} L^{\mu\nu} W_{\mu\nu} \,, \tag{B.2}$$

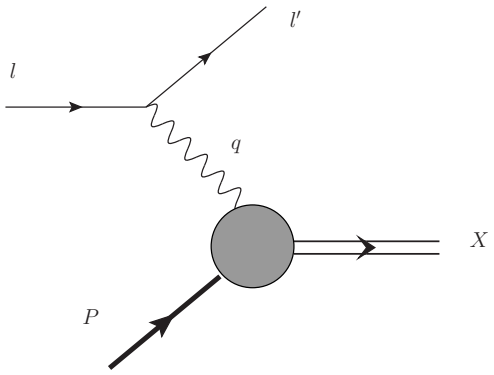

Figure B.1: Inclusive Deep Inelastic Scattering.

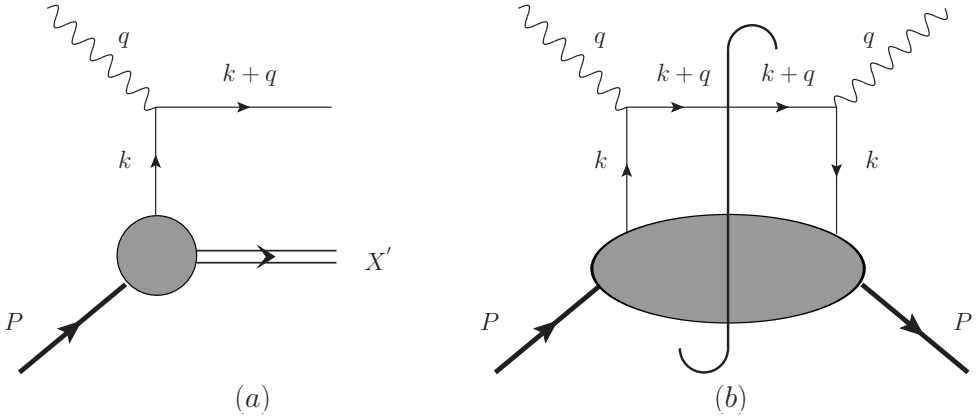

Figure B.2: DIS amplitude with a quark in the final state (a) and handbag diagram for the corresponding cross section (b).

where we separated the contributions from the leptonic tensor

$$L^{\mu\nu}(l,l';s) = \frac{1}{2}\sum_{s'}\left(\bar{u}_{s'}(l')\gamma^{\mu}u_s(l)\right)^{*}\left(\bar{u}_{s'}(l')\gamma^{\nu}u_s(l)\right), \tag{B.3}$$

and the hadronic tensor

$$W^{\mu\nu}(q,P;S) = \frac{1}{2\pi}\sum\!\!\!\!\!\!\int_X (2\pi)^4\delta^4\left(p_X - P - q\right)\,\langle P,S|J^{\mu}(0)|X\rangle\,\langle X|J^{\nu}(0)|P,S\rangle\ . \tag{B.4}$$

Here $J^{\mu}(x) = e_f\bar{\psi}(x)\gamma^{\mu}\psi(x)$ is the electromagnetic current related to a quark with charge e_f in units of e.[1] The leptonic tensor takes into account the electromagnetic interaction of the probe with the active parton and can be hence calculated perturbatively. The hadronic tensor, instead, contains all the non-perturbative information about the target.

Let us now split the final state $|X\rangle$ in Eq. (B.4) into a free quark with

[1]To be precise, a flavor index should be attached to each fermion field and, consequently, to the quark currents. We will omit it for better readability of the equations.

momentum $k' = k + q$ and mass m and a remnant state $|X'\rangle$, as shown in diagram (a) of Fig. B.2. By using the on-shell condition to rewrite

$$\int \frac{\mathrm{d}^3 k'}{(2\pi)^3 2k'^0} = \int \mathrm{d}^4 k\, \delta\left(k'^2 - m^2\right) \theta(k'^0 - m) \tag{B.5}$$

and the completeness for $|X'\rangle$, we obtain

$$\begin{aligned} W^{\mu\nu}(q, k, P; S) = \sum_f e_f^2 \int \mathrm{d}^4 k\, \delta\left((k+q)^2 - m^2\right) \theta\left(k^0 + q^0 - m\right) \int \frac{\mathrm{d}^4 z}{(2\pi)^4} e^{ik\cdot z} \\ \times \left[\left\langle P, S|\bar{\psi}(0)\psi(z)|P, S\right\rangle \gamma^\mu (\not{k} + \not{q} + m)\gamma^\nu \right. \\ \left. + \left\langle P, S|\psi(0)\bar{\psi}(z)|P, S\right\rangle \gamma^\nu (\not{k} + \not{q} + m)\gamma^\mu \right] . \end{aligned} \tag{B.6}$$

The second term in square brackets in Eq. (B.6) refers to the situation where, instead of a quark, we have an antiquark interacting with the virtual photon; we will drop it in the present discussion from now on.
We refer to Fig. B.2 for a diagrammatic interpretation of Eq. (B.6). It is easy to recognize that the right-hand side corresponds to the square of the amplitude described by diagram (a), "amputated" of the virtual photon line. Thanks to the optical theorem [46], we can represent the square of (a) with the handbag diagram (b), where the cut indicates that, in addition to the usual Feynman rules, we have to integrate over the final states and insert the on-shell condition $\delta\left(P_X^2 - m_X^2\right) \theta\left(p_X^0\right)$ for each particle in the final state. Furthermore, imaginary parts in the propagators change sign going from the left side to the right side of the cut.
We finally relate the hadronic tensor with the correlator at vanishing momentum transfer by rewriting

$$\begin{aligned} W^{\mu\nu} = \sum_f e_f^2 \int \mathrm{d}^4 k\, \delta\left((k+q)^2 - m^2\right) \theta\left(k^0 + q^0 - m\right) \\ \times \mathrm{Tr}\left[\Phi_S(k; P)\gamma^\mu \left(\not{k} + \not{q} + m\right)\gamma^\nu\right] , \end{aligned} \tag{B.7}$$

where

$$\Phi_S(k; P) = \int \frac{\mathrm{d}^4 z}{(2\pi)^4} e^{ik\cdot z} \left\langle P, S|\bar{\psi}(0)\psi(z)|P, S\right\rangle \tag{B.8}$$

coincides with Eq. (4.27) once we integrate over k^-. The diagrammatic representation of the correlator is shown in Fig. 4.4. It corresponds to the "lower part" of the handbag diagram (b) of Fig. B.2, obtained by removing the fermion propagator and the virtual photons, but still including the cut. This can be seen by reinserting the completeness on the hadronic final state $|X'\rangle$ in Eq. (B.8):

$$\Phi_S(k; P) = \sum\!\!\!\!\!\!\int_{X'} \left\langle P, S|\bar{\psi}(0)|X'\right\rangle \left\langle X'|\psi(0)|P, S\right\rangle \delta^{(4)}\left(P - k - P_{X'}\right) . \tag{B.9}$$

B.2 TMD gauge invariance

In Section 5.3.2 we showed that, in Feynman gauge, the leading-twist TMDs at order α receive contributions from three different diagrams, namely (a) to (c) in Fig. 5.5. It was then demonstrated in Section 5.3.3 that these contributions can be identified with the three terms coming from diagram (a) alone, but written with the light-cone gauge photon propagator. Here we summarize how the T-even TMDs reported in Eqs. (5.64) to (5.70) can be decomposed in the sum of these three terms:

$$f_1^A(x,\boldsymbol{k}_\perp) = \frac{1}{(2\pi)^3}\left[\frac{\boldsymbol{k}_\perp^2 + m^2(1-4x+x^2)}{x}\right]\varphi^2(x,\boldsymbol{k}_\perp)\,,$$
$$f_1^B(x,\boldsymbol{k}_\perp) = f_1^C(x,\boldsymbol{k}_\perp) = \frac{1}{(2\pi)^3}\left[\frac{\boldsymbol{k}_\perp^2 + m^2(1-x)^2}{(1-x)^2}\right]\varphi^2(x,\boldsymbol{k}_\perp)\,. \tag{B.10}$$
$$g_{1L}^A(x,\boldsymbol{k}_\perp) = \frac{1}{(2\pi)^3}\left[\frac{\boldsymbol{k}_\perp^2 - m^2(1+x^2)}{x}\right]\varphi^2(x,\boldsymbol{k}_\perp)\,,$$
$$g_{1L}^B(x,\boldsymbol{k}_\perp) = g_{1L}^C = \frac{1}{(2\pi)^3}\left[\frac{\boldsymbol{k}_\perp^2 + m^2(1-x)^2}{(1-x)^2}\right]\varphi^2(x,\boldsymbol{k}_\perp)\,. \tag{B.11}$$
$$g_{1T}^A(x,\boldsymbol{k}_\perp) = -\frac{2m^2}{(2\pi)^3}\,\varphi^2(x,\boldsymbol{k}_\perp)\,, \quad g_{1T}^B(x,\boldsymbol{k}_\perp) = g_{1T}^C(x,\boldsymbol{k}_\perp) = 0\,. \tag{B.12}$$
$$h_{1L}^A(x,\boldsymbol{k}_\perp) = -\frac{2m^2}{(2\pi)^3 x}\,\varphi^2(x,\boldsymbol{k}_\perp)\,, \quad h_{1L}^B(x,\boldsymbol{k}_\perp) = h_{1L}^C(x,\boldsymbol{k}_\perp) = 0\,. \tag{B.13}$$
$$h_{1T}^{\perp\,A}(x,\boldsymbol{k}_\perp) = h_{1T}^{\perp\,B}(x,\boldsymbol{k}_\perp) = h_{1T}^{\perp\,C}(x,\boldsymbol{k}_\perp) = 0\,. \tag{B.14}$$
$$h_{1T}^A(x,\boldsymbol{k}_\perp) = -\frac{2m^2}{(2\pi)^3}\,\varphi^2(x,\boldsymbol{k}_\perp)\,,$$
$$h_{1T}^B(x,\boldsymbol{k}_\perp) = h_{1T}^C(x,\boldsymbol{k}_\perp) = \frac{1}{(2\pi)^3}\left[\frac{\boldsymbol{k}_\perp^2 + m^2(1-x)^2}{(1-x)^2}\right]\,, \tag{B.15}$$

where for each TMD $f^e(x,\boldsymbol{k}_\perp)$ the notation $f^e(x,\boldsymbol{k}_\perp) = f^A(x,\boldsymbol{k}_\perp) + f^B(x,\boldsymbol{k}_\perp) + f^C(x,\boldsymbol{k}_\perp)$ is understood. We observe in particular that for the TMDs g_{1T}^e and h_{1L}^e the second and third term are vanishing: this means that their evaluation in Feynman and light-cone gauge would coincide even omitting the insertion of the Wilson line.

B.3 Eikonal approximation in the Drell-Yan process

In Section 5.3.2 we described the eikonal approximation for the SIDIS case and showed how to isolate the sub-diagram corresponding to the electron correlator from the handbag diagram, in presence of a gauge photon. The key result of the approximation is the introduction of the eikonal propagator (5.58) to which we associate the Feynman rules illustrated in Fig. 5.7. Here we provide the

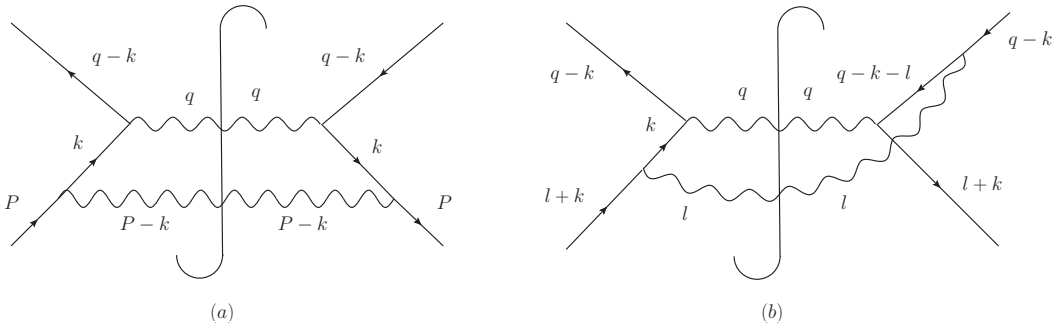

Figure B.3: Cut diagram for the electron-positron annihilation, with a gauge photon.

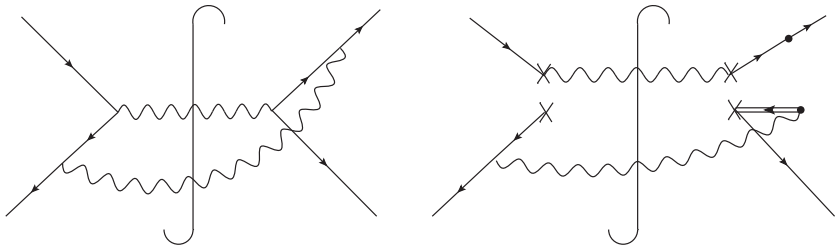

Figure B.4: Cut diagram for the electron-positron annihilation, split into its upper and lower part, which is the one contributing to the correlator. Diagrams are meant to be joined by attaching crosses with crosses and circles with circles.

analog derivation of the eikonal propagator for the QED Drell-Yan scattering, where the partonic content of the dressed electron is probed by a positron that annihilates with the internal electron, producing an outgoing photon.
The amplitude of the Drell-Yan process can be obtained by evaluating the cut diagram in Fig. B.3 (a); its factorization into an upper and lower part is trivial. We thus focus on diagram (b) in Fig. B.3, where we consider the same process with the inclusion of a initial-state interaction with a gauge photon. The corresponding amplitude reads

$$\begin{aligned}\mathcal{M}^2 =& \frac{e^4}{(2\pi)^3}\delta(l^2)\delta(q^2)\bar{v}_{S'}(q-k)\gamma_\mu\frac{\not{k}+m}{k^2-m^2+i\epsilon}\gamma_\nu u_S(l+k)\\ &\times\bar{u}_S(l+k)\gamma^\mu\frac{\not{q}-\not{k}-\not{l}-m}{(q-k-l)^2-m^2-i\epsilon}\gamma^\nu v_{S'}(q-k)\,. \end{aligned}\tag{B.16}$$

Let us apply the eikonal approximation to the fermion propagator with momentum $q-l-k$: similarly to Eq. (5.58), we obtain:

$$\frac{\not{q}-\not{k}-\not{l}-m}{(q-k-l)^2-m^2-i\epsilon}\simeq-\frac{(q-k)^-\gamma^+}{2(q-k)^-k^+ +i\epsilon}=\frac{\gamma^+}{-2k^+ +i\epsilon'}\,,\tag{B.17}$$

where $\epsilon' = -\epsilon/(q-k)^-$ is still positive since $q-k$ is the momentum of the outgoing positron. Therefore, with respect to the SIDIS case, here we have a

Figure B.5: Feynman rules for the eikonal propagator and vertex in the Drell-Yan case; the rules refer to the left-hand side of the cut.

sign difference in the momentum of the eikonal propagator.
In Fig. B.4 we show the diagrammatic representation of the splitting. The Feynman rules for the eikonal propagator in the Drell-Yan case are indicated in Fig. B.5. Notice that the position of the cross and the circle in the eikonal propagator are flipped, with respect to the SIDIS case.

Appendix C

From momentum to position space

C.1 Overlap representation of GPDs in the impact-parameter space

We show how to derive Eqs. (6.104) to (6.106), reporting the discussion in Ref. [148].
In momentum space, the LFWF overlap representation of GPDs can be recovered from that of (proper combinations of) GTMDs by integrating over the active quark's transverse momentum $\boldsymbol{k}_\perp$. Referring to the scalar-diquark model, one has, for $\xi^+ = 0$:

$$H(x,\boldsymbol{\Delta}_\perp) = \int \frac{\mathrm{d}^2\boldsymbol{k}_\perp}{2(2\pi)^3}\left[\psi_+^{+\,*}(x,\boldsymbol{k}'_\perp)\psi_+^+(x,\boldsymbol{k}_\perp)+\psi_-^{+\,*}(x,\boldsymbol{k}'_\perp)\psi_-^+(x,\boldsymbol{k}_\perp)\right], \quad \text{(C.1)}$$

$$E(x,\boldsymbol{\Delta}_\perp) = -\frac{2M}{\Delta_L}\int \frac{\mathrm{d}^2\boldsymbol{k}_\perp}{2(2\pi)^3}\left[\psi_+^{+\,*}(x,\boldsymbol{k}'_\perp)\psi_+^-(x,\boldsymbol{k}_\perp)+\psi_+^{+\,*}(x,\boldsymbol{k}'_\perp)\psi_-^-(x,\boldsymbol{k}_\perp)\right], \quad \text{(C.2)}$$

$$\tilde{H}(x,\boldsymbol{\Delta}_\perp) = \int \frac{\mathrm{d}^2\boldsymbol{k}_\perp}{2(2\pi)^3}\left[\psi_+^{+\,*}(x,\boldsymbol{k}'_\perp)\psi_+^+(x,\boldsymbol{k}_\perp)-\psi_-^{+\,*}(x,\boldsymbol{k}'_\perp)\psi_-^+(x,\boldsymbol{k}_\perp)\right], \quad \text{(C.3)}$$

where $\boldsymbol{k}'_\perp = \boldsymbol{k}_\perp + (1-x)\boldsymbol{\Delta}_\perp$.
Let us consider a generic function G in the form

$$G(\boldsymbol{\Delta}_\perp) = \int \frac{\mathrm{d}^2\boldsymbol{k}_\perp}{(2\pi)^2} f^*(\boldsymbol{k}_\perp - a\boldsymbol{\Delta}_\perp) g(\boldsymbol{k}_\perp) \quad \text{(C.4)}$$

for some arbitrary parameter a. If the functions f and g satisfy

$$f(\boldsymbol{k}_\perp) = \int \mathrm{d}^2\boldsymbol{r}_\perp\, e^{-i\boldsymbol{r}_\perp\cdot\boldsymbol{k}_\perp}\tilde{f}(x,\boldsymbol{r}_\perp), \quad \text{(C.5)}$$

$$g(\boldsymbol{k}_\perp) = \int \mathrm{d}^2\boldsymbol{r}_\perp\, e^{-i\boldsymbol{r}_\perp\cdot\boldsymbol{k}_\perp}\tilde{g}(x,\boldsymbol{r}_\perp), \quad \text{(C.6)}$$

where $\tilde{f}$ and $\tilde{g}$ denote the respective Fourier transforms, we can write:

$$\int \frac{\mathrm{d}^2\boldsymbol{\Delta}_\perp}{(2\pi)^2}\, e^{i\boldsymbol{b}_\perp\cdot\boldsymbol{\Delta}_\perp} G(\boldsymbol{\Delta}_\perp) = \frac{1}{|a|^2}\, \tilde{f}^*\left(\frac{\boldsymbol{b}_\perp}{a}\right)\tilde{g}\left(\frac{\boldsymbol{b}_\perp}{a}\right) . \tag{C.7}$$

If we apply the last relation to Eqs. (C.1) to (C.3) with $a = (1-x)$, $\boldsymbol{r}_\perp = \boldsymbol{b}_\perp/(1-x)$, we recover the overlap representation in Eqs. (6.104) to (6.106).

C.2 Hankel transform

Let us now consider the Fourier transform (6.101) of the LFWFs to the impact-parameter space. In order to recover Eqs. (6.102) and (6.103), we need the two-dimensional Fourier transform $\tilde{f}(x_\perp)$ of a generic function $f(p_\perp)$, where $p_\perp = |\boldsymbol{p}_\perp|$ and $x_\perp = |\boldsymbol{x}_\perp|$:

$$\tilde{f}(x_\perp) = 2\pi \int_0^\infty \mathrm{d}p_\perp\, g(p_\perp)\, J_0(x_\perp p_\perp)\, p_\perp . \tag{C.8}$$

Here $J_0(z)$ is the zeroth order Bessel function of the first kind; these functions have, for generic n, the following integral representation:

$$J_n(z) = \frac{1}{2\pi i^n} \int_0^{2\pi} \mathrm{d}\phi\, e^{-iz\cos\phi}\, e^{in\phi} . \tag{C.9}$$

In the following, we will need the Hankel transform of a function g in the form $g(p_\perp) = 1/(a^2+p_\perp^2)$, that is given by

$$\int \mathrm{d}^2\boldsymbol{p}_\perp \frac{e^{i\,\boldsymbol{x}_\perp\cdot\boldsymbol{p}_\perp}}{a^2+p_\perp^2} = 2\pi K_0(a x_\perp) , \tag{C.10}$$

where $K_n(z)$ is the n-th order modified Bessel function of the first kind.
We now use Eq. (C.8) to derive the Fourier transforms of the light-front wave functions (6.98)-(6.99). The wave functions Ψ_+^+ and Ψ_-^- depend on $\boldsymbol{k}_\perp^2$ only through the function $\varphi(x,\boldsymbol{k}_\perp^2)$ in Eq. (6.100). Therefore, we can directly apply to them (C.10), with $a = u(x,m_D^2)$, and obtain Eq. (6.102).
In order to evaluate the Fourier transforms of ψ_-^+ and ψ_+^-, instead, we first need to switch to polar coordinates, and set:

$$\boldsymbol{b}_\perp = b_\perp(\cos\phi_b, \sin\phi_b) , \quad \boldsymbol{k}_\perp = k_\perp(\cos\phi_k, \sin\phi_k) .$$

Let us consider ψ_-^+ as an example; we can rewrite its Fourier transform as:

$$\begin{aligned}\psi_-^+(x,\boldsymbol{b}_\perp) = \int_0^{+\infty} \frac{k_\perp\,\mathrm{d}k_\perp}{2(2\pi)^3} \int_0^{2\pi} \mathrm{d}\phi_k\, e^{ib_\perp k_\perp(\cos\phi_b\cos\phi_k+\sin\phi_b\sin\phi_k)} \\ \times \frac{g\sqrt{1-x}}{(2\pi)^2}\, \frac{k_\perp\, e^{i\phi_k}}{k_\perp^2+u(x,m_D^2)} .\end{aligned} \tag{C.11}$$

The integral in the angular variable is:

$$\int_0^{2\pi} \mathrm{d}\phi_k \, e^{ib_\perp k_\perp \cos(\phi_b-\phi_k)} \, e^{-i(\phi_b-\phi_k)} e^{-i\phi_b} \equiv \int_0^{2\pi} \mathrm{d}\phi_k \, e^{-ib_\perp k_\perp \cos\phi_k} \, e^{-i\phi_k} e^{i\phi_b} = (2\pi i) \, e^{i\phi_b} \, J_1(b_\perp k_\perp) \, , \tag{C.12}$$

where we used (C.9). The intermediate step is allowed, because the complex exponentials are 2π-periodic, and we are integrating over a whole period 2π. By inserting Eq. (C.12) into Eq. (C.11), the latter becomes:

$$\Psi_-^+(x, \boldsymbol{b}_\perp) = -i \frac{g\sqrt{1-x}}{2\pi} e^{i\phi_b} \int_0^{+\infty} \mathrm{d}k_\perp \frac{k_\perp^2}{k_\perp^2 + u(x, m_D^2)} \, J_1(b_\perp k_\perp) \, . \tag{C.13}$$

By substituting $\alpha = 1$, $\beta = 0$, $z^2 = u(x, m_D^2)$ and $s = b_\perp$ in the identity [93]

$$\int_0^{+\infty} \mathrm{d}t \, \frac{t^{\alpha+1}}{(t^2+z^2)^{\beta+1}} \, J_\alpha(st) = \frac{s^\beta z^{\alpha-\beta}}{2^\beta \Gamma(\beta+1)} \, K_{\alpha-\beta}(sz) \, ,$$

where $\Gamma(r)$ is the Gamma function, we arrive at the final result (6.103).

C.3 Kinetic and canonical orbital angular momentum

Proving the equality between Eqs. (6.114) and (6.115) amounts to establishing the following identity

$$\int_0^1 \mathrm{d}x \, \frac{1}{1-x} \left[(1-x)(x^2M^2 - m^2) + (1+x)\, u \right] Z K_0(Z) K_1(Z) = \int \mathrm{d}x \, \frac{1-3x}{1-x} \, u \left[K_1(Z) \right]^2 \, , \tag{C.14}$$

Using

$$\frac{1}{Z} \frac{\partial Z}{\partial x} = \frac{1}{2u} \frac{\partial u}{\partial x} + \frac{1}{1-x}, \qquad x \frac{\partial u}{\partial x} = u + x^2 M^2 - m^2, \tag{C.15}$$

we find that

$$\frac{1}{1-x} \left[(1-x)(x^2M^2 - m^2) + (1+x)\, u \right] Z = 2ux \frac{\partial Z}{\partial x}. \tag{C.16}$$

Noting now that

$$\frac{\mathrm{d}(Z^2 \left[K_1(Z) \right]^2)}{\mathrm{d}Z} = -2Z^2 K_0(Z) K_1(Z), \tag{C.17}$$

we can rewrite the LHS of Eq. (C.14) as

$$\int_0^1 \mathrm{d}x \, \frac{1}{1-x} \left[(1-x)(x^2M^2 - m^2) + (1+x)\, u \right] Z K_0(Z) K_1(Z) = -\int_0^1 \frac{xu}{Z^2} \frac{\partial (Z^2 \left[K_1(Z) \right]^2)}{\partial x}. \tag{C.18}$$

Integrating by parts, the boundary term vanishes identically for $b_\perp > 0$ and we obtain the RHS of Eq. (C.14).

Bibliography

[1] M. Born, W. Heisenberg, and P. Jordan. Zur Quantenmechanik. II. *Z. Phys.*, 35(8-9):557, 1926.

[2] P. A. M. Dirac. Quantum theory of emission and absorption of radiation. *Proc. Roy. Soc. Lond.*, A114:243, 1927.

[3] S. S. Schweber. *QED and the men who made it: Dyson, Feynman, Schwinger, and Tomonaga*. 1994.

[4] P. A.M. Dirac. Forms of Relativistic Dynamics. *Rev. Mod. Phys.*, 21:392, 1949.

[5] The proton mass: At the heart of most visible matter. `https://phys.cst.temple.edu/~meziani/proton-mass-workshop-2016/`, 2016.

[6] 2nd workshop on the proton mass: At the heart of most visible matter. `http://www.ectstar.eu/node/2218`, 2017.

[7] E. Leader and C. Lorcé. The angular momentum controversy: What's it all about and does it matter? *Phys. Rept.*, 541(3):163, 2014.

[8] B. L. G. Bakker et al. Light-Front Quantum Chromodynamics: A framework for the analysis of hadron physics. *Nucl. Phys. Proc. Suppl.*, 251-252:165, 2014.

[9] S. J. Brodsky, H. Pauli, and S. S. Pinsky. Quantum chromodynamics and other field theories on the light cone. *Phys. Rept.*, 301:299, 1998.

[10] H. Leutwyler and J. Stern. Relativistic Dynamics on a Null Plane. *Annals Phys.*, 112:94, 1978.

[11] S. Fubini and G. Furlan. Renormalization effects for partially conserved currents. *Physics*, 1(4):229, 1965.

[12] S. Weinberg. Dynamics at infinite momentum. *Phys. Rev.*, 150:1313, 1966.

[13] L. Susskind. Model of selfinduced strong interactions. *Phys. Rev.*, 165:1535, 1968.

[14] K. Bardakci and M. B. Halpern. Theories at infinite momentum. *Phys. Rev.*, 176:1686, 1968.

[15] S. Chang and S. Ma. Feynman rules and quantum electrodynamics at infinite momentum. *Phys. Rev.*, 180:1506, 1969.

[16] J. D. Bjorken. Asymptotic sum rules at infinite momentum. *Phys. Rev.*, 179:1547, 1969.

[17] J. B. Kogut and D. E. Soper. Quantum Electrodynamics in the Infinite Momentum Frame. *Phys. Rev.*, D1:2901, 1970.

[18] S. D. Drell, D. J. Levy, and T. Yan. Theory of deep-inelastic lepton-nucleon scattering and lepton-pair annihilation processes. i. *Phys. Rev.*, 187:2159, 1969.

[19] S. D. Drell, D. J. Levy, and T. Yan. Theory of deep-inelastic lepton-nucleon scattering and lepton-pair annihilation processes. iii. deep-inelastic electron-positron annihilation. *Phys. Rev. D*, 1:1617, 1970.

[20] S. D. Drell, D. J. Levy, and T. Yan. Theory of deep-inelastic lepton-nucleon scattering and lepton pair annihilation processes. ii. deep-inelastic electron scattering. *Phys. Rev. D*, 1:1035, 1970.

[21] S. J. Brodsky, R. Roskies, and R. Suaya. Quantum Electrodynamics and Renormalization Theory in the Infinite Momentum Frame. *Phys. Rev.*, D8:4574, 1973.

[22] M. Sawicki. Light front limit in a rest frame. *Phys. Rev.*, D44:433, 1991.

[23] J. D. Bjorken, John B. Kogut, and Davison E. Soper. Quantum Electrodynamics at Infinite Momentum: Scattering from an External Field. *Phys. Rev.*, D3:1382, 1971.

[24] D. E. Soper. Infinite-momentum helicity states. *Phys. Rev.*, D5:1956, 1972.

[25] M. Burkardt. Impact parameter space interpretation for generalized parton distributions. *Int.J.Mod.Phys.*, A18:173, 2003.

[26] S. J. Brodsky, Dae S. Hwang, B. Ma, and I. Schmidt. Light cone representation of the spin and orbital angular momentum of relativistic composite systems. *Nucl. Phys.*, B593:311, 2001.

[27] L. Susskind and G. Frye. Theory of self-induced strong interactions. *Phys. Rev.*, 164:2003, 1967.

[28] C. Lorcé and B. Pasquini. Quark Wigner Distributions and Orbital Angular Momentum. *Phys. Rev.*, D84:014015, 2011.

[29] S. J. Chang and T. M. Yan. Quantum field theories in the infinite momentum frame. 2. Scattering matrices of scalar and Dirac fields. *Phys. Rev.*, D7:1147, 1973.

[30] N. E. Ligterink and B. L. G. Bakker. Equivalence of light front and covariant field theory. *Phys. Rev.*, D52:5954, 1995.

[31] B. L. G. Bakker, M. A. DeWitt, C. R. Ji, and Y. Mishchenko. Restoring the equivalence between the light-front and manifestly covariant formalisms. *Phys. Rev.*, D72:076005, 2005.

[32] N. C. J. Schoonderwoerd and B. L. G. Bakker. Equivalence of renormalized covariant and light front perturbation theory. 2. Transverse divergences in the Yukawa model. *Phys. Rev.*, D58:025013, 1998.

[33] N. C. J. Schoonderwoerd and B. L. G. Bakker. Equivalence of renormalized covariant and light front perturbation theory. 1. Longitudinal divergences in the Yukawa model. *Phys. Rev.*, D57:4965, 1998.

[34] C. R. Ji, Z. Li, and A. T. Suzuki. Electromagnetic gauge field interpolation between the instant form and the front form of the Hamiltonian dynamics. *Phys. Rev.*, D91(6):065020, 2015.

[35] A. Misra and S. Warawdekar. Equivalence of covariant and light front QED at one loop level. *Phys. Rev.*, D71:125011, 2005.

[36] S. M. Patel and A. Misra. Equivalence of Covariant and Light Front QED: Generating Instantaneous Diagrams. *Phys. Rev.*, D82:125024, 2010.

[37] L. Mantovani, B. Pasquini, X. Xiong, and A. Bacchetta. Revisiting the equivalence of light-front and covariant QED in the light-cone gauge. *Phys. Rev.*, D94(11):116005, 2016.

[38] L. Mantovani, A. Bacchetta, B. Pasquini, and X. Xiong. The Gauge-Field Propagator in Light-Cone Gauge: Which is the Correct One? *Few Body Syst.*, 58(2):84, 2017.

[39] A. T. Suzuki and J. H. O. Sales. Light front gauge propagator reexamined. *Nucl. Phys.*, A725:139, 2003.

[40] A. Harindranath. An Introduction to light front dynamics for pedestrians. In *International School on Light-Front Quantization and Non-Perturbative QCD (To be followed by the Workshop 3-14 Jun 1996) Ames, Iowa, May 6-June 2, 1996*, 1996.

[41] A. T. Suzuki and J. H. O. Sales. Light-front gauge propagator reexamined-II. hep-th/0304065.

[42] D. Mustaki, S. Pinsky, J. Shigemitsu, and K. Wilson. Perturbative renormalization of null plane QED. *Phys. Rev.*, D43:3411, 1991.

[43] P. P. Srivastava and S. J. Brodsky. Light front quantized QCD in light cone gauge. *Phys. Rev.*, D64:045006, 2001.

[44] S. Weinberg. *The Quantum theory of fields. Vol. 1: Foundations*. Cambridge University Press, 2005.

[45] G. P. Lepage and S. J. Brodsky. Exclusive Processes in Perturbative Quantum Chromodynamics. *Phys. Rev.*, D22:2157, 1980.

[46] M. E. Peskin and D. V. Schroeder. *An Introduction to quantum field theory*. 1995.

[47] A. T. Suzuki and J. H. O. Sales. The Light front gauge propagator: The Status quo. In *Light cone physics: Hadrons and beyond: Proceedings. 2003*, 2004.

[48] J. Collins. *Foundations of perturbative QCD*. Cambridge University Press, 2013.

[49] S. Meissner, A. Metz, and M. Schlegel. Generalized parton correlation functions for a spin-1/2 hadron. *JHEP*, 0908:056, 2009.

[50] S. Meissner, A. Metz, . Schlegel, and K. Goeke. Generalized parton correlation functions for a spin-0 hadron. *JHEP*, 08:038, 2008.

[51] M. Diehl. Introduction to GPDs and TMDs. *Eur. Phys. J.*, A52(6):149, 2016.

[52] C. Lorcé, B. Pasquini, and M. Vanderhaeghen. Unified framework for generalized and transverse-momentum dependent parton distributions within a 3Q light-cone picture of the nucleon. *JHEP*, 1105:041, 2011.

[53] K. Goeke, A. Metz, and M. Schlegel. Parameterization of the quark-quark correlator of a spin-1/2 hadron. *Phys. Lett.*, B618:90, 2005.

[54] R. L. Jaffe. Spin, twist and hadron structure in deep inelastic processes. In *The spin structure of the nucleon. Proceedings, International School of Nucleon Structure, 1st Course, Erice, Italy, August 3-10, 1995*, page 42, 1996.

[55] J. C. Collins and D. E. Soper. Parton Distribution and Decay Functions. *Nucl. Phys.*, B194:445, 1982.

[56] C. J. Bomhof, P. J. Mulders, and F. Pijlman. Gauge link structure in quark-quark correlators in hard processes. *Phys. Lett.*, B596:277, 2004.

[57] C. J. Bomhof, P. J. Mulders, and F. Pijlman. The Construction of gauge-links in arbitrary hard processes. *Eur. Phys. J.*, C47:147, 2006.

[58] C. Lorcé and B. Pasquini. Structure analysis of the generalized correlator of quark and gluon for a spin-1/2 target. *JHEP*, 09:138, 2013.

[59] M. G. Echevarria, . Idilbi, K. Kanazawa, C. Lorcé, A. Metz, B. Pasquini, and M. Schlegel. Proper definition and evolution of generalized transverse momentum dependent distributions. *Phys. Lett.*, B759:336, 2016.

[60] X. Ji. Viewing the proton through 'color' filters. *Phys. Rev. Lett.*, 91:062001, 2003.

[61] A. V. Belitsky, X. D. Ji, and F. Yuan. Quark imaging in the proton via quantum phase space distributions. *Phys. Rev.*, D69:074014, 2004.

[62] P. J. Mulders and R. D. Tangerman. The Complete tree level result up to order 1/Q for polarized deep inelastic leptoproduction. *Nucl. Phys.*, B461:197, 1996. [Erratum: Nucl. Phys.B484,538(1997)].

[63] V. Barone, A. Drago, and P. G. Ratcliffe. Transverse polarisation of quarks in hadrons. *Phys. Rept.*, 359:1, 2002.

[64] A. Bacchetta, M. Diehl, K. Goeke, A. Metz, P. J. Mulders, and M. Schlegel. Semi-inclusive deep inelastic scattering at small transverse momentum. *JHEP*, 02:093, 2007.

[65] M. Diehl. Generalized parton distributions. *Phys. Rept.*, 388:41, 2003.

[66] X. Ji. Gauge-Invariant Decomposition of Nucleon Spin. *Phys. Rev. Lett.*, 78:610, 1997.

[67] A. V. Belitsky and A. V. Radyushkin. Unraveling hadron structure with generalized parton distributions. *Phys. Rept.*, 418:1, 2005.

[68] S. Boffi and B. Pasquini. Generalized parton distributions and the structure of the nucleon. *Riv. Nuovo Cim.*, 30:387, 2007.

[69] U. D'Alesio and F. Murgia. Azimuthal and Single Spin Asymmetries in Hard Scattering Processes. *Prog. Part. Nucl. Phys.*, 61:394, 2008.

[70] C. Lorcé and B. Pasquini. On the Origin of Model Relations among Transverse-Momentum Dependent Parton Distributions. *Phys. Rev.*, D84:034039, 2011.

[71] S. Meissner, A. Metz, and K. Goeke. Relations between generalized and transverse momentum dependent parton distributions. *Phys. Rev.*, D76:034002, 2007.

[72] A. Bacchetta, D. Boer, M. Diehl, and P. J. Mulders. Matches and mismatches in the descriptions of semi- inclusive processes at low and high transverse momentum. *JHEP*, 08:023, 2008.

[73] D. Boer and P. J. Mulders. Time reversal odd distribution functions in leptoproduction. *Phys. Rev.*, D57:5780, 1998.

[74] D. W. Sivers. Single Spin Production Asymmetries from the Hard Scattering of Point-Like Constituents. *Phys. Rev.*, D41:83, 1990.

[75] M. Burkardt. Impact parameter dependent parton distributions and off forward parton distributions for zeta —> 0. *Phys. Rev.*, D62:071503, 2000. [Erratum: Phys. Rev.D66,119903(2002)].

[76] E. Wigner. On the quantum correction for thermodynamic equilibrium. *Phys. Rev.*, 40:749, 1932.

[77] C. Lorcé and B. Pasquini. Multipole decomposition of the nucleon transverse phase space. *Phys. Rev.*, D93(3):034040, 2016.

[78] T. Liu and B. Ma. Quark Wigner distributions in a light-cone spectator model. *Phys. Rev.*, D91:034019, 2015.

[79] A. Rajan, A. Courtoy, M. Engelhardt, and S. Liuti. Parton Transverse Momentum and Orbital Angular Momentum Distributions. *Phys. Rev.*, D94(3):034041, 2016.

[80] A. Courtoy and A. S. Miramontes. Quark Orbital Angular Momentum in the MIT Bag Model. *Phys. Rev.*, D95(1):014027, 2017.

[81] M. Engelhardt. Quark orbital dynamics in the proton from Lattice QCD – from Ji to Jaffe-Manohar orbital angular momentum. *Phys. Rev.*, D95(9):094505, 2017.

[82] D. Chakrabarti, T. Maji, C. Mondal, and A. Mukherjee. Quark Wigner distributions and spin-spin correlations. *Phys. Rev.*, D95(7):074028, 2017.

[83] A. Mukherjee, S. Nair, and V. K. Ojha. Wigner distributions for gluons in a light-front dressed quark model. *Phys. Rev.*, D91(5):054018, 2015.

[84] X. Ji, F. Yuan, and Y. Zhao. Hunting the Gluon Orbital Angular Momentum at the Electron-Ion Collider. *Phys. Rev. Lett.*, 118(19):192004, 2017.

[85] Y. Hatta, Y. Nakagawa, F. Yuan, Y. Zhao, and B. Xiao. Gluon orbital angular momentum at small-x. *Phys. Rev.*, D95(11):114032, 2017.

[86] J. Zhou. Elliptic gluon generalized transverse-momentum-dependent distribution inside a large nucleus. *Phys. Rev.*, D94(11):114017, 2016.

[87] Y. Hatta, B. Xiao, and F. Yuan. Probing the Small- x Gluon Tomography in Correlated Hard Diffractive Dijet Production in Deep Inelastic Scattering. *Phys. Rev. Lett.*, 116(20):202301, 2016.

[88] Y. Hagiwara, Y. Hatta, and T. Ueda. Wigner, Husimi, and generalized transverse momentum dependent distributions in the color glass condensate. *Phys. Rev.*, D94(9):094036, 2016.

[89] S. Bhattacharya, A. Metz, and J. Zhou. Generalized TMDs and the exclusive double Drell–Yan process. *Phys. Lett.*, B771:396, 2017.

[90] M. Diehl, T. Feldmann, R. Jakob, and P. Kroll. The Overlap representation of skewed quark and gluon distributions. *Nucl. Phys.*, B596:33, 2001.

[91] S. J. Brodsky, M. Diehl, and D. S. Hwang. Light cone wave function representation of deeply virtual Compton scattering. *Nucl. Phys.*, B596:99, 2001.

[92] M. Burkardt and B. Pasquini. Modelling the nucleon structure. *Eur. Phys. J.*, A52(6):161, 2016.

[93] P. Hoyer and S. Kurki. The Transverse shape of the electron. *Phys. Rev.*, D81:013002, 2010.

[94] G. A. Miller. Electron structure: Shape, size, and generalized parton distributions in QED. *Phys. Rev.*, D90(11):113001, 2014.

[95] T. Liu and B. Q. Ma. Angular momentum decomposition from a QED example. *Phys. Rev.*, D91:017501, 2015.

[96] N. Kumar and C. Mondal. Wigner distributions for an electron. *hep-ph/1705.03183*, 2017.

[97] S. J. Brodsky and G. P. Lepage. Exclusive Processes in Quantum Chromodynamics. *Adv. Ser. Direct. High Energy Phys.*, 5:93, 1989.

[98] C. Lorcé, B. Pasquini, X. Xiong, and F. Yuan. The quark orbital angular momentum from Wigner distributions and light-cone wave functions. *Phys. Rev.*, D85:114006, 2012.

[99] L. Mantovani, A. Bacchetta, and B. Pasquini. The Electron in Three-Dimensional Momentum Space. *Few Body Syst.*, 57(7):515, 2016.

[100] A. Bacchetta, L. Mantovani, and B. Pasquini. Electron in three-dimensional momentum space. *Phys. Rev.*, D93(1):013005, 2016.

[101] D. Boer, P. J. Mulders, and F. Pijlman. Universality of T odd effects in single spin and azimuthal asymmetries. *Nucl. Phys.*, B667:201, 2003.

[102] X. Ji and F. Yuan. Parton distributions in light cone gauge: Where are the final state interactions? *Phys. Lett.*, B543:66, 2002.

[103] J. C. Collins and D. E. Soper. Back-To-Back Jets in QCD. *Nucl. Phys.*, B193:381, 1981. [Erratum: Nucl. Phys.B213,545(1983)].

[104] X. Ji, J. Ma, and F. Yuan. QCD factorization for semi-inclusive deep-inelastic scattering at low transverse momentum. *Phys. Rev.*, D71:034005, 2005.

[105] S. M. Aybat and T. C. Rogers. TMD Parton Distribution and Fragmentation Functions with QCD Evolution. *Phys. Rev.*, D83:114042, 2011.

[106] M. G. Echevarria, A. Idilbi, and I. Scimemi. Factorization Theorem For Drell-Yan At Low q_T And Transverse Momentum Distributions On-The-Light-Cone. *JHEP*, 07:002, 2012.

[107] J. C. Collins and T. C. Rogers. Equality of Two Definitions for Transverse Momentum Dependent Parton Distribution Functions. *Phys. Rev.*, D87(3):034018, 2013.

[108] M. G. Echevarria, A. Idilbi, A. Schäfer, and I. Scimemi. Model-Independent Evolution of Transverse Momentum Dependent Distribution Functions (TMDs) at NNLL. *Eur. Phys. J.*, C73(12):2636, 2013.

[109] M. G. Echevarría, A. Idilbi, and I. Scimemi. Soft and Collinear Factorization and Transverse Momentum Dependent Parton Distribution Functions. *Phys. Lett.*, B726:795, 2013.

[110] A. Bacchetta, M. Boglione, A. Henneman, and P. J. Mulders. Bounds on transverse momentum dependent distribution and fragmentation functions. *Phys. Rev. Lett.*, 85:712, 2000.

[111] A. V. Belitsky, X. Ji, and F. Yuan. Final state interactions and gauge invariant parton distributions. *Nucl. Phys.*, B656:165, 2003.

[112] P. J. Mulders and J. Rodrigues. Transverse momentum dependence in gluon distribution and fragmentation functions. *Phys. Rev.*, D63:094021, 2001.

[113] K. Goeke, S. Meissner, A. Metz, and M. Schlegel. Checking the Burkardt sum rule for the Sivers function by model calculations. *Phys. Lett.*, B637:241, 2006.

[114] J. C. Collins and T. C. Rogers. The Gluon Distribution Function and Factorization in Feynman Gauge. *Phys. Rev.*, D78:054012, 2008.

[115] D. Boer, S. Cotogno, T. van Daal, P. J. Mulders, A. Signori, and Y. Zhou. Gluon and Wilson loop TMDs for hadrons of spin ≤ 1. *JHEP*, 10:013, 2016.

[116] M. Burkardt. Sivers mechanism for gluons. *Phys. Rev.*, D69:091501, 2004.

[117] M. Burkardt. Quark correlations and single spin asymmetries. *Phys. Rev.*, D69:057501, 2004.

[118] M. Diehl and P. Hägler. Spin densities in the transverse plane and generalized transversity distributions. *Eur. Phys. J.*, C44:87, 2005.

[119] D. Boer, S. J. Brodsky, P. J. Mulders, and C. Pisano. Direct Probes of Linearly Polarized Gluons inside Unpolarized Hadrons. *Phys. Rev. Lett.*, 106:132001, 2011.

[120] D. Boer, W. J. den Dunnen, C. Pisano, M. Schlegel, and W. Vogelsang. Linearly Polarized Gluons and the Higgs Transverse Momentum Distribution. *Phys. Rev. Lett.*, 108:032002, 2012.

[121] C. Pisano, D. Boer, S. J. Brodsky, M. G. A. Buffing, and P. J. Mulders. Linear polarization of gluons and photons in unpolarized collider experiments. *JHEP*, 10:024, 2013.

[122] S. Catani and M. Grazzini. QCD transverse-momentum resummation in gluon fusion processes. *Nucl. Phys.*, B845:297, 2011.

[123] J. C. Collins. Leading twist single transverse-spin asymmetries: Drell-Yan and deep inelastic scattering. *Phys. Lett.*, B536:43, 2002.

[124] Y. Hatta. Notes on the orbital angular momentum of quarks in the nucleon. *Phys. Lett.*, B708:186, 2012.

[125] M. Wakamatsu. Is gauge-invariant complete decomposition of the nucleon spin possible? *Int. J. Mod. Phys.*, A29:1430012, 2014.

[126] K. Liu and C. Lorcé. The Parton Orbital Angular Momentum: Status and Prospects. *Eur. Phys. J.*, A52(6):160, 2016.

[127] C. Lorcé. Spin–orbit correlations in the nucleon. *Phys. Lett.*, B735:344, 2014.

[128] M. V. Polyakov. Generalized parton distributions and strong forces inside nucleons and nuclei. *Phys. Lett.*, B555:57, 2003.

[129] M. V. Polyakov and A. G. Shuvaev. On'dual' parametrizations of generalized parton distributions. hep-ph/0207153.

[130] K. Goeke, J. Grabis, J. Ossmann, M. V. Polyakov, P. Schweitzer, A. Silva, and D. Urbano. Nucleon form-factors of the energy momentum tensor in the chiral quark-soliton model. *Phys. Rev.*, D75:094021, 2007.

[131] C. Cebulla, K. Goeke, J. Ossmann, and P. Schweitzer. The Nucleon form-factors of the energy momentum tensor in the Skyrme model. *Nucl. Phys.*, A794:87, 2007.

[132] L. Adhikari and M. Burkardt. Angular Momentum Distribution in the Transverse Plane. *Phys. Rev.*, D94(11):114021, 2016.

[133] C. Lorcé, L. Mantovani, and B. Pasquini. Spatial distribution of angular momentum inside the nucleon. hep-ph/1704.08557.

[134] F. J. Belinfante. *Physica*, 6:887, 1939.

[135] F. J. Belinfante. *Physica*, 7:449, 1940.

[136] L. Rosenfeld. *Mém. Acad. Roy. Belg.*, 18:1, 1940.

[137] C. Lorcé. The light-front gauge-invariant energy-momentum tensor. *JHEP*, 08:045, 2015.

[138] C. Lorcé. Geometrical approach to the proton spin decomposition. *Phys. Rev.*, D87(3):034031, 2013.

[139] C. Lorcé. Gauge symmetry and background independence: Should the proton spin decomposition be path independent? *Nucl. Phys.*, A925:1, 2014.

[140] B. L. G. Bakker, E. Leader, and T. L. Trueman. A Critique of the angular momentum sum rules and a new angular momentum sum rule. *Phys. Rev.*, D70:114001, 2004.

[141] R. G. Sachs. High-Energy Behavior of Nucleon Electromagnetic Form Factors. *Phys. Rev.*, 126:2256, 1962.

[142] C. Lorcé. New and simple covariant expressions for Dirac bilinears. hep-ph/1705.08370.

[143] E. Leader. New relation between transverse angular momentum and generalized parton distributions. *Phys. Rev.*, D85:051501, 2012.

[144] E. Leader. On the controversy concerning the definition of quark and gluon angular momentum. *Phys. Rev.*, D83:096012, 2011. [Erratum: Phys. Rev.D85,039905(2012)].

[145] Elliot Leader. A critical assessment of the angular momentum sum rules. *Phys. Lett.*, B720:120–124, 2013. [Erratum: Phys. Lett.B726,927(2013)].

[146] S. J. Brodsky and S. D. Drell. The Anomalous Magnetic Moment and Limits on Fermion Substructure. *Phys. Rev.*, D22:2236, 1980.

[147] M. Burkardt and Hikmat BC. Angular Momentum Decomposition for an Electron. *Phys. Rev.*, D79:071501, 2009.

[148] N. Kumar and H. Dahiya. Charge and magnetization densities in transverse coordinate and impact parameter space. *Phys. Rev.*, D90(9):094030, 2014.

[149] K. Kanazawa, C. Lorcé, A. Metz, B. Pasquini, and M. Schlegel. Twist-2 Generalized TMDs and the Spin/Orbital Structure of the Nucleon. *Phys. Rev.*, D90:014028, 2014.

[150] M. A. Alonso. Wigner functions in optics: describing beams as ray bundles and pulses as particle ensembles. *Adv. Opt. Photon.*, 3(4):272, 2011.

[151] L. Maccone and C. C. Rusconi. State estimation: A comparison between direct state measurement and tomography. *Phys. Rev. A*, 89:022122, 2014.

[152] T. Muta. *Foundations of Quantum Chromodynamics: An Introduction to Perturbative Methods in Gauge Theories, (3rd ed.)*, volume 78 of *World scientific Lecture Notes in Physics*. World Scientific, Hackensack, N.J., 2010.